IAEA TECDOC SERIES

IAEA-TECDOC-CD-1798

High Burnup Fuel: Implications and Operational Experience

Proceedings of a Technical Meeting Held in Buenos Aires, 26–29 November 2013

IAEA
International Atomic Energy Agency

HIGHT BURNUP FUEL: IMPLICATIONS AND OPERATIONAL EXPERIENCE

The following States are Members of the International Atomic Energy Agency:

AFGHANISTAN
ALBANIA
ALGERIA
ANGOLA
ANTIGUA AND BARBUDA
ARGENTINA
ARMENIA
AUSTRALIA
AUSTRIA
AZERBAIJAN
BAHAMAS
BAHRAIN
BANGLADESH
BARBADOS
BELARUS
BELGIUM
BELIZE
BENIN
BOLIVIA, PLURINATIONAL STATE OF
BOSNIA AND HERZEGOVINA
BOTSWANA
BRAZIL
BRUNEI DARUSSALAM
BULGARIA
BURKINA FASO
BURUNDI
CAMBODIA
CAMEROON
CANADA
CENTRAL AFRICAN REPUBLIC
CHAD
CHILE
CHINA
COLOMBIA
CONGO
COSTA RICA
CÔTE D'IVOIRE
CROATIA
CUBA
CYPRUS
CZECH REPUBLIC
DEMOCRATIC REPUBLIC OF THE CONGO
DENMARK
DJIBOUTI
DOMINICA
DOMINICAN REPUBLIC
ECUADOR
EGYPT
EL SALVADOR
ERITREA
ESTONIA
ETHIOPIA
FIJI
FINLAND
FRANCE
GABON
GEORGIA
GERMANY
GHANA
GREECE
GUATEMALA
GUYANA
HAITI
HOLY SEE
HONDURAS
HUNGARY
ICELAND
INDIA
INDONESIA
IRAN, ISLAMIC REPUBLIC OF
IRAQ
IRELAND
ISRAEL
ITALY
JAMAICA
JAPAN
JORDAN
KAZAKHSTAN
KENYA
KOREA, REPUBLIC OF
KUWAIT
KYRGYZSTAN
LAO PEOPLE'S DEMOCRATIC REPUBLIC
LATVIA
LEBANON
LESOTHO
LIBERIA
LIBYA
LIECHTENSTEIN
LITHUANIA
LUXEMBOURG
MADAGASCAR
MALAWI
MALAYSIA
MALI
MALTA
MARSHALL ISLANDS
MAURITANIA
MAURITIUS
MEXICO
MONACO
MONGOLIA
MONTENEGRO
MOROCCO
MOZAMBIQUE
MYANMAR
NAMIBIA
NEPAL
NETHERLANDS
NEW ZEALAND
NICARAGUA
NIGER
NIGERIA
NORWAY
OMAN
PAKISTAN
PALAU
PANAMA
PAPUA NEW GUINEA
PARAGUAY
PERU
PHILIPPINES
POLAND
PORTUGAL
QATAR
REPUBLIC OF MOLDOVA
ROMANIA
RUSSIAN FEDERATION
RWANDA
SAN MARINO
SAUDI ARABIA
SENEGAL
SERBIA
SEYCHELLES
SIERRA LEONE
SINGAPORE
SLOVAKIA
SLOVENIA
SOUTH AFRICA
SPAIN
SRI LANKA
SUDAN
SWAZILAND
SWEDEN
SWITZERLAND
SYRIAN ARAB REPUBLIC
TAJIKISTAN
THAILAND
THE FORMER YUGOSLAV REPUBLIC OF MACEDONIA
TOGO
TRINIDAD AND TOBAGO
TUNISIA
TURKEY
TURKMENISTAN
UGANDA
UKRAINE
UNITED ARAB EMIRATES
UNITED KINGDOM OF GREAT BRITAIN AND NORTHERN IRELAND
UNITED REPUBLIC OF TANZANIA
UNITED STATES OF AMERICA
URUGUAY
UZBEKISTAN
VANUATU
VENEZUELA, BOLIVARIAN REPUBLIC OF
VIET NAM
YEMEN
ZAMBIA
ZIMBABWE

The Agency's Statute was approved on 23 October 1956 by the Conference on the Statute of the IAEA held at United Nations Headquarters, New York; it entered into force on 29 July 1957. The Headquarters of the Agency are situated in Vienna. Its principal objective is "to accelerate and enlarge the contribution of atomic energy to peace, health and prosperity throughout the world''.

IAEA-TECDOC-1798

HIGH BURNUP FUEL: IMPLICATIONS AND OPERATIONAL EXPERIENCE

PROCEEDINGS OF A TECHNICAL MEETING HELD IN BUENOS AIRES, 26–29 NOVEMBER 2013

INTERNATIONAL ATOMIC ENERGY AGENCY
VIENNA, 2016

For further information on this publication, please contact:

Nuclear Fuel Cycle and Materials Section
International Atomic Energy Agency
Vienna International Centre
PO Box 100
1400 Vienna, Austria
Email: Official.Mail@iaea.org

Printed by the IAEA in Austria
August 2016

HIGH BURNUP FUEL: IMPLICATIONS AND OPERATIONAL EXPERIENCE
IAEA-TECDOC-CD-1798
ISBN 978-92-0-155316-4
ISSN 1684-273

FOREWORD

A trend towards increasing the discharge burnup of nuclear fuel has been a feature of the operation of virtually all types of nuclear power plant for many years. The increase of the fuel burnup has been implemented in response to the economic challenge to reduce costs associated with nuclear power. Increased dwell allows smaller fuel inventories and fabrication costs on the one hand, and reduced spent fuel volumes to handle and to store or reprocess on the other hand, typically at the expense of higher enrichments. It is also possible to design longer fuel cycles in the reactor, which can mean higher availability and capacity factors as well as fewer handling operations. However, there are also increased costs associated with high burnup, apart from increased enrichment: larger specific decay heats and increased dose rates during transport due to larger neutron source intensities in highly burnt fuel have been identified at the back end, as well as new regulatory challenges associated with the precise quantification of safety margins, for example criticality safety, to guarantee high performance during reactor operation and fuel robustness and integrity overall.

It is thus necessary to evaluate safety margins obtained in practice for high burnup fuel from the operational experience in different Member States, to compare these experiences and to assess whether the expected benefits have been obtained in reality.

The Technical Meeting on High Burnup Fuel Experience and Economics, held in Buenos Aires, Argentina, 26–29 November 2013, was a follow up of two previous meetings, held in Argentina in 1999 and in Bulgaria in 2006, with the purpose to revisit and update the current operational experience and economic conditions associated with high burnup fuel. The meeting was strongly supported at the Technical Working Group on Fuel Performance and Technology held in April 2013, with the aim of bringing together experts with significant experience in experimental programmes on high burnup fuel, to compare their respective experiences and to evaluate physical limitations at pellet, cladding and structural component levels, with a wide focus including fabrication, core behaviour, transport and intermediate storage for most types of commercial nuclear power plant. The meeting was hosted by the National Atomic Energy Commission of Argentina (Comisión Nacional de Energía Atómica, CNEA), and was held at the Biblioteca Nacional in Buenos Aires.

The meeting was attended by 44 specialists from 12 countries, the IAEA and the European Commission (JRC Institute for Transuranium Elements) representing R&D institutions, nuclear utilities and state nuclear regulatory and licensing authorities. Seventeen papers were presented in five technical sessions, covering experimental data and modelling in normal and accident conditions, operating experience and lessons learned, fuel design and fuel cycle, R&D and fabrication, and licensing and regulatory aspects.

The IAEA wishes to thank the hosts and participants for their contribution to the meeting and especially the local coordinator, L. Alvarez (Argentina) for the organization of the Technical Meeting and the technical visit to the Atucha 2 nuclear power plant and F. Jatuff (Switzerland) for active participation in the preparation of the meeting summary. The officer responsible for this publication was V. Inozemtsev of the Division of Nuclear Fuel Cycle and Waste Technology.

EDITORIAL NOTE

This publication has been prepared from the original material as submitted by the contributors and has not been edited by the editorial staff of the IAEA. The views expressed remain the responsibility of the contributors and do not necessarily represent the views of the IAEA or its Member States.

Neither the IAEA nor its Member States assume any responsibility for consequences which may arise from the use of this publication. This publication does not address questions of responsibility, legal or otherwise, for acts or omissions on the part of any person.

The use of particular designations of countries or territories does not imply any judgement by the publisher, the IAEA, as to the legal status of such countries or territories, of their authorities and institutions or of the delimitation of their boundaries.

The mention of names of specific companies or products (whether or not indicated as registered) does not imply any intention to infringe proprietary rights, nor should it be construed as an endorsement or recommendation on the part of the IAEA.

The IAEA has no responsibility for the persistence or accuracy of URLs for external or third party Internet web sites referred to in this publication and does not guarantee that any content on such web sites is, or will remain, accurate or appropriate.

CONTENTS

SUMMARY

INTRODUCTION

The Technical Meeting on High Burnup Fuel Economics and Operational Experience held in Buenos-Aires, Argentina, from 26 to 29 November 2013 was a follow up of two previous meetings. The first one was held in Argentina in 1999 to consider, for the first time at the IAEA level, the technical and economic limits to fuel burnup extension in the different Member States. It covered both high burnup experience and the issues and limits imposing economic constraints [1]. The second one was held in Bulgaria in 2006 and focussed on the operating experience since 1999, high burnup fuel behaviour and the economic conditions surrounding high burnup fuel at the time [2]. The present meeting strongly supported at the *Technical Working Group on Fuel Performance and Technology* (TWGFPT) was held in April 2013 as a follow-up of the previous two meetings and in order to update the basic perspectives of the contributing member states to this field, including possible new regulatory views following the Fukushima accident in Japan in 2011. Seventeen papers from twelve countries and one international organisation were presented during five technical sessions, covering *Experimental Data and Modelling in Normal and Accident Conditions*, chaired by Thierry Wiss, *Operating Experience and Lessons Learned*, chaired by Gabriel Ruggirello, *Fuel Design and Fuel Cycle*, chaired by Catherine Cottrell, *R&D and Fabrication*, chaired by Raj Bhushan Bhatt, and *Licensing and Regulatory Aspects*, chaired by Juraj Rovny. Two more papers were presented, respectively by Patrick Blanpain and Catherine Cottrell, but their full texts were not submitted to the IAEA and correspondingly were not included into this publication. Fabian Jatuff of Kernkraftwerk Gosgen-Daniken AG, Switzerland actively participated in the discussion of meeting's results and preparation of this Summary.

Meeting was opened by N.L. Boero, Director of the CNEA in Argentina, who welcomed the participants and introduced the status of activities in her country, mentioning in particular the finalisation of the Atucha II NPP project and the construction begin of the national small modular reactor CAREM at the Atucha site. D. Marchi from CNEA presented basic features of the Argentinian nuclear programme at the different sites. F.Reale from the national nuclear fuel producer company CONUAR, sponsor of the meeting, presented his company and the advance of activities in the areas nuclear fuel production, special materials and services, and special alloys. V. Inozemtsev thanked the local organisers on behalf of the IAEA and described the work programme carried out by the Agency in the field of the nuclear fuel cycle and material technologies, among others in the framework of the series of Coordinated Research Projects (CRPs) FUMEX (Fuel Modelling at Extended Burnup-FUMEX-I, 1993-1996 [3] FUMEX-II, 2002-2007 [4] and FUMEX-III, 2008-2012 [5]).

A visit was arranged for the participants of the Technical Meeting to see the final stage of construction of the Atucha II NPP near Lima, about 100 km from the Buenos Aires capital city. The reactor is a PHWR of a pressure-vessel type, designed for 745 MWe output and fuelled with natural or slightly enriched uranium like Atucha I. The first core is already loaded with its 450 fresh fuel assemblies and primary circuit tests have been successfully conducted with light water and external heating coming from the operation of the two primary pumps. Entry into service is expected during 2014.

The results of the Technical Meeting need to be separated according to reactor type. Regarding light water reactors (LWRs), fuel burnup license was effectively extended up to 70 MWd/kgU in some countries since several years, without technical obstacles even with the present enrichment limit of 5 wt% as already envisaged [1-2]. This is in particular the case of some pressurised water reactors (PWRs) in Europe, and VVERs are slowly being upgraded

towards this limit; boiling water reactors (BWRs) are following the trend but remain at slightly lower values. There is though no further incentive to increase these burnup limits, challenges now being associated with the high burnup structure (HBS) and the pellet and cladding behaviour during accident conditions in view of more stringent regulatory requirements expected in the future e.g. reactivity insertion and loss-of-coolant accidents (RIA and LOCA), requiring better experimental data and more refined modelling capabilities compared to those available today. A significant aspect in this context is the transportability of high burnup fuel assemblies following a long-term dry storage, due to possible degradation mechanisms such as creep, hydride reorientation, loss of ductility, etc. that may take place under relatively high temperature conditions during very long periods under dry storage. Safety aspects of spent fuel storage are presented in the IAEA Specific Safety Guide SSG-15 [6].

Pressurised heavy water reactors (PHWRs), on the other hand, are fully exploiting their flexibility to increase very significantly, in relative terms, their discharge burnups and to expand their fuel cycle capabilities; they are doing so and they will continue to do it in the near future. In Argentina this has been implemented through the successful use of slightly enriched uranium (SEU), also expected for Atucha II. Particularly in Asia the trend is worth mentioning, where the use of uranium mixtures in Chinese and mixed oxide (MOX) in Indian CANDU-type reactors is progressing significantly. Fabrication advances include uranium mixtures coming from reprocessed uranium (RepU) with depleted uranium leading to natural uranium equivalent (NUE), and also light concentrations of plutonium mixtures for MOX-type fuel. Technological advances, such as more efficient sintering processes and revisited materials such as boron-bearing UO_2, free standing cladding and optimal plenum design, are being pursued for PHWRs.

The next four sections present in detail the general focus of the Technical Meeting (Background), the individual presentations (Summaries and Comments), the identified limitations (Problems, Challenges and Perspectives), and finally a brief description of open fields (Recommendations for Future Work) before the individual contributions.

BACKGROUND

There are many opportunities for increasing the burnup of fuels by changing the fuel design and also by using alternative fuel cycles. Many countries are attempting to increase the utilization of their resources by increasing the burnup values of the fuel in order to increase the economics of nuclear power. The drivers and the optimization mechanisms being used to achieve these higher burnup values depend on various priorities and differ from country to country. For example, many countries are employing enrichment of uranium in order to achieve higher burnup fuels and thus improve the economics of the reactor. Whereas, other countries are exploring alternative fuel cycles such as RU in order to ensure a secure supply of fuel inventory, achieve higher burnup values and reduce their front end fuel cycle costs.

Regulatory aspects remain to play an important role in fuel type selection and fuel cycles modification. Safety aspects of reactor core design and fuel refuelling patterns are presented in Refs [7, 8]. Utilities, on the one hand, tend to optimize their fuel cycle costs loading more modern fuel types and increasing average burnup of discharged fuel. On the other hand these steps are limited by particular regulatory regimes and fuel safety requirements. New fuel types as well as increased burnup are subject to more stringent licensing requirements in most of the countries. Regulatory bodies are paying renewed attention to deepen into particular limits such as maximum enthalpy deposition in LWR-MOX fuel during RIAs, the behaviour of the high burnup structure (HBS) during very fast ramps in RIAs, and fuel fragmentation, relocation and dispersal following ballooning and burst during LOCAs. Transport and storage

conditions are being scrutinised in detail, to guarantee that high burnup fuel could be safely transported and handled following a long-term dry storage, because of possible degradation mechanisms such as creep, hydride reorientation, loss of ductility, etc. that may take place under relatively high temperature conditions during decades of storage.

These new efforts to complete and deepen safety assessments of high burnup fuels in these fields require more and better experimental data, particularly well designed and conducted tests in research reactor loops, and refined modelling capabilities for accident situations. The papers presented during the sessions reflect in detail these trends.

SUMMARY OF THE TECHNICAL SESSIONS

The first session, under the title Experimental Data and Modelling in Normal and Accident Conditions, grouped seven papers. This Session 1 was chaired by T. Wiss, from the EC JRC Institute for Transuranum Elements (European Commission).

In the first presentation entitled *Pushing the Limits of the Simulation of Nuclear Materials and Fuels by using the BaCo code and M³ (Multiscale Modelling of Materials)*, A. Marino of CNEA Centro Atomico Bariloche, Argentina briefly presented the BaCo code also trying to properly include accident conditions. The BaCo code was developed to simulate the nuclear fuel rods behaviour under irradiation and it has good compatibility with PHWR, PWR, VVER, among others type of fuels (commercial, experimental or prototypes). The code includes additional extensions for 3D calculations, statistical analysis, fuel design, a full core analysis and accident conditions at work. Research on new fuels (GEN IV) and cladding materials properties based on *ab initio* (from the beginning) and multiscale's modelling of materials (M³) are currently under development to be included in the BaCo code modelling. Examples of the code by using the cases of the IAEA Coordinated Research Projects D-COM (1981-1985) [9], FUMEX I (1993-1996) [3], FUMEX II (2001-2005) [4] and FUMEX III (2008-2011) [5] but also new fuel conditions, such as fuel burnup extension, have been presented.

In the second presentation by T. Wiss (*Properties of high burnup structure in LWR fuels*) it was shown that the HBS is rather well characterized and that HBS does not compromise the safe operation of high burnup fuel under normal operating conditions. More specifically it was shown that fission gases are not released when HBS is formed, that the intrinsic thermal conductivity even recovers when HBS is formed and that softening due to HBS formation is observed being beneficial for pellet-clad mechanical interaction (PCMI). However, no model fully explaining the HBS formation exists today. The HBS behaviour under severe accident conditions (fast ramps) still needs to be determined To this effect more recent and ongoing campaigns are focused, among others, on the evolution of HBS at ultra-high burnup, on the comparison of high burnup structures in LWR fuel (UO_2, MOX) and other fuel systems, and on the incorporation of HBS properties in the TRANSURANUS fuel performance code.

In the third presentation shared between C. Syrewicz and A. Bonelli from Nucleoelectrica Argentina (NASA), on the *Assessment of PCI failure prediction capabilities of TRANSURANUS code for natural uranium fuel based on operational fuel pin failures of Atucha I NPP* it was shown how the TRANSURANUS code capabilities regarding PCI failure prediction for Atucha type fuels have been assessed by the use of operational experience. On 14/06/85, ten fuel rods were detected failed in CNA-I after a severe power cycle. The failure mechanism was pellet-cladding interaction (PCI). The source code was modified (subroutine SPAKOR): some material properties of the clad and ABKRIT (burnup critical value) parameter were changed. This version led to much more satisfactory results. The elasticity modulus of Zry-4 and yield and rupture stresses for burst tests, provided by the fuel vendor CONUAR, were included. Overall results were compared and finally an Atucha-

suited re-compiled code executable was selected for oncoming PCI calculations of Atucha-type fuels. Furthermore, uncertainties in power history data were identified and therefore it was concluded that boundary conditions provided in the performed calculations highly influenced failure/non failure code predictions. In light of this, it was concluded that results had to be analyzed on a global basis for each of the calculated sensitivity cases.

The performed assessment contributed in gaining confidence on TRANSURANUS code predictions when simulating natural uranium fuels of low burnup, for which phenomena have not been deeply investigated lately, as this type of fuels is rather unusual among the fuel designs currently found in the nuclear industry.

In the fourth presentation, A. Denis from CNEA – Centro Atomico Constituyentes, Argentina discussed the high burnup models incorporated to the DIONISIO code. Several subroutines, oriented to high burnup, were recently incorporated into the code which can be applied to various types of fuels from PWR, PHWR, BWR, VVER and CAREM, and has meanwhile integrated 40 interconnected models to represent extended burnups. It has the capability of calculating the radial distribution of power density, neutron flux and burnup as well as the radial distribution of the more relevant U and Pu isotopes but also the radial distribution of Cs, Nd and Xe. Additionally, the evolution of pore and grain size and pores number density in the rim zone and the accumulation of fission gas in the closed pores can be determined. A very elegant approach using empirical expressions is used for fitting the cross sections calculations. Thermal conductivity of UO_2 in terms of the content of Gd (burnable poison) and the accumulated burnup is also calculated with the newest version of the code.

The fifth presentation by A. Soba from CNEA - Centro Atomico Constituyentes, Agentina on the *Simulation with DIONISIO 2.0 of a whole nuclear fuel rod under extended irradiation* was supplementary to the previous one. In its new architecture the code can represent a complete rod, which is divided into a number of axial segments. All the subroutines were subject to numerous separate tests, including parametric analyses and comparison with experimental data. These models were introduced in DIONISIO. The predictive ability of the code as a whole was tested by comparison of its results with experimental data. The extension of the modelling to the whole rod, by sectors, gave good results without the loose of the local prediction, basically the details of PCMI. The inclusion of high burnup models allowed to extend the range of prediction of DIONISIO 2.0 to the actual range of results obtained worldwide in PWRs, BWRs and PHWRs, that mean about 60-80 MWd/kg_{HM}.

The sixth presentation by Z. Hozer of Hungarian Academy of Sciences Centre for Energy Research was on the Simulation of high burnup fuel fragmentation in high temperature transients. Fragmentation and relocation of the high burnup fuel pellets was observed in Halden LOCA tests and in Studsvik hot cell experiments. A simple model has been developed for the analysis of the mechanical behaviour of the fuel pellet to explain the fragmentation mechanism. High pore pressure and porosity can cause such stresses in high burnup fuel pellet that can lead to fragmentation of UO_2 during a LOCA when the fracture strength is reached. The model presented is suitable for predicting the fragmentation of the HBS of the fuel pellets with average burnups between 56 and 102 MWd/kgU and the ensuring extra fission gas release during LOCA.

In the last presentation of the Session 1, Maria Sypchenko of JSC A.A. Bochvar High-technology Research Institute of Inorganic Materials, Russian Federation *(Experimental and computational studies of VVER high burnup fuel behaviour under LOCA conditions (MIR-LOCA/60))* showed both experimental and modelling studies on the VVER high burnup fuel behaviour under LOCA conditions. The LOCA/60 experiment with VVER high-burnup fuel was performed in the MIR research reactor (SSC-RIAR) in 2010. Experimental fuel assembly

with 16 fresh and 3 refabricated VVER-1000 type test fuel rods with burnup of 58.1 - 58.6 MWd/kgU was tested. The purpose of the MIR-LOCA/60 experiment was the study of thermo-mechanical behaviour of VVER high burnup fuel at typical conditions for LOCA design accidents including also research on cladding deformations and rupture conditions, claddings oxidation, fuel pellets fragmentation and relocation in the ballooning area of cladding. In this experiment the duration of cladding temperature above 700°C was about 1 minute. Post-test neutron, thermohydraulic and thermomechanical calculations were carried out (benchmark between 5 codes). In this test there was a rupture of claddings of four fresh fuel rods with large hoop strain deformations. There was cracking of pellets into large fragments and relocation of fragments in the ballooning area but the refabricated fuel rods kept their tightness. Thus, in this test there was no condition for destruction of fuel pellets with burnup 58 MWd/kgU.

Session 2, operating experience and lessons, consisted of four papers and was chaired by Gabriel Ruggirello from CNEA, Argentina. The first two of them comprehensively described the operating experiences showing main results in high burn up programs in LWRs and the other two showed the achievement and the problems found in the implementation of the increased burnup programs in PHWRs.

The first presentation of Session 2 was *Issues for Increasing Burnup*, authored by P. Blanpain from AREVA, France and given by V. Inozesmtsev, which was based essentially in the author's presentation during the last TWGFTP meeting in April 2013. The presenter gave a comprehensive overview of discharge burnup of reactors worldwide during 2010-2013, discriminated by their type. Special details were described for particular cases of reactors in Germany, France and the USA. The advantages and disadvantages of burnup extension and the operational and regulatory aspects were thoroughly analyzed. The author's basic conclusion is that current maximum batch-averaged discharged burnups of ~65 GWd/t_{HM} are already representative of fuel assembly or fuel rod licensing limits and there are no more economic incentives for burnups beyond these values. Unfortunately only Power Point version of this presentation was available and therefore not included into the Proceedings.

The second presentation, *Fuel Failure Issues Related to Increasing Burnup*, was given by O. Yousaf from the Chashma NPP, Pakistan; he described the incentives for high burn up programs and the potential failure mechanisms at high burn up expected. The case of using extended burnup in a postulated accident like the one in Fukushima was analyzed and this gave valuable insights about this scenario.

Fabian Jatuff from Switzerland gave the third presentation of Session 2 entitled *High burn up fuel technical and economic lessons learned at Swiss nuclear power plants*. First, the front-end incentive in Switzerland to achieve higher burnups, with fixed annual cycles and national back-end policies restricting reprocessing, was described. Then the Swiss high-burnup research programme followed by the Gösgen NPP was reported, which achieved very high burnup upgrades that led to world-record commercial values, with licensing limits on rod-average and peak (pellet-averaged) burnups of 75 and 82 GWd/tU for UO_2 fuel, respectively. The presentation considered economic attractiveness of having introduced high burnups, as well as future challenges, among others those corresponding to the transportability of high burnup fuel following a long dry storage.

The fourth and last presentation of Session 2 was given by the session chair, G. Ruggirello from CNEA, under the title *Post-Irradiation Visual Inspection and Metrology of a New Design Atucha I Fuel Element*. The goal of the development is the use of SEU with 0.85 wt% enrichment and the increase of the uranium mass in order to achieve a higher burnup, as well bringing a frequency reduction of on-line refuelling in the Atucha I PHWR. These goals

involved a modification in several parameters, among others in the pellet stack and in the structure design of the fuel element. The visual inspection and metrology controls performed assured the progressive implementation of the uranium mass increase programme.

Session 3, fuel designs and fuel cycles, was chaired by Catherine Cottrell from CANDU Energy, Canada and consisted of three presentations from Argentina, Brazil and Canada, respectively. These sessions are summarized below.

The first presentation of the session, *Status of Fuel Engineering Activities on Extended Burnup Fuel for the Argentine Fleet of PHWRs*, was given by Alejandro Bussolini from CNEA. In Argentina, there are three nuclear reactors: Embalse CANDU 6 PHWR and the Atucha I and Atucha II Siemens/KWU PHWRs. The Embalse and Atucha-1 reactors are operational whereas the Atucha-2 reactor is near completion, with fuel assemblies loaded and the commissioning phase in the advanced stage. Typical burnup values for PWRs are around 50 000 MWd/tU and operators are working to increase burnup values to high or ultrahigh levels of 60 000 to 70 000 MWd/tU; a relative increase of 20 – 40%. For PHWRs the intent is to increase the burnup values from 7500 MWd/tU to values of 15 000 – 25000 MWd/tU; an enormous relative increase in the range 115 – 250%. The extended burnup values were achieved by using SEU in the Atucha I reactor by employing a step-by-step approach. Over six years, the SEU was gradually introduced into the reactor until achieving a full core loading in 2001. The higher burnup values result in several benefits including a decrease in fuel cost impact on the total electricity cost, uranium resource savings, and a reduction in spent fuel volumes. In order to utilize SEU in the Atucha I reactor, the fuel design was optimized in the following manner: plenum length was increased, bearing pads redesigned to have longer contact surfaces, cladding ductility increased and the elastic sliding shoe material was replaced with Inconel-718. Optimization resulted in achieving a maximum local burnup of close to 15 000 MWd/tU with a fuel dwell time of almost twice that of natural uranium (300 to 50 FPDs). These results translate into a reduction of spent fuel volume of approximately 42% and a reduction on the cost of the fuel included in the cost of electricity of about 30 – 40%. This fuel has been assessed for use in the Atucha II reactor and has been shown to be feasible. Feasibility study was also performed for the Embalse CANDU 6 PHWR which showed that by using 0.9 wt% U-235 SEU a burnup value of 14 000 MWd/tU could be achieved resulting in an estimated fuel savings of approximately 20%.

The second contribution in Session 3 was given by the session chair C. Cottrell, with the title *CANDU Reactor Fuel Cycle Flexibility*. Unfortunately only Power Point version of this presentation was available and therefore not included into the Proceedings. The presentation discussed the use of recycled uranium (RU) and thorium fuels in the CANDU reactors. This is a different approach to increasing the burnup of the fuel – by reusing the fuel you are in essence increasing the burnup of the starting material. The driver for using these alternative fuels is the projected increase in nuclear power requirements in the next few decades, primarily in China, resulting in a strain on the uranium supply. Since China has an existing fleet of both PWRs and CANDU reactors, the use of RU in the CANDU fleet exploited the synergy between the two technologies. There are ample existing and projected quantities of RU for use in CANDU reactor applications. It is advantageous to use the RU in CANDU reactors because it can be done in a direct manner without the need for re-enrichment needed for PWR use which is more difficult and costly. The use of RU in CANDU reactors is technically and economically attractive. The RU fuel in the form of natural uranium Equivalent, a mixture of RU and depleted uranium has been tested in one of the Qinshan CANDU reactors in Haiyan, China. Based upon the successful testing, a full core application of this fuel in the two Qinshan CANDU stations is underway. Canada with its Chinese partners are using the success of the NUE fuel as the basis of a new reactor design, the

Advanced Fuel CANDU Reactor (AFCR), which will utilize RU or Th-based fuels at higher burnup values. As with the PHWRs in Argentina, the typical burnup value for the CANDU reactor is 7 500 MWd/tU using natural uranium fuel. The target burnup for the AFCR is 10 000 MWd/tU for RU-based fuel and 20 000 MWd/tU for Th-based fuel. The RU-based fuel not only has the economic benefit resulting from higher burnup capacities but also from the lower cost required to acquire the resource. Unfortunately only Power Point version of presentation was presented therefore was not included into these Proceedings.

The third and last contribution in Session 3, entitled *Core Management Improvements at Angra Unit 1 Using an Advanced 16x16 Westinghouse type PWR Fuel Assembly*, was presented by Lelia Custodio Panetto from Industrias Nucleares do Brasil (INB). Brazil has three operating Westinghouse PWRs referred to as Angra-1, Angra-2 and Angra-3. INB in partnership with KEPCO Nuclear Fuel Company and Westinghouse Electric Company designed an advanced 16x16 PWR fuel assembly in order to increase burn up values and thermal margin capability while significantly reducing fuel cycle costs. The 16x16 fuel assembly was modified by optimizing the fuel rod diameter, introducing low parasitic neutron components, improved departure from nucleate boiling margin and other mechanical features to improve design margins and reliability. Analyses were performed to select the optimum FROD, to optimize cost, fuel cycle management and nuclear reactivity. Based on these three criteria only, the optimized FROD was 0.350 inches. This optimization resulted in negative impacts to DNB margin, fuel rod performance experience, fuel rod bow models/experience and a desire for longer fuel cycles (~430 EFPDs). Due to customer's requirement for longer cycles and the upper limit that exists in enrichment to be used as well as previous experience, the optimized FROD selected was 0.360 inches. In addition, an axial blanket optimization study was undertaken to determine which axial blanket enrichment and length would provide better fuel cycle cost-benefit. It was determined that fuel cycle costs for using ZIRLO mid grids was 1.6% lower when compared to using Inconel mid grids.

Session 4 was devoted to R&D and fabrication and was chaired by Raj Bhushan Bhatt from BARC, India. Three presentations were given during this session. Two presentations were on R&D related to fuel pellets and clad material and one was on fabrication of MOX fuel. The papers were related to developments which would help in improving the burnup.

The first paper in Session 4, entitled *Fabrication of (UO_2-0.4 % PuO_2) MOX fuel for PHWRs*, was presented by the session chair R. B. Bhatt. The work dealt with fabrication procedure of MOX fuel for PHWR (CANDU) and the results of irradiation. It mentioned the design changes required as compared to natural uranium UO_2 fuel. The additional steps required for fabrication of MOX fuel were also discussed. The limitations of the use of glovebox for fabrication of MOX fuel was discussed in detail. Finally, it was concluded that 50 MOX bundles of PHWR loaded in one of the Indian PHWR were successfully irradiated to high burnups of around 10 000 MWd/tU, which could be achieved in all the 50 bundles without any failure.

The second presentation of the session was entitled *Low Temperature Sintering of UO_2 at Reducing Atmosphere and its Application* and presented by Y. W. Rhee from KAERI, Korea, Republic of. The contribution dealt with work carried out to achieve high density at low sintering temperature using sintering additive aiming at a HBS-type already for the fresh fuel, using a two-step sintering. The former method involved addition of MnO, which in turn accelerates the diffusion so the sintering can be carried out at low temperature. The same method was also found suitable for boron-compound-dispersed UO_2 fuel. BN has been chosen as boron compound over other boron compounds for its thermal stability. MnO-added UO_2 pellets can be densified up to 95% of the theoretical density (TD) after sintering at 1250°C for 1 hour in H_2 atmosphere. UO_2 pellets with 0.1 wt% BN and 0.2 wt % MnO has a

sintered density of about 94% TD after sintering for 1 h, and sintered density increased up to around 96% TD after sintering for 4 hours. Microstructure of HBS is characterized by very small grain of 300 nm in diameter. HBS can be obtained by using nano-sized powders as raw materials. These nano-sized powders pose difficulties in fabrication. By using 2 stages sintering, 300-400 nm grain size structure was achieved, with 0.1 micron size powder.

The last presentation of Session 4, entitled *Work Plan to Achieve the Technology for the Introduction of Oxygen Micro-Addition and Beta–Niobium Second Phase Particles with Optimum Size and Distribution in the Zirconium Matrix of Zr-1%Nb Alloy"*, was presented by Paula Regina Alonso from CNEA, Argentina. The presentation described the work plan to achieve the technology for oxygen micro addition and beta- niobium second phase particles with optimum size and distribution in matrix of Zr-1%Nb alloy, for the production of the national equivalent of the M5 alloy. The author presented the specific goals and the road map to achieve them. The first goal was to fabricate ingots of Zr-1% Nb- 0.12% O by melting with consumable arc electrode in a two fusion process. The second goal was to use a thermo mechanical process to obtain strips of particles of second phase with optimal size and distribution. The last goal was to characterise the microstructure and evaluate the mechanical properties of the material produced.

Licensing and regulatory aspects was the subject of Session 5, chaired by Juraj Rovny from Slovenske Elektrarne, Slovakia. In this session, the following two papers were presented: *Challenges for the Regulatory Body during Transition to Use the Fuel with High Burnup*, from S. Popova of the Bulgarian Nuclear Regulatory Agency and *Licensing and Operational Experience with High Burnup Fuel in Slovak NPPs*, given by the session chair J. Rovny.

Though there were only two presentations given, all of the participants confirmed that there are specific legislative requirements dedicated to fuel licensing in their countries. There seems to be quite large difference in practices applied in each individual country regarding fuel type and burnup licensing. Existing legal basis allows for application of permitting higher burnup in almost any of the countries; however, the scope and nature of documentation to be submitted differs from country to country. This resulted in wide range of maximum reached burnups of different NPPs worldwide. While some utilities operate its fuel cycles with limiting burnups below 55 MWd/kgU (max. fuel rod average) there are countries, as for example Switzerland, that go up to 75 MWd/kgU.

PROBLEMS, CHALLENGES AND PERSPECTIVES

From the current perspective there is no indication that a common and widely accepted view on high burnup issues could be reached as a kind of consensus among majority of countries or regulatory bodies. While there are countries that reached successfully relatively high burnup values there is still a large proportion of operators that operate its fuel cycles with burnups in moderate regions. This difference is expected to remain also in the future. The experts are of the opinion that at least LWRs need to be grouped separately from PHWRs (CANDU or pressure vessel type) regarding problems, challenges and perspectives for burnup extensions and future trends, and this chapter is organised thus in this way.

But before treating these two groups of reactors separately, it is worth indicating some challenges that apply to all of them, namely transition cores and plant performance issues. The experts are of the opinion that individual high burnup issues need also to be considered in the frame of the transition cores needed to achieve the burnup target and in the frame of overall plant performance. When optimizing for higher burnup it is not possible to improve in every aspect because there are several constraints. Trade-offs between technical requirements, upper limits to enrichment, licensing limitations, uncertainties (depending on

the burnup value desired; behaviour of pellets) and customer requirements, etc. determine the extent of high burnup values that can be achieved. Impacts on existing reactor systems limit the extent to which higher burnup values can be achieved in operating reactors. In existing reactors, there are several constraints that must be met (i.e., existing licensing basis) and the fuel must be designed to meet these requirements. For future reactor designs, however, the capability of the reactors to utilize higher burnup fuels should be accommodated already by the design. There are also general challenges, reactor type independent, at organizational and regulatory level. Most of the utilities rely on fuel vendors for the development of licensing documentation. Nevertheless fuel vendors do not always satisfy the scope and depth of calculations and experiments required by foreign regulatory bodies. This is caused both by the fact that the scope and nature of documentation required differs between particular countries and by the fact that fuel vendors protect their know-how. Some of the utilities decrease the dependence on fuel vendors by performing or supporting independent research activities. This is a very cost-intensive alternative but frequently well balanced by benefits resulting from optimized fuel cycle costs. On the contrary there are cases when utility relying on fuel vendor and external Technical Support Organizations (TSOs) over a long period may loose the majority of its competences in fuel cycle optimization and licensing. Another type of problems that could arise during fuel type licensing is the unpredictability of licensing period duration Regulatory bodies usually come up with additional requirements during the licensing process. Equally utilities and NPPs have to comprehend the extent of impact that modification of fuel type can have on NPPs systems and related documentation. Proper analysis and correct preparation are necessary in order to estimate licensing process duration properly.

LIGHT WATER REACTORS

For LWRs burnups are approaching the regulatory limits assuming the 5% enrichment upper bound; economic advantages do not appear to be great in going beyond in enrichment or burnup (say, maximum assembly-average burnup of ~70 GWd/tU). Although several reactors are operating safely already at this relatively high burnup values, the meeting expert's panel sees a number of challenges at pellet, cladding and fuel assembly structure level, for design or beyond design accident conditions, as described below.

Pellet Behaviour: The formation of the HBS is possibly the most significant example of the restructuring processes affecting high burnup nuclear fuel in-pile. In commercial fuel the HBS forms at the relatively cold outer rim of the fuel pellet, where the local burnup is 2-3 times higher than the average pellet burnup, under the combined effect of irradiation and thermomechanical conditions determined by the power regime and the fuel rod configuration. The main features of the transformation are the subdivision of the original fuel grains into new sub-micron grains, the relocation of the fission gas into newly formed intergranular pores, and the absence of large concentrations of extended defects in the fuel matrix inside the subdivided grains. The qualification of the newly formed structure is a key requirement to ensure that high burnup fuel operates within the safety margins. The safe burnup extension can also be very different for different reactor types and higher burnup does not necessarily result in the formation of the HBS. The studies on the behaviour of the HBS should be aligned with the needs of the industry and it should be guaranteed not to overlook at artefacts or not well described operation/irradiation/PIE-tests conditions (e.g. fragmentation tests); for example, the status of research and development suggests today that the HBS at the pellet rim shows an appropriate thermal conductivity and even better mechanical properties to prevent detrimental interaction with the cladding. On the other hand, accident conditions still need to be investigated on very high burnup fuel to guarantee a good knowledge of the behaviour of such fuels. There is concern about rapid power ramps or LOCA conditions that could lead to

pellet swelling and fragmentation of the HBS (and of the rest of the pellet), which combined with cladding ballooning and burst, could lead to fuel relocation and dispersal. Further investigations are here envisaged.

Cladding Behaviour: A potential degradation of fuel performance due to extended burnup is the uniform corrosion of zirconium alloy claddings, depending on water chemistry parameters, which could lead to enhanced oxidation, hydrogen pickup, zirconium hydride precipitation, and thus to loss of ductility of the cladding. Dimensional changes in terms of diameter and length variation are also of concern, for extended fuel dwell. Increased fuel rod internal pressure, pellet-cladding interaction and pellet-cladding mechanical interaction effects need to be monitored carefully. Apart from the above-mentioned general issues there has been a particular safety-related issue discussed during the meeting. Recent Halden reactor project tests denoted as IFA-650 attracted attention of several regulatory bodies and required response of utilities. The tests pointed to a possible fuel fragmentation and fuel relocation phenomena that could have a strong impact on burnup values licensed by regulators if the test conditions are transferable to power reactor conditions.

Long-Term Dry Storage: Ageing of structural materials and casks / baskets is also being put under scrutiny. There are still many uncertainties that have not been finally bounded when transitioning to higher burnup values. Despite the availability of some solid experimental evidence, existing data may not be sufficient for definitive conclusions. In particular, once the higher burnup value is achieved a new challenge of dealing with the spent fuel in terms of transportability after long-term dry storage becomes a potential issue. The concern of possible degradation mechanisms such as creep and hydride reorientation must be addressed. This topic reflects here as well the discussions held during the 11th Meeting of the Technical Working Group on Nuclear Fuel Cycle Options and Spent Fuel Management on 5-7 June 2013 at IAEA headquarters in Vienna, in relation with the fundamental differences between the behaviour of fuel in wet and dry storage and further differences between dry storage systems. In the case of dry storage there does not appear to be enough data at the moment to support defining any limit on the duration of spent fuel storage.
[https://www.iaea.org/OurWork/ST/NE/NEFW/Technical-Areas/NFC/twgnfco-meeting-2013.html]

Experimental Data and Modelling: In order to refine the conclusions on the properties and their evolution during irradiation and post-irradiation, dedicated experiments and selected PIEs should be performed. This is especially the case for irradiation in accident conditions, typically RIA and LOCA. The data to be integrated in models/fuel performance codes (FPCs) should be carefully examined before concluding on specific behaviour.

PRESSURISED HEAVY WATER REACTORS

For CANDU- or pressure vessel-type heavy water reactors, the range of burnups is in absolute terms much smaller than LWRs high burnups and thus some challenges of LWRs such as HBS and heavy duty cladding utilisation is less of a concern. Also several possible degradation mechanisms during dry storage are less important or non-existent; decay heats and associated temperatures are much smaller, neutron source intensities virtually null and hydrogen pickup and cladding embrittlement less problematic. In this sense, the further extension of burnup for PHWRs is much more straightforward than in LWRs. Nevertheless, fuel designers, operators and regulatory bodies could benefit enormously from the LWR experience, when PHWR regimes begin to touch some of the well-known LWR phenomena or limits. It refers, for example, to the design of free-standing cladding for PHWRs, increase of fission gas release, pellet-cladding gap closure and mechanical interaction during normal operation, etc.

For achieving higher burnups, uranium mixtures and uranium-plutonium oxides could be used. Utilization of reprocessed uranium can allow PHWRs to achieve higher burnup values without the requirement for costly re-enrichment and additional poison loadings, and also have significantly lower front end fuel cycle costs. The 10 000 – 12 000 MWd/tU average burnup can be achieved in PHWRs by increasing the fissile content either by using SEU or MOX. This may require slight or no changes in the current design of the fuel rod. For achieving higher burn ups (~20 000 MWd/tU) free standing clad instead of collapsible clad, which is currently being used in PHWRs, may be needed. Mixtures of plutonium oxide in the form of MOX can also be carried out. This required few design changes such as use of free standing clad, provision of plenum space, end plug adaptation, etc. Current and other additives can be tried for achieving better results. Two stage sintering can be tried on boron-bearing UO_2. The two-stage sintering in achieving HBS looks very promising. Detail study of this technique would be useful in a production scale plant. Addition of other alloying elements in Zr – 1%Nb is being currently studied.

RECOMMENDATIONS FOR FUTURE WORK

It is clear that modification in fuel types and fuel cycle strategies will remain in constant change also in future. This is driven mainly by the motivation to reach lower operational costs through improved fuel economy and to maintain or improve safety margins. Operating fuels closer to their limits and implementing latest state of the art fuel types impose increased demand on licensing from the applicant as well as from the regulatory point of view.

At pellet level, investigations on the possible impact of the HBS under accident conditions during operation, and at normal and accident conditions during extended storage and transportation also in view of final disposal in a geologic repository, should continue to be addressed. It is thus recommended to continue with high burnup fuel experiments that would facilitate understanding of all related phenomena including fuel fragmentation and relocation in order to address these issues properly within the licensing process. Predictive capabilities of FPC for higher burnups have also been implemented since many years as well as the accuracy of the various models integrated in FPCs. However, a full description of the mechanisms leading to the formation of the HBS are not yet available and basic processes need to be further investigated by designed experiment combined with modelling. The HBS in fuel pellet is very important in retaining the fission gases. The inclusion of dopants, two-stage sintering and other low-temperature sintering processes could contribute to prevent a heterogeneous pellet structure or to minimize fission gas release during accidents. It is thus encouraged to develop FPCs further to accompany these industrial trends.

At cladding level, it is recommended to make the best synergy between the studies on the fuel and on the cladding, especially by analyzing the interface and the behaviour of the fuel in constraint conditions. One should also not neglect the evolution of the fuel during cooling before performing any PIE. To get more experimental evidence by PIE experiences to guarantee the transportability of very high burnup spent fuel following a long-term dry storage: creep, hydride reorientation, embrittlement, etc. Safety demonstrations to license the operation of high burnup fuel and a very solid experimental program are required. Underwater inspection and advance metrology techniques continue to be unavoidable tools for monitoring fuel assembly behaviour.

In order to refine the modelling at a multi-scale level, basic mechanisms (single effect studies) still need to be investigated and understood. The multi-scale approach formulating the basic mechanisms (*ab initio*) governing the phenomena observed at meso-scale, such as defects or dislocation behaviour, and finally responsible for the evolution of the fuel rod needs to be further developed. However, the time scale and the parallel between the

development of the basic experiments (e.g. ion implantation) and the modelling tools and data are not fully in-line with the needs of the industry to licence fuel with higher burnups today.

Finally, there is a strong recommendation from the expert's panel to continue and improve the collaboration and information exchange. Some of this is relatively straightforward, such as the SEU experience on increased burnup in Atucha I being translated to Atucha II in Argentina, and also to equivalent programs in other PHWRs. More challenging is the information exchange between different organizations and between member states, whereby the Agency plays already a significant role, so it is recommended to continue the series of Technical Meetings. It is recognized thereby that given the variety of core designs (PWR, BWR, VVER, and PHWR) the qualification of high burnup fuel management must be conducted for each of these separately. However, cross comparisons are necessary to enlarge the qualification database supporting the core and mechanistic fuel design codes. Cross calculations between LWR fuel designers and PHWR fuel designers should be beneficial as the operating conditions of these two fuels are widely different, although similar basic mechanisms are involved. It is also recommended in this sense to get direct contributions from relevant countries such as the USA, Germany and Japan, which unfortunately were absent during this meeting.

Another benefit could be reached by promoting harmonization and regulatory cooperation in the area of fuel types and fuel cycles licensing in order to minimize different approaches to licensing among particular countries particularly if operating similar technologies and fuel types. Even higher degree of standardization could be reached by development of standardized scope of licensing documentation for licensing higher burnups. A good example of this is the recently launched collaboration between the regulatory bodies of Brazil, the Netherlands, Sweden and Switzerland, based on a number of symmetries and similar conditions of their national nuclear industries. Such initiatives are welcomed and it is recommended to continue and strengthen them.

REFERENCES

[1] INTERNATIONAL ATOMIC ENERGY AGENCY, Technical and economic limits to fuel burnup extension, Proc. of a Technical Committee Meeting held in San Carlos de Bariloche, Argentina, 15-19 Nov. 1999, IAEA-TECDOC-1299, Vienna July 2002.

[2] INTERNATIONAL ATOMIC ENERGY AGENCY, High burnup fuel experience and economics, Working Material after a Technical Committee Meeting held in Sofia, Bulgaria, 26-28 September 2006.

[3] INTERNATIONAL ATOMIC ENERGY AGENCY, Fuel modelling at extended burnup, Report of the Co-ordinated Research Programme on Fuel Modelling at Extended Burnup-FUMEX, 1993-1996, IAEA-TECDOC-998, Vienna (1998).

[4] INTERNATIONAL ATOMIC ENERGY AGENCY, Fuel Moelling at Extended Burnup (FUMEX-II), Report of a Coordinated Research Project 2002-2007, IAEA-TECDOC-1687, Vienna (2012).

[5] INTERNATIONAL ATOMIC ENERGY AGENCY, Improvement of Computer Codes Used for Fuel Behaviour Simulation (FUMEX-III), Report of a Coordinated Research Project 2008-2012, IAEA-TECDOC-1697, Vienna (2013).

[6] INTERNATIONAL ATOMIC ENERGY AGENCY, IAEA Safety Standards, Storage of Spent Nuclear Fuel, Specific Safety Guide SSG-15, Vienna (2012).

[7] INTERNATIONAL ATOMIC ENERGY AGENCY, IAEA Safety Standards, Design of the Tractor Core for Nuclear Power Plants, Safety Guide No. NS-G-1.12 Vienna (2005).

[8] INTERNATIONAL ATOMIC ENERGY AGENCY, IAEA Safety Standards Series, Core Management and Fuel Handling for Nuclear Power Plants, Safety Guide No. NS-G-2.5 Vienna (2002).

[9] INTERNATIONAL ATOMIC ENERGY AGENCY, Development of computer models for fuel element behaviour in water reactors, Survey Report of a Coordinated Research Programme (D-COM), IAEA-TECDOC-418, Vienna (1987).

EXPERIMENTAL DATA AND MODELLING IN NORMAL AND ACCIDENT CONDITIONS

(SESSION 1)

Chairperson

T. Wiss

European Commission

PUSHING THE LIMITS OF THE SIMULATION OF NUCLEAR MATERIALS AND FUELS BY USING THE BACO CODE AND M³ (MULTISCALE MODELLING OF MATERIALS)

A.C. MARINO [a, b]

[a] Comisión Nacional de Energía Atómica (CNEA), Centro Atómico Bariloche (CAB)
[b] Universidad Nacional de Cuyo (UNCuyo), Instituto Balseiro (IB)
San Carlos de Bariloche, Río Negro, Argentina
marino@cab.cnea.gov.ar

Abstract. The BaCo code was developed to simulate the nuclear fuel rods behaviour under irradiation. BaCo has good compatibility with PHWR, PWR, VVER, among others type of fuels (commercial, experimental or prototypes). The code includes additional extensions for 3D calculations, statistical analysis, fuel design, a full core analysis and accident conditions –at work–. Research on new fuels and cladding materials properties based on *ab initio* and multiscale modelling of materials (M³) are currently under development to be included in the BaCo code modelling. Examples of the code by using the cases of the CRP FUMEX of IAEA, new fuel conditions, such as fuel burnup extension, dry storage and an approach of new materials, and an overview of our present results of M³ will be presented.

1. INTRODUCTION

The BaCo code ('Barra Combustible', Spanish expression for 'fuel rod') was developed at the end of the 70´s in CNEA (Atomic Energy National Commission of Argentina) with the purpose of studying the fuel rod behaviour under irradiation conditions [1, 2] and during storage conditions [3, 4, 5]. BaCo gave the modelling support for the design of advanced PHWR (CNEA-MOX [6] fuels CARA fuel [7]) and innovative PWR fuels (as the fuel for the CAREM reactor [8]). The confidence in the results regarding the description of the fuel behaviour under irradiation enables the inclusion of the BaCo code in several international fuel code comparison programs as D-COM [9], CRP FUMEX I [10], II [11] and III. Although the development of BaCo was focused on PHWR fuels, as CANDU [12] and Atucha ones [13], the code holds a full compatibility with commercial –as PWR, BWR, and VVER [14]–, advanced, experimental, prototypes and/or unusual fuels (as for example uranium nitride and carbide at least for illustrative and comparative purpose).

The BaCo code includes additional tools as the software package for finite elements 3D calculations [15] and the statistical analysis for advanced fuel designs by taking into account the as fabricated fuel rod parameters and their statistical uncertainties [16]. BaCo allows the calculation of a complete set of irradiations as for example the calculation of a full reactor core [13]. It is of crucial importance nowadays to develop a better experimental and theoretical knowledge of the processes related with the evolution of defects and the accumulation of fission products for modelling the fuel behaviour under different operating conditions and the evolution of a spent fuel over long period of time. The current experimental database could be enough to support empirical correlations and modelling for current fuels [17]. Nevertheless, new approaches are required if the actual fuel computer codes will be used to simulate new materials and extreme situations as ultra-high burnup. The unavailable data needed for new fuels development will be obtained through a multiscale modelling (M^3), a methodology that will provide the theoretical approach to model the properties of materials through *ab initio*, molecular dynamics, kinetic Monte Carlo and finite elements calculations over the relevant length and time scales of each method [18].

2. THE BACO CODE

2.1. Main assumptions of the code

BaCo assumes azimuthal bi-dimensional symmetry in cylindrical coordinates for the fuel rod [1]. Although angular coordinates are not considered explicitly, angular dependent phenomenon, as well as radial cracking, are simulated through the angular averaging method [19]. Also axial pellet cracking and relocation are included in BaCo. The hypotheses of axial symmetry and modified plane strains (constant axial strain) are used in the numerical modelling. The fuel rod is separated in axial sections in order to simulate its axial power profile dependence. Rod performance is numerically simulated using finite time steps (finite differential scheme). The modular structure of the code allows the description of phenomena observed in the UO_2 pellet and the Zry cladding behaviour. The current version of BaCo can be applied to any geometrical dimensions of cylindrical fuel rods mainly with UO_2 pellets (either compact or hollow, with or without dishing) and Zry cladding. However, the code allows us to calculate fuel rods with other materials for the pellets and the cladding as metallic uranium, uranium carbide, uranium nitride (for pellets) and silicium carbide (for cladding), at least for illustrative and comparative purpose, due to the simplicity of the modelling included in BaCo of those materials.

2.2. Advanced Features of BaCo

BaCo 3D tools [15], parametric analysis [16], statistical analysis [16], full core calculations [13] and graphical data post processing improve the code performance and the analysis of the calculations [2].

2.2.1. 3D extensions

Although the BaCo code uses a quasi bidimensional approach, the use of several three dimensional (3D) finite element features allow a complementary analysis of 3D properties, as for example the stress-strain state at a specific period of time during the irradiation [15].

The BaCo code results were enhanced by using ‘ad hoc’ tools developed at the MECOM and SiM³ Divisions (Bariloche Atomic Centre, CNEA) [20]. The temperature profile, the crack pattern and the boundary conditions (as the inner pressure, pellet stack weight, etc.), among others, are calculated with BaCo as the input data to the 3D stress-strain state and the average deformations of the UO_2 pellet.

The analysis of the radial fuel pellet deformation is presented as an example of the 3D BaCo extensions. The Figure 1 includes the finite element mesh (with radial cracks), used for the calculation, and the 3D stress-strain state represented with the radial deformations, hoop stress and von Misses equivalent stress. We find a stress release close to the ridge position due to the presence of the cracks and a similar situation due to the central hole. The Figure 2 shows a comparison between a VVER flat pellet and a pellet with a central hole. The second plot of the Figure 2 shows a comparison between two pellets with and without a central hole; here fuel cracks are included in the calculation. We observe that the central hole reduces the radial deformations and the ridging at the fuel pellet. A preliminary conclusion of this analysis is that pellets with central hole are more conservative that a solid one.

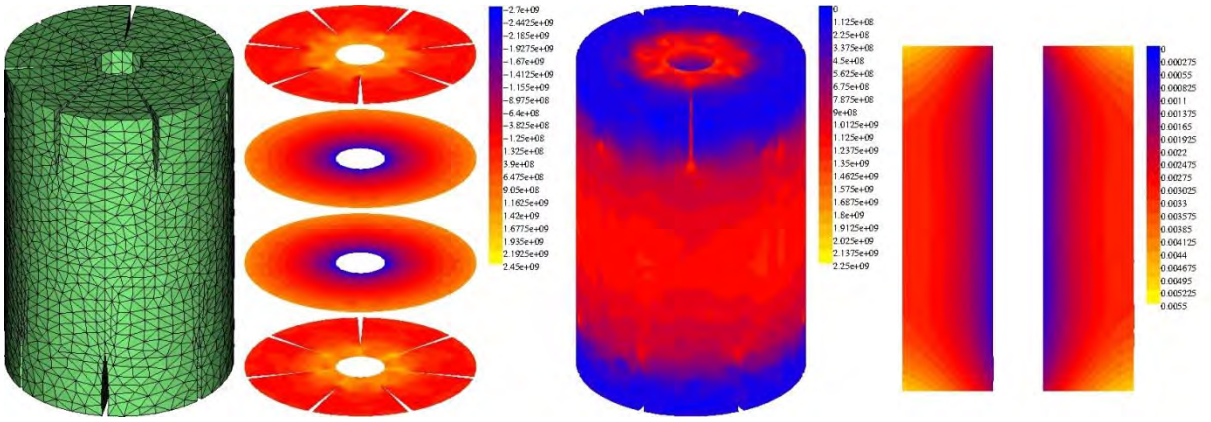

FIG. 1. 3D mesh of a VVER pellet (with the central hole and 7 radial cracks), hoop tress (tangential stresses), von Misses equivalent stresses and radial deformations as it was calculated with the 3D BaCo tools.

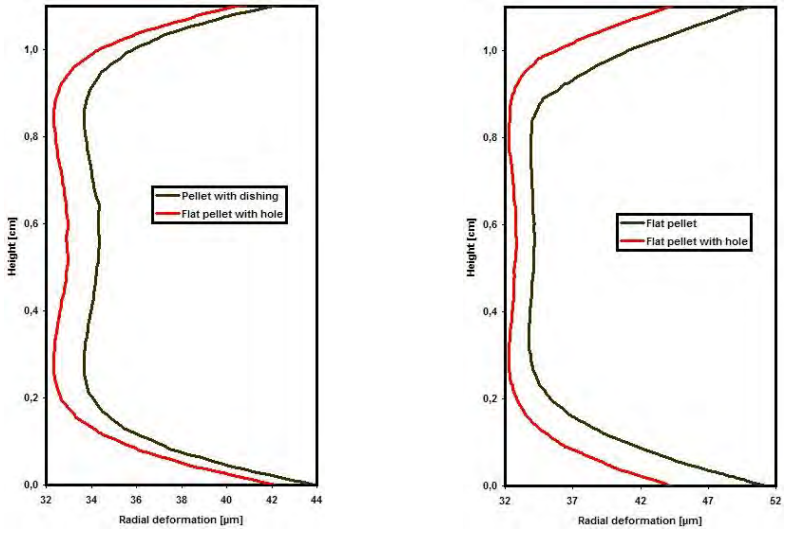

FIG. 2. Radial deformation of a VVER pellet. On the left: a comparison of the use of a pellet with a dishing and a flat pellet with a central hole. On the right: a flat pellet compared with a similar pellet with a central hole by using a mesh with seven radial cracks.

We properly define BaCo as a quasi bidimensional code. However, the inclusions of the axial power profile, the 3D extension and the original treatment of the pellet cracks, could allow us to present BaCo as a quasi 3D code. In particular because there are self-defined 3D codes typically use simetry of revolution, a reduced rod length, no axial power profile and/or axially and radially distributed cracks. BaCo keeps its definition of a quasi bidimensional code.

2.2.2. Parametric analyses

The 'parametric analysis' is the study of the individual influence of each fuel rod parameter in the fuel rod behaviour (temperatures, stresses, deformations, pressures, etc.). With this analysis we find the correct weight of each fuel rod parameter in order to understand the fuel behaviour with a far and wide scope. This technique is the second step in order to tune the as fabricated tolerances with an engineering overview especially when we are designing fuel elements [2].

This BaCo tool can be extended to the parameters of the models of behaviour included in the code. Then we can analyze the relative influence of each individual model and its parameters in the full behaviour of the fuel rod.

2.2.3. Statistical improvements

For a better understanding of the uncertainties and their consequences, the mechanistic approach must therefore be enhanced by the statistical analysis [16]. BaCo includes a probability analysis within their code structure covering uncertainties in fuel rod parameters, in the code parameters and/or into the fuel modelling taking into account their statistical distribution. As consequence, the influence of some typical fabrication parameters on the fuel cycles performance can be analyzed. It can also be applied in safety analyses and economics evaluation to define the operation conditions and to assess further developments. These tools are particularly valuable for the design of nuclear fuel elements since BaCo allows the calculation of a complete set of irradiations.

Figure 3 presents the result of the probabilistic analysis for the pellet center temperature. There is a temperature band with less than 200°C of uncertainty after reshuffling. This band does not represent a big change in pellet grain morphology and the pattern of cracks. In fact we find two bands, an upper wide band without pellet cladding contact and a narrow band at the bottom of the calculated curves where pellet cladding contact is present. The difference in the width of the bands is due to the uncertainty in the gap size (and the corresponding uncertainty in the gap conductance). Points disappear from the upper band when burnup increases and PCI is done, then the curve jump to the narrow bottom band and the uncertainty in gap conductance is at a minimum.

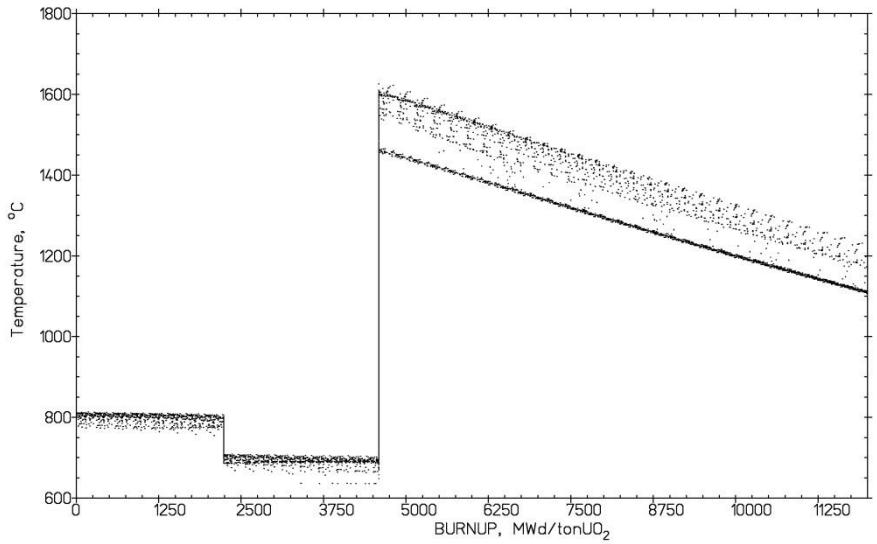

FIG. 3. Pellet center temperature results from the BaCo code probabilistic analysis of a SEU fuel rod of Atucha I (Slightly Enrichment Uranium).

Figure 4 shows the hoop stress (tangential stress at the inner surface of the cladding) of probably the most demanding fuel of the CAREM reactor [8]. The plot is including:

- The BaCo code calculation by using the standard values of the fuel;
- The calculation by using a combination of the fuel parameters which produces the maximum temperature in the fuel (obtained by the estimation of the maximum gap between pellet and cladding compatible with the as fabricated tolerances);

- The calculation by using a combination of the fuel parameters which produces the maximum hoop stress in the cladding (obtained by the estimation of the minimum gap between pellet and cladding compatible with the as fabricated tolerances);
- The statistical calculation (in the background of the plot) showing the statistical dispersion by taking into account a big set of calculation using random, and realistic, fuel parameters as BaCo input data compatible with the as fabricated tolerances.

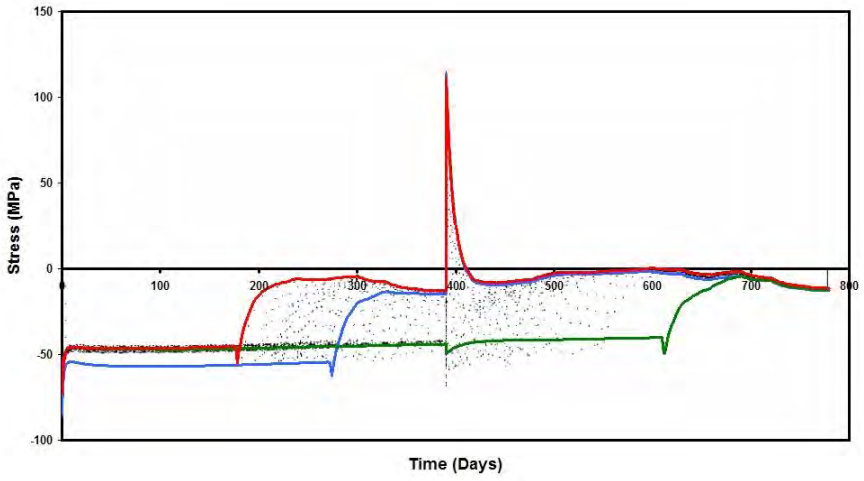

FIG. 4. Hoop stress analysis of the most demanding fuel rod segment of the CAREM fuel. It is included the standard calculation (blue curve), the 'maximum temperature' situation (green curve) and the 'maximum hoop stress' situation (red curve).

The obtained results showed a conservative design due to that the maximum stress is under the defined value for a failure in this fuel rod.

2.2.4. Full core calculation

BaCo allows the calculation of a complete set of irradiations of the same fuel design and the calculation of a complete core. We illustrate the performance analysis with the study of the first SEU core of the Atucha I NPP [13]. Using the detailed power history of all fuel elements, BaCo was used to calculate fuel behaviour indicators, like stresses, temperatures, dimensions, pressures and gases releases. Figure 5 presents the maximum hoop stress reached at the inner surface of the cladding for each fuel rod during each individual irradiation. The average hoop stress values increase slightly with burnup and change from ~60 to ~40 MPa depending on burnup. All the fuel rods are well below the σ_{scc} value to produce a failure due to PCI-SCC (σ_{scc} = 170 MPa) [21]. Stress reversal was found just in one fuel rod. The rest of the rods are under compression during the irradiation. Figure 6 includes de maximum temperatures. All the fuel presents a maximum temperature below ~1900°C with an average value of 1700ºC which decreases with burnup. We could expect columnar grains at the pellet center of the fuel and for a few pellets a small hole. The values are acceptable for Atucha fuel, because it has a relative thick pellet as compared with other self standing rods like present PWR and BWR.

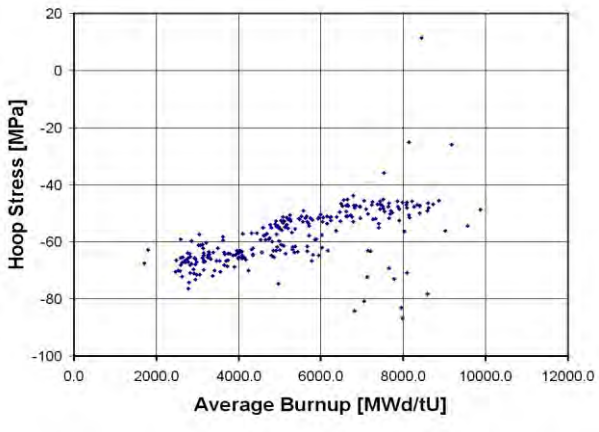

FIG. 5. Maximum hoop stress at the inner surface of the cladding calculated for each fuel of the first SEU core of the Atucha 1 NPP.

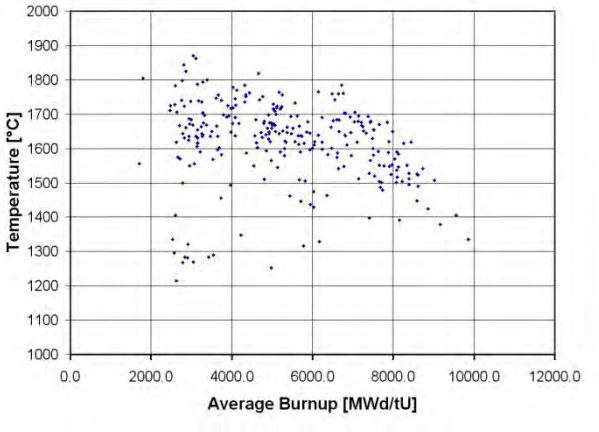

FIG. 6. Maximum pellet center temperature calculated with BaCo for each fuel of the first SEU core of the Atucha 1 NPP.

2.2.5. Accidental conditions with BaCo –at work–

At the 80's it was developed a set of BaCo expansions in order to simulate the thermal phenomena taking place in a nuclear fuel rod. In particular the transients characterized for high thermal gradients or fast temporal changes in the power generation or at the boundary conditions. Phase changes may occur in the materials as a consequence of this evolution. Those phenomena take place during accident conditions [22].

In case such accidents involving fuel material melting, the thermal process is transformed into a heat transport phenomenon with a change of phase of the first order with absorbing of energy. This problem, known as Stefan problem, in the case of a nuclear fuel has the particularity of the existence of internal heat sources and high latent heat of the material.

A set of tools were developed in order to solve the thermal transients (program TRANS), to solve the thermal transients with phase change and melting of the fuel and to model the UO_2 melting under irradiation taking into account the nuclear fissions, the behaviour of the fission fragments and the statistical theory of percolation (program MSA). Figure 7 shows the radial temperature of a UO_2 pellet at different time steps during a high and fast power increment as it was calculated with MSA plus BaCo [22]. The increase is compatible with a severe accident and it is included the liquid phase in the figure.

Currently we are reissuing these programs in order to properly adapt it to the current version of BaCo.

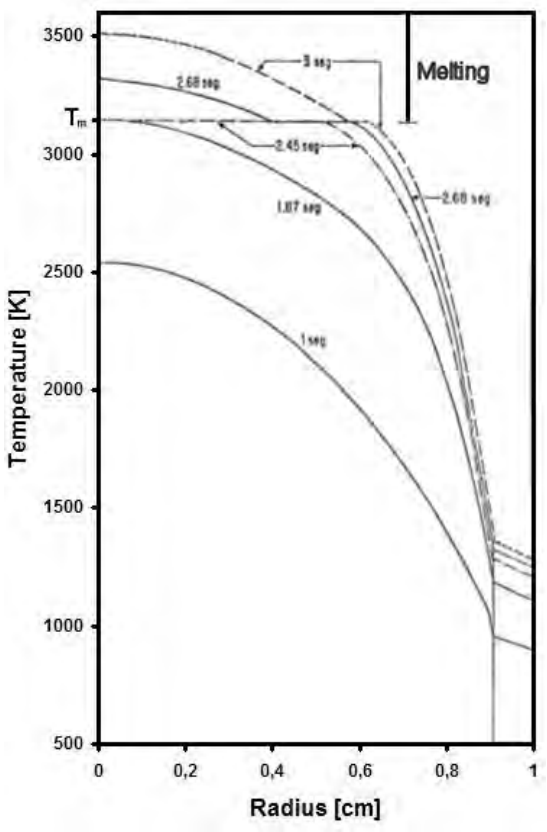

FIG. 7. Pellet radial temperatures at different time steps including the liquid phase [22].

2.3. Advanced Applications of the BaCo code

In order to illustrate the use of the BaCo code with advanced applications we will present a few appointments about our participation in the series of CRP FUMEX of the IAEA, the simulation of the dry storage of spent fuels, the intention to simulate new materials for pellets and cladding and the intention to couple BaCo with M³ tools in order to obtain a sustainable database of physical parameters of the materials of the fuel elements.

2.3.1. CRP FUMEX

The confidence in the BaCo code results regarding the description of the fuel behaviour under irradiation enables the inclusion of the BaCo code in several international fuel code comparison programs as D-COM [9], CRP FUMEX I [10], II [11] and III.

The first edition (1993-1996) of the CRP FUMEX (Coordinate Research Project on Fuel Modelling at Extended Burnup) of the IAEA (International Atomic Energy Agency) was originally focussed on thermal and mechanical calculations; finally the thermal affairs were mainly assessed. Several blind tests by using experimental data were provided for the OECD HRP (Halden Reactor Project) [10]. Figure 8 shows the FGR (Fission Gas Release) at EOL End of Life), main result of the case 1. Figure 9 include the gas pressure calculated with BaCo and the experimental data at specific shutdowns. We obtain an excellent agreement between calculation and experimental data for both cases.

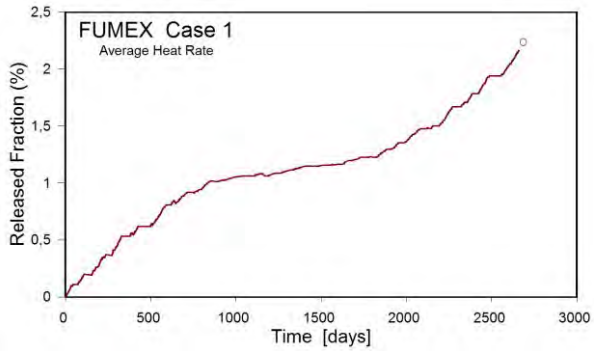

FIG. 8. BaCo calculation for Fraction of FGR, case 1 of CRP FUMEX I. The experimental result at EOL (End of Life) was FGR = 1.8 %.

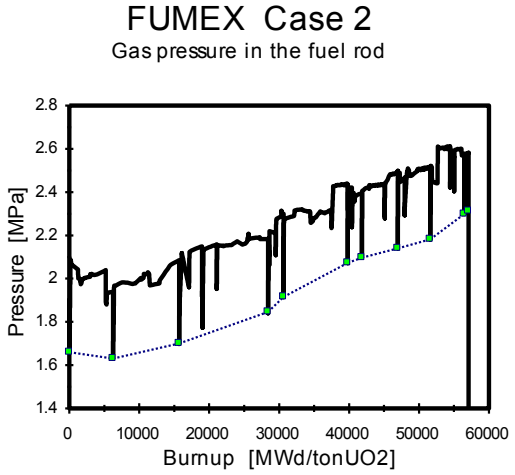

FIG. 9. Pressure in the rod vs. burnup for case 2. The experimental data are the squared dots at the shutdowns.

CRP FUMEX II (2001-2006) was mainly devoted to FGR modelling. One of the most demanding simulations was the case 15. The Risø National Laboratory in Denmark has carried out programs of slow ramp and hold tests, the good agreement between the BaCo calculation with the experimental data is presented in Figure 10. Figure 11 shows an idealized and realistic representation of ultra high burnup experiment provided for AREVA. We obtain good results in the range of the realist fuels without major changes in the fuel models of the BaCo code.

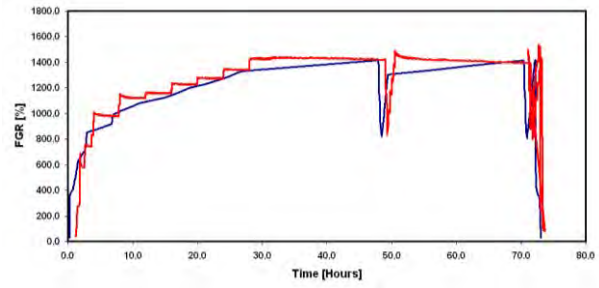

FIG. 10. Pellet centreline data and calculation during the bump test. Case 15 of CRP FUMEX II.

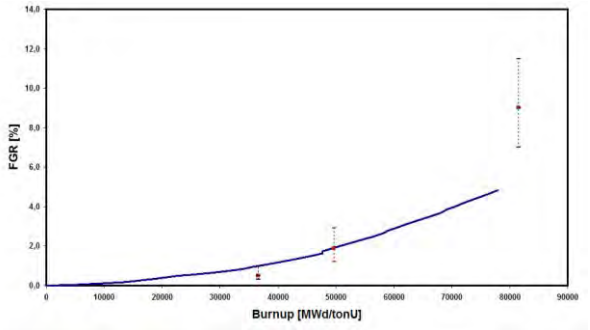

FIG. 11. BaCo code calculation of FGR (idealized case provided by AREVA).

Case 27-a of CRP FUMEX II was a computational experiment to study the effects of linear rating on FGR by comparing the differences between codes via parametric studies. We are pushing the limits of the codes with this simulation due to the ultra high burnup at EOL of this CANDU fuel. Those fuels have not plenum and they can not accommodate the FGR. Due to that reason and the high power (and fuel temperature) we obtained high levels of inner gas pressure not compatible with the integrity of the fuel rod (see Figure 12). They were presented similar situations of overpressure for the others participants of the CRP who presents their results.

A complement of the CRP FUMEX II was carried out with PHWR experimental data produced for BARC, India [23, 24]. Figure 13 shows the calculations of all the participants of these exercises where a great dispersion was found. It was clear the need of an improvement in the modelling of PHWR fuels at high power.

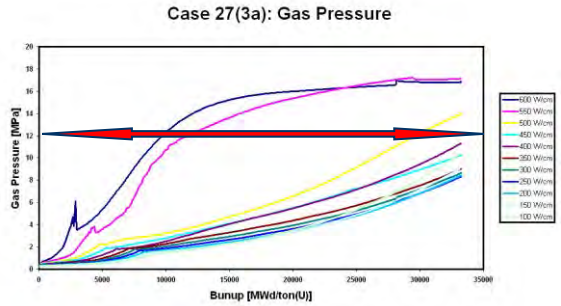

FIG. 12. Internal gas pressure (BaCo, CNEA, Argentina). Coolant pressure as reference. A PHWR case of CRP FUMEX II.

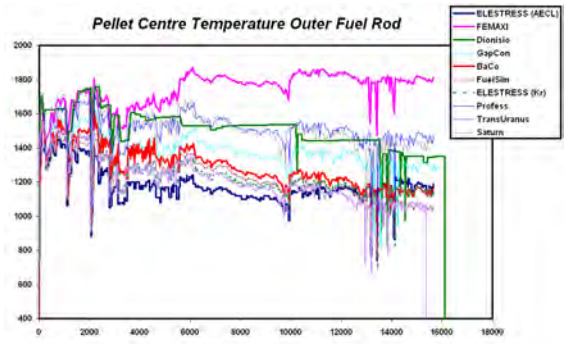

FIG. 13. Code calculations of the pellet center temperature of an outer fuel rod of the PHWR bundle K1-56504 of BARC, India.

Figure 14 includes the BaCo calculation of the pellet center temperature of an outer fuel rod of the AECL-JC-Bundle at three axial segments It was included the Vitanza threshold in order to take a first approach to FGR [23]. The calculation of the expected behaviour at dry storage conditions will presented below.

Figure 15 show the statistical dispersion of the hoop stress of a MOX fuel experiment provided for CNEA at the IFPE and selected as a mandatory case of the CRP FUMEX III [6]. We obtain a top value over the threshold for a PCI-SCC failure [21]. These calculations were performed previous to the experiment due to the fact that BaCo was used in order to define the parameters of this experiment and as a frame to analyse the PIE [6].

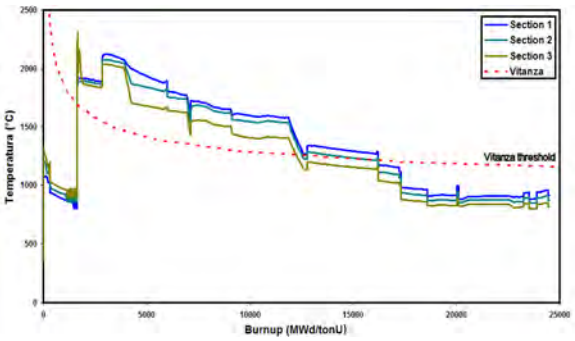

FIG. 14. Fuel pellet center temperature. Outer fuel rod of the Bundle AECL-JC.
A PHWR case of CRP FUMEX III

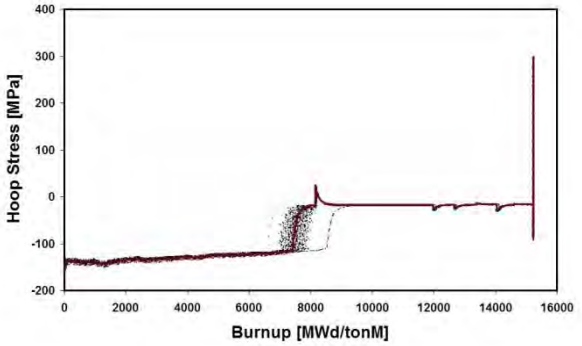

FIG. 15. Hoop stress (including a sensibility analysis) of the CNEA-MOX-RAMP case (CRP FUMEX III).

2.3.2. Fuel behaviour under dry storage conditions

It is usually accepted that the fuel element must not fail during the operation of the power plant. However, the fuel integrity must also be kept during the intermediate storage at pools and/or silos. The simulation of the fuel behaviour under dry storage conditions can be calculated by using BaCo as an extension of the normal application of the analysis of nuclear fuel elements under irradiation. The safe conditions of storage, in particular the temperature of the dry storage system [25], can be analyzed and the results are briefly presented here [3-5].

We simulate that condition with BaCo by using an extension of the normal power history under irradiation. We continue the calculation after end of life (EOL) with new boundary conditions (in particular the pressure and the temperature of the dry system of storage) and without an inner source of heat in the pellet (zero power and burnup). The calculation is

strongly simplified and the behaviour will just present small variations but with a widest time scale. Figure 16 includes de FGR (Fission gas release) against burnup with those conditions for an advanced CANDU fuel included as an exercise of code comparison in the CRP FUMEX III of the IAEA. The peak at EOL represents the FGR for ~10 years of storage in dry conditions (in this case with a temperature of 300°C). There is an increment of the FGR due to the thermal condition of storage. Figure 17 is the same of the previous one but against the time. FGR increases continuously in time due to a process thermally activated as it was found in Ref. [25] by using the semi empirical FGR model included in BaCo [1, 2].

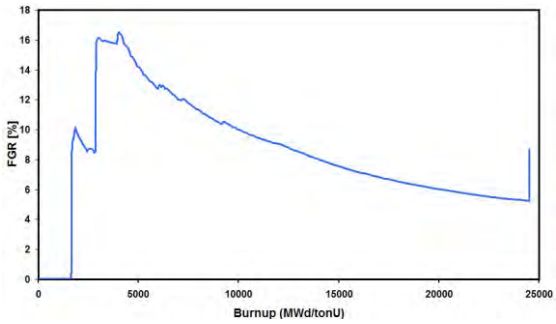

FIG. 16. FGR during irradiation and dry storage conditions vs. average burnup. The FGR at EOL (End Of Life) is ~6%, the final peak is the release (~10%) during dry storage at 300ºC (without irradiation conditions –no burnup-).

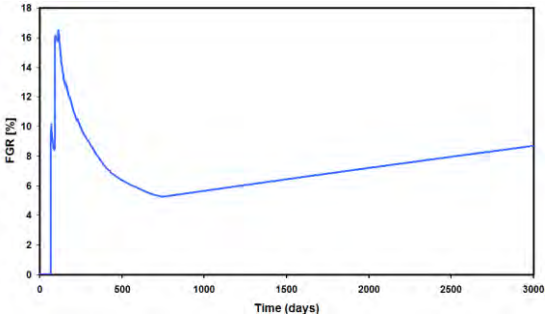

FIG. 17. The plot of the Fig. 1 but vs. time. FGR is due to a process thermally activated. Temperature of storage 300°C.

Figures 18 and 19 shows a stress analysis of two different PHWR fuels during the operation and during the dry storage. We found that there is a small increment of stresses and gas pressure into the fuel rod due to a small fission gas release thermally activated in the presence of the corrosive elements or compounds as I, Cs, CsI, etc, due to the accumulated burnup [21]. A stress corrosion cracking (SCC) failure could be achieved in the fuel due to the accumulated damage of the cladding during irradiation and the small but constant increment of FGR [3, 4, 5, 25]. The result of the statistical analysis of BaCo indicates that the integrity of the fuel is determined by the manufacture tolerances and mainly the solicitations during the NPP irradiation. The main conclusion of the present study is that the fuel temperature of the device should be carefully controlled in order to ensure safe storage conditions.

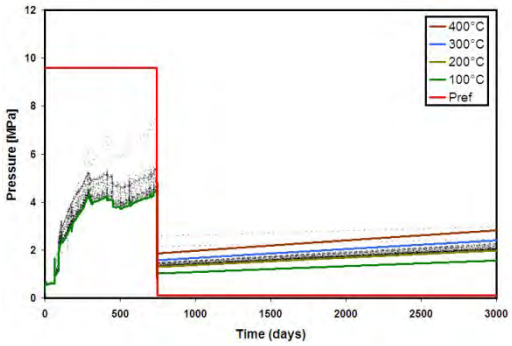

FIG. 18. Inner pressure of the fuel rod due to the free gases of an experimental CANDU fuel (one of the CRP FUMEX III cases). The red curve is the pressure outside of the cladding (the pressure of the coolant during irradiation and the ambient pressure -1 atm- during storage). The coloured curves are the parametric analysis by changing the temperature of the dry storage device (from 100°C to 400°C). The plot includes the statistical analysis of the inner pressure of the fuel rod due to a storage temperature of 300°C (cyan line in the plot).

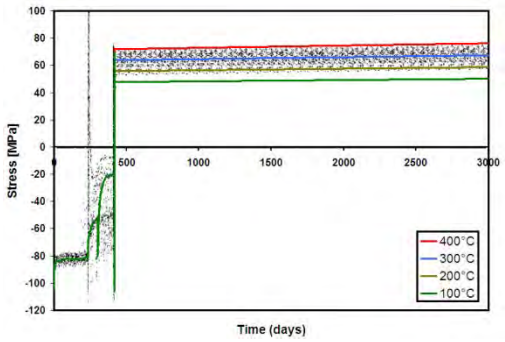

FIG. 19. Hoop stress of the Atucha I fuel during irradiation (mainly the cladding is under a compression state of stresses) and during the dry storage at four different temperatures for the storage (where the cladding is under a tensile state). The plot includes the statistical analysis of the hoop stress with a temperature of the storage device of 300°C (cyan line in the plot).

2.3.3. New materials for new fuels with BaCo

The symmetry of revolution adopted for the fuel rod and the modular structure of the code allows us to include new materials for the fuel pellet, the cladding and/or the filling gases by taking into account the requirements of the new reactors defined in the Generation IV initiative [26]. Two examples of the use of BaCo are presented as an approach of the behaviour of SiC claddings, Figure 20 includes a comparison of the evolution of the UO_2 pellet radius by using a Zry-4 and SiC claddings in PWR conditions. The difference of behaviour is due to that Zry is a metallic alloy and SiC is a ceramic. Figure 21 shows the temperature radial profile by using different materials for the pellets (metallic U, Uranium Carbide, Uranium Nitride and UO_2). It is clearly shown the strong reduction of the fuel temperature when a material with a good thermal conductivity is used. The previous results highlight that the BaCo code is ready to be applied to Generation IV reactors where that geometrical condition of the fuel is included for these materials or another ones under development.

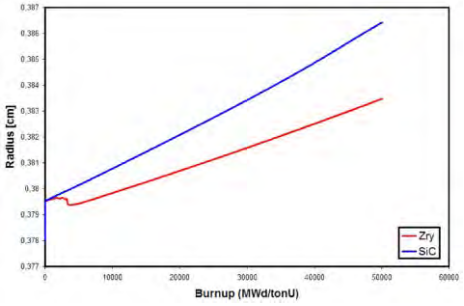

FIG. 20. Pellet radius evolution of two fuel rods with Zry-4 and SiC cladding irradiated in PWR conditions and at constant power.

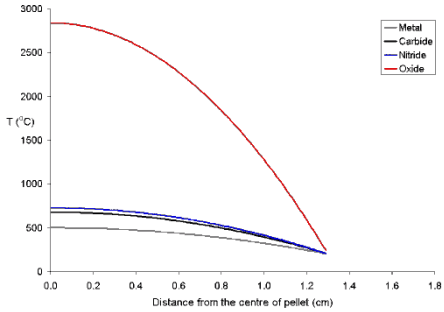

FIG. 21. Fuel pellet center temperature of a 26 mm diameter CANDU pellet with a power density of 250 W per cubic meter.

3. TOWARDS THE M³ OF NUCLEAR FUEL MATERIALS FOR GENERATION IV REACTORS

There has been a considerable interest in actinide nitrides and carbides during the last years due to the Generation IV reactor initiative. The current experimental database could be enough to support empirical correlations and modelling for current fuels. However, the development of new theoretical approaches are required if the fuel computer codes available nowadays will be used to simulate new materials and extreme situations in future research

programs. The Multiscale Modelling of Materials (MMM or M³) allows the study of complex phenomena as the behaviour of new fuels and cladding materials and could provide a theoretical methodology to obtain the required information. The M³ methodology is based on the electronic structure calculations through *ab initio* codes followed by the development of effective or model potentials to be used in molecular dynamics and kinetic Monte Carlo codes. However, molecular dynamics simulations require an intensive use of powerful computers and therefore the interatomic potentials to be used must be computationally efficient as well as physically appropriate for the description of the properties of the fuels and cladding materials to be used in the Generation IV reactors. Although there are several possibilities for developing an interatomic potential, by fitting the parameters to experimental or theoretical data, the approach followed in this research is different. Mainly, it is an attempt to compute the physical and thermal properties through a parameter-free pairwise potential computed from the first principles calculations of the cohesive energy coupled to the Chen-Mobius lattice inversion method [27, 28]. Pure Th, in the *fcc* (faced centred cubic) structure, was used in this work as a test element to check the accuracy of this methodology to describe their thermal and elastic properties. In doing so, this study focuses on the ability of a parameter-free pairwise potential to maximize the information by examining the accuracy of predicted properties against both *ab initio* and experimental results. It will be shown that it is possible to describe with a high accuracy the behaviour with temperature of the *fcc* Th properties without using molecular dynamic or *ab initio* phonon calculations.

The cohesive energy was obtained from the full potential LAPW method as it is implemented in the WIEN2k code [29, 30]. The energy curve of *fcc* Th thus obtained was fitted with the equation of state (EOS) of Birch-Murnaghan to obtain the lattice parameter, equilibrium volume *Vo*, the bulk modulus *Bo* and its derivative *Bo`*. The temperature effects on *fcc* Th properties can be computed by using the pair potential combined with the quasiharmonic approximation [31]. Based on the computed elastic constant and by applying the quasi-harmonic approximation, it is possible to study the thermodynamic properties of Th such as thermal expansion coefficient, Grüneisen parameters, and Debye temperature. The calculated lattice parameter, bulk modulus, elastic constants at T=0 K and related magnitudes are summarized in Table 1. They are compared with experimental data and previous theoretical results computed from *ab initio* phonon calculations.

TABLE 1. PHYSICAL AND THERMAL PROPERTIES OF *fcc* TH

	a [Å^3/at]	Bo [GPa]	*Bo`*	C_{11} [GPa]	C_{12} [GPa]	C_{44} [GPa]	θ_D [K]
Experiments							
Armstrong [32]	32.95	58		78	48.2	51.3	
Greinier [33]	32.88	60.37		80.79	50.16	50.31	
Vohra [34]	32.88	54/55/	3.0/3.8/4.				
Evans[35]	32.66	59	1				
Bellusi[36]							
Lawson[37]		58	4.2				163 ± 3
ab initio results							
FP-LMTO[38, 39]	29.6	63		55.3	35.3	45.9	
ABINIT [40, 41]	31.7	56		86	39.5	58.4	
WIEN2k [42]	32.43	57.11	3.05	75.6	40.87	52.76	
model potential [43]		67.5		78.3	62.2	39.9	
phonon T = 300K [44]	32.43	50.01	4.08	81.4	40.73	49.47	
WIEN2k (this work) free-parameter	32.31	57.1		82.0	40.7	56.5	

	a [Å^3/at]	Bo [GPa]	*Bo`*	C_{11} [GPa]	C_{12} [GPa]	C_{44} [GPa]	θ_D [K]
potential (this work, [45])	32.77	54.6	3.6	75.6	44	44	161.7

***a**: lattice parameter, **Bo**: bulk modulus, **Bo`**: bulk modulus derivative, C_{11}, C_{12} and C_{44}: lattice constants, and θ_D: Debye temperature.*

It is important to remark here that the behaviour of the elastic constant versus temperature is one of the most relevant and difficult set of properties to be described accurately by any interatomic potential or *ab initio* method. Their calculations require the resolution of small energy shifts that arise when the lattice is slightly distorted by applying different strains. Previous theoretical results show an average error around 8% in Th compared to experiment. The elastic constant obtained in this work are in well agreement with the expected results obtained from a pair potential with an error of 0.3% and 8% for the elastic constants C_{11} and C_{12}, respectively. The errors are similar or less than previous theoretical results based on *ab initio* phonon calculations, as shown in Table 1.

The methodology under current development [45] has proven to be very useful also in the determination of the volume dependence of the free energy at a given temperature and the description of the temperature and pressure effects on the Th properties. It is shown that the parameter-free pair potential presented in this work describes the structural properties of *fcc* Th, as volume vs. pressure and lattice parameter vs T with accuracy comparable to *ab initio* phonon calculations. Figures 22 and 23 show these results. Figure 24 compares the theoretical results of this work for the behaviour of the C_{11} and C_{12} elastic constants and Poisson's ratio versus temperature with previous *ab initio* methods and experimental data.

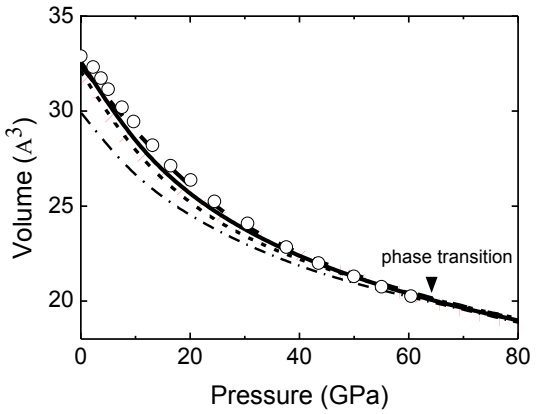

FIG. 22. Volume vs. pressure equation of state for fcc Th. The experimental result of [46] (open circles) are compared with ab initio phonon calculations [40] (short-dashed line) and [44] (red full circles), the FP-LMTO calculation [38] (dot-dashed line), the ab initio plus mean field potential approach [47] (dashed line) and the results of this work (solid line).

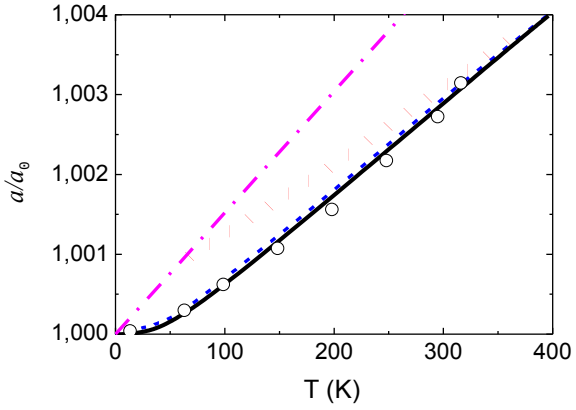

FIG. 23. Reduced lattice constants a(T)/a(0) versus temperature for fcc Th. The experimental results of Armstrong et al [32] (red full circles) and Lawson et al [37] (open circles) are compared with the ab initio phonon calculations [44] (dashed line), ab initio plus Debye model [48] (dot-dashed line) and this work (solid line).

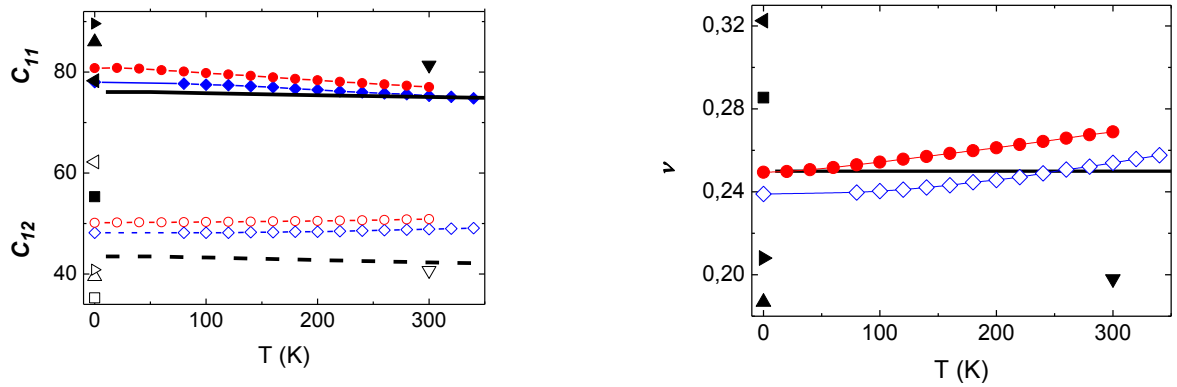

a) *b)*

FIG. 24. a) Elastic constants C_{11} *(full symbols) and* C_{12} *(open symbols) (in GPA) versus temperature (in K); b) Poisson's ratio* ν *versus temperature. The experimental values are from Armstrong et al [32] (diamond) and Greiner et al [33] (circles). The theoretical calculations are from the ab initio phonon calculation of Refs. [40] (up triangle) and [44] (down triangle), the ab initio results of Refs. [38] (square), [42] (right triangle) and [43] (left triangle), and the free energy approach of this work (solid and dashes lines for* C_{11} *and* C_{12}*, respectively. Solid lines for Poisson's ratio).*

The methodology under current development [45] has proven to be very useful also in the determination of the volume dependence of the free energy at a given temperature and the description of the temperature and pressure effects on the Th properties. It is shown that the parameter-free pair potential presented in this work describes the structural properties of *fcc* Th, as volume vs. pressure and lattice parameter vs T with accuracy comparable to *ab initio* phonon calculations. Figures 22 and 23 show these results. Figure 24 compares the theoretical results of this work for the behaviour of the C_{11} and C_{12} elastic constants and Poisson's ratio versus temperature with previous *ab initio* methods and experimental data.

It is noteworthy the agreement between the result of this work with the experimental and previous theoretical ones based on phonon calculations. The results presented here highlight the point that although the thermodynamics properties like lattice parameter vs. T and pressure EOS are accurately described, it is needed to compute the elastic properties with more precision and less dispersion between the theoretical methods, as it is shown in Figure 24. The next step in our research will be to build an n-body free-parameter potential suitable to be used in molecular dynamic calculations in order to predict the microstructure evolution and atomic site redistribution in *fcc* Th and multicomponent Th-based nuclear fuel.

4. CONCLUSIONS

The modular structure of BaCo allows the inclusion of new models and material properties. Taking into account this advantage, this work presents an overview of the BaCo code capabilities by using the cases of the CRPs FUMEX of IAEA, the analysis of the fuel behaviour under dry storage conditions and the use of new materials, as SiC, for the fuel cladding and advanced nuclear fuel materials for the pellets, as UN and UC. The condition to start these analyses is to keep the symmetry of revolution of the fuel. But, new approaches are required if the actual fuel computer codes will be used to simulate new materials and extreme situations in future research programs. Those needs could be covered by using M³ in order to extend the field of application of the modelling and the code. Actinides nitride and carbide represent examples of the limitation found in the research of new fuel and materials due to the limited available experimental information. The results presented in this work suggests that modelling has reached the point where effective and practical answers can be obtained, becoming a source of experimental information to current relevant problems in Generation IV

framework. This work highlight that BaCo is ready to be applied to Generation IV reactors, if the fuel has symmetry of revolution. *Ab initio* and M³ can enhance the field of application of the code by including a strong physical basement covering the unavailable data needed for those improvements.

We emphasized the use of the codes for the simulation of the behaviour of nuclear materials and fuels in order to promote the concept of modelling support for nuclear fuel design and experiments instead of experimental support for fuel modelling.

ACKNOWLEDGMENTS

The main author of this review paper about the BaCo code and its applications is deeply grateful for participation, comments and commitments made by J. Garcés, E. Losada, V. Martín, X. Lago, G. La Mattina, L. Juanicó, S. Harriague, C. Baigorria, G. Demarco, L. Furlano, H. Lestani, R. Maturana, H. Mosca and S. Jaroszewicz of CNEA and M. Ordoñez and F. Reale of CONUAR.

REFERENCES

[1] MARINO, A. C. et al., BaCo (BArra COmbustible) Code Version 2.20: a thermomechanical description of a nuclear fuel rod, Journal of Nuclear Materials **229** (1996) 155-168.

[2] MARINO, A.C., Starting Point, Keys and Milestones of a Computer Code for the Simulation of the Behaviour of a Nuclear Fuel Rod, *Science and Technology of Nuclear Installations*, Volume 2011, Article ID 326948 (2011).

[3] MARINO, A. C., PHWR fuel rod behaviour during dry storage, Water Reactor Fuel Performance (Proc. WRFPM 2009/Top Fuel meeting, September 6-10, 2009, Paris, France) No. 2022.

[4] MARINO, A. C., CANDU Fuel Rod Behaviour during Dry Storage, CANDU Fuel (Proc. 11th International Conference, Niagara Falls, Ontario, Canada, October 17-20, 2010).

[5] MARINO, A. C., An overview of the dry storage of nuclear fuels with the BaCo code, VVER Fuel Performance, Modelling and Experimental Support (Proc. 8th International Conference, Burgas, Bulgaria, September 26-October 4, 2009).

[6] MARINO, A. C., ADELFANG, P. and PÉREZ, E. E., Irradiation of Argentine MOX fuels. Post-irradiation results and experimental analysis with the BACO code, Journal of Nuclear Materials **229** (1996) 169-186.

[7] BRASNAROF, D. O. et al, A New Fuel Design for Two Different HW Type Reactors, Science and Technology of Nuclear Installations (2011) Article ID 194650.

[8] BOADO MAGAN, H. et al, CAREM Projects Status, Science and Technology of Nuclear Installations, Volume 2011, Article ID 326948.

[9] MISFELD, I., The D-COM blind problem on fission gas release, IAEA, International Working Group on Fuel Performance and Technology for Water Reactors, OECD-NEA-CSNI/IAEA Specialist's Meeting on Water Reactor Fuel Safety and Fission Products Release in Off-Normal and Accident Conditions, RISØ National Laboratory, IWGFTP/16 (1983).

[10] INTERNATIONAL ATOMIC ENERGY AGENCY, Fuel modelling at extended burnup, Report of the Co-ordinated Research Programme on Fuel Modelling at Extended Burnup-FUMEX-, 1993-1996, IAEA-TECDOC-998, Vienna (1998).

[11] KILLEEN, J. et al, Fuel modelling at extended burnup: IAEA coordinated research project FUMEX-II, LWR Fuel Performance (Proc. Int. Meeting (Top Fuel '06), Salamanca, Spain, October 2006).

[12] MARINO, A. C., Computer simulation of the behaviour and performance of a CANDU fuel rod, CANDU Fuel (Proc. 5th International Conference, Toronto, Canada, September 1997).
[13] MARINO, A. C. et al, High power ramping in commercial PHWR fuel at extended burnup, Nuclear Engineering & Design **236** 13 (2006) 1371–1383.
[14] MARINO, A. C., An approach to VVER fuels with BaCo, VVER Fuel Performance, Modelling and Experimental Support (Proc. 7th International Conference Albena, Bulgaria, September 17-21, 2007).
[15] DEMARCO, G. L., & MARINO, A. C., 3D Finite Elements Modelling for Design and Performance Analysis of UO_2 Pellets, Science and Technology of Nuclear Installations, **2011** (2011), Article ID 843491.
[16] MARINO, A. C., et al, Sensitivity analysis applied to nuclear fuel performance related to fabrication parameters and experiments, Structural Mechanics in Reactor Technology (Proc. 14th Int. Conf., Lyon, France, August 1997).
[17] TURNBULL, J. A., et al, Experimental data on PCI and PCMI within the IFPE database, Pellet-Clad Interaction in Water Reactor Fuels (Proc. International Seminar PCI '04, Aix-en-Provence, France, March 2004).
[18] MARINO, A. C., et al, Present and Future Trends in PHWR Fuel Material Modelling with the BaCo code, Structural Mechanics in Reactor Technology (Proc. 21st Int. Conf. SMiRT 21, November 6-11, 2011, New Delhi, India).
[19] MARINO, A. C., Crack and dishing evolution models and PCI-SCC considerations for fuel pellets in a quasi-bidimensional environment, Pellet-Clad Interaction in Water Reactor Fuels (Proc. of the Les Journées de Cadarache 2004, International Seminar, Aix en Provence, France, March 9-11, 2004).
[20] BUSCAGLIA, G. et. al., Un programa general de elementos finitos en paralelo, in Proceedings of the 6to Congreso Argentino de Mecánica Computacional, MECOM'99, September 1999, Mendoza, Argentina.
[21] SPINO, J., Fragilización de la vaina de Zircaloy-4 en elementos combustibles PWR por acción de los productos de fisión volátiles. Fenómeno de corrosión bajo tensiones activado por iodo. Influencia interna de la química interna del combustible, Ph. D. thesis Instituto Balseiro, Universidad Nacional de Cuyo, Argentina, February (1988).
[22] BAIGORRIA, C. C., Fenómenos Térmicos en Barras de Combustible nuclear, Ph. D. thesis Instituto Balseiro, Universidad Nacional de Cuyo, Argentina, December 1983.
[23] MARINO, A. C., CRP FUMEX PHWR cases a BaCo Code Point of View and Its Results, IAEA TM on Fuel Integrity During Normal Operating and Accident Conditions in Pressurized Heavy Water Reactor (PHWRs), 24-27 September, 2012, Bucharest, Romania.
[24] SAH D, N. et al., Blind prediction exercise on modelling of PHWR fuel at extended burnup, Nuclear Engineering & Design **383** (2008) 144-149.
[25] PAVLOV, S. V. et al., Results of investigation of the VVER-1000 fuel rods after thermal testing under conditions simulating different modes of spent nuclear fuel dry storage, VVER Fuel Performance, Modelling and Experimental Support (Proc. of the 7th International Conference Albena, Bulgaria, September 17-21, 2007).
[26] AZPITARTE, O., Reactores Nucleares de IVta Generación, in Proceedings of the XXXVII Annual Meeting of the Argentine Association of Nuclear Technology (AATN XXXVII), Buenos Aires, Argentina, November 22-26, 2010.
[27] CHEN, N. X., CHEN, Z. D., and WEI, Y. C., Multidimensional inverse lattice problem and a uniformly sampled arithmetic Fourier transform, Phys. Rev. E 55, R5 (1997).
[28] CHEN, N. X., GE, X. J., ZHANG, W. Q., and ZHU F. W., Atomistic analysis of the field-ion microscopy image of Fe_3Al, Phys. Rev. B 57, 14203 (1998).

[29] BLAHA, P. et al., WIEN2k, An Augmented PlaneWave + Local Orbitals Program for Calculating Crystal Properties (Karlheinz Schwarz, Techn. Universitat Wien, Austria), 2001. ISBN 3-9501031-1-2.
[30] PERDEW, J. P., BURKE, K. and ERNZERHOF, M., Generalized Gradient Approximation Made Simple, Phys. Rev.Lett. **77**, 3865 (1996).
[31] MORUZZI, V. L., JANAK, J. F. and SCHWARZ K., Calculated thermal properties of metals, Phys. Rev. **B 37**, 790 (1988).
[32] ARMSTRONG, P. E., CARLSON, O. N., and SMITH, J. F., Elastic constants of thorium single crystals in the range 77-400°K, J. Applied Phys. **30**, 36 (1959).
[33] GREINER, J. D., PETERSON, D. T., and SMITH, J. F., Comparison of the single-crystal elastic constants of Th and a ThC 0.063 alloy, J. Applied Physics. **48**, 3357 (1977).
[34] VOHRA, Y. K., HOLZAPFEL, W. B., Thorium under strong compression-a test case for the evaluation of EOS data by different forms and procedures, High Press. Res. 11, 223 (1993).
[35] EVANS, D. S. and RAYNOR, G. V., The lattice spacing of thorium, with reference to contamination, J. Nucl. Mater. 3, **281** (1959).
[36] BELLUSSI, G., BENEDICT, U. and HOLZAPFEL, W. B., High pressure X-ray diffraction of thorium to 30 GPa, Less Common Met. **78**, 147 1981.
[37] LAWSON, A.C., MARTINEZ, B., ROBERTS, J.A., BENNETT, B.I., RICHARDSON Jr., J.W., Melting of the light actinides, Philosophical Magazine B, **80**, 53 (2000).
[38] SÖDERLIND, P., ERIKSSON, O., JOHANSSON, B. and WILLS, J. M., Theoretical investigation of the high-pressure crystal structures of Ce and Th, Phys. Rev. B **52**, 13169 (1995).
[39] SÖDERLIND, P., ERIKSSON, O., WILLS, J. M., and BORING, A. M., Elastic constants of cubic f-electron elements: Theory, Phys. Rev. B **48**, 9306 (1993).
[40] BOUCHET, J., JOLLET, F. and ZRAH, G., High-pressure lattice dynamics and thermodynamic properties of Th: An ab initio study of phonon dispersion curves, Phys. Rev. B **74**, 134304 (2006).
[41] BOUCHET, J. and ALBERS, R. C., Elastic properties of the light actinides at high pressure, J. Phys.: Condens. Matter **23**, 215402 (2011).
[42] GUPTA, S., JOSHI, K. D. and BANERJEE, S., Met. And Mat. Transactions **39A**, 1593 (2008).
[43] BARIA, J. K. and JANI, A. R., Experimental and theoretical investigations on d and f electron systems under high pressure. Lattice dynamics of La, Yb, Ce and Th, Physica B, 405, 2065 (2010).
[44] CUI-E HU, ZHAO-YI ZENG, LIN ZHANG, XIANG-RONG CHEN, LING-CANG CAI, Phase transition and thermodynamics of thorium from first-principles calculations, Solid State Communications **150**, 393 (2010).
[45] JAROSZEWICZ, S., MOSCA, H.O., GARCÉS, J.E., The temperature behaviour of the elastic and thermodynamic properties of fcc thorium, Journal of Nuclear Materials, **429**, Issues 1–3 (October 2012) 136-142.
[46] GHANDEHARI, K. and VOHRA, Y. K., Onset of structural transformation in thorium metal at high pressures, Scripta Met. et Mat., **27** (1992) 195.
[47] LI LI and TI WANG, Thermodynamic properties of the actinide metals Th and U: A first-principles study, Phys. Rev. B, **63**, 245108 (2001).
[48] JOSHI, K. D., GUPTA, S. C. and BANERJEE, S., Ab-initio theoretical analysis of thermal expansivity, thermal vibrations and melting of thorium, Phil. Mag., **88**, 3145 (2008).

PROPERTIES OF THE HIGH BURNUP STRUCTURE IN LWR

T. WISS, V.V. RONDINELLA, R.J.M. KONINGS, D. STAICU, D. PAPAIOANNOU, S. BREMIER, P. PÖML, O. BENES, J.-Y. COLLE, I. HOLT, P. VAN UFFELEN

European Commission, Joint Research Centre, Institute for Transuranium Elements, Postfach 2340, 76125 Karlsruhe, Germany
E-mail: thierry.wiss@ec.europa.eu

Abstract. The formation of the RIM- or High Burnup Structure (HBS) is possibly the most significant example of the restructuring processes affecting commercial nuclear fuel in-pile. The HBS forms at the relatively cold outer rim of the fuel pellet, where the local burnup is 2-3 times higher than the average pellet burnup, under the combined effects of irradiation and thermo-mechanical conditions determined by the power regime and the fuel rod configuration. The main features of the transformation are the subdivision of the original fuel grains into new sub-micron grains, the relocation of the fission gas into newly formed intergranular pores, and the absence of large concentrations of extended defects in the fuel matrix inside the subdivided grains. The characterization of the newly formed structure and its impact on thermo-physical or mechanical properties is a key requirement to ensure that high burnup fuel operates within the safety margins. This paper presents a synthesis of the main findings from extensive studies performed at JRC-ITU during the last 25 years to determine properties and behaviour of the HBS. In particular, microstructural features, thermal transport, fission gas behaviour, and thermo-mechanical properties of the HBS will be discussed. The main conclusion of the experimental campaigns is that the HBS does not compromise the safety of nuclear fuel during normal operations.

1. INTRODUCTION

Extension of the authorised burnup of LWR fuel is an important issue for nuclear reactor operation. The benefits of increased fuel burnup are a decrease in the volume of spent fuel discharged and fuel cycles cost. It also leads to less refuelling operations and thus higher availability. With the increase of the burnup, it has become important to establish the practical limitations that may arise from the physical evolution of the fuel. A possible limitation being the restructuring of the UO_2 fuel that occurs at the pellet periphery in high burnup LWR fuel. This restructuring was observed for the first time in very high burnup fuel in the late 1950s as described by Belle [1]. It is generally called the high burnup structure (HBS) or rim structure. This structure starts to form when the local burnup exceeds about 60MWd/kgHM. The formation of the HBS is characterised by four consecutive phases: sub-division of the original grains by polygonisation, loss of xenon from the new grain structure, formation of micrometer sized pores in the re-crystallized new structure as a result of diffusion of fission gas out of the new grain structure, growth of the new pores with increase in the local burnup as they collect the gas that continuously flow from the surrounding re-crystallised grains.

The HBS has been extensively investigated for almost 25 years and many properties and characteristics of this structure have been measured, including microstructure changes, fission gas release and xenon depletion, porosity, thermal conductivity, oxidation state, and lattice parameter [2-10]. But there are still some discussions about this high burnup structure formation processes [11] and its behaviour in accidental condition.

2. MICROSTRUCTURE

2.1. Microscopy

At average burnups above about 45 GWd.t^{-1}, a porous outer ring is formed in nuclear UO_2 fuels with a typical thickness of 100 to 200 µm (which corresponds to 4-8% of the fuel volume) [12]. In this region, the local bumup is largely increased by a factor 2-3 due to Pu-formation by resonance absorption of neutrons [13].

The new structure, today called High Burnup Structure (HBS) is more precisely characterized by grain subdivision and redistribution of fission gases and extended defects. The original grains, with a typical size of around 10 µm, subdivide by a factor of ~10^4 into sub-micron grains with a size of about 0.1 – 0.3 µm. The fission gas is removed from the fuel matrix, and is retained in a high concentration of micron-sized intergranular closed pores; reported values for the porosity fraction in the HBS can exceed 20% [14]. The microstructure of the subdivided grains appears free of extended defects as will be shown below.

From the ceramographies shown in Figure 1, from fuel irradiated within a broad range of burnups and temperatures it can be clearly seen that an extensive porosity forms at a burnup and temperature threshold which has also been unambiguously confirmed by the scanning electron microscopy (SEM) images shown in Figure 2. These thresholds lay around 70 GWd.t^{-1} for the burnup and ~ 1100 °C for the irradiation temperature respectively. The discrete irradiation conditions do not allow more refined values at the time.

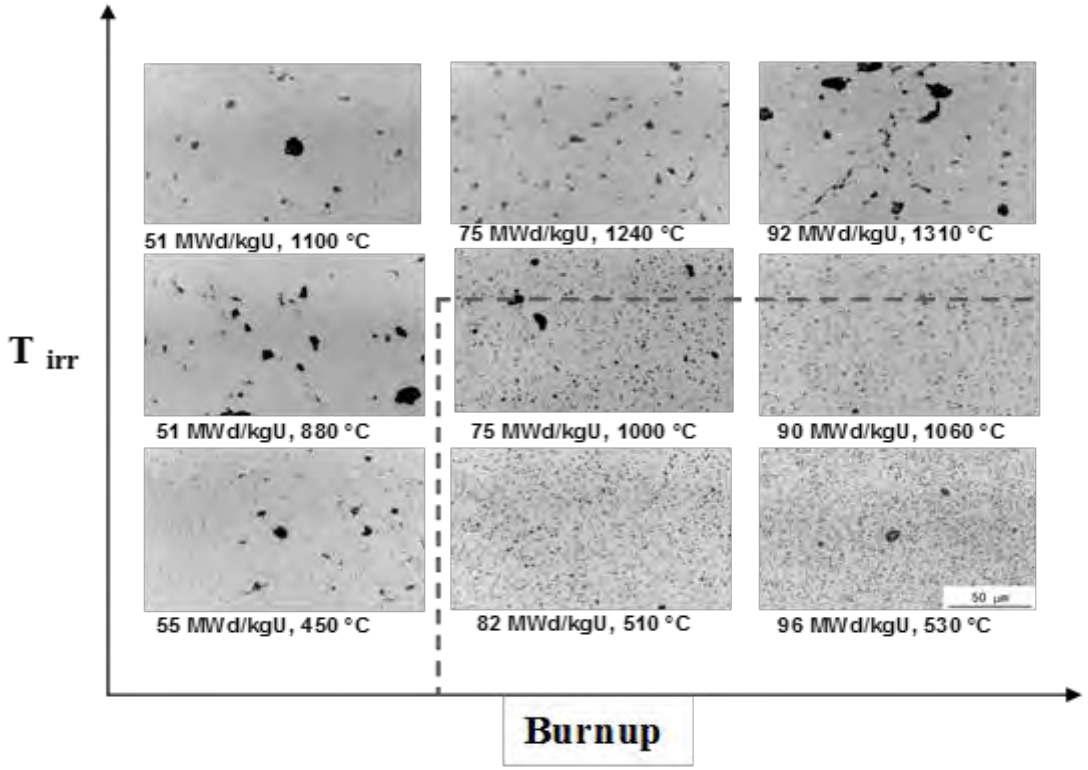

FIG. 1. Ceramographies of a series of samples irradiated in a matrix of burnup and temperature range in the frame of the HBRP program rim. The dashed line indicates the threshold temperature and burnup for the HBS formation (lower right corner) as evidenced from the increase in porosity.

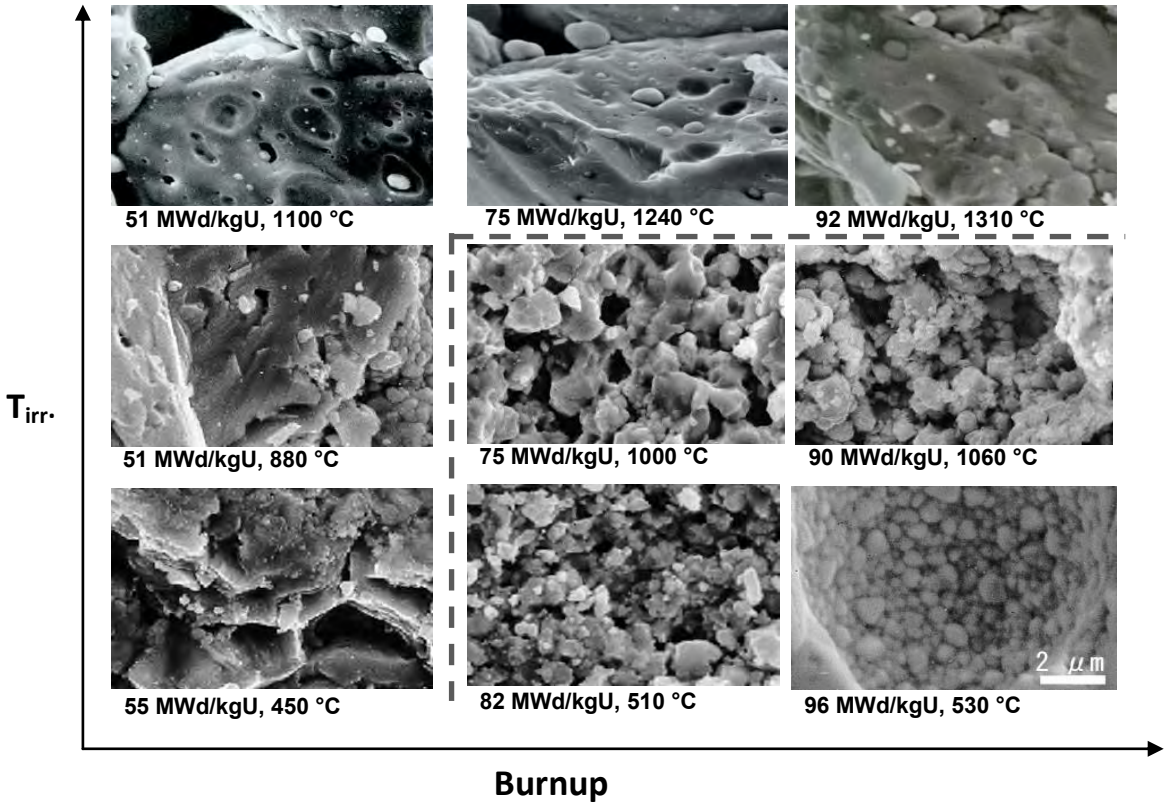

FIG. 2. SEM observations on the fracture surfaces of specimens irradiated at different burnups and temperatures. All pictures have the same magnification. The dashed line shows the threshold for the HBS formation (lower right corner).

Figure 2 shows the typical SEM images in the test matrix of burnup and temperature. Before restructuring, most of the specimen has a structure characterized by original grains whose average size is ~ 10 μm. After restructuring, small divided grains with size ranging between 100 nm and 2 μm are observed.

More in detail, two structures, rounded grains at open surfaces and (bulk) polyhedral grains, have been identified in the high burnup region of the fuel [15]. In one of his paper [12] Matzke has introduced the term 'cauliflower' structure to describe the appearance of the fuel, other authors have named the phenomenon the 'rim effect'. The formation of smaller grains at open surfaces (e.g. pores) shows a fractal appearance with the smaller grains having a size of less than 10 nm as can be seen in Figure 3 on the 3 SEM micrographs. The determined fractal dimension was 2.2 very close to the one of the cauliflower as the HBS was earlier referred to [12]. The surface reorganization has been observed by scanning electron microscopy [12, 16] and is accompanied by a bulk restructuring that is also observable by scanning electron microscopy (see Figure 2) but is mostly investigated by transmission electron microscopy (TEM) [17, 18]. The fuel transforms by a sub-division process in polyhedral grains surrounding pores. The newly formed tiny grains are often found to be slightly disoriented (a few degrees) [18]. A recent observation of a memory effect of the original grains structure supports this assumption [9].

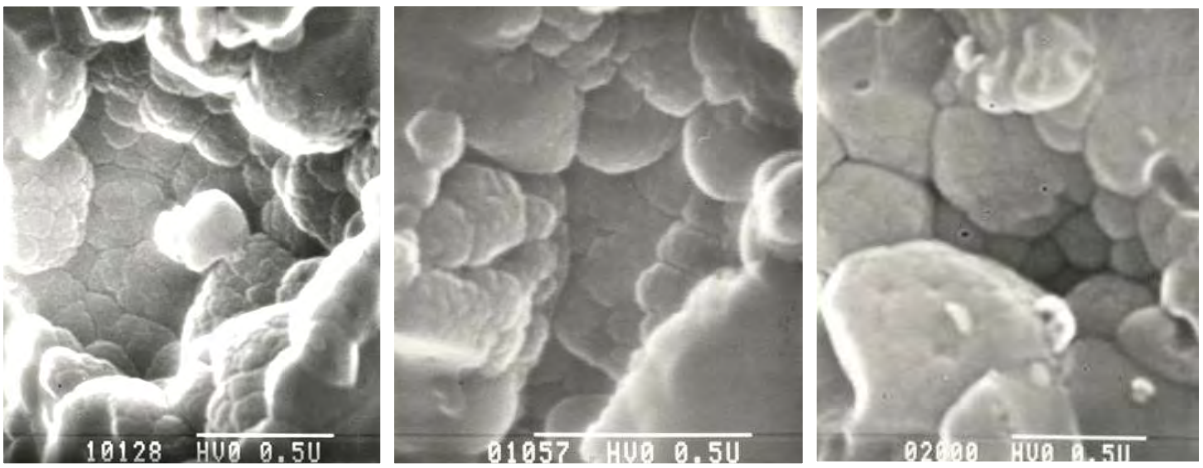

FIG. 3. Secondary electron images showing the restructured pattern inside a pore of the HBS. The fractal aspect can be noted at the different magnification.

More evidence of the restructuring can be visualized from TEM investigations [5, 7, 18-20]. The resolution of the instrument allows observing nanometer sized features being five metal precipitates, nanobubbles, dislocations (lines, loops), etc. It is not intended to detail the various microstructural aspects here but there is a clear difference between regular grains and re-structured grains providing they differ only from the burnup point of view.

In the TEM micrographs of Figure 4 the burnup and temperature threshold for the HBS formation are clearly seen if one accepts the formation of the ~200 nm size grains as a significant result of re-structuring of the original ~ 10 µm size grains. More specifically, the images of the samples irradiated below 55 GWd.t^{-1} show that no re-structuring occurred and that the grains contain numerous intragranular bubbles, dislocation loops or metallic precipitates associated with fg bubbles. On the contrary for the samples with burnups above 70 GWd.t^{-1} and irradiated at temperatures below 1060 °C the formation of small grains with sizes of about 250 nm is clearly seen. These grains do not contain visible defects and only some remaining small fg bubbles are observed. Even if most of the gas is swiped out from the re-structured grains the continuous process of fission will produce fission gases which will start to cumulate in the small grains prior their release in the larger pores of the HBS. This can be observed on the image of the sample irradiated at 1000 C and 75 GWd.t^{-1} where small intragranular bubbles are visible. In addition string of bubbles precipitated at the grain boundaries are also observed in this later sample, whose connection can produce pathways for gas diffusion towards the intergranular pores. It should be noted that depending on the orientation of the grains towards the electron beam (diffraction conditions are limited in terms of tilting in the modified TEM) the bubbles are not always visible or the contrast is different. This is for example the case in the image of the sample irradiated at 82 GWd.t^{-1} at 510 C where the bubbles can be seen as black dots (in the preceding described sample they were visible both as white and black dots in adjacent grains hence having different orientation towards the electron beam).

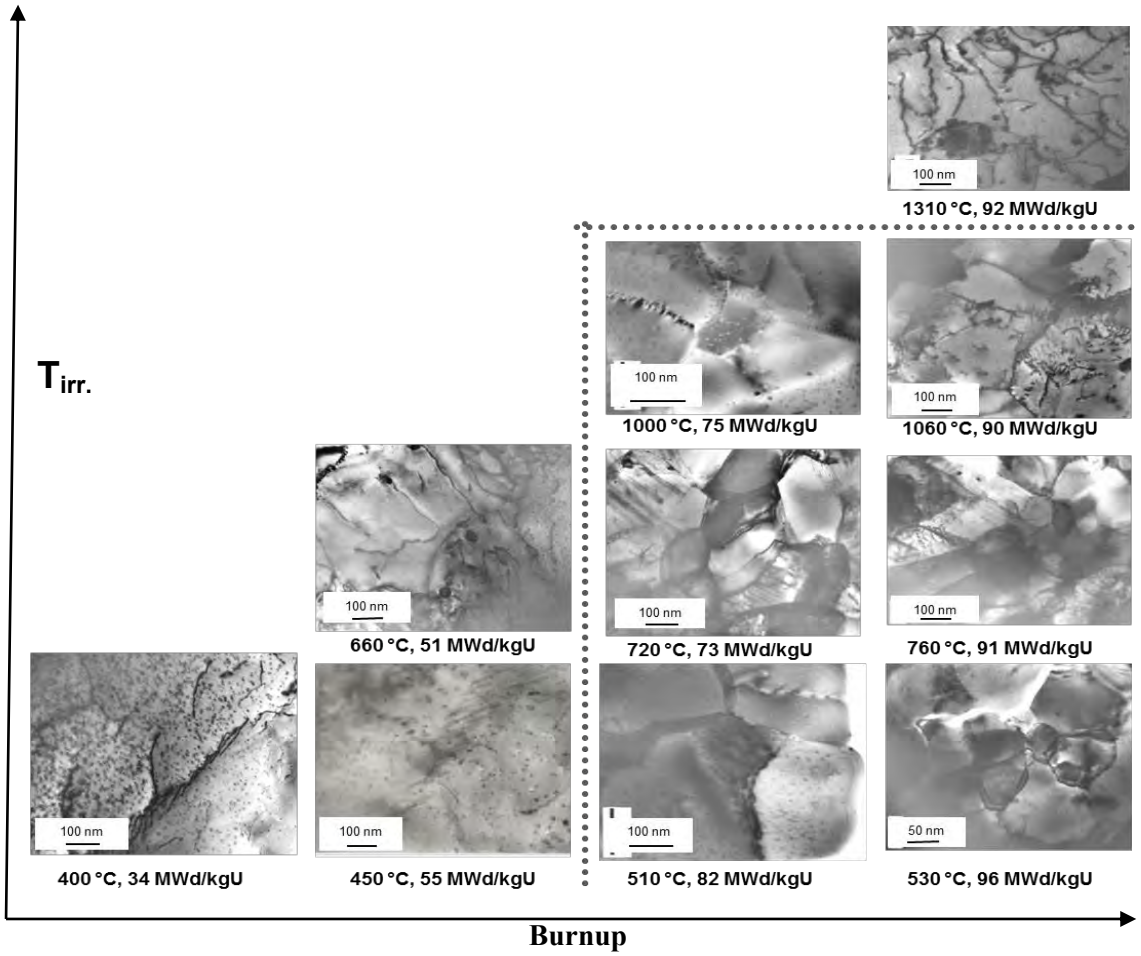

FIG. 4. Series of TEM bright field micrographs showing the microstructure evolution as a function of the irradiation conditions (burnup, temperature). These images have been acquired in the frame of the HBRP program [2]. The small restructured grains are clearly visible in the lower right corner below the dashed line indicating the threshold for the HBS formation.

For the sample irradiated at very high burnup (92 GWd.t^{-1}) and at very high temperature (1310 °C) no re-structuring is observed. Rather a high concentration of dislocations is observed highlighting the plastic behaviour of the fuel at this temperature. Most of the defects produced at this temperature will also probably anneal reducing the facto the number of extended defects that can be involved in the formation of sub-boundaries by sequences of dislocation pinning-piling up-slight tilting of sub-grains.

Figure 5 allows one to define the burnup and irradiation temperature threshold of the HBS formation: the burnup threshold is between 45 and 70 GWd.t^{-1}, and the temperature threshold could be around 1100°C [21]. In the restructured specimen, polyhedral grains with size ranging between 0.5 and 2 μm were observed away from the coarsened bubbles, while rounded grains in the size range 150–350 nm are only observed on the inner surface of coarsened bubbles, as shown in Figure 3. The size of polyhedral grains decreases as burnup increases. This can be explained by assuming that a homogeneous grain sub-division process takes place in the grains, forming smaller polyhedral grains. The formation of rounded grains might be due to the effect of free surfaces. This, in turn, would suggest that the HBS structure formation is independent from the existence of pores.

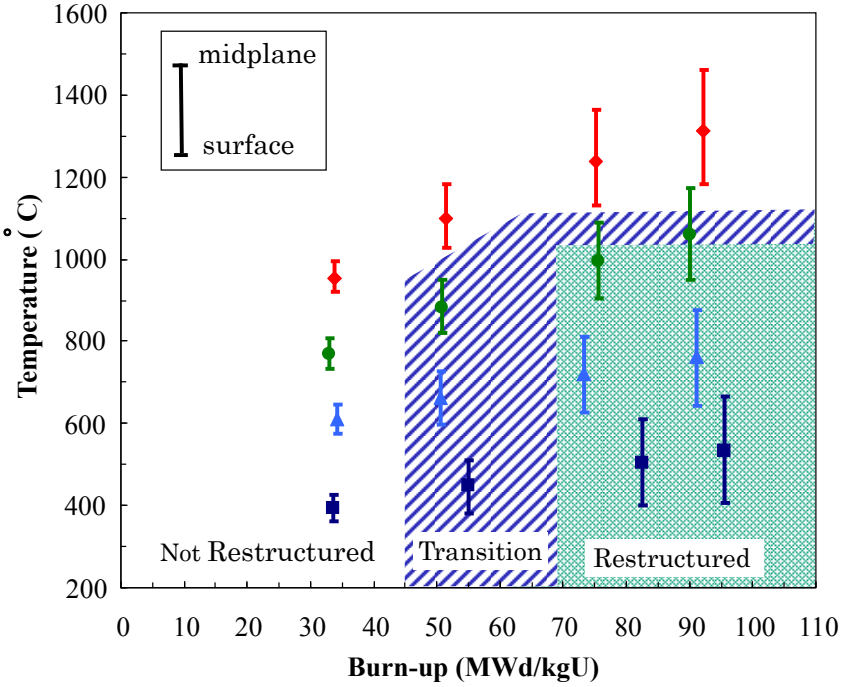

FIG. 5. Burnup and average irradiation temperature of the 16 stacks of HBRP. The extremes represent the temperature difference between the surface and the centre of the discs, obtained by a finite element calculation [2]. The outer dark blue dashed area delineates the burnup temperature range where re-structuring is partly achieved and the light blue the area where full restructuring is observed.

2.2. Electron Probe Micro-analysis (EPMA) and Secondary Ion Mass spectrometry (SIMS)

In addition to the characteristic grain restructuring and porosity development in the HBS one of the main question concerns the fate of the fg. Mogensen et al. [22] determined the radial xenon concentration profiles by X-ray fluorescence (XRF) and EPMA of commercial low-enriched BWR fuel with burn-ups of 44.8–54.9 GWd.t^{-1} and high enriched PWR fuel with burnups from 62.5 to 83.1 GWd.t^{-1}. They found that the percentage of gas released from the UO_2 grains in the outer region of the fuel was generally small compared with the percentage released from the pellet cross-section. This is consistent with the current understanding that most of the fission gas released from the fuel when the high burnup structure forms is retained in the new pore structure. This has been also confirmed by Spino [3, 23-25] who showed that at least up to 250 GWd.t^{-1} local burnup and 25% local porosity no relevant interconnecting paths between pores were present in the HBS as well as by Knudsen cell fission product release measurements by [9]. Electron probe microanalysis was used in ITU to estimate the radial extent of the transformation of the microstructure by measuring the distance from the pellet edge over which Xe depletion in the fuel matrix occurs. In Fig. 6 the local Xe concentration measured in the outer regions of UO_2 fuel sections is plotted as a function of the local burnup. The steep fall of the Xe concentration at burnup around 60 GWd.t^{-1} marks the onset of the recrystallisation process. At burnups over 120 GWd.t^{-1} the constant low Xe concentration indicates that the fuel microstructure transformation is complete.

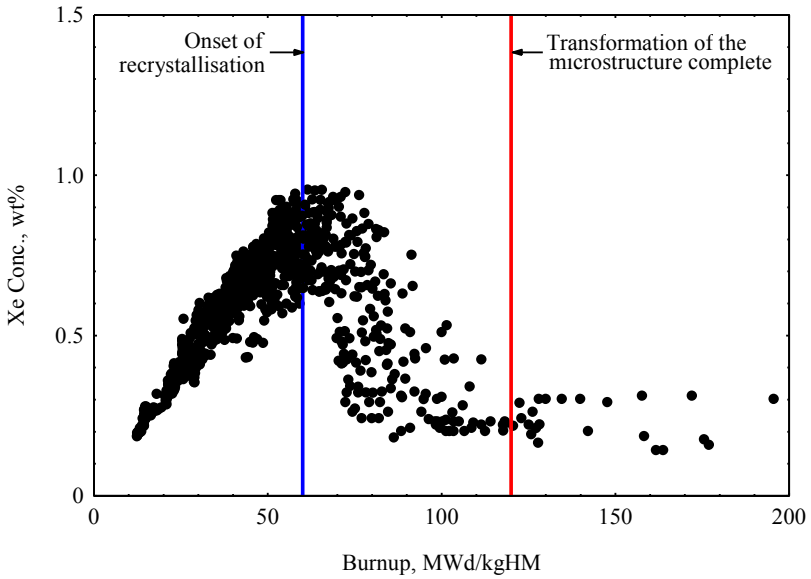

FIG. 6. EPMA results for the local concentration of xenon in the outer region of UO_2 fuel related to the local burnup. The peak concentration at 60 to 75 MWd/kgHM marks the burnup threshold for the formation of the high burnup structure.

Using SIMS [26] it has been confirmed that the fission gas lost from the matrix is contained in the pores of the high burnup structure (Figure 7) and that little gas, if any, is released to the rod free volume either when recrystallization occurs, or with increase in burnup above the threshold value once the high burnup structure is established (Figure 8).

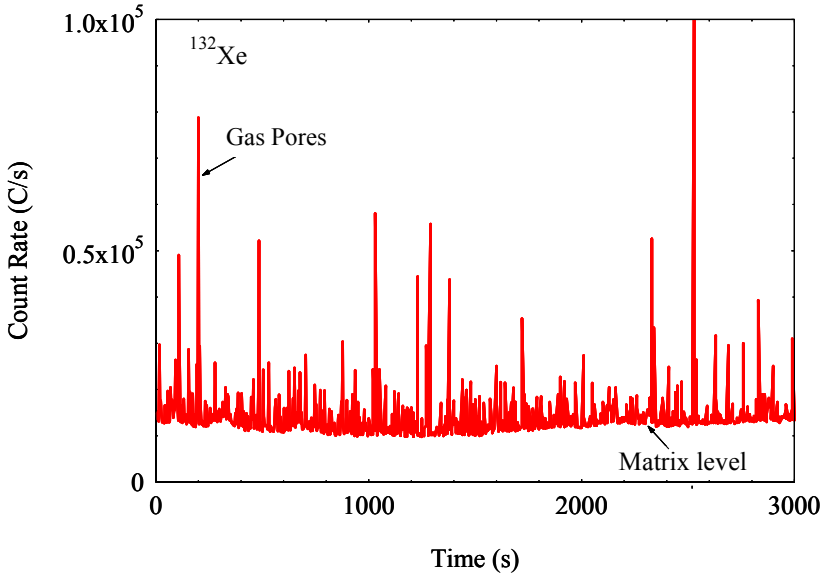

FIG. 7. SIMS depth profile for ^{132}Xe in the high burnup structure produced with a $\left(^{16}O\right)_2^+$ primary ion beam at a high current density of 154 mA/cm^2. The spikes are caused by the expulsion of gas from the pores in the microstructure. Time is equivalent to erosion depth.

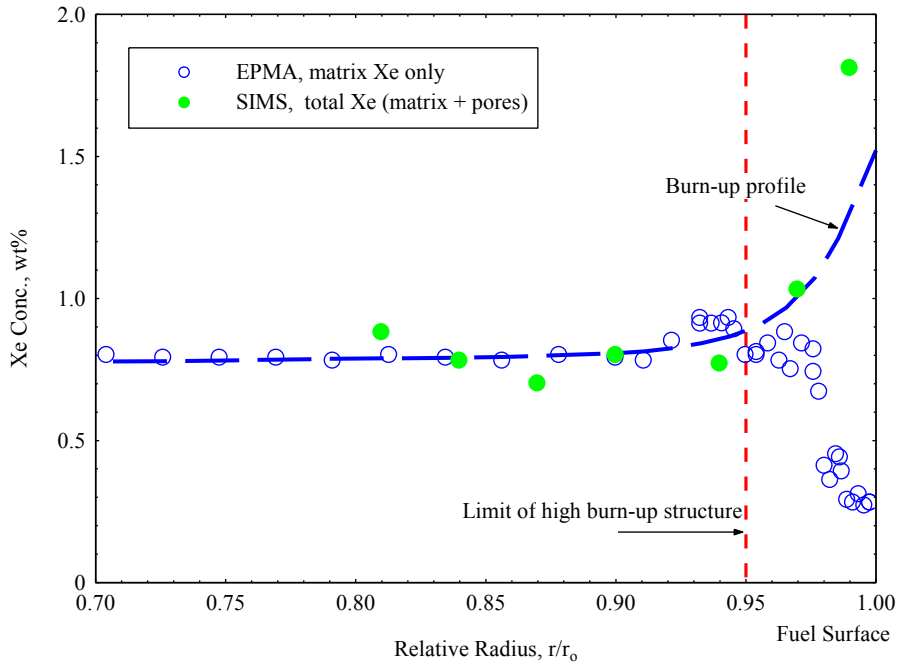

FIG. 8. The local concentration of retained xenon in the outer region of UO_2 fuel as measured by SIMS and EPMA. The steep increase in the SIMS profile at the fuel surface indicates that almost all the gas missing from the UO_2 matrix is contained in the pores of the high burnup structure. Note that in the interval between r/r_o =0.80 and 0.95, the gas is present as an atomic dispersion.

An important question with implications for the behaviour of the high burnup structure during a reactor accident is the pressure of the gas in the pores. The Xe intensity spikes in the SIMS depth profile in Figure 7 can be converted to concentration using the matrix intensity level which is known from EPMA to correspond to about 0.25 wt%. Knowing the size distribution of the pores in the high burnup structure, the gas pressure can then be estimated from the Xe concentration using a hard sphere equation of state [26]. With this method the average pressure of the gas in the pores was found to be 45 MPa. Thus, the pores of the high burnup structure are overpressurised, but generally not excessively so. Consequently, it would appear that few of the pores present in the high burnup structure are sufficiently overpressurised to initiate fragmentation of the fuel during a reactor accident as could be experimentally observed during a laboratory high temperature annealing of a very high burnup sample [9].

3. GAS RELEASE

Fission gas (fg) release from the fuel pellet, hence excessive internal pressurization of the fuel rod could lead to a reduction of the thermal contact between fuel and cladding, thus increasing the fuel temperature. This may ultimately lead to fuel rod failure in the case of accidental transients. It was feared that the formation of the HBS could lead to a slight increase in the oxygen potential starting at a local burnup of 80 MWd/kgU [23]. It could therefore be expected that the release of the fission gases could be enhanced. However, as previously reported [23, 27, 28] the LWR fuel remains stoichiometric or slightly hypostoichiometric. It was also thought that the HBS porosity would induce an enhanced mobility of the fission gases during normal conditions and that there was a new source for fission gas release occurring directly from the restructuring at high burnup.

The release of fg is in fact strongly affected by the irradiation temperature. During normal operating conditions LWR fuel experiences temperatures between ~13001500 K at the pellet

center and ~600-800 K at the rim. Measurements of fg release both in-pile and after fuel rod discharge do indicate an increase of the fraction of gas released with increasing burnup. For instance, post-irradiation examination data from rod puncturing tests reported by Manzel and Walker [29] indicate fg release between 5-10% at an average burn-up of 50 GWd.t^{-1}, and up to almost 25% for fuel with a very high average burnup of 100 GWd.t^{-1}. The exact radial location in UO_2 fuel pellets and the mechanisms responsible for fg release at high burnup are not yet fully understood. However, it is now generally agreed that this release does not originate from the HBS, but rather from higher temperature regions towards the axial center of the fuel pellet, where temperature effects allow interconnection among intergranular fg bubbles and the opening of pathways for fg release along the grain boundaries. Both special irradiation [2, 10] and commercial fuel data [14, 24] indicate that almost all locally generated fg is retained in the intergranular HBS porosity.

In addition to the analyses of fg by EPMA and SIMS some thermal desorption analyses were performed using a Knudsen cell device [31].

Figure 9 shows the normalized fractional release of Krypton during a Knudsen cell effusion test on very high burnup specimens (90-96 GWd.t^{-1}). In this graph it appears clearly that the release of krypton is associated to the irradiation temperature and hence since the burnup is very high to the microstructure of the fuel. Although the onset for release is similar for the five samples, irradiated at the (almost) same burnup but at different temperatures, the normalized fractional release profile is very sharp for the restructured samples on the contrary of those irradiated at temperatures where restructuring does not occur (above 1100 °C).

The quantity of gas released from the HBS was shown to correspond to the theoretical inventory and therefore that the restructuring process does not cause the release of the fg out of the fuel pellet which is clearly a positive feature of the HBS.

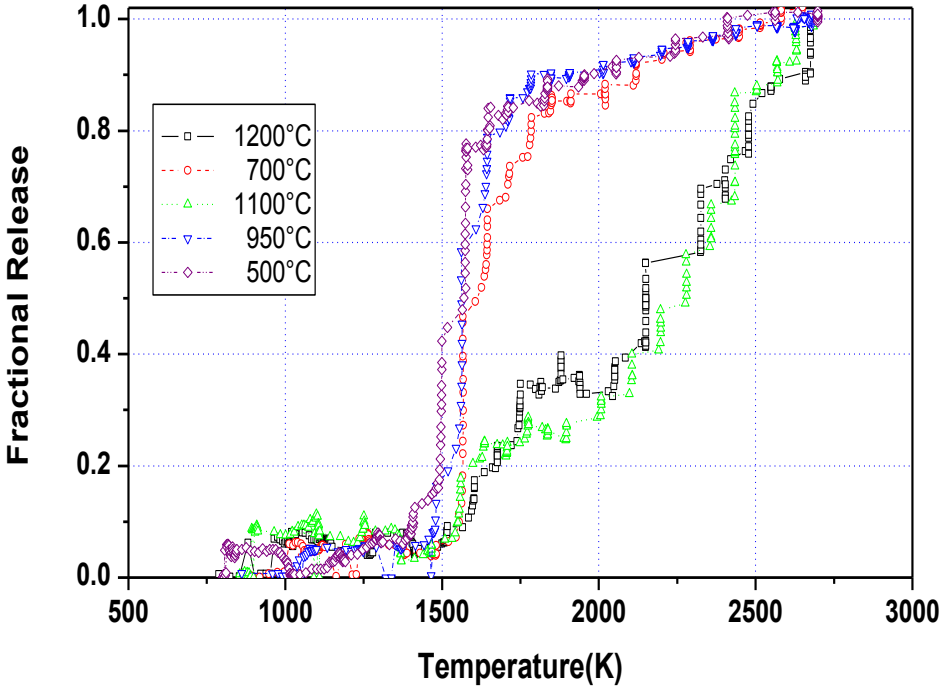

FIG. 9. ^{85}Kr normalized fractional release from UO_2 samples (HBRP) irradiated in the BU range 90-96 GWd.t^{-1} at various temperatures.

4. THERMO-PHYSICAL PROPERTIES

In fuel performance codes, the effect of the HBS on the heat transfer is generally included in a correlation describing the thermal conductivity degradation

$$\lambda = \frac{1}{A_0 + A_1 \cdot bu + B \cdot T}$$

and the porosity build up in the HBS as well as in an improved gap conductance in order to account for the bonding layer between the ceramic pellets and the metallic cladding. To this end, for example, the cladding and pellet roughness is empirically reduced above a certain burnup to account for the filling up by mainly zirconium oxide, which has a higher thermal conductivity than that of the mixture of He and Xe in the residual gap.

Thermal conductivity degradation of the fuel is sometimes considered to saturate:

$$\lambda = \frac{\sqrt{\lambda_0}}{D\sqrt{bu}} \arctan\left(D\sqrt{bu}\sqrt{\lambda_0}\right) + \lambda_{el}$$

with $\lambda_0 = 1/(A+BxT)$ and D is a constant. It can be shown that in the low burnup limit this expression tends to the classical form of λ_0. Occasionally partial thermal conductivity restoration is even considered when the HBS is created. In this way account is made for the 'cleaning' of the matrix from point defects and fission products, which relies on an empirical formulation of the lattice parameter variation. The latter approach seems to be in line with recent experimental data.

The thermal diffusivity and the heat capacity of irradiated high burnup UO_2 fuels were measured, and laboratory thermal annealing cycles with increasing maximum temperatures were applied to examine recovery effects [32]. The most conspicuous decrease in diffusivity was observed in high burnup samples subjected to in-pile temperatures of 600 K – 800 K. These samples showed a decrease in conductivity of up to a factor of four compared to fresh fuel. Analysis of the experimental measurements shows that the effective decrease of the thermal conductivity during reactor irradiation is due to: a) atomically dispersed FP, b) irradiation and self-irradiation defects, c) fission gas and volatile FP dynamically frozen in the fuel during irradiation, d) fission gas precipitation and porosity evolution.

The important effects due to fission gas were interpreted by considering the possible states, from gas-in-solid through bubble precipitation until intergranular swelling conditions. Thermal annealing leads to defect annihilation, and to healing of the lattice with a consequent recovery of thermal diffusivity.

The formation of the HBS has a positive effect by limiting the decrease in thermal conductivity with burnup. The effect of this restructuring, which entails a significant decrease in the fission-gas concentration dynamically dissolved in the matrix, can be clearly seen in the graphs: the thermal conductivity at EOL, plotted in Figure 10 as a function of irradiation temperature for different values of burnup, shows that the formation of the HBS has a positive effect on the lattice thermal conductivity (i.e., if the trivial diminution due to fission-gas swelling is not taken into account).

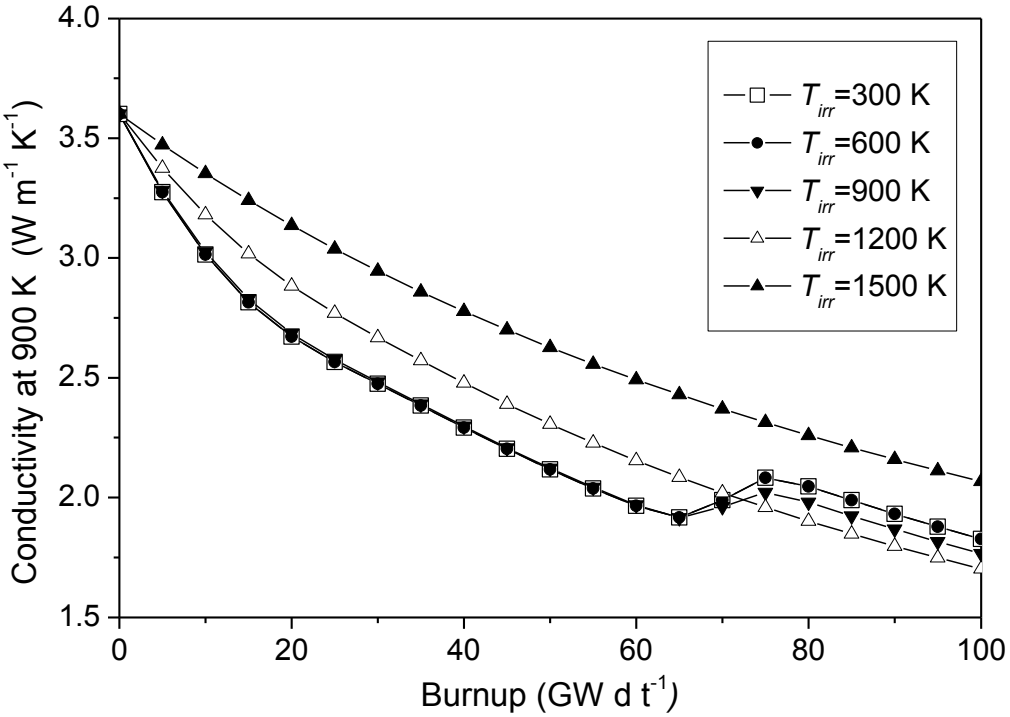

FIG. 10. Lattice thermal conductivity at EOL as a function of burnup for different irradiation temperatures.

Figure 11 shows the evolution with burnup of the conductivity measured at 900 K, for different irradiation temperatures, normalised to 5% porosity. It can be seen that the samples displaying the HBS have higher lattice conductivity than those irradiated at about 1200 K, a temperature at which the HBS is not formed. One can see that only in samples irradiated at T_{irr} >1500 K does the lattice conductivity become higher than that measured in the HBS.

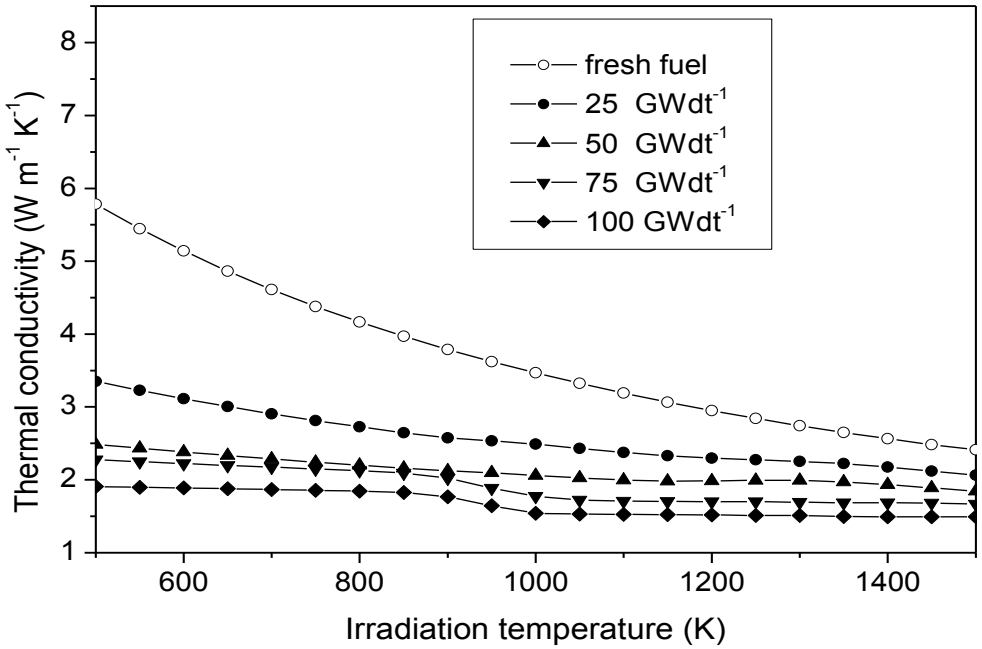

FIG. 11. Evolution with burnup of the conductivity measured at 900 K, for different irradiation temperatures, normalized to 5% porosity.

In spite of the formation of the high burnup structure, the thermal diffusivity of the fuel at 100 $MWd.t^{-1}$ was 55% higher than the value expected to result from the degradation caused by the build up of fission products and point defects in the fuel lattice at this burnup. Clearly, the higher thermal diffusivity and conductivity caused by the HBS formation is a consequence of the removal of fission product atoms from the fuel lattice and healing of radiation defects that accompanies restructuring of the fuel grains (part of the HBS formation mechanisms). Moreover, the role of the pores of the high burnup structure as sinks for the fission gas expelled from the fuel lattice during restructuring is more important than the counter acting effect as barriers to heat transport. With the increase of burnup, large stresses are produced in the matrix during laboratory annealing with sudden development of cracks. The higher is the fuel burnup, the lower the temperature at which these processes are activated. At 100 $GWd.t^{-1}$ the fuel fragments at temperatures just above the in-pile temperature. Therefore, a prediction of the thermal transport performance of the outer pellet region of high burnup fuel (which exhibit the HBS) under transient conditions is still uncertain, and further measurements must be conducted where the thermal diffusivity is measured under restrained conditions.

5. THERMO-MECHANICAL PROPERTIES

The effect of the long irradiation time in the mechanical analysis by means of fuel performance codes is mostly accounted for in the cladding properties. In fuel, on the other hand a reduction of the micro-hardness (Fig.12) and Young's modulus (Fig. 13) has been observed in high burnup fuel pellets, but this is not yet included in the fuel performance codes. This also holds for the bond between pellet and cladding. On the one hand, it improves the pellet-cladding interaction resistance since it is much softer than UO_2. On the other hand, the pellet-clad bonding would make the cladding subjected to a bi-axial stress state due to pellet stack elongation. This bi-axial stress state is a mechanically more tough condition for cladding.

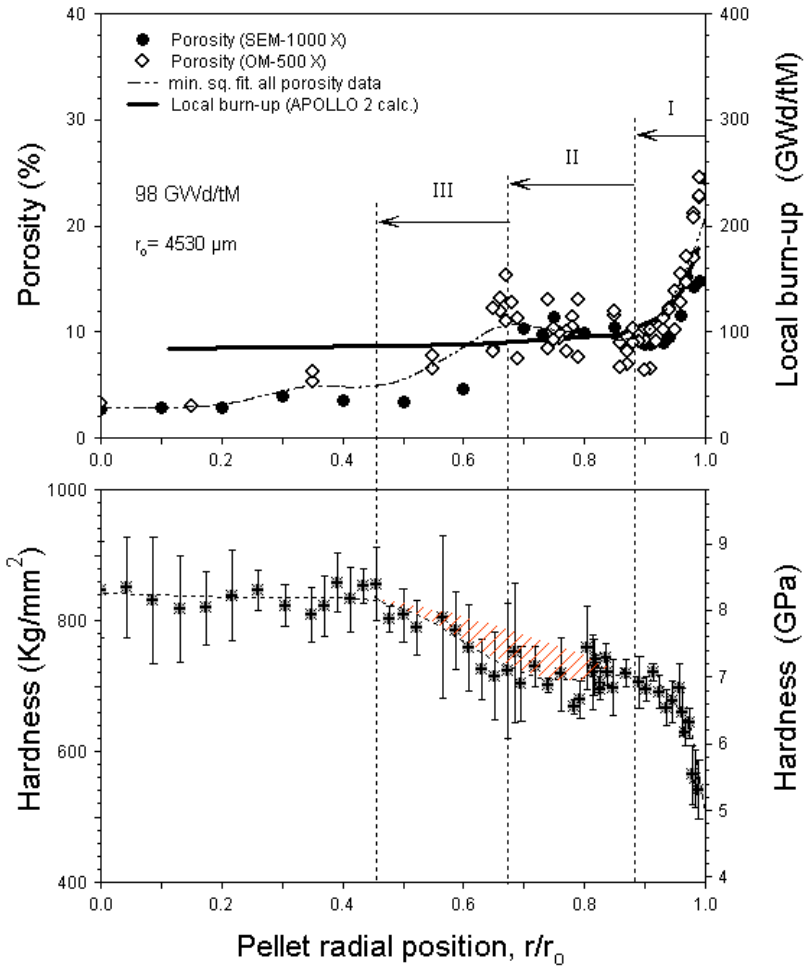

FIG. 12. Experimental values for micro-hardness of irradiated UO_2 fuel with a burnup of 98 GWd.t^{-1}

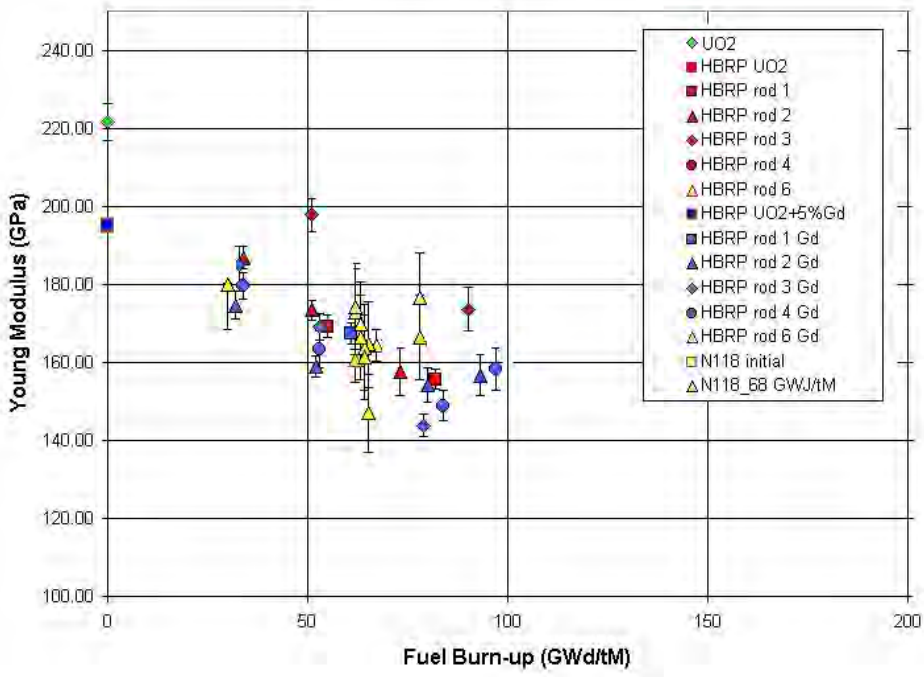

FIG. 13. Experimental Young's modulus of irradiated LWR fuels as a function of burnup.

6. MODELLING OF FISSION GAS BEHAVIOUR

The first simple model for the HBS formation in oxide fuels that was implemented in the TRANSURANUS code [33] was proposed by Lassmann and relied on the local burnup value alone. More precisely, above a certain local burnup threshold, the HBS formation was assumed to start, resulting in the reduction of the fission product concentration in the matrix, concomitant with the formation of large HBS pores. Above a second burnup threshold, the HBS was assumed to be saturated, leading to a release of any additional gas arriving at the HBS pores. This second assumption has been questioned, since more recent analysis showed that the HBS pores remain closed up until local volume swelling values of 25 % and negligible release was observed from the HBS during normal operating conditions.

The open questions about the HBS formation mechanisms and properties triggered new experimental campaigns, largely based on disc irradiations in order to assess the separate effect of the local temperature and burnup. The results revealed that the HBS formation only takes place below a certain temperature limit, which is attributed to defect healing. Therefore Khvostov et al. [34] proposed a so called effective burnup, which accounts for the fact that when the temperature exceeds a certain limit defect annealing will prevent further accumulation of the effective local burnup that is used for predicting the onset of the HBS formation. A recent critical re-analysis of published and new data along with a multi-scale and multi-physics simulation provided lead to the suggestion of a new temperature dependent effective burnup:

$$\Delta bu_{eff} = \begin{cases} \Delta bu, T \le T_{thres} \\ 0, T > T_{thres} \end{cases}$$

where T is the local fuel temperature expressed in °C, Δbu is the considered burnup increment and T_{thres} is the temperature threshold in °C for healing of defects.

The swelling caused by the HBS pores is mostly modelled separately with a very simple linear or quadratic function of burnup (Figure 14).

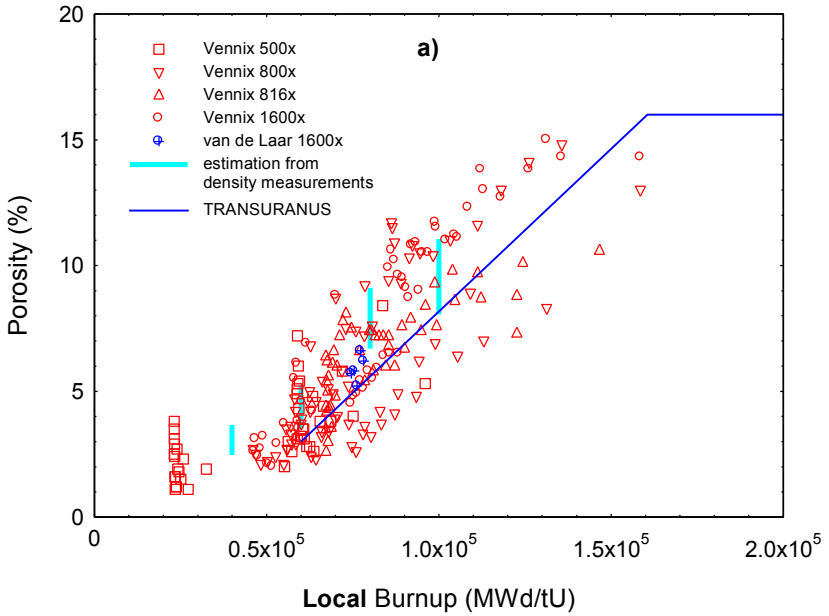

FIG. 14. Porosity as a function of the local burnup for highly irradiated fuel, and the corresponding correlation adopted in the TRANSURANUS code.

Based on the new model for the HBS formation as a function of temperature and burnup, a new model for the release from this structure under design basis accident (DBA) is being developed, which depends on the local temperature levels, the effective burnup and should account for any constraint effect. It relies on local experimental data obtained from HBS samples in a Knudsen Cell that is coupled with a mass spectrometer [31], as well as on the basis of integral results observed in fuel rod segments. The internal gas pressure, especially after a RIA, is remarkably enhanced by the burst release of fission gas following the grain separation, and is generally correlated with the peak fuel enthalpy. The fission gas originates mainly from the intergranular gas bubbles, even though some contribution comes from gas pores within the grains and the high burnup structure. Although few models consider the thermal diffusion process of fission gas atoms from inside the grains, it is generally considered that it can be substantially neglected. This is mostly explained by the short duration of the high temperature period of the pellet (e.g. a few or several tens of seconds) to allow for the thermal diffusion to contribute significantly to the FGR increase, even if the fuel pin runs into a DNB phase. In the case of a LOCA, the time-interval is much longer and the mechanical constraint on the fuel - hence the HBS pores and grain boundary bubbles - is lower, causing a larger contribution to the internal gas pressure increase. The constraint effect must therefore be accounted for in the model describing the behaviour of the HBS pores during DBAs.

7. CONCLUSIONS

The acquisition of experimental data specifically targeted at assessing key properties and behaviour of HBS has produced a widespread consensus on the main features and properties of the HBS structure. The technology concerns related to fg behaviour, swelling and fuel cladding mechanical interaction, and thermal conductivity of high burnup fuel under normal operating conditions have been positively addressed and today's LWR fuel operates to burnup levels which encompass the formation of HBS with no specific reported issues. The experimental data on HBS are incorporated in some fuel performance codes with good success [30, 33, 34].

HBS is the self-reorganization of the fuel to respond to the radiation damage and harsh thermo-mechanical conditions established in-pile. All the models proposed converge and show evidence that the formation of the HBS is ultimately driven by and results in the minimization of the local internal energy of the system.

Several campaigns have been undertaken to test possible routes (including fuel grain additives and special fabrication procedures) to delay or avoid the onset of the HBS formation, mainly for concern of enhanced fg release from restructured fuel during off-normal conditions (e.g. sudden temperature excursions).
There are still open questions concerning the mechanisms driving the HBS formation and its evolution during continued irradiation (data for UO_2 fuel with a local burn-up in the range 160-250 $GWd.t^{-1}$were collected [6, 9, 29]. Further investigations, combining microstructural and microanalytical experimental studies using state of the art characterization tools (e.g. TEM and SIMS) and a multi-scale modelling approach will possibly provide answers to these questions.

ACKNOWLEDGEMENTS

The authors are indebted with many colleagues at ITU (impossible to mention all of them) for all the work performed over almost 3 decades on the topic of the high burnup structure. Most

of them will appear in the citations. The contribution by AREVA for supplying irradiated LWR fuel samples was essential, so as the important role played by the HBRP irradiation and examination programmes.

REFERENCES

[1] BELLE, J., Uranium Dioxide: Properties and Nuclear Applications, in: N.R. Handbooks (Ed.), United States Atomic Energy Commission, 1961.

[2] KINOSHITA, M., SONODA, T., KITAJIMA, S., SASAHARA, A., KAMEYAMA, T., MATSUMURA, T., KOLSTAD, E., RONDINELLA, V.V., RONCHI, C., HIERNAUT, J.P., WISS, T., KINNART, F., EJTON, J., PAPAIOANNOU, D., MATZKE, H., High Burnup Rim Project: (III) properties of rim-structured fuel, LWR Fuel Performance, (Proc. 2004 International Meeting, ANS, Orlando, Fl, USA, 2004) 207-213.

[3] SPINO, J., BARON, D., COQUERELLE, M., STALIOS, A.D., High burn-up rim structure: evidences that xenon-depletion, pore formation and grain subdivision start at different local burn-ups, Journal of Nuclear Materials, **256** (1998) 189-196.

[4] SONODA, T., KAMEYAMA, T., SASAHARA, A., KITAJIMA, S., NAUCHI, Y., KINOSHITA, M., RONDINELLA, V.V., WISS, T., HIERNAUT, J.P., PAPAIOANNOU, D., SHEINDLIN, M., STAICU, D., Clarification of rim structure effects on properties and behaviour of LWR UO2 fuels and gadolinia doped fuels, LWR Fuel Performance/Top Fuel (Proc. American Nuclear Society - 2007) 340-346.

[5] SONODA, T., KINOSHITA, M., RAY, I.L.F., WISS, T., THIELE, H., PELLOTTIERO, D., RONDINELLA, V.V., MATZKE, H., Transmission electron microscopy observation on irradiation-induced microstructural evolution in high burn-up UO2 disk fuel, Nuclear Instruments and Methods in Physics Research, Section B: Beam Interactions with Materials and Atoms, **191** (2002) 622-628.

[6] WALKER, C.T., STAICU, D., SHEINDLIN, M., PAPAIOANNOU, D., GOLL, W., SONTHEIMER, F., On the thermal conductivity of UO2 nuclear fuel at a high burn-up of around 100 MWd/kgHM, Journal of Nuclear Materials, **350** (2006) 19-39.

[7] RAY, I.L.F., THIELE, H., MATZKE, H., Transmission electron microscopy study of fission product behaviour in high burnup UO_2, J. Nucl. Mater., 188 (1992) 90-95.

[8] NOIROT, J., DESGRANGES, L., LAMONTAGNE, J., Detailed characterisations of high burn-up structures in oxide fuels, Journal of Nuclear Materials, **372** (2008) 318-339.

[9] HIERNAUT, J.P., WISS, T., COLLE, J.Y., THIELE, H., WALKER, C.T., GOLL, W., KONINGS, R.J.M., Fission product release and microstructure changes during laboratory annealing of a very high burn-up fuel specimen, J. Nucl. Mater., 377 (2008) 313-324.

[10] KONINGS, R.J.M., WISS, T., GUÉNEAU, C., Nuclear Fuels, in: L.R. Morss, N.M. Edelstein, J. Fuger (Eds.) The Chemistry of the Actinides and Transactinides Elements, Springer, Dordrecht (2010) 3665-3811.

[11] RONDINELLA, V.V., WISS, T., The high burn-up structure in nuclear fuel, Mat. Today, 13 (2010) 24-32.

[12] MATZKE, H., BLANK, H., COQUERELLE, M., LASSMANN, K., RAY, I.L.F., RONCHI, C., WALKER, C.T., J. Nucl. Mater., **166** (1989) 165.

[13] MATZKE, H., Radiation damage in crystalline insulators; oxides and ceramic nuclear fuels, Radiation Effects, **64** (1982) 3-33.

[14] SPINO, J., STALIOS, A.D., SANTA CRUZ, H., BARON, D., Stereological evolution of the rim structure in PWR-fuels at prolonged irradiation: Dependencies with burn-up and temperature, Journal of Nuclear Materials, **354** (2006) 66-84.
[15] LOZANO, N., DESGRANGES, L., AYMES, D., NIEPCE, J.C., Hugh magnification SEM observations for two types of granularity in a high burnup PWR fuel rim, J. Nucl. Mater., 257 (1998) 78-87.
[16] UNE, K., NOGITA, K., KASHIBE, S., IMAMURA, M., Microstructural change and its influence on fission gas release in high burnup UO_2 fuel, J. Nucl. Mater., 188 (1992) 65.
[17] UNE, K., NOGITA, K., SHIRATORI, T., HAYASHI, K., Rim structure formation of isothermally irradited UO_2 fuel discs, J. Nucl. Mater., 288 (2001) 20-28.
[18] RAY, I.L.F., MATZKE, H., THIELE, H., KINOSHITA, M., An electron microscopy study of the RIM structure of a UO2 fuel with a high burnup of 7.9% FIMA, J. Nucl. Mater.,, 245 (1997) 115-123.
[19] WISS, T, THIELE, H., JANSSEN, A., PAPAIOANNOU, D., RONDINELLA, V.V., KONINGS, R.J.M., Recent results of Microstructural Characterization of Irradiated Light Water Reactor Fuels using Scanning and Transmission Electron Microscopy, JOM, **64** (2013) 1390-1395.
[20] NOGITA, K., UNE, K., Nucl. Instrum. Meth. B, B91 (1994) 301.
[21] HOLT, L., SCHUBERT, A., VAN UFFELEN, P., WALKER, C.T., FRIDMAN, E., SONODA, T., Sensitivity study on Xe depletion in the high burn-up structure of UO_2, Journal of Nuclear Materials, **452** (2014) 166-172.
[22] MOGENSEN, M., PEARXE, J., WALKER, C.T., J. Nucl. Mater., 264 (1999) 99-112.
[23] SPINO, J., PEERANI, P., Oxygen stoichiometry shift of irradiated LWR-fuels at high burn-ups: Review of data and alternative interpretation of recently published results, Journal of Nuclear Materials, **375** (2008) 8-25.
[24] SPINO, J., PAPAIOANNOU, D., GLATZ, J.P., Comments on the threshold porosity for fission gas release in high burn-up fuels, Journal of Nuclear Materials, **328** (2004) 67-70.
[25] SPINO, J., REST, J., GOLL, W., WALKER, C.T., Matrix swelling rate and cavity volume balance of UO_2 fuels at high burn-up, Journal of Nuclear Materials, **346** (2005) 131-144.
[26] WALKER, C.T., BREMIER, S., PORTIER, S., HASNAOUI, R., GOLL, W., SIMS analysis of an UO_2 fuel irradiated at low temperature to 65 MWd/kgHM, J. Nucl. Mater., **393** (2009) 212-223.
[27] KLEYKAMP, H., The chemical state of LWR high-power rods under irradiation, Journal of Nuclear Materials, **84** (1979) 109-117.
[28] WALKER, C.T., RONDINELLA, V.V., PAPAIOANNOU, D., WINCKEL, S.V., GOLL, W., MANZEL, R., On the oxidation state of UO2 nuclear fuel at a burn-up of around 100 MWd/kgHM, Journal of Nuclear Materials, **345** (2005) 192-205.
[29] MANZEL, R., WALKER, C.T., EPMA and SEM of fuel samples from PWR rods with an average burn-up of around 100 MWd/kgHM, Journal of Nuclear Materials, **301** (2002) 170-182.
[30] VAN UFFELEN, P., KONINGS, R.J.M., VITANZA, C., TULENKO, J., Analysis of reactor fuel rod behaviour, in: D.G. Cacuci (Ed.) Handbook of nuclear engineering, Springer, 2010, pp. 1519-1627.
[31] COLLE, J.Y., MAUGERI, E., THIRIET, C., TALIP, Z., CAPONE, F., HIERNAUT, J.P., KONINGS, R.J.M., WISS, T., A mass spectrometry method for quantitative and kinetic analysis of gas release from nuclear materials and its application to helium desorption from UO_2 and fission gas release from irradiated fuel, J. Nucl. Sci. tech., **51** (2014) 700-711.

[32] RONCHI, C., SHEINDLIN, M., STAICU, D., KINOSHITA, M., Effect of burn-up un the thermal conductivity of uranium dioxide up to 100.000 MWd/t, J. Nucl. Mater., **327** (2004) 58-76.
[33] LASSMANN, K., TRANSURANUS: a fuel rod analysis code ready for use, in: H.M. Schumacher (Ed.) Nuclear Materials for Fission Reactors, Elsevier, Oxford, 1992, pp. 295-302.
[34] KHVOSTOV, G., MIKITYUK, K., ZIMMERMANN, M.A., A model for fission gas release and gaseous swelling of the uranium dioxide fuel coupled with the FALCON code, Nuclear Engineering and Design, **241** (2011) 2983-3007.

ASSESMENT OF PCI FAILURE PREDICTION CAPABILITIES OF TRANSURANUS CODE FOR NATURAL URANIUM FUEL BASED ON OPERATIONAL FUEL PIN FAILURES OF ATUCHA I NPP

SYREWICZ, MARÍA CECILIA, BONELLI, ANALIA NOEMÍ

Licensing, Nuclear Safety and Core Design, UG-CNAII-IVCN-Nucleoeléctrica Argentina S.A, Lima, B2806AEL Buenos Aires, Argentina
csyrewicz@na-sa.com.ar, abonelli@na-sa.com.ar

Abstract.

Atucha I is a pressurized heavy water reactor, cooled and moderated with heavy water by two separate systems. In the year 1985, several natural uranium fuel elements failed owing to pellet-cladding interaction (PCI), after a cycle of power.

The aim of this work is to assess TRANSURANUS Code capabilities regarding PCI failure prediction for Atucha-type fuels by using the available information from the above mentioned incident. Input preparation required the revision of old site data, recount on historical fuel rod design changes, and the execution of new neutronic simulations. A base case was calculated with as-delivered code executable and using recommended input parameters. Afterwards, a very detailed sensitivity study was conducted. The purpose of it was to assess the influence on results of model parameters and especially of fuel material properties. The SPAKOR PCI model on TRANSURANUS code was also studied and some model parameters were updated for Atucha type fuels, in particular Young modulus of Zr-4 and yield and rupture stresses for burst tests, provided by the fuel vendor (CONUAR). Overall results were compared and finally an Atucha-suited re-compiled code executable was selected for oncoming PCI calculations of Atucha-type fuels. Furthermore, uncertainties in power history data were identified and therefore it was concluded that boundary conditions provided in the performed calculations highly influenced failure/non failure code predictions. In light of this, it was concluded that results had to be analyzed on a global basis for each of the calculated sensitivity cases.

The performed assessment contributed to gaining confidence on TRANSURANUS Code predictions when simulating natural uranium fuels of low burnup, for which phenomena have not been deeply investigated lately, as this type of fuels is rather unusual among the fuel designs currently found in the nuclear industry.

1. INTRODUCTION

TRANSURANUS Code is a computational program used to perform the thermal-mechanical analysis of the fuel rods from nuclear facilities. In spite of the large amount of successful validations, rarely do they base on data of PHWR fuels of low extraction burn up.

As this software has been lately utilized to predict Atucha 2 fuels behaviour in different conditions, the need of assessing it for Atucha-type fuels arose. This work was performed to gain confidence on the predictions of PCI/SCC failure made by SPAKOR subroutine of TRANSURANUS Code. By simulating a real event occurred in Atucha 1, code results were assessed and the modification of some parameters from the source code was justified for this type of fuels.

2. OVERVIEW OF THE STUDIED TRANSIENT

Atucha 1 nuclear power plant is a two loop, nearly 345MWe Pressurized Heavy Water Reactor nuclear power plant, constructed by Siemens KWU, which is in operation since 1974 in Lima, Argentina. In the 1980s Atucha 1 was not operated as a base loaded plant, so it was usual to cycle power according to the electrical power output demand. As an example of this, the evolution of global power from June 11th to June 14th 1985 is shown in the figure below (Figure 1).

On June 14th of 1985 10 fuel elements failed owing to PCI/SCC as a consequence of a severe power transient. In order to perform the cycling maneuver shown in Figure 1, control rods were partially introduced in the upper half of the reactor. This movement of the control rods caused a misshaping of the axial power profile which produced local overpower on several fuel assemblies, reaching local linear heat rates over 600 W/cm, even though the global power was at worst scarcely over 100% Full Power.

An example of the distortions that took place during the transient is presented in Figure 2, which corresponds to the fuel element in channel J24 on June 14th of 1985 at 8:25 (14.9 hours after the beginning of the considered event). In this case, the maximum axial factor was over 1.8.

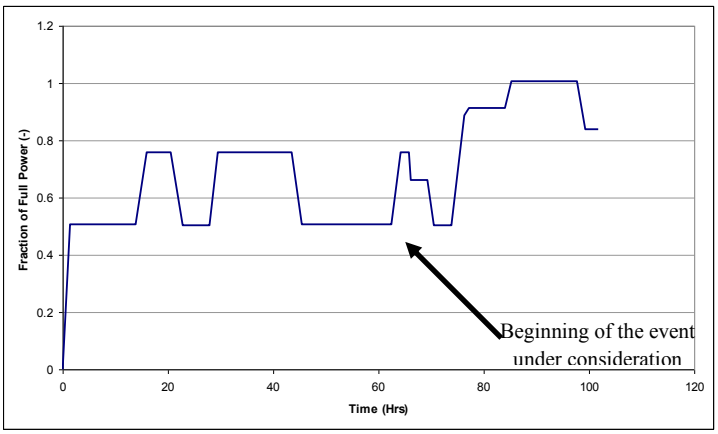

FIG. 1. Capacity factor as a function of time from June 11th to June 14th 1985.

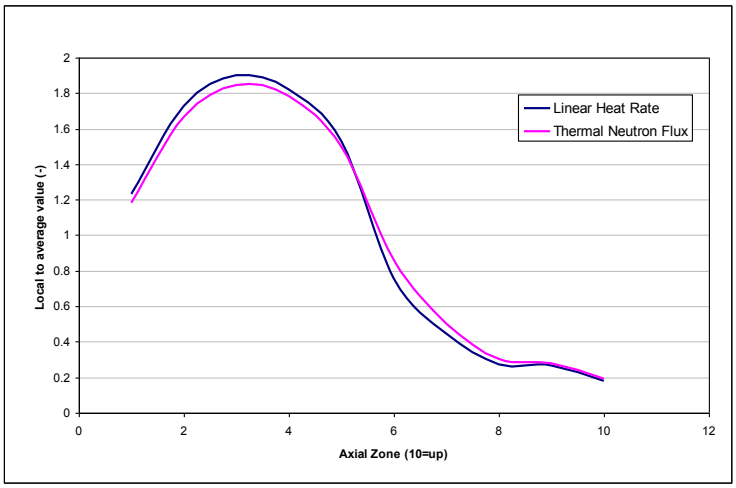

FIG. 2. Thermal neutron flux and linear heat rate of channel J24 14.9 hours after the beginning of the transient.

3. DESCRIPTION OF TRANSURANUS PCI/SCC MODEL

TRANSURANUS is a computer program for the thermal and mechanical analysis of fuel rods in nuclear reactors [1]. It is widely used in the industry for fuel rod design, and for the simulation of normal, off-normal and accident conditions such as LOCA and RIA.

Within TRANSURANUS code, SPAKOR is the subroutine that predicts PCI/SCC failure [1]. It is based mainly on the model developed by Mattas, Yangee and Neimark [2]. The model considers that these kind of failures start as an intergranular fracture, which is caused

independent on the applied stress. At some point of its growth the crack becomes a 'cleavage and flutting' fracture and it can be described by linear elastic fracture mechanics.

One strong supposition of the model is that crack growth initiates if all the following conditions are fulfilled: burnup must exceed a critical value (called ABKRIT and equal to 5000 MWd/tU), cladding temperature must exceed 270ºC, hoop stress in the cladding must be positive and strain rate of the cladding must exceed a temperature dependant critical strain. During the intergranular phase, crack growth rate is assumed to decrease exponentially with crack length, until a critical length is reached, that depends on cladding hoop stress and on the threshold stress intensity factor for SCC (KISCC). At this point, the 'cleavage and fluting' phase starts and proceeds up to failure, that takes place if the crack length exceeds either the cladding wall thickness, or the length at which the net section stress exceeds a rupture strength (σ_{rs}^{SPAKOR}). For the evaluation of KISCC the following simple correlation is adopted:

$$K_{ISCC}\left[MPa \cdot m^{1/2}\right] = 24.5 - 0.0325\sigma_{ys}^{SPAKOR} \qquad (1)$$

Where σ_{ys}^{SPAKOR} is thezxx cladding yield strength (in MPa). It is worth noting that Zircaloy properties (yield strength and rupture strength) used in SPAKOR are fitted parameters of the model, for which the approximate values: $\sigma_{ys}^{SPAKOR} = 560\ MPa$ and $\sigma_{rs}^{SPAKOR} = 690\ MPa$ are used.

4. TRANSURANUS MODEL AND CALCULATION METHOD

4.1. Input data for TRANSURANUS code

The fuel rod consists of a stack of natural UO_2 sintered pellets, of compensation pellets in Al_2O_3, a supporting tube and a compression spring. Everything is placed into a Zircaloy-4 (stress relieved) cladding tube. The main fuel data are summarized in Table 1.

TABLE 1. CNA 1 FUEL DATA

Fuel Assembly	Value/description	
Number of Fuel Assemblies in the reactor	251	
Number of Fuel Rods per FA	36	
Fuel Pellet	**Value/description**	**Unit**
Material	UO_2	
Density	10.55 ±0.15	g/cm^3
U/O ratio	0.0711	at/at---
Pellet diameter	10.62	mm
Pellet length	12 ±1	mm
Number of pellets	441	---
Enrichment	0.00711	g/gHM
Volume of dishing per pellet	21 ±5	mm^3
Cladding		
Material	Zircaloy-4	---
Density	6.6 10^3	kg/m^3
Otuside Diameter	11.9	mm
Inside Diameter	10.8	mm
Fuel Rod		
Total Length	5557.2 ±1.4	mm
Active Length	5300	mm
Pellet/Cladding gap thickness	0.09	mm
Gas plenum length	212	mm

Fill gas	Helium	---
Fill gas pressure	2.25	MPa (abs)

The active length of the fuel rod is divided into 10 axial segments, called 'slices' (Figure 3). In TRANSURANUS code, the analysis is performed slice per slice starting from slice No. 1 up to slice No. 10. An additional slice is modeled to consider the gas plenum volume. To account for the additional structures in the upper plenum, a user supplied factor is considered (AOPL factor). The fuel pellet dishing is accounted for as well (PRODIS factor). For the radial discretization, the fuel and the cladding are divided into 6 rings (called 'coarse zones'), 5 for the fuel and 1 for the cladding, in which the elasticity modulus E and Poisson's number are constants. These rings are further subdivided into 94 so called 'fine zones' in which numerical integration is performed.

The boundary conditions implemented in TRANSURANUS v1m1j11 code are as follows: (1) linear heat rate (LHR) at ten axial positions as a function of time; (2) coolant temperature at inlet of the channel (one value); (3) heat transfer coefficient (one value); (4) fast neutron flux at the same positions of the LHR as a function of time; and (5) pressure (one value). The source of the used data is presented in the following sections. The methodology is similar to that presented in [3-5].

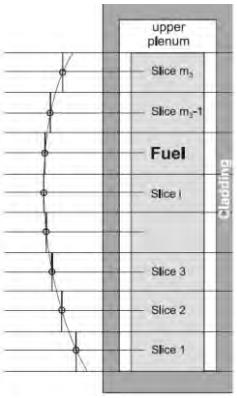

FIG. 3. Schematic representation of the axial discretization in TU code.

4.2. Atucha 1 Fuel Management Overview

The CNA-1 reactor has on-power refuelling that is performed by a refuelling machine. In general, there is just one refuelling path which depends upon burnup (Tabale 2, Figure 4). Fresh fuel enters zone 2, stays until a transition burnup is reached (see Table 2), moves to 1 (central zone), stays until a transition burnup, moves to 3 and stays there until it reaches the exit burnup and leaves the core (see Figure 4). Being this path the one followed by most fuel elements, there are some exceptions that were not considered here.

TABLE 2. MOVEMENTS FOR BURNUP MANAGEMENT

Zone	Shuffling Burn up [MWd/tU]
2 → 1	2770
1 → 3	5100
3→Pools	6000

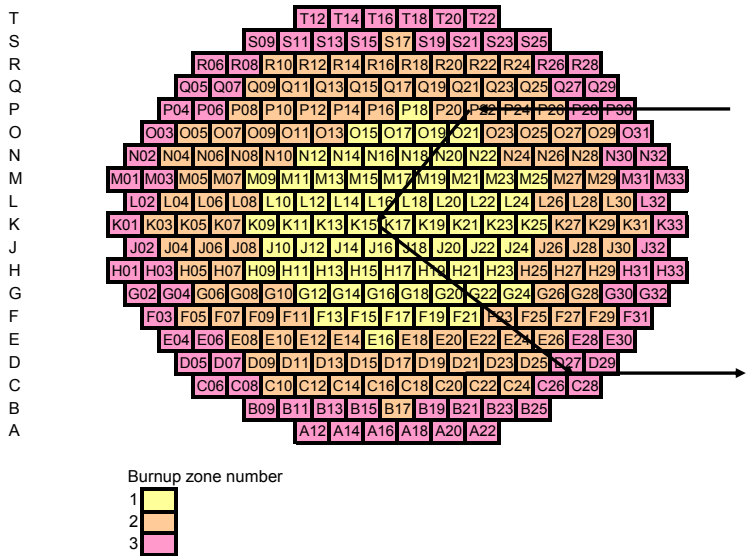

FIG. 4. CNA-1 burnup zones for fuel management.

4.3. Base irradiation

When codes are validated against experimental data, measurements on Linear Heat Rate, system pressure, temperature, etc are available for the input preparation. Given the fact that this simulation is based on an actual occurrence, only some of these data are available. Thus it is necessary to make best-estimate considerations to build up the previous irradiation history of each of the modeled fuel pins, in order to achieve the burnup that we estimate correct at the beginning of the studied transient.

To start with, power is not measured locally on each fuel assembly in Atucha 1. Thus, the reactor state is calculated regularly by using a neutronic code called PUMA and a model of the complete core. This calculation is performed approximately every 2 full power days which have been carefully recorded since the start of the plant operation, and were made available for the present analysis.

To correctly model the state of the fuel pin at the beginning of the transient, it was very important to achieve the correct average burnup. This information was taken from fuel management forms that the operators record every time a fuel bundle is introduced, shuffled or taken out of the core. The position in the core and the time at which the FA is placed there, given as full power days, are recorded in those forms. The Fuel Bundle inlet and outlet average burnup could then be tracked from the PUMA outputs already mentioned.

With all these data, average Linear Heat Rate for each location in the core was calculated according to the following equations:

$$\Delta bu_{MPR}(z_i) = \frac{\bar{q}'^{\,MPR}_{CHj}(z_i)}{m_l \cdot c_f} \cdot \Delta dfp_{CHj} \Rightarrow \bar{q}'^{\,MPR}_{CHj}(z_i) = \frac{\Delta bu_{MPR}(z_i)}{\Delta dfp_{CHj}} \cdot m_l \cdot c_f \quad (2)$$

$$\Delta bu_{MPR}(z_i) = \Delta bu_{PUMA}(z_i) \cdot f \quad (3)$$

Where:

$\bar{q}'^{\,MPR}_{CHj}(z_i)$: average linear heat rate per axial slice of the rod submitted to the maximum power in channel j

$\Delta bu_{MPR}(z_i)$: burnup difference per axial slice between the outlet and the inlet of the fuel bundle to the channel j

Δdfp_{CHj} : full power days between the outlet and the inlet of the bundle to the channel j.

m_l : mass per unit length

c_f : capacity factor (% Full Power)

$\Delta bu_{PUMA}(z_i)$: burnup difference for an axial slice between the outlet and the inlet of the fuel bundle to the channel j, reported in PUMA calculation output.

f : factor which takes into account the radial peak factor, the 5% of power dissipated in the moderator, the tolerances and the structural tube factor.

Capacity factors c_f were extracted from graphics of percentage of full power as a function of time (Figure 1), while constant values of 11.5 MPa for coolant pressure, 278 ºC for coolant inlet temperature were used. This type of thermal boundary condition for the cladding was selected because only coolant inlet data was available for steady state plant conditions. The value for the Heat Transfer Coefficient was considered to be constant for each of the hydraulic zones of the core in which the considered FA was placed, which was a good approximation according to full plant steady state RELAP 5 thermohydraulic calculations, from which input values were taken.

4.4. Power transient

Given that the above mentioned neutronic calculations did not provide an adequate level of detail of the boundary conditions during the power transient, a new PUMA calculation was performed starting from the equilibrium burnup at the beginning of it, and covering the 21 hours it lasted. Thus, linear heat rate, neutron flux and burnup profiles were obtained at least once every hour throughout the simulation time span.

TRANSURANUS requires inputting the fast neutron flux as a function of time, while PUMA provides total neutron flux. To determine the fast neutron flux, a direct relation to total neutron flux and power at the beginning of the transient was used, following a calculation method provided in [6]:

As an example, Figure 5 shows the Linear Heat Rate for the simulated fuel rod in channel J24. A zoom of the power transient zone is to be seen. Table 3 includes further information for all analyzed pins. The location of the analyzed rods in the core is shown in Figure 6 [7].

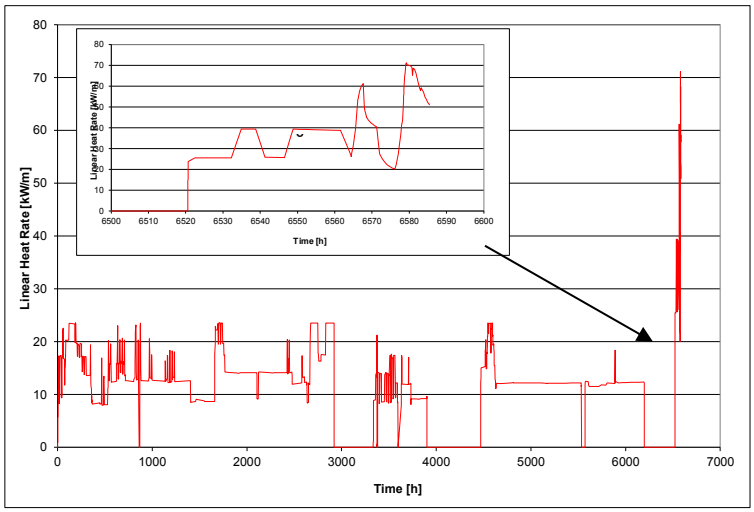

FIG. 5. Linear heat rate as a function of time for the simulated fuel rod in channel J24.

TABLE 3. BOUNDARY CONDITIONS FOR STUDIED RODS

Channel	State after event	Average BU [MWd/tU]	q' Conditioning [W/cm]	ΔLHR [W/cm]	Maximum LHR [W/cm]	Max. Ramp Rate [W/cm·h]
E18	NF	3214	374.2	287.1	661.3	168.26
E20	NF	2179	375.1	296.3	671.4	183.90
F17	NF	4986	372.3	274.0	646.3	141.55
F21	NF	5123	369.1	292.1	661.2	173.84
G18	NF	5127	370.9	269.6	640.5	162.41
G20	NF	3609	388.0	296.5	684.5	183.06
G22	NF	5057	372.4	295.7	668.1	178.13
G24	NF	3373	376.4	306.6	683.0	182.98
H17	NF	4617	354.9	238.9	593.8	128.17
H21	NF	5487	367.0	281.5	648.5	167.92
H25	NF	230	368.2	301.7	669.9	178.46
J18	NF	4162	336.3	226.6	562.9	132.41
J26	NF	2745	371.7	305.3	677.0	182.24
K19	NF	5502	321.2	225.2	546.4	129.32
K21	NF	3157	374.4	279.8	654.2	170.22
K23	NF	4735	377.7	296.7	674.4	178.75
K25	NF	3405	381.6	309.4	691.0	197.91
L20	NF	4588	348.4	250.3	598.7	144.10
L26	NF	2199	367.6	299.9	667.5	185.08
M21	NF	5106	359.3	267.2	626.5	158.14
M25	NF	3509	365.3	294.0	659.3	178.95
N16	NF	3637	368.8	242.1	610.9	112.41
N18	NF	5408	353.4	243.2	596.6	138.14
N22	NF	3184	377.3	289.4	666.7	176.81
N24	NF	3213	367.6	291.7	659.3	180.72
O15	NF	2891	382.4	259.1	641.5	161.68
O19	NF	4988	357.5	259.3	616.8	154.03
P16	NF	241	358.2	253.0	611.2	153.13
P18	NF	3374	362.5	263.2	625.7	162.16
F19	F	3193	389.0	297.8	686.8	164.30
H19	F	4351	367.4	266.0	633.4	154.76
H23	F	4552	380.1	303.7	683.8	186.67
J20	F	4624	360.0	263.5	623.5	158.42
J22	F	3485	384.7	298.4	683.1	157.41
J24	F	2785	393.9	317.1	711.0	200.19
L22	F	3844	377.6	288.8	666.4	170.11
L24	F	4649	372.4	296.4	668.8	178.92
M23	F	4998	367.7	287.0	654.7	172.29
O17	F	4474	368.2	256.4	624.6	148.12

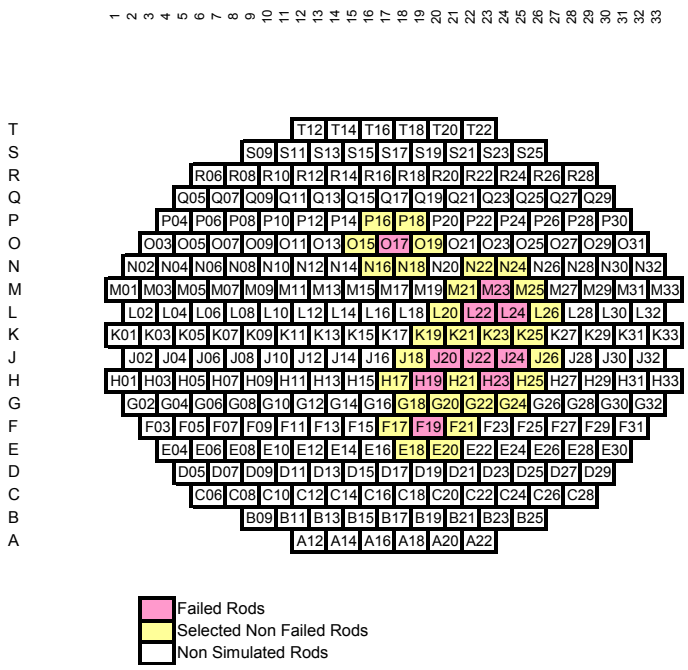

FIG. 6. Location of analyzed channels.

5. RESULTS

5.1. Standard TRANSURANUS case

A first set of calculations was made using the version v1m1j11 of TRANSURANUS code as-delivered. Results have been presented in Table 4 and Table 5 (case TU STD). In the first one, the total amount of right predictions of the code for rods that have failed or remained sound at the end of the event is presented. Table 5 shows a detailed failure/non failure result list, together with sensitivity tests results presented in the following section.

TABLE 4. SUMMARY OF RESULTS

Case		ABKRIT	SigmaY, SigmaR and E	IHGAP	IRELOC	ncracks	fine zones	Correct predictions of failed rods	Correct predictions of non-failed rods	Total number of correct predictions	Total number of calculated failed rods
TU STD		5000	TU	0	8	6	94	0/10	24/29	24	5
1	A	3000	TU	0	8	6	94	1/10	17/29	18	13
	B	0	TU	0	8	6	94	1/10	16/29	17	14
2	A	0	TU	0	2	6	94	2/10	20/29	22	11
	B	0	TU	0	5	6	94	1/10	28/29	29	2
3	A	5000	CNA1	0	8	6	94	3/10	22/29	25	10
	B	0	CNA1	0	8	6	94	7/10	15/29	22	21
4	A	0	CNA1	3	8	6	94	7/10	15/29	22	21
	B	0	CNA1	4	8	6	94	7/10	15/29	22	21
5	A	0	CNA1	0	2	6	94	7/10	14/29	21	22
	B	0	CNA1	0	5	6	94	7/10	15/29	22	21
6	A	0	CNA1	0	8	4	94	10/10	6/29	16	33
	B	0	CNA1	0	8	8	94	0/10	25/29	25	4
7		0	CNA1	0	8	6	120	7/10	15/29	22	21
8		0	CNA1	4	5	8	94	0/10	29/29	29	0
9		0	CNA1	0	5	4	94	8/10	7/29	15	30
10		0	CNA1-B	0	8	6	94	1/10	20/29	21	10

TABLE 5. DETAILED RESULTS OF CALCULATED CASES. GRAY-COLOURED CHANNELS (FROM F19 TO O17) INDICATE FAILED RODS DURING THE REAL EVENT. F=FAILED; NF=NON FAILED

Channel Nr.	Real Rod	TU STD.	1A	1B	2A	2B	3A	3B	4A	4B	5A	5B	6A	6B	7	8	9	10
E18	NF	NF	F	F	F	NF	NF	F	F	F	F	NF	F	NF	F	NF	F	F
E20	NF	NF	NF	NF	NF	NF	NF	NF	NF	NF	NF	NF	F	NF	NF	NF	F	NF
F17	NF	F	F	F	F	NF	F	F	F	F	F	NF	F	F	F	NF	F	F
F21	NF	F	F	F	F	NF	F	F	F	F	F	NF	F	F	F	NF	F	NF
G18	NF	F	F	F	F	NF	F	F	F	F	F	NF	F	NF	F	NF	F	F
G20	NF	NF	F	F	NF	NF	NF	F	F	F	F	F	F	NF	F	NF	F	NF
G22	NF	F	F	F	NF	NF	F	F	F	F	F	NF	F	F	F	NF	F	NF
G24	NF	NF	F	F	F	NF	NF	F	F	F	F	NF	F	NF	F	NF	F	NF
H17	NF	NF	NF	NF	NF	NF	NF	NF	NF	NF	NF	NF	NF	NF	NF	NF	NF	NF
H21	NF	NF	NF	NF	F	NF	F	F	F	F	F	NF	F	NF	F	NF	F	F
H25	NF	NF	NF	NF	NF	NF	NF	NF	NF	NF	NF	NF	NF	NF	NF	NF	NF	NF
J18	NF	NF	NF	NF	NF	NF	NF	NF	NF	NF	NF	NF	NF	NF	NF	NF	NF	NF
J26	NF	NF	F	F	NF	NF	NF	F	F	F	F	NF	F	NF	F	NF	F	F
K19	NF	NF	NF	NF	NF	NF	NF	NF	NF	NF	NF	NF	NF	NF	NF	NF	NF	NF
K21	NF	NF	NF	NF	NF	NF	NF	NF	NF	NF	NF	NF	F	NF	NF	NF	F	NF
K23	NF	F	F	F	F	NF	F	F	F	F	F	F	F	NF	F	NF	F	F
K25	NF	NF	F	F	F	NF	NF	F	F	F	F	NF	F	NF	F	NF	F	F
L20	NF	NF	NF	NF	NF	NF	NF	NF	NF	NF	NF	NF	NF	NF	NF	NF	NF	NF
L26	NF	NF	NF	NF	NF	NF	NF	NF	NF	NF	NF	NF	F	NF	NF	NF	F	F
M21	NF	NF	F	F	NF	NF	F	F	F	F	F	NF	F	NF	F	NF	F	NF
M25	NF	NF	NF	NF	NF	NF	NF	NF	NF	NF	NF	NF	F	NF	NF	NF	F	NF
N16	NF	NF	F	F	F	F	NF	F	F	F	F	F	F	F	F	NF	F	F
N18	NF	NF	NF	NF	NF	NF	NF	NF	NF	NF	NF	NF	F	NF	NF	NF	NF	NF
N22	NF	NF	NF	NF	NF	NF	NF	NF	NF	NF	F	NF	F	NF	NF	NF	F	NF
N24	NF	NF	NF	NF	NF	NF	NF	F	F	F	F	NF	F	NF	F	NF	F	NF
O15	NF	NF	NF	NF	NF	NF	NF	NF	NF	NF	NF	NF	F	NF	NF	NF	F	NF
O19	NF	NF	NF	NF	NF	NF	NF	NF	NF	NF	NF	NF	F	NF	NF	NF	NF	NF
P16	NF	NF	NF	NF	NF	NF	NF	NF	NF	NF	NF	NF	NF	NF	NF	NF	NF	NF
P18	NF	NF	NF	NF	NF	NF	NF	NF	NF	NF	NF	NF	F	NF	NF	NF	NF	NF
F19	F	NF	NF	NF	NF	NF	NF	F	F	F	F	F	F	NF	F	NF	F	NF
H19	F	NF	NF	NF	NF	NF	NF	NF	NF	NF	NF	NF	F	NF	NF	NF	F	NF
H23	F	NF	NF	NF	NF	NF	NF	F	F	F	F	F	F	NF	F	NF	F	NF
J20	F	NF	NF	NF	NF	NF	NF	NF	NF	NF	NF	NF	F	NF	NF	NF	NF	NF
J22	F	NF	NF	NF	NF	NF	NF	F	F	F	F	F	F	NF	F	NF	F	NF
J24	F	NF	F	F	F	F	NF	F	F	F	F	F	F	NF	F	NF	F	F
L22	F	NF	NF	NF	NF	NF	F	F	F	F	F	NF	F	NF	F	NF	F	NF
L24	F	NF	NF	NF	F	NF	F	F	F	F	F	NF	F	NF	F	NF	F	NF
M23	F	NF	NF	NF	NF	NF	F	F	F	F	F	NF	F	NF	F	NF	F	NF
O17	F	NF	NF	NF	NF	NF	NF	NF	NF	NF	NF	NF	F	NF	NF	NF	NF	NF

As it can be seen, none of the failed fuel rods was predicted failed while 24 out of 29 of the sound rods were predicted correctly. Owing to this, the need to improve SPAKOR results was identified. The study of the model's parameters as well as the adaptation of material properties to CNA-1 specific ones was performed, following an approach similar to that presented in [8].

5.2. Sensitivity analysis performed

5.2.1. ABKRIT

Previous calculations and analysis for Atucha-type fuels, had demonstrated that ABKRIT parameter presented in Section 4.1, has a strong influence in results. Fuels have a very low exit burnup in PHWR-natural uranium reactors, compared to exit burnup of PWRs and BWRs. Owing to the fact that ABKRIT=5000 MWd/tU is relatively near to the exit burnup for CNA-1 fuels, and PCI failure cannot occur if burnup is lower than ABKRIT, the percentage of fuel rods that would be assessed by SPAKOR subroutine in a whole-core analysis would be very low. To force the code to enter in this subroutine independently of Burnup-level, ABKRIT was modified to be zero.

Tables 4 and 5 (Case 1-B), show that the number of total predicted failures for this case increases considerably. Results obtained with an intermediate value of ABKRIT=3000 are also presented (Case 1-A). It is observed that the influence of partially lowering the critical burnup value from 3000 MWd/tU to 0 MWd/tU is almost negligible.

5.2.2. Pellet fragments relocation model

TRANSURANUS has 6 different Relocation Models, of which 3 were identified to be suitable for CNA-1 Fuel Type. Recommended models are IRELOC 8 (Modified FRAPCON-3 Model) and 5 (Modified KWU-LWR Model- ITU Calibration), of which the first one was chosen for the Base Case (TU STD Case). For this sensitivity, also IRELOC 2 (Original KWU-LWR model) has been assessed. Results in Table 4 show that changes in IRELOC have a stronger influence in cases with TRANSURANUS-SPAKOR original Yield and Rupture strength values (see Section 7.2.3), than in cases with CNA-1 values. In the former, the failure threshold is elevated by changing from IRELOC 8 to 2 to 5 (Cases 1-B, 2-A and 2-B), while in the latter, changes in IRELOC have almost no influence on results (Cases 3-B, 5-A and 5-B). This suggests that relocation models play a more important role when SPAKOR rupture and yield strengths are set to higher values.

5.2.3. Material properties

Young's modulus of elasticity of Zircaloy for CNA-1 material is temperature dependent and follows the following relation:

$$E(T) = 99404 - 65.4 * T \tag{4}$$

Where:

$E = \text{Young Modulus}(\text{N/mm}^2)$

$T = \text{Temperature}(^{\circ}\text{C})$

According to Figure 7 there is a discrepancy to the Young Modulus equation implemented in TU code of about 700MPa at room temperature.

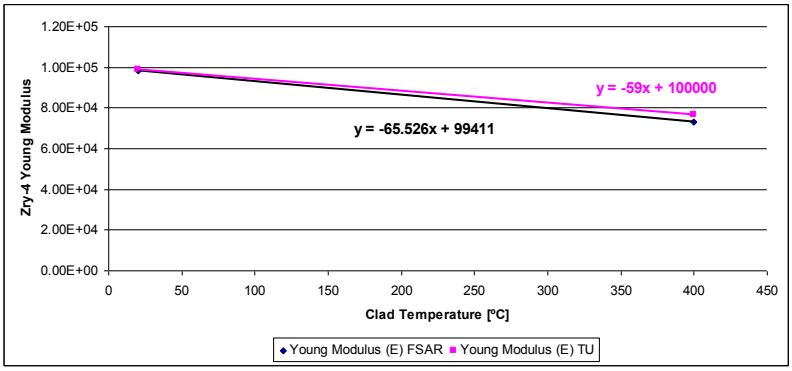

FIG. 7. Young's Modulus of Elasticity of Zircaloy for Atucha fuels and as implemented in TRANSURANUS.

According to fuel vendor, Strengths of Zircaloy-4 of Atucha Fuels [9] are the ones reported in Table 6. In between those values, linearity is assumed.

TABLE 6. YIELD AND RUPTURE STRENGTHS OF ATUCHA FUEL ZIRCALOY-4

Yield Strength	
≥ 350 N/mm^2	at room Temperature (20ºC)
200 to 300 N/mm^2	at 400ºC
Rupture Strength	
≥ 480 N/mm^2	at room Temperature (20ºC)
≥ 270 N/mm^2	at 400ºC

In SPAKOR subroutine, model fitted parameters known as Yield and Rupture Stress have a constant value of $\sigma_{ys}^{SPAKOR} = 560\ MPa$ and $\sigma_{rs}^{SPAKOR} = 690\ MPa$ respectively. After observing the difference in SPAKOR parameters and Yield and Rupture Strengths reported for Atucha fuels, the idea arose that these model parameters could be updated to the available data. Therefore an Atucha-fitted version of the code was compiled, adapting Young Modulus and Yield and Rupture Stress in SPAKOR subroutine to the previously mentioned values.

Results obtained can be seen in Tables 4 and 5. Cases 3 to 9 (identified as SIGMA-CNA1) have been run using this modified executable, obtaining in general a higher number of predicted failed rods, as it was expected.

5.2.4. Gap conductance model

Pellet-cladding gap heat transfer coefficient is the limiting resistance in heat transfer from the pellet periphery to the cladding outer surface. Therefore it influences the temperature profile and all the dependant models upon it. Gap conductance model incorporated in TRANSURANUS code is the well documented URGAP model (1979), revised and recalibrated in 1986. Among the four available options for gap conductance models (IHGAP), IHGAP=0 is the recommended option (Gas Bonding thermal conductivity of mixture according to Lindsay and Bromeley, in which accommodation coefficients are taken into account). For the sensitivities IHGAP=3 (Case 4-A) (as standard option but without considering accommodation coefficients) and IHGAP=4 (Case 4-B) (specific model option gas bonding, thermal conductivity of mixture according to Tondon and Saxena – accommodation coefficients taken into account) were tested. Table 4 shows that changing the IHGAP model does not affect results for the burnup and linear heat rates studied here.

5.2.5. Number of cracks in the fuel

In TRANSURANUS the number of cracks in which fuel pellet is divided is an input parameter. To input six cracks is recommended. Nevertheless, the influence of this arbitrary number was studied by making two sensitivities: four (Case 6-A) and eight (Case 6-B) cracks were considered. As it can be derived from Table 4, the lower the number of cracks the higher the amount of failed rods calculated, and vice versa. Results obtained for eight cracks (Case 6-B and 8) were discarded because the failure threshold resulted so high that almost no fuels were predicted failed.

5.2.6. Number of mesh points

The number of mesh points was studied by increasing the number of fine zones mentioned in Section 6.1 (94 mesh points) to the maximum possible number, that is to say, 20 per each radial zone (120 in total). This modification has shown no change on the obtained results (see Table 4 - Case 7 vs 3-B).

5.2.7. Effect of combined sensitivities

The effect of combining the simultaneous change of the previously studied parameters is shown for cases 8 and 9 in Table 5. Setting IRELOC=5 rises the failure threshold, as well as increasing the number of cracks to 8. The combined effect of both changes resulted as expected in a major increase of the failure threshold, that is to say, a lower amount of failed fuel rods (Case 8 vs 3-B). On the other hand, setting the number of cracks to four showed to have a stronger influence in increasing the number of failed rods, than the effect of setting IRELOC=5 (Case 9 vs. 6-B and Case 9 vs. 5-A).

As none of these parameters combinations resulted in a considerable increase of correctly predicted results, they were discarded as the selected base case.

5.2.8. Updated mechanical properties

Later in time during the assessment, results from burst tests were provided by the fuel vendor. It was then discussed that due to the formulation of SPAKOR model equations, a burst stress would better represent the yield and rupture strengths used in the model, than the available ones from the FSAR, obtained from traction tests (Table 6). A new case number 10 was run, setting the yield strength of SPAKOR to $\sigma_{ys}^{Burst-CNA2} = 250\ MPa$ and the rupture stress to $\sigma_{rs}^{Burst-CNA2} = 333\ MPa$. If Cases 3B and 10 are compared, the total number of failed rods is lower in case 10, as expected, due to the use of higher yield and rupture strength limits.

5.3. Selected Cases

Cases 3 B and 10 have been selected to be the most suitable set of input parameters and source code modifications for Atucha-type fuels for best estimate analysis, because of the reasonably good results obtained, especially regarding the fact that IRELOC, nCracks and IHGAP match either the standard values or the ones recommended by the code manual. Also some SPAKOR model parameters related to Zircaloy-4 Material Properties have been fitted to available Atucha fuel values. The adaptation of Material Properties (Young Modulus in this case) to analyzed fuel-specific values is also in line with the recommended practice.

For Case 3B, the amount of correctly predicted failures is as high as 70%. For the non-failed rods on the other hand, an important overprediction of failures was observed (48%), however it was considered to be conservative. On the other hand, Case 10 showed almost the same total correct predictions than Case 3B, but the total number of failed rods was 10, exactly as those in the real event.

In Table 5, some of the lines have been shadowed in colours. These lines identify fuel rods that consistently presented the same failure/non failure result, regardless of the case being calculated. This suggests that the results in these cases strongly depend on boundary conditions and not in models selections or modifications made to the code. As it has been previously mentioned, there were many uncertain parameters needed for the set up of the base irradiation. In particular, neutronic calculations were redone only for the high power event being studied, and not for the whole irradiation history. Information coming from different input models thus considered could have lead to some misleading boundary conditions being calculated. TRANSURANUS code results had to be assessed then, taking into consideration this modelling limitation external to the code.

These uncertainties in the boundary conditions suggest that a Case calculating more accurately the total amount of failed rods is more suitable than one getting to predict right the failure of the real rods by also increasing the total amount of calculated failures. Adding the fact that SPAKOR model description suggests that *"Zircaloy properties (yield strength σ_{ys} and rupture strength σ_{rs}) need to be known precisely in order to apply the model correctly"* (Ref. [1]), it was concluded that Case 10 gave the most suitable results. The executable with the aforementioned modifications was selected to be used in future PCI assessment of Atucha-type fuels.

6. CONCLUSIONS

A thorough analysis of Atucha-type fuel behaviour related to PCI/SCC failure has been presented here. A real power transient that occurred during June 1985 has been modeled with TRANSURANUS code for 10 fuel rods that failed during the event, and for 29 adjacent rods that remained sound after the transient. The aim of the calculation was to evaluate failure/non-failure prediction capabilities of the code for low burnup natural uranium PHWR fuel rods.

A first set of calculations named as TRANSURANUS Standard Case was done with as-delivered TRANSURANUS Code. Given the low accuracy in failure/non-failure prediction, SPAKOR model was analyzed. A model-specific parameter (ABKRIT) was suited so that the code could account for PCI/SCC failure even for low burnup fuels. Also SPAKOR model parameters for Zircaloy-4 yield and rupture strengths were updated to values reported for CNA-1 Zircaloy cladding. With the so-fitted version of the subroutine, a series of sensitivity analysis was performed, in order to study the influence of pellet-cladding gap conductance model, fuel pellets fragments relocation models and number of cracks in the pellet. Also the number of mesh points used for the numerical integration in the code was changed to study the influence on results. A second executable with more rigorous material data was created leading to more satisfactory results.

After performing the sensitivities, it was confirmed that using the modified TRANSURANUS version of the code (setting ABKRIT to zero and SPAKOR yield and rupture values to CNA-1 specific ones, obtained in burst tests), and selecting standard or recommended models for the studied parameters led to reasonably good results. Selected Case 10, showed an exact prediction of the total amount of failed rods while the number of total correct predictions was very similar than that obtained for other cases.

It is also important to point out that only the failure or non-failure of fuel rods was assessed after the transient. In the reality, no measure of how close the sound fuel rods were to failure was available, so many of the 29 selected non-failed fuel rods could have been very close to failure even though this condition was actually not reached. A very slight change in boundary conditions considered for the calculations presented here, could have been strong enough to shift the prediction of the code in many of the sensitivity cases here analyzed.

In relation to this, and due to the lack of availability of on-line measurements for many of the boundary conditions (pressure and temperature of coolant, etc), many sources of uncertainties were identified:

- Burnup at the beginning of the transient.
- Local linear heat rate and neutron fast flux (for the previous irradiation history)
- Fuel characteristics that influence in results: grain size of UO_2; mechanical properties of Zircaloy-4; thermal properties of Zircaloy and UO_2

By taking into consideration that there were many uncertainties in the boundary conditions used for the calculations, it was concluded that a case calculating more accurately the total amount of failed rods is more suitable than one getting to predict right the failure of the real rods by also conservatively increasing the total amount of calculated failures.

As the above mentioned uncertainties are at the present impossible to avoid, an extension of the work presented here has been identified. In the first place a statistical study of the complete-core is projected, in order to assess the influence of boundary conditions and fabrication tolerance of some relevant parameters. At last, the influence of simplifying assumptions in input data such as thermohydraulic boundary conditions will be further

analyzed, given the fact that no experimental measurements are available apart from the failed/non failed condition of the studied rods.

ACKNOWLEDGEMENTS

Special thanks to Dr. Daniel Roqueta, who performed the neutronic calculations with PUMA Code, and to Eng. Miguel A. Schivo and Eng. Gustavo Salom, who collaborated in the analysis of results and the understanding of the physical phenomena involved. The authors also wish to thank Paul Van Uffelen and Arndt Schubert (TRANSURANUS developer's team) for the fruitful discussions and the helpful technical support.

REFERENCES

[1] LASSMANN, K., SCHUBERT, A., VAN UFFELEN, P., GYORY, CS., VAN DE LAAR, J., TRANSURANUS Handbook, version *v1m1j11*, JRC, EC, ITU, January 2011.

[2] MATTAS, R.F., YAGGEE, F.L., NEIMARK, L.A., Iodine stress-corrosion cracking in irradiated zircaloy cladding, Light Water Reactor Fuel (Proc. Topical Meeting, Portland, Oregon (1979) , American Nuclear Society) CONF-790441-7.

[3] ADORNI, M., DEL NEVO, A., D'AURIA, F., MAZZANTINI, O., A Procedure to Address the Fuel Rod Failures during LB-LOCA Transient in Atucha-2 NPP, Science And Technology of Nuclear Instalations – Nuclear Activities in Argentina – 2010; HINDAWI Volume 2011, Article ID 929358.

[4] ADORNI, M., Methodology for the Analysis of Fuel Behaviour During LOCA and RIA, PhD Thesis in Nuclear Engineering, Department of Mechanics, Nuclear and Production Engineering, University of Pisa, Pisa (I), June 10, 2011.

[5] ADORNI, M., DEL NEVO, A., D'AURIA, F., Methodology for the analysis of fuel behaviour during LOCA and RIA for licensing purposes, ICONE20-POWER2012-54698, August 2012.

[6] ROQUETA, D., SALOM, G., SCHIVO, M., Historias de irradiación de las barras combustibles en condiciones desfavorables durante transición BOL-BEQ, Informe de Trabajo LN-BN-000074, 01/11/2010, Nucleoeléctrica Argentina (Internal Report).

[7] FERRERI, A., SIDELNIK, J., GRANT, C. et al., Simulación del transitorio de potencia ocurrido en la CNA-1, el 14/6/85. Tomando en cuenta la dependencia espacial del Xenón, Informe de Trabajo 1114/86 –CNEA – Dirección de Centrales Nucleares (Internal Report).

[8] ROZZIA, D., ADORNI, M., DEL NEVO, A., D'AURIA, F., Capabilities of TRANSURANUS code in simulating power ramp tests from the IFPE database, Nuclear Engineering and Design 241 (2011) 1078-1086.

[9] Final Safety Analysis Report (FSAR) CNA2 - Chapter 4.2: Fuel Safety Design. Rev.0.

HIGH BURNUP MODELS INCORPORATED TO THE DIONISIO CODE

A. SOBA, M. LEMES, GONZÁLEZ, M.E., A. DENIS

Gerencia Ciclo del Combustible Nuclear, Comisión Nacional de Energía Atómica (CNEA), Centro Atómico Constituyentes (CAC), Buenos Aires, Argentina

Abstract. Due to the extension of the permanence time of the nuclear fuels within the reactor, physical and chemical modifications take place in the fuel material, especially in the external ring of the fuel pellet. The codes for simulating the rod behaviour during reactor operation need adequate models to describe these phenomena and be capable of making accurate predictions in the whole burnup range. A complex group of subroutines has been included in DIONISIO to represent the radial distribution in the pellet of the power density, burnup, porosity and concentration of diverse nuclides, particularly those capable of undergoing fissions, in terms of overall parameters like initial enrichment and average burnup. In this work we summarize the models recently developed, related to the high burnup scenario. On the one hand, empirical expressions representing the absorption and capture cross sections of several uranium and plutonium isotopes, as functions of the initial enrichment in ^{235}U, average burnup and radial coordinate are presented. In addition, new models that give the distribution of porosity, fission gas retention and release in the pellet edge are described. Moreover, an empirical formula that relates the thermal conductivity of the fuel material with the burnup and the content of gadolinium, usually added as burnable poison, is presented. Subroutines corresponding to each of these models have been incorporated to the DIONISIO code. With these improvements the code was used to simulate data provided by the FUMEX I/II/III NEA data bank. The results presented here make evident the good agreement between experiments and simulations.

1. INTRODUCTION

When the residence time of the nuclear fuel rods is increased beyond a given level, several properties of the pellet material (usually uranium oxide) suffer changes which need to be adequately represented by the simulation tools. A threshold of about 40-45 MWd/kgHM for the average burnup can be established on an empirical basis for the manifestation of the first signs of the high burnup structure. Beyond this threshold some distinctive features of the structure progressively develop: small grains and large pores as compared with those of the original material, absence of Xe from the solid lattice (although it continues to be dissolved in the rest of the pellet). The porous microstructure at the pellet edge deteriorates the thermal conductivity [1, 4] and the mechanical integrity of the pellet. The inclusion in DIONISIO of the subroutines dedicated to the simulation of the microstructural aspects of the rim region was reported elsewhere [2, 3].

It is accepted nowadays that the source of these transformations are the resonant peaks of the absorption cross section of ^{238}U and the consequent chains of nuclear reactions that give birth to several Pu isotopes. Among them, ^{239}Pu and ^{241}Pu, of fissile character, increase the fissions density, particularly in the pellet rim. As a result, the power generation rate and the burnup increase radially towards the outer boundary and for sufficiently high burnup levels can reach local values two or three times higher at this ring than in the rest of the pellet [4].

A detailed analysis of the aspects described above demands the formulation of the balance equations of all the isotopes that are created and destroyed during the irradiation process, in the whole neutron energy range involved. This is the formidable task of the codes specialized in reactor physics. Codes like WIMS-E [5, 6], HELIOS [7, 8], CONDOR [9] and HUEMUL [10] solve the Boltzmann transport equations [11] in a number of energy intervals (typically 69 energy groups), and include adequate considerations in the region of the resonant absorption peaks of ^{238}U. They predict with high precision the radial distribution of neutron flux, burnup and concentration of every isotope, fissile, fissionable or fertile, gaseous or solid, within the rod, relevant to the overall process, all of them as functions of time. But a

fuel performance code, designed to describe the large number of thermomechanical and thermochemical processes within the fuel rod, cannot include such a detailed description. To avoid these difficulties but without losing the required completeness, a simplified treatment was proposed in the past consisting in limiting the analysis to the more abundant isotopes and reducing the energy spectrum to a single group. The first antecedent in this type of analysis is found in the RADAR model [12] which was validated against the WIMS code. The present work is inspired by the models RAPID [13] and TUBRNP, the latter included in the TRANSURANUS code [14].

In this work the predictions of the reactor cell codes HUEMUL and CONDOR were used as the basis on which empirical expressions were fitted to represent, with the higher possible approximation degree, the absorption, capture and fission cross sections of the more abundant isotopes of U and Pu: ^{235}U, ^{236}U, ^{238}U, ^{239}Pu, ^{240}Pu, ^{241}Pu and ^{242}Pu. These parameters were evaluated as functions of the initial enrichment in ^{235}U (in the range from natural uranium to 12%), the average burnup (from fresh fuel to 120 MWd/kgHM) and the radial coordinate, assuming a single energy group. A function to express the total flux as a function of the linear power, the enrichment and the flux of thermal neutrons within the pellet was also fitted. The curves so obtained were carefully tested via comparison with both reactor codes and then were incorporated to DIONISIO. A large number of experimental results were successfully simulated with the code thus improved. These results were reported in [3, 15].

Additionally, an expression to describe the burnup induced degradation of the thermal conductivity of UO_2 along the fuel operation time was recently elaborated. The formula also evaluates the conductivity of fuels with some content of Gadolinium in the range from 0 to 8wt%, which is the usual proportion in the UO_2 fuels with burnable poisons. The new model was firstly compared with conductivity experimental data and was then implemented into the DIONISIO code. Some results of this code aspect were reported in [16]. Moreover, empirical expressions representing the amounts of caesium, neodymium and xenon, mainly following K. Lassmann et al. [17, 18], were compared with experimental data and incorporated in DIONISIO as new subroutines.

These improvements together with the structural modifications described in a different work presented in this meeting gave origin to the new code version DIONISIO 2.0. The recently incorporated models, the calculation methods used and the separate verifications performed are summarized here. Moreover, a considerable number of experiments compiled in the IAEA data bases were simulated with the present code structure. The comparisons are also presented.

2. MODELS

2.1. One energy group calculations

The balance equations listed below relate the variation rate of the concentration N (atoms/cm^3) of each of the relevant isotopes considered in DIONISIO with the instantaneous value of the concentration. They are identified by subscripts formed by the name of the element and the mass number of the isotope. The cross section σ (expressed in barns) is labeled with a subscript a, c or f to indicate absorption, capture or fission, respectively, and with a superscript to identify the nuclide. The same superscript is used to label the decay constant λ (measured in 1/s). ϕ (neutrons/(cm^{2}s)) indicates the one-group neutron flux. N and ϕ are considered as functions of the irradiation time (t) and the radial position (r) in the

pellet; σ is assumed to depend on the radius, the average burnup (b) and the initial enrichment (q) in ^{235}U measured in wt%.

$$(1)\quad \frac{\partial N_{U235}}{\partial t} = -N_{U235}(t,r)\sigma_a^{235}(r,b,q)\phi(t,r)$$

$$(2)\quad \frac{\partial N_{U236}}{\partial t} = -N_{U236}(t,r)\sigma_a^{236}(r,b,q)\phi(t,r) + N_{U235}(t,r)\sigma_c^{235}(r,b,q)\phi(t,r)$$

$$(3)\quad \frac{\partial N_{U238}}{\partial t} = -N_{U238}(t,r)\sigma_a^{238}(r,b,q)\phi(t,r)$$

$$(4)\quad \frac{\partial N_{Pu239}}{\partial t} = -N_{Pu239}(t,r)\left(\sigma_a^{239}(r,b,q)\phi(t,r) + \lambda^{239}\right) + N_{U238}(t,r)\sigma_c^{238}(r,b,q)\phi(t,r)$$

$$(5)\quad \frac{\partial N_{Pu240}}{\partial t} = -N_{Pu240}(t,r)\left(\sigma_a^{240}(r,b,q)\phi(t,r) + \lambda^{240}\right) + N_{Pu239}(t,r)\sigma_c^{239}(r,b,q)\phi(t,r)$$

$$(6)\quad \frac{\partial N_{Pu241}}{\partial t} = -N_{Pu241}(t,r)\left(\sigma_a^{241}(r,b,q)\phi(t,r) + \lambda^{241}\right) + N_{Pu240}(t,r)\sigma_c^{240}(r,b,q)\phi(t,r)$$

$$(7)\quad \frac{\partial N_{Pu242}}{\partial t} = -N_{Pu242}(t,r)\left(\sigma_a^{242}(r,b,q)\phi(t,r) + \lambda^{242}\right) + N_{Pu241}(t,r)\sigma_c^{241}(r,b,q)\phi(t,r)$$

Reactor codes generally divide the neutrons energy spectrum in two broad categories described as *thermal* (neutrons with energies below 0.65 eV) and *fast* (neutrons with higher energies). Both ranges are used in the balance equations (1)-(7) to predict the behaviour of each species.

To evaluate the cross section functions to be introduced in (1)-(7) the codes CONDOR and HUEMUL were run assuming the conditions of a generic UO_2 pellet; the initial enrichment is varied from 0.7% to 12 %; the final average burnup is given values ranging from fresh fuel to 120 MWd/kgU. With these results, empirical expressions were fitted for the absorption, capture and fission cross sections of each relevant isotope, neutron flux and local burnup, all of them as functions of *r*, *b* and *q*. The expressions generated in this manner are valid in a continuous three-dimensional domain defined by the limiting values of the parameters *r*, *b* and *q*. The formulae fitted in the present work can be grouped in the following function shapes:

$$(8)\quad f_1(r,b,q) = a_0 + a_1 r + a_2 b + a_3 r^2 + a_4 rb + a_5 b^2 + a_6 r^3 + a_7 r^2 b + a_8 rb^2 + a_9 b^3$$

$$(9)\quad f_2(r,b,q) = a_0(a_1 + a_2 b + a_3 b^2 + a_4 b^3)\left(a_5 + a_6 \exp\left(a_7\left(1 - \frac{r}{r_{\max}}\right)^{a_8}\right)\right)$$

$$(10)\quad f_3(r,b,q) = \frac{P_{vol}}{3.2\times 10^{-11}\sum_i \sigma_f^i(r,0,1)N_i} \cdot\left(a_0 + a_1 b + a_2 q + a_3 b^2 + a_4 bq + a_5 q^2 + a_6 b^3 + a_7 b^2 q + a_8 bq^2 + a_9 q^3\right)$$

In the election of the coefficients the criterion was to optimize the fitting in the intermediate ranges of burnup and/or initial enrichment, i.e. from 20 to 80 MWd/kgHM and from 3 to 8 w%^{235}U, respectively, since these are the values of interest in the present fuel development

studies. In (10), which is used to determine the total neutron flux, $\sigma_f^i(r,0,1)$ represents the fission cross section of isotope *i* in the reference condition corresponding to fresh fuel (*b*=0) and enrichment 1wt% (*q*=1), and P_{vol} is the volumetric power density expressed in W cm^{-3}.

To exemplify, the empirical expressions obtained for σ_a^{235}, σ_a^{236}, σ_a^{240} and σ_a^{242} (representing the absorption cross section of ^{235}U, ^{236}U, ^{240}Pu and ^{242}Pu, respectively) and those for ϕ_{tot} are displayed in Table 1. Similar correlations, not listed in this table, were obtained for the rest of the cross sections used in the equations system (1)(7); some of them were reported in [15].

TABLE 1. CORRELATION FORMULAE AND THE CORRESPONDING COEFFICIENTS FOR THE ABSORPTION CROSS SECTIONS OF ^{235}U, ^{236}U, ^{240}Pu AND ^{242}Pu, AND THE TOTAL NEUTRON FLUX, CALCULATED FOR A SINGLE ENERGY GROUP

$\sigma_a^{235} = a_0 + a_1 r + a_2 b + a_3 r^2 + a_4 rb + a_5 b^2 + a_6 r^3 + a_7 r^2 b + a_8 rb^2 + a_9 b$ with

$a_0 = 8.5663\times10^{+01} - 1.452\times10^{+01} q + 7.9068\times10^{-01} q^2$

$a_1 = -9.3400\times10^{-04} + 4.5791\times10^{-04} q - 8.1504\times10^{-06} q^2 + 5.7252\times10^{-07} q^3 - 1.2767\times10^{-07} q^4$

$a_2 = 1.3955\times10^{+01} + 4.4988\times10^{-01} q$

$a_3 = 5.9610\times10^{-09} - 2.6213\times10^{-09} q + 5.5749\times10^{-10} q^2 - 3.3465\times10^{-11} q^3$

$a_4 = -5.8722\times10^{+01} - 2.8297 q$

$a_5 = -5.7726\times10^{-14} + 4.700\times10^{-14} q - 1.4529\times10^{-14} q^2 + 1.7064\times10^{-15} q^3 - 6.7250\times10^{-17} q^4$

$a_6 = 1.1990\times10^{+02} + 4.6660 q - 1.2529\times10^{-01} q^2$

$a_7 = -1.0488\times10^{-05} + 1.4527\times10^{-07} q + 2.6736\times10^{-06} q^2 - 2.0278\times10^{-07} q^3$

$a_8 = 1.2862\times10^{-10} + 7.3720\times10^{-11} q - 2.6430\times10^{-11} q^2 + 1.6497\times10^{-12} q^3$

$a_9 = -3.0515\times10^{-05} - 6.0782\times10^{-06} q - 2.5616\times10^{-06} q^2 + 6.0349\times10^{-07} q^3 - 2.9614\times10^{-08} q^4$

$\sigma_a^{236} = f_1(r,b,q)$, eq. (8), with

$a_0 = 1.6057 - 6.8713 q + + 9.6081\times10^{-01} q^2 - 4.6908\times10^{-02} q^3 - 1.0528\times10^{-05} q^4$

$a_1 = 9.7599\times10^{-02} - 6.8512\times10^{-02} q + 2.1897\times10^{-02} q^2 - 2.8643\times10^{-03} q^3 + 1.3365\times10^{-04} q^4$

$a_2 = 4.6102\times10^{+01} + 7.6858\times10^{+01} q - 1.2920\times10^{+01} q^2 + 9.6226\times10^{-01} q^3 - 2.6040\times10^{-02} q^4$

$a_3 = -2.2220\times10^{-03} + 8.3287\times10^{-04} q - 1.8398\times10^{-04} q^2 + 1.8434\times10^{-05} q^3 - 6.7646\times10^{-07} q^4$

$a_4 = -1.7051\times10^{+02} - 2.7093\times10^{+02} q + 4.9345\times10^{+01} q^2 - 4.1398 q^3 + 1.3432\times10^{-01} q^4$

$a_5 = 1.21073\times10^{-05} - 1.3072\times10^{-06} q + 8.4640\times10^{-08} q^2$

$a_6 = 1.9650\times10^{+02} + 2.9111\times10^{+02} q - 5.6125\times10^{+01} q^2 + 5.0616 q^3 - 1.7933\times10^{-01} q^4$

$a_7 = 1.1519\times10^{-01} - 1.1481\times10^{-03} q - 4.3180\times10^{-02} q^2 + 8.5555\times10^{-03} q^3 - 4.8473\times10^{-04} q^4$

$a_8 = -5.0679\times10^{-04} - 9.1153\times10^{-04} q + 3.2156\times10^{-04} q^2 - 4.4494\times10^{-05} q^3 + 2.1812\times10^{-06} q^4$

$a_9 = -1.0871\times10^{-01} + 2.1636\times10^{-01} q - 6.5612\times10^{-03} q^2 - 3.2417\times10^{-03} q^3 + 2.6291\times10^{-04} q^4$

$\sigma_a^{240} = f_1(r,b,q)$, eq. (8), with

$$a_0 = 2.4356\times10^{+02} - 7.4465\times10^{+01}q + 2.0205\times10^{+01}q^2 - 2.3110q^3 + 9.0858\times10^{-02}q^4$$
$$a_1 = -5.4351\times10^{-03} - 3.5277\times10^{-04}q + 1.2257\times10^{-04}q^2 - 9.4641\times10^{-06}q^3 + 2.7345\times10^{-07}q^4$$
$$a_2 = -9.0926\times10^{+01} + 5.6823\times10^{+02}q - 1.5718\times10^{+02}q^2 + 1.7378\times10^{+01}q^3 - 6.7179\times10^{-01}q^4$$
$$a_3 = 6.2413\times10^{-08} + 4.1771\times10^{-09}q - 1.6026\times10^{-09}q^2 + 1.2766\times10^{-10}q^3 - 3.7148\times10^{-12}q^4$$
$$a_4 = -8.3656\times10^{+01} - 1.9650\times10^{+03}q + 5.4960\times10^{+02}q^2 - 6.0663\times10^{+01}q^3 + 2.3410q^4$$
$$a_5 = -2.4281\times10^{-13} + 1.4976\times10^{-14}q$$
$$a_6 = 6.59769\times10^{+02} + 1.9983\times10^{+03}q - 5.7275\times10^{+02}q^2 + 6.3522\times10^{+01}q^3 - 2.4543q^4$$
$$a_7 = 3.9184\times10^{-03} - 3.0028\times10^{-03}q + 7.9302\times10^{-04}q^2 - 9.0454\times10^{-05}q^3 + 3.5730\times10^{-06}q^4$$
$$a_8 = -2.1097\times10^{-08} - 1.0837\times10^{-09}q + 2.8649\times10^{-11}q^2 + 3.4214\times10^{-11}q^3 - 2.0635\times10^{-12}q^4$$
$$a_9 = -4.2931\times10^{-04} + 4.8312\times10^{-03}q - 1.1840\times10^{-03}q^2 + 1.2638\times10^{-04}q^3 - 4.8460\times10^{-06}q^4$$

$\sigma_a^{242} = f_1(r,b,q)$, eq. (8), with

$$a_0 = 3.0118\times10^{+01} - 6.5618\times10^{-01}q$$
$$a_1 = 7.3847\times10^{-02} - 7.2747\times10^{-02}q + 2.7282\times10^{-02}q^2 - 3.1957\times10^{-03}q^3 + 1.1832\times10^{-04}q^4$$
$$a_2 = 6.4450 + 2.1587\times10^{-01}q - 2.4665\times10^{-02}q^2$$
$$a_3 = -4.0275\times10^{-04} - 2.8568\times10^{-04}q + 2.5461\times10^{-05}q^2$$
$$a_4 = -2.7537\times10^{+01} + 7.4897\times10^{-01}q$$
$$a_5 = 4.1927\times10^{-06} + 4.0962\times10^{-07}q - 6.7322\times10^{-08}q^2$$
$$a_6 = 3.0368\times10^{+01} - 5.8145\times10^{-01}q$$
$$a_7 = 9.7741\times10^{-03} - 2.0036\times10^{-02}q + 1.1978\times10^{-03}q^2$$
$$a_8 = -5.1067\times10^{-04} + 1.5204\times10^{-04}q - 7.4631\times10^{-06}q^2$$
$$a_9 = 1.5474\times10^{-01} - 1.1565\times10^{-03}q - 5.4451\times10^{-04}q^2$$

$\phi_{total} = f_2(r,b,q)$, eq.(9), with

$$a_0 = 0.700$$
$$a_1 = -3.0432\times10^{-9}$$
$$a_2 = 0.0113$$
$$a_3 = 3.5805\times10^{-17}$$
$$a_4 = 5.2119\times10^{-11}$$
$$a_5 = -0.0013$$
$$a_6 = -1.1270\times10^{-25}$$
$$a_7 = -1.6796\times10^{-18}$$
$$a_8 = 1.3674\times10^{-11}$$
$$a_9 = 2.7321\times10^{-5}$$

2.1.1. Comparison with reactor codes

Figures 1 to 5 were selected to show the comparison between the empirical formulae fitted in this work and the results obtained with the reactor codes HUEMUL and CONDOR for the local burnup, concentration and cross sections of absorption, capture and fission of the U and Pu isotopes.

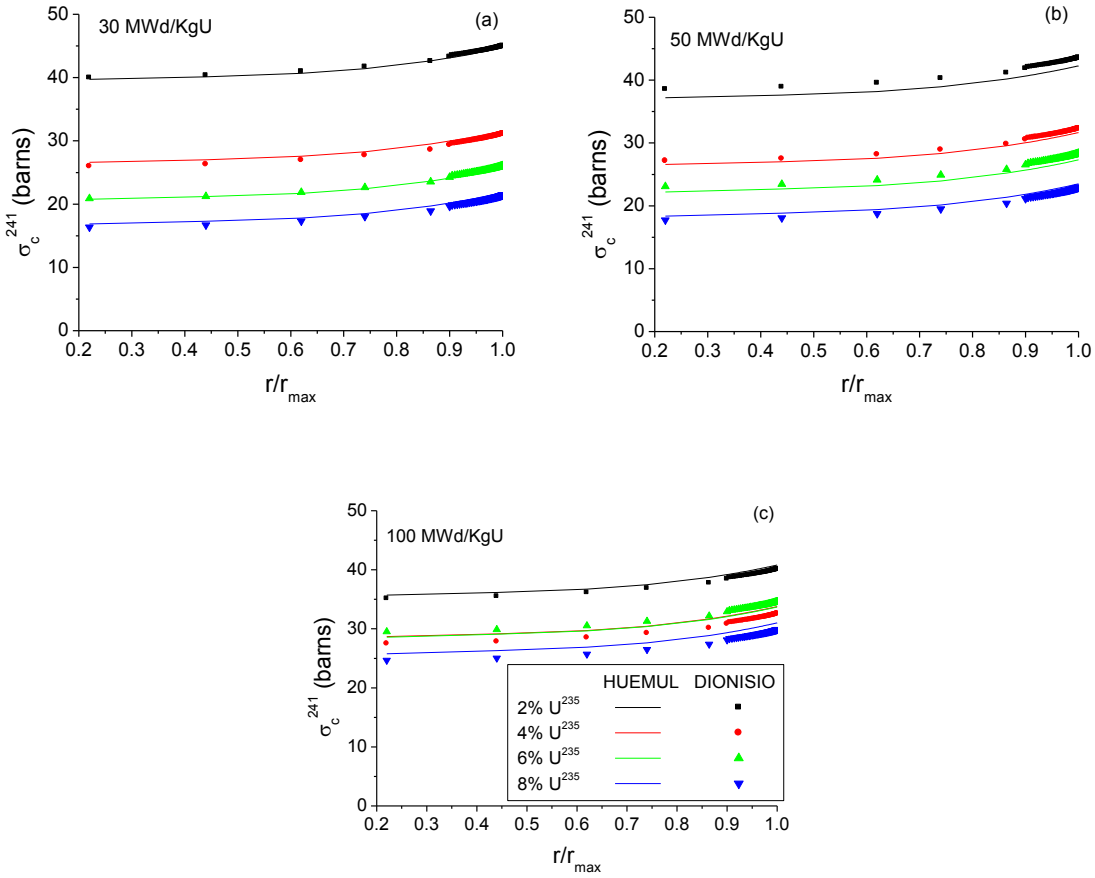

FIG. 1. Capture cross section (σ_c^{241}) of ^{241}Pu vs. the relative radius for different values of the initial enrichment and average burnup levels of (a) 30 MWd/kgU; (b) 50 MWd/kgU and (c) 100 MWd/kgU. Comparison between the values predicted by HUEMUL and the functions included in DIONISIO. The legend in (c) applies for the three plots.

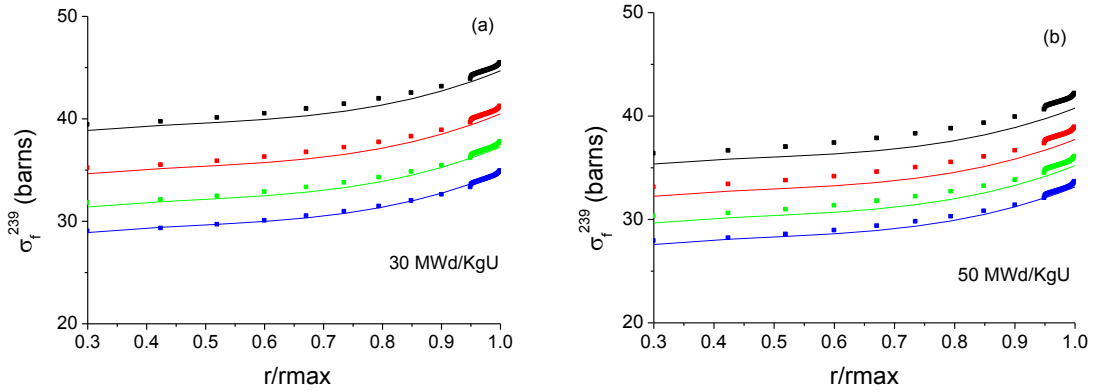

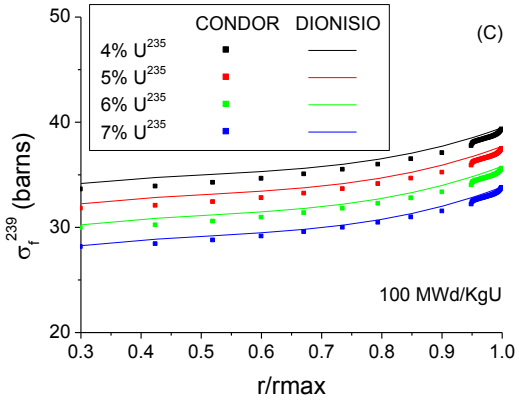

FIG. 2. Fission cross section (σ_f^{239}) of ^{239}Pu vs. the relative radius for different values of the initial enrichment and average burnup levels of (a) 30 MWd/kgU; (b) 50 MWd/kgU and (c) 100 MWd/kgU. Comparison between the values predicted by CONDOR and the functions included in DIONISIO. The legend in (c) applies for the three plots.

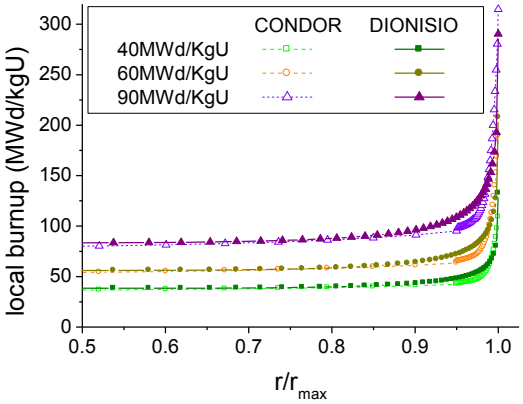

FIG. 3. Comparison between the distribution of burnup obtained with the correlation laws developed in DIONISIO and the results given by CONDOR, for different levels of average burnup.

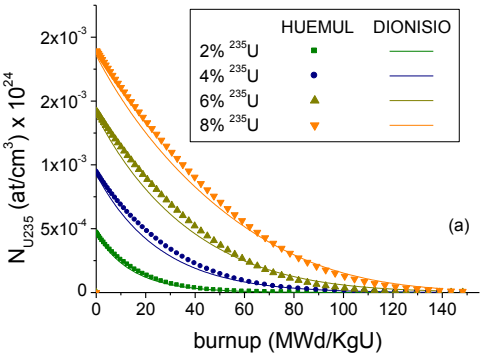

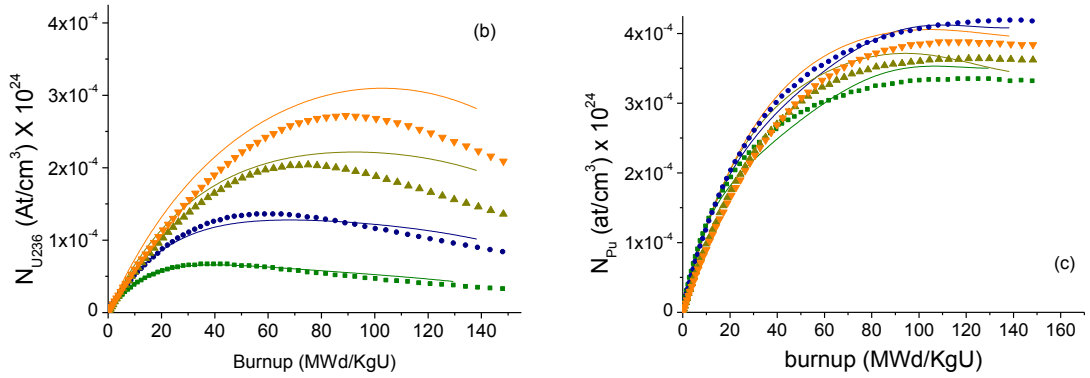

FIG. 4. Concentration of (a) ^{235}U,(b) ^{236}U and (c) total Pu in the middle of the pellet (r/r_{max}~0.5) vs. the average burnup. Comparison between the predictions of HUEMUL and DIONISIO for different initial enrichments. The legend in (a) applies for the three plots.

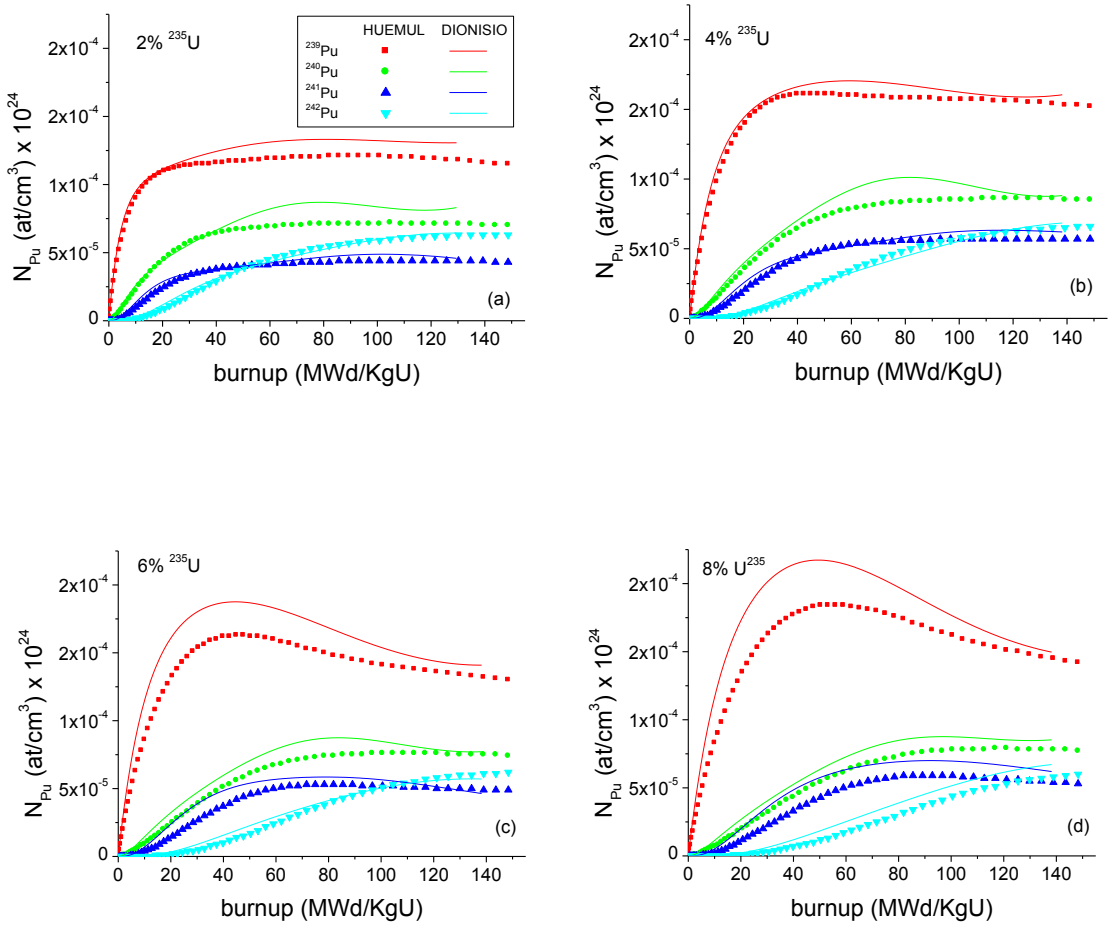

FIG. 5. Concentration of ^{239}Pu, ^{240}Pu, ^{241}Pu and ^{242}Pu at r/r_{max}~0.85 vs. the average burnup. Comparison between the predictions of HUEMUL and DIONISIO for initial enrichments of (a) 2%; (b) 4%; (c) 6% and (d) 8%. The legend in (a) applies for the four plots.

2.2. Content of Cs, Nd and Xe

The experimental determinations [17] show that the fission yield of Cs, Nd and Xe can be reasonably approximated by constants, so that the generation rates of these elements per unit volume (involving the different isotopes and their decay chains) are proportional to the fission rate. The rate laws are thus expressed as $\frac{\partial C_i}{\partial t} = Y_i \dot{f}$ where i indicates the element, C is the concentration in atoms/cm^3, $\dot{f}$ is the local fission rate in fissions/(cm^{3}s) and the respective fission yields are $Y_{Cs} \approx 0.150$, $Y_{Nd} \approx 0.199$ and $Y_{Xe} \approx 0.268$. These expressions are used in the TRANSURANUS code and were also adopted in DIONISIO.

The proportionality between the local concentration of Nd and the local burnup is experimentally verified. Something similar also holds for Cs, but with a larger dispersion. Due to this property, Nd and Cs concentrations are used as a measure of the local burnup level. With respect to Xe, the EPMA determinations show the decrease of the gas dissolved in the matrix for burnups higher that a certain level. Xe concentration is experimentally used to locate the burnup threshold Bu_o. For $Bu > Bu_o$, the high burnup microstructure forms, and a considerable fraction of Xe is collected by the large pores. The depletion of gas from the matrix is well represented by the following empirical expression [17] which was adopted for the concentration of Xe dissolved in the matrix

$$(11)\; C_{Xe} = 1.46\times10^{-2}\left(\left(\frac{1}{\alpha}\right)+\left(Bu_o-\left(\frac{1}{\alpha}\right)\right)e^{-\alpha(Bu-Bu_o)}\right)$$

where $\alpha = 0.058$ is a fitting parameter. These expressions are compared with experimental data. In particular, the determinations performed on the A3-6-4 rod of the HBEP3 experiment [19] are shown in Fig. 6 and compared with the curves obtained with this approximation.

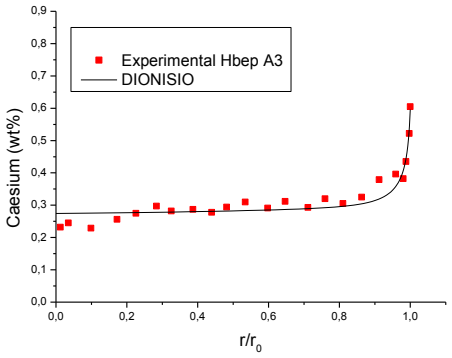

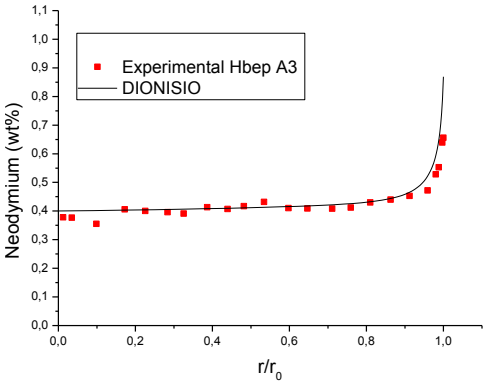

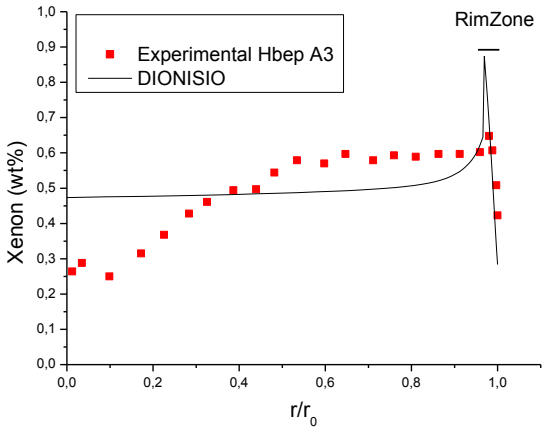

FIG. 6. Local concentration of (a) Cs, (b) Nd and (c) Xe measured in the rod A3-6-4 of the HBEP3 experiment and simulations with the fitting formulae included in DIONISIO.

2.3. Thermal conductivity of UO_2 and (U, Gd) O_2

Computer codes used for simulating the thermo-mechanical behaviour of nuclear fuels must include an adequate description of the thermal conductivity, since it plays a key role on the accuracy of the prediction of temperature distribution in the system, and in consequence of all the physical properties of the whole system. The thermal conductivity of UO_2 is a function not only of temperature, but of variables such as burnup level, porosity, stoichiometry, Pu and Gd content, etc.

In this work, different thermal conductivity models published in the open literature have been evaluated, for UO_2, (U, Pu) O_2 and (U, Gd) O_2 fuels, as well as a large amount of related experimental data. Starting from an expression published by J. Fink [20], modifications were introduced to reflect the degradation of thermal conductivity due to burnup and to the presence of Gd in the lattice and to give the best possible fitting to the experimental data available in the literature. The expression adopted is

$$(12)\quad k(T) = (1-p^{2/3})\left[\frac{1}{A+BT+CT^2+a_{Gd}w_{Gd}(b_{Gd}-T)+h_D(T,Bu)} + (1-c_{Gd}w_{Gd})\frac{D}{T^{5/2}}\exp\left(-\frac{E}{T}\right)\right] \text{ in } \frac{\text{W}}{\text{cm°C}}$$

where p is the material porosity, T the absolute temperature and w_{Gd} the weight fraction of Gd. For the function h_D the expression [20]

$$(13)\quad h_D(Bu) = A_D + B_D \exp\left(-\frac{Bu}{C_D}\right)$$

was adopted. The fitting parameters of this formula as well as a_{Gd}, b_{Gd} and c_{Gd} in the previous one were selected according to the experimental data compiled in [20] and [21]. Fig. 7 shows the effect of burnup on the thermal conductivity of UO_2. Generally speaking, in the range 0-1660°C, the determinations of different authors are similar evidencing the decrease of conductivity with temperature. For higher temperatures a tendency to grow is observed and the dispersion is clearly larger. The effect of burnup is more visible in the lower temperature range. For temperatures about 1600°C and Bu>60MWd/kgU the conductivity is about 0.02W/cm°C.

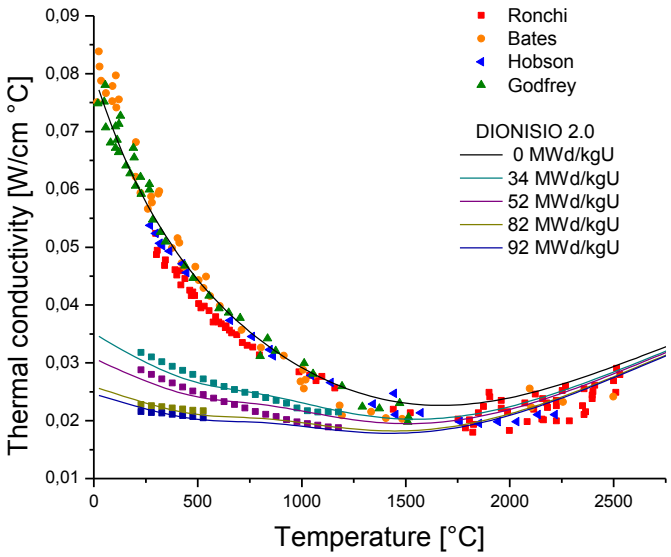

FIG. 7. Effect of burnup on the thermal conductivity of UO_2.

Fig. 8 shows of the effect on the thermal conductivity of unirradiated UO_2 of the addition of Gd, normally in the form of gadolinia, Gd_2O_3. The conductivity degradation increases with the Gd content, although its influence is relatively lower for high temperatures and burnup levels.

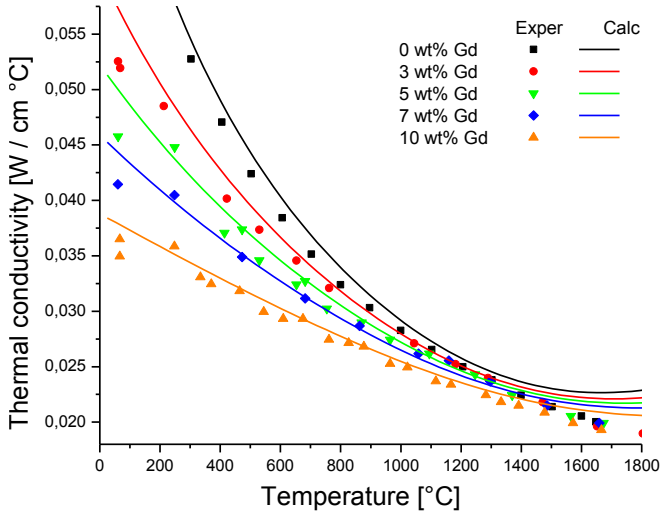

FIG. 8. Effect of the Gd content on the thermal conductivity of UO_2.

2.4. Microstructural changes in the rim zone

For extended irradiation periods, the new microstructure that develops in the pellet periphery (rim zone), characterized by small grains and large pores as compared with those of the original material and absence of Xe from the solid lattice, causes local changes in the mechanical and thermal properties, thus affecting the overall fuel behaviour. The evolution of

porosity in the high burnup structure (HBS) is assumed to be determinant of the retention capacity of the fission gases released by the matrix. This is the reason why, during the latest years a considerable effort has been devoted to characterizing the parameters that influence porosity.

Starting from several works published in the open literature, a model was developed to describe the behaviour and development of porosity at local burnup values ranging from 60 to 300 MWd/KgHM. The model is mathematically expressed by a system of non-linear differential equations. Phenomena like the growth of pores radius by vacancies trapping, the interactions of different orders between open and closed pores (coalescence), the evolution of the pores number density, the internal pressure and over pressure within the closed pores, interactions between pores and the free surface (gas venting), the fission gas retained in the matrix and released to the closed pores and to the free volume of the rod are analyzed.

The HBS can be conventionally considered to start at ≈60 MWd/kgU. Two parameters, porosity and pores number density, become useful to describe the HBS. Both show a change of behaviour at a burnup threshold of about 100 MWd/kgU. In the interval between 60 and 100 MWd/kgU, porosity increases with burnup at a rate of about 1.7 % / 10 MWd/kgU until it reaches about 10% at the burnup critical value (Figure 9). For burnups higher than 100 MWd/kgU, the porosity increase rate is about 0.6 % / 10 MWd/kgU [22]. The pores number density, instead, increases with burnup until reaching a maximum of about 10^8 pores/mm^3 at the burnup threshold value and then decreases [22]. This fact reveals that after ≈100 MWd/kgU the pores coalescence process becomes significant. In the burnup range beyond the critical value, the pores density decreases while larger pores are generated as the burnup increases.

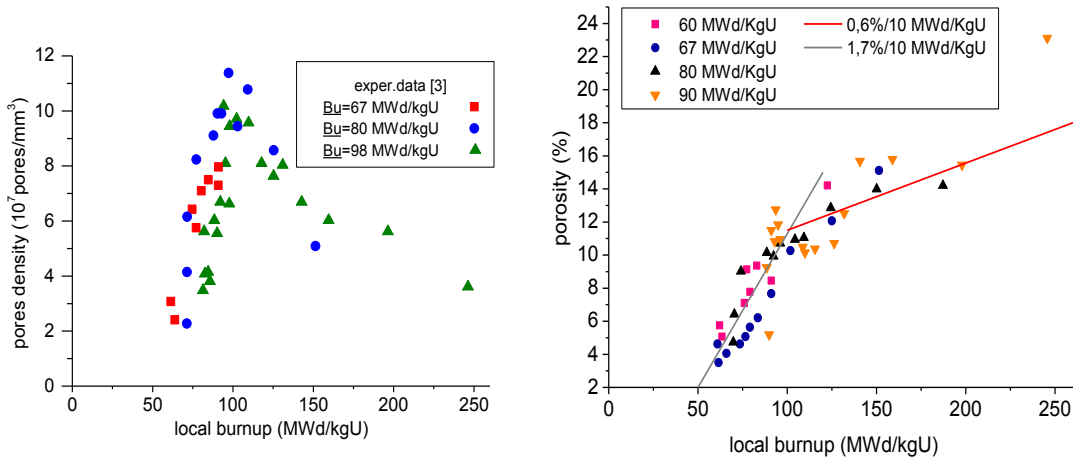

FIG. 9. Experimental data of (a) porosity and (b) number density vs. local burnup for different level of average burnup.

For these reasons, two different schemes have been adopted to represent the system state in terms of the local burnup level: *model 1*, valid for burnups between 60 and 100 MWd/kgU and *model 2*, for burnups above 100 MWd/kgU. For local burnups even higher, the pores next to the pellet surface acquire an increasing probability of making contact with the free surface and thus becoming open pores. The microstructure adopts a typical aspect referred to [23] as *ultra-high burnup structure* (UHBS). The gas contained in the formerly closed pores is released to the free volume of the fuel rod. The experimental data reveal that the fraction of

open pores remains low and limited to a very narrow layer in the pellet periphery. J. Spino et al. [24] determined that a local burnup as high as 250 MWd/kgU is necessary for reaching a total porosity of 24%. Below this burnup level, the open porosity represents less than 7% of the total porosity. These very high local burnup levels are needed in order that the pores make contact with the pellet surface thus releasing its gas content. The fraction of open pores decreases towards the pellet interior so that the vented zone is limited to the outer 20 μm layer.

This model was published elsewhere [2, 3]. Only the more relevant aspects will be described here.

- Pores are assumed of spherical shape with radius R_p. The pores population within the material is characterized by the porosity (σ) and pores number density (n_p), which are related by $\sigma = \frac{4}{3}\pi R_p^3 n_p$.
- The accumulation of fission gas within the closed pores gives rise to a certain overpressure on the pore surface given by $\Delta\zeta = P_p - \frac{2\gamma}{R_p} - P_h$ where P_p is the pressure due to the gas within the pore, P_h is the hydrostatic pressure and γ is the surface energy of the pore, estimated in $\gamma \approx 1 J/m^2$.
- The gas enclosed in the pores, mainly Xe, is assumed to obey the Van der Waals equation. Then, $P_p(\frac{4}{3}\pi R_p^3 - \omega_{Xe} N_p) = N_p kT$ where $\omega_{Xe} \approx 8.5\times10^{-29}$ m^3/atom, is the specific volume for Xe, N_p is the number of gas atoms in a pore and T is the absolute temperature. The number of fission gas atoms enclosed in the pores per unit volume of the material is $C_p = N_p n_p$ and then $P_p(\sigma - \omega_{Xe} C_p) = C_p kT$.
- The fission gas generated during fuel irradiation, c_{gen}, is distributed among pores, c_p, matrix, c_{matrix}, and rod free volume, c_{rel}, i.e.: $c_{gen} = c_p + c_{matrix} + c_{rel}$, all of them measured as weight per cent of fuel. The expressions for c_{gen} and c_{matrix} were given in section 0.
- In the burnup range corresponding to *model one* c_{rel} is very low and can be approximated by $c_{rel} \approx 1.6\times10^{-6}$ wt%.

  The empirical expression $\sigma = [\frac{(0.015 + 0.008\lambda)Bu}{1 - 0.0135\times Bu + 6\times10^{-5} Bu^2}] - (0.036 - \sigma_0)$ was developed for porosity in terms of local burnup. It includes the possible effects of pellet-cladding mechanical interaction ($\lambda = 1$ when pellet-cladding contact exists and $\lambda = 0$ when it does not). σ_0 represents the porosity reached by the fuel material when Bu=Bu_o=60 MWd/kgU, i.e. when the high burnup range starts. The value of σ_0 is usually in the range 3% to 6%, depending on the fabrication route and base irradiation conditions.
- *Model two* includes the mechanisms of pore growth due to trapping of vacancies and interstitials, and to interactions of diverse orders between pores (closed or open) and of pores with the pellet surface. According to the pore radius growth rate is given by $\frac{dR_p}{dt} = \frac{1}{R_p}[D_v X_v^0 (1 - \exp(-\frac{\Delta\zeta\Omega}{kT})) - D_i X_i^0 (1 - \exp(\frac{\Delta\zeta\Omega}{kT}))]$ where Ω indicates the volume associated to the point defects assumed equal to the volume per uranium atom in the UO_2

lattice ($\Omega = 4.09 \times 10^{-29} m^3$), the term $\Delta\zeta\Omega$ in both exponents represents the work invested in moving an atom under a pressure $\Delta\zeta$ thus creating a point defect of volume Ω; $X_{v,i} = \Omega C_{v,i}$ indicates the fraction of sites occupied by vacancies/interstitials. A system of coupled differential equations is solved to obtain the fractional concentrations of vacancies and interstitials, which lead to the pore radius R_p.

The complete model is compared with experimental data obtained from the open literature [28-31]. The results are shown in Figure 10.

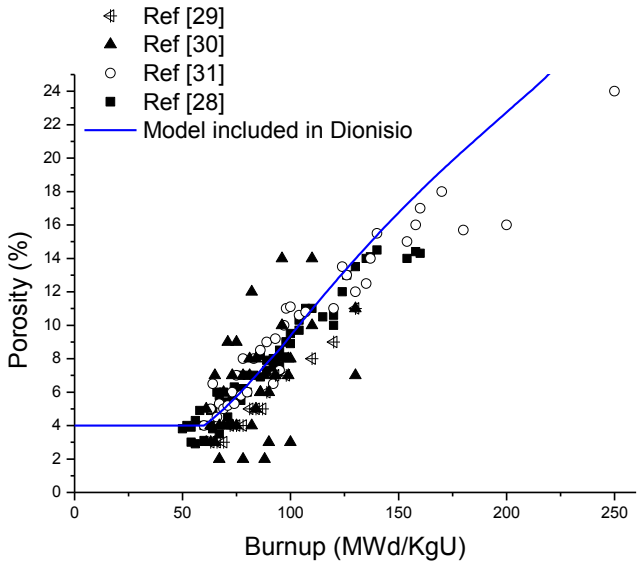

FIG. 10. Porosity vs. burnup. Comparison between experimental data from the open literature and the model included in DIONISIO.

3. INCORPORATION OF THE MODELS IN DIONISIO

The models just described were introduced in DIONISIO and the predictive ability of the code as a whole was tested by comparison of its results with experimental data corresponding to the high burnup range. The results of this testing and the modifications in the code architecture are the subject of the next presentation.

4. CONCLUSIONS

Several subroutines have been incorporated to the DIONISIO code in recent times. They are oriented to extending the scope of the code to the high burnup range. The radial profiles of the more significant uranium and plutonium isotopes are evaluated, assuming that the resonant absorption of epithermal neutrons by ^{238}U is responsible for the formation of the rim structure. The degradation of thermal conductivity with burnup as well as its dependence with the content of Gd, usually included as burnable poison, was also considered. Empirical models describing the production of Nd, Cs and Xe were incorporated to the code.

A more complex model aimed at describing the formation and progress of the high burnup microstructure was also incorporated. The evolution of parameters like porosity and pores number density of closed and open pores, overpressure provoked by the fission gas enclosed in the pores, concentration of point defects in the vicinity of these pores, inventory of gas

retained in the solid matrix of the transformed pellet region, trapped in the pores and released to the rod free volume are considered in terms of the burnup, in the range comprised between 60 and 300 MWd/kgU, as well as in terms of the radial position within the fuel pellet in its outer ring.

All the subroutines were subjected to numerous separate tests that included parametric analyses spanning a wide range of temperature, burnup, fission rate, surface/volume ratio, among others. The model testing also covered comparison of its results with experimental information mostly obtained from the FUMEX II/III data bank showing a good agreement both in average burnup as total plutonium produced.

With the improvements recently introduced, involving subroutines for the physical and chemical properties of the fuel material in the high burnup range, the code DIONISIO in its version 2.0 evidenced a good performance in the numerous simulations of experimental situations typical of PWR, BWR and PHWR fuels. On this basis, DIONISIO 2.0 can be regarded as an adequate simulation tool even for average burnup levels as high as 60 MWd/kgU.

REFERENCES

[1] CUNNINGHAM, M., FRESHLEY, M. and LANNING, D., Development and characteristics of the rim region in high burnup UO_2 fuel pellets. J. Nucl. Mater. **188** (1992) 19-27.

[2] LEMES, M., Estudio analítico y numérico de los efectos de la irradiación hasta alto quemado en combustibles de reactores de potencia, Master Thesis, April 2013.

[3] SOBA, A., DENIS, A., LEMES, M., An empirical formulation to describe the evolution of the high burnup structure, sent for publication.

[4] MATZKE, Hj., On the rim effect in high burnup UO_2 LWR fuels, J. Nucl. Mater. **189** (1992) 141-148.

[5] NEWTON, T., HUTTON, J. in: PARK, M. (Ed.), Proceedings of PHYSOR 2002 – International Conference on the New Frontiers of Nuclear Technology: Reactor Physics, Safety and High-Performance Computing, 14A-04, American Nuclear Society, Seoul, Korea, Republic of, 7–10 October 2002.

[6] HUTTON, J., NEWTON, T., PERRY, R., POWNEY, D., Proceedings of PHYSOR 2004 – The Physics of Fuel Cycles and Advanced Nuclear Systems: Global Developments, Session 1D, American Nuclear Society, Chicago, Illinois, USA, 25–29 April 2004.

[7] STAMMLER, R., BOERRESEN, S., CASAL, J., FORSLUND, P., Proceedings of PHYSOR 1996 – International Conference on Physics of Reactors, American Nuclear Society, Mito, Ibaraki, Japan, 16–20 September 1996

[8] HELIOS Methods, Program Manual Rev. 1, Program HELIOS 1.4, Studsvik-Scandpower, 1998.

[9] VILLARINO, E., CONDOR calculation package. PHYSOR 2002, Seoul, Korea, Republic of, October 7-10, 2002.

[10] GRANT, C., User handbook of the HUEMUL code (in preparation).

[11] GLASSTONE, S., SESONSKE, A., Ingeniería de Reactores Nucleares. Ed. Reverté, S.A. Buenos Aires, 1975.

[12] PALMER, I., HESKETH, K., JACKSON, P., in: J. Gittus (Ed.), Water Reactor Fuel Element Performance Computer Modelling, Applied Science, Barking, UK, 1983, p. 321.

[13] LEE, C., KIM, D., SONG, J., BANG, J., JUNG, Y., RAPID model to predict radial

burnup distribution in LWR UO_2 fuel. J. Nucl. Mater. **282** (2000) 196-204.
[14] SCHUBERT, A., van UFFELEN, P., van de LAAR, J., WALKER, C., HAECK, W., Extension of the TRANSURANUS burn-up model. J Nucl. Mater. **376** (2008) 1–10.
[15] SOBA, A., DENIS, A., ROMERO, L., VILLARINO, E., SARDELLA, F., A high burnup model developed for the DIONISIO code, J. Nucl. Mater. **433** (2013).
[16] GONZÁLEZ, M., DENIS, A., SOBA, A., Modelización de la conductividad térmica del UO_2 y $(U,Gd)O_2$ bajo irradiación. Implementación en el código DIONISIO, 98º Reunión Anual de la Asociación Física Argentina, 24 – 27 de septiembre de 2013, Bariloche, Argentina.
[17] LASSMANN, K., WALKER, C., van de LAAR, J., LINDSTRÖM, F., Modelling the high burnup UO_2 structure in LWR fuel, J. Nucl. Mater., **226**, pp 1-8 (1995).
[18] LASSMANN, K., SCHUBERT, A.,van de LAAR, J.,Recent developments of the transuranus code with emphasis on high burnup phenomena. International Conference on Nuclear Fuel for Today and Tomorrow (2003).
[19] LYON, W.,US-PWR 16x16 LTA Extended Burnup Demonstration Program Summary File (2005).
[20] FINK, J., Review: Thermophysical properties of Uranium Dioxide, J. Nucl. Mater. **279** (2000) 1.
[21] RONCHI, C., SCHEINDLIN, M., STAICU, D., KINOSHITA, M., Effect of burn-up on the thermal conductivity of Uranium dioxide up to 100.000 MWd/t, J. Nucl. Mater. **327** (2004) 58.
[22] SPINO, J., STALIOS, A., SANTA CRUZ, H., BARON, D., Stereological evolution of the rim structure in PWR-fuels at prolonged irradiation: Dependencies with burnup and temperature, J. Nucl. Mater. **354** (2006) 66–84.
[23] ROMANO, A., HORVATH, M., RESTANI, R., Evolution of porosity in the high-burnup fuel structure, J. Nucl. Mater. **361** (2007) 62-68.
[24] SPINO, J., VENNIX, K., COQUERELLE, M., Detailed characterization of the rim microstructure in PWR fuels in the burn-up range 40-67 GWd/tM, J. Nucl. Mater. **231** (1996) 179-190.
[25] OLANDER, D., Fundamental aspects of nuclear reactor fuel elements. Department of Nuclear Engineering, University of California, Berkeley (1976).
[26] KHVOSTOV, G., MIKITYUK, K., ZIMMERMANN, M., A model for fission gas release and gaseous swelling for the uranium dioxide fuel coupled with the FALCON code, J. Nucl. Eng. Des. **241** (2011) 2983-3007.
[27] BLAIR, P., PhD Thesis, Modelling of fission gas behaviour in high burnup nuclear fuel, École Polytechnique Federale, Lausanne, Switzerland (2008).
[28] NOIROT, J., DESGRANGES, L., LAMONTAGNE, J., Detailed characterizations of high burn-up structures in oxide fuels, J. Nucl. Mater. **372** (2008).
[29] UNE, K., NOGITA, K., SHIRATORI, T., HAYASHI, K., Rim structure formation of isothermally irradiated UO_2 fuel discs, J. Nucl. Mater., **288** (2001).
[30] SPINO, J., REST, J., GOLL, W., WALKER, C., Matrix swelling rate and cavity volume balance of UO_2 fuels at high burnup, J. Nucl. Mater., **346** (2005).
[31] NOIROT, L., An Advanced Mechanistic Model of Fission Gas Behaviour in Nuclear Fuel, J. Nucl. Sci. Techn., **43** (2006).

SIMULATION WITH DIONISIO 2.0 OF A WHOLE NUCLEAR FUEL ROD UNDER EXTENDED IRRADIATION

A. SOBA, M. LEMES, A. DENIS

Gerencia Ciclo del Combustible Nuclear, Comisión Nacional de Energía Atómica (CNEA), Centro Atómico Constituyentes (CAC), Buenos Aires, Argentina

Abstract.

The version 2.0 of the DIONISIO code has been recently developed with the purpose of improving the accuracy of the simulation of the whole fuel rod. To this end, the rod is divided into a number of axial segments. The local values of linear power and coolant temperature are given as input data to DIONISIO 1.0 which is executed in each segment obtaining as outputs the local values of temperature, stress, strain, among other physical variables. Then, the general rod parameters (internal rod pressure, amount of fission gas released, pellet stack elongation, etc.) are evaluated at the end of every time step, conveniently combining the results of all the axial segments. The new code architecture allows taking into account the axial variation of the linear power and, consequently, evaluating the dependence of all the significant rod parameters with the longitudinal coordinate. Moreover, new calculation tools designed to extend the application range of the code to high burn up have also been incorporated to DIONISIO 2.0 in recent times and are the subject of other presentation. With these improvements, the code results are compared with some experiments published in the IAEA data base, covering more than 380 fuel rods irradiated up to average burnup levels of 40-60 MWd/kgU. The results of these comparisons, which are presented here, reveal the good quality of the simulations.

1. INTRODUCTION

The fuel performance code DIONISIO version 1.0 was designed to describe most of the main phenomena occurring in a PWR/PHWR fuel rod throughout its life under normal operation conditions. The code is two-dimensional, discretizes one half of an axial section of a pellet and the corresponding cladding segment, assumes cylindrical symmetry for the rod and also symmetry with respect to the middle pellet plane and uses the finite element method to integrate the non-linear differential equations of heat diffusion and stress-strain. Starting from an idealized power history, it predicts the temperature distribution in the domain, elastic and plastic stress and strain, creep, swelling and densification, release of fission gases, caesium and iodine to the internal volume of the rod, gas mixing, pressure increase, irradiation growth of the Zircaloy cladding, development of an oxide layer on its surface and hydrogen uptake, restructuring and grain growth in the pellet. The effects of a corrosive atmosphere (SCC) either on the internal or external cladding wall as well as the possibility of pellet-cladding interaction (PCI) are also considered [1–6].

After performing the above mentioned calculations in a single fuel pellet, the results are generalized in DIONISIO 1.0 to the rod length. This scheme implies the assumption that the linear power and the coolant temperature are uniform in the whole rod. Although a large number of properties are adequately simulated taking the average values of the input parameters, it is to be admitted that in certain instances this may lead to underestimation of some output variables. Initiation of fission gas release is an example of this limitation since the release surely starts at the middle of the rod, when the average linear power indicates that no release has to occur yet. On the opposite edge, but for the same reasons, a simulation performed with the maximum of linear power would overestimate the amount of gas released. It is worth mentioning that a correct prediction of gas release, both in regard to the time of initiation or to the amount released is crucial for a correct simulation of the composition of

the internal atmosphere in the rod, which affects the evolution of the internal pressure and temperature profile and therefore all the physical parameters of the system.

A new version of the code, DIONISIO 2.0, has been recently developed with the purpose of giving a more accurate simulation of the behaviour of the whole rod. To this end, the rod is divided into a number of user defined axial segments. In each one DIONISIO 1.0 is executed taking as input data the local parameters of the rod (linear power, coolant temperature). The complete problem is solved in each segment obtaining the relevant local output parameters (temperature, stress and strain distributions, among others). Then, the general rod parameters (internal rod pressure, amount of fission gas released, pellet stack elongation, etc.) are evaluated at the end of every time step, conveniently combining the results of all the axial segments. The new code architecture allows taking into account the axial variation of the linear power and coolant temperature and, consequently, evaluating the dependence of all the significant rod parameters with the longitudinal coordinates.

Although the following aspects are not analyzed in the present work, we mention for completeness that calculation tools designed to extend the application range of the code to high burnup have also been incorporated to DIONISIO 2.0 in recent times and are the subject of another presentation. On the one hand, a group of subroutines, which are tuned for UO_2 fuels in LWR conditions, predict the evolution of the radial distribution of the isotopes ^{235}U, ^{236}U, ^{238}U, ^{239}Pu, ^{240}Pu, ^{241}Pu and ^{242}Pu [2]. On the other hand, a set of subroutines has been included to simulate the microstructural modifications that the pellet suffers at its external edge under high and very high burnup conditions [3]. Furthermore, subroutines designed to predict the distribution of caesium, iodine; neodymium and xenon in the pellet solid lattice were also integrated to DIONISIO 2.0 [4], on the basis of experimental information reported in Refs [5, 6].

2. DESCRIPTION OF THE NEW FEATURES OF THE CODE

2.1. New domain of resolution

With the aim of reaching a better simulation of the phenomena involved in a fuel bar, a partition of the complete rod is introduced in this new version of DIONISIO. These sections represent partitions of the real rod submitted to different values of the linear power according to the non-uniform longitudinal distribution of neutron flux in the reactor.

Figure 1 shows, in the left side scheme, the active portion of a whole fuel rod. A magnification is given in the center of the figure where several axial sections are shown, each one containing a given number of pellets. In each axial section the differential equations (heat, stress, strain) are solved in a representative pellet and the corresponding cladding segment, using the finite elements method. The pellet is assumed symmetrical with respect to the middle transversal plane. Hence, only one half of the pellet needs to be analyzed. Moreover, cylindrical symmetry is assumed. The system is well represented by the domain in the *r-z* plane shown in the right side scheme, where rectangular finite elements are used for the discretization.

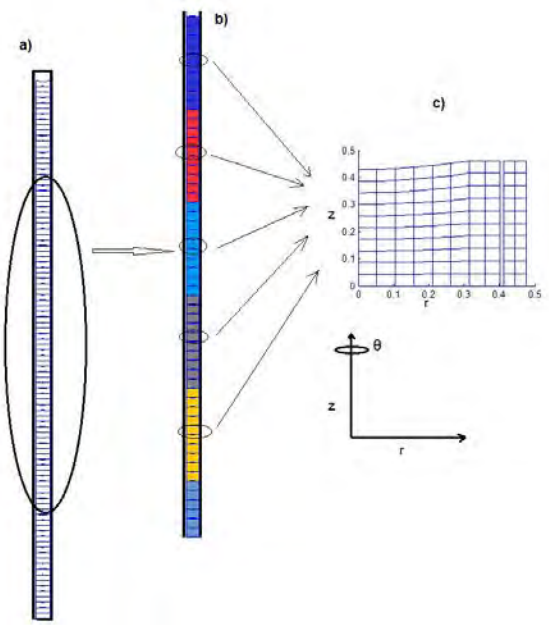

FIG. 1. a) Scheme of the active part of a whole fuel rod. b) Magnification of a portion of the rod where several segments, each one containing a number of pellets, is shown. c) In each sector a half domain (pellet and cladding) is solved using the finite elements method with axial symmetry.

In every time step, a complete description of the system variables is obtained for each axial section starting from the local values of the linear power and coolant temperature. After that the amount of gas released by each rod segment is evaluated on the whole rod, adding the contribution of each sector. The composition of the gas mixture in the gap and its thermal conductivity are recalculated in every time step. The internal rod pressure is calculated with the ideal gas law using the total number of gas atoms released, the total free volume within the rod and the average of the gap temperatures in all the segments.

2.2. High burnup considerations

When the residence time of nuclear fuel rods of uranium oxide is increased beyond a given threshold value, several properties of the pellet material suffer changes and hence the subsequent behaviour of the rod is significantly altered. Due to the absorption of epithermal neutrons by ^{238}U (its absorption cross section exhibits resonant peaks in the energy range comprised between 5 and 2000 eV) and to the chains of nuclear reactions that take place thereafter, several Pu isotopes are born especially at the pellet periphery. In particular, the fissile character of ^{239}Pu and ^{241}Pu is the cause of the increased number of fission events that occur in that ring. For this reason, the radial dependence of the power generation rate and the burnup accumulation need to be considered. These parameters, which at low and intermediate burnup levels can be considered with a reasonably good approximation as uniformly distributed, reach values two or three times higher at the pellet edge than at the rest of the pellet when the average burnup exceeds a certain magnitude. The numerical codes designed to simulate fuel behaviour under irradiation must include the radial distribution of power density, burnup and concentration of diverse nuclides to produce predictions valid in the high burnup range.

The complete treatment of all the isotopes involved in the nuclear reactions within the pellet encompassing the whole energy spectrum is the task of the codes specialized in reactor physics. A simplified treatment consisting in reducing the energy spectrum to a single group

was proposed in the past [7]. The calculation scheme chosen for DIONISIO consists in adopting this simplification and restricting the balance equations to the more abundant isotopes: ^{235}U, ^{236}U, ^{238}U, ^{239}Pu, ^{240}Pu, ^{241}Pu and ^{242}Pu. Starting from reliable values of the isotopes concentrations obtained with the neutronic codes CONDOR [8] and HUEMUL [9] in a range of irradiation conditions, empirical expressions were fitted to represent, with the higher possible accuracy, the absorption, capture and fission cross sections of these isotopes as functions of the initial enrichment in ^{235}U, the average burnup and the radial coordinate, within the approximation of one neutron energy group.

The general trend to extending the time of residence of the fuel in the reactor is generally accomplished by increasing the initial loading of fissile elements in the fuel via enrichment. This originates the need of introducing some neutron absorber material in the core to compensate the reactivity in excess in the fresh fuel. One of the usual strategies consists in including Gd_2O_3 as burnable absorber in the UO_2 matrix. Its presence has significant effects on the fuel performance: radial modification of the power profile, degradation of the thermal conductivity of the fuel and reduction of the fuel melting point. DIONISIO 2.0 is capable of simulating UO_2 fuels doped with Gd_2O_3 as a burnable poison. The system of equations described above is enlarged to include the Gd 155 and 157 isotopes that play a role in the burnup process, particularly at the beginning of fuel irradiation.

The inhomogeneous distribution of fissile Pu isotopes that builds up for extended irradiation periods and the consequent increase of local burnup in the pellet periphery (rim zone) originate the gradual development of a new microstructure characterized by small grains and large pores as compared with those of the original material. In this region Xe is absent from the solid lattice (although it continues to be dissolved in the rest of the pellet). The porous microstructure in the pellet edge causes local changes in the mechanical and thermal properties, thus affecting the overall fuel behaviour.

A model was developed to describe the behaviour and progress of porosity at local burnup values ranging from 60 to 300 MWd/kgU [8]. The analysis includes the interactions of different orders between open and closed pores (as in Refs [10, 11]), the growth of the pore radius by capturing vacancies, the evolution of the number density of pores, the overpressure within the closed pores and the inventory of fission gas dissolved in the matrix, retained in the closed pores and released to the free volume of the rod.

3. CODE VALIDATIONS

Several experimental data reported in IAEA data basis that cover the extended burnup range were simulated with the recent version 2.0 of DIONISIO. Some of the many results are presented below and compared with the measurements or with the results of other codes.

With the aim of showing the improvement obtained with the axial partition of the rod, the conditions of the PRIMO (PWR Reference Irradiation of MOX Fuels) experiment were simulated [12]. This program that started in 1986 was cosponsored by several institutions and fuel vendors, with the aim of testing the performance of eight codes from different countries [13]. It consisted in the irradiation of a single instrumented rod, named BD8, in the BR3 reactor during cycles 4D1 and 4D2 prior to being transferred to the ISABELLE 1 loop for ramping in the OSIRIS reactor. The data for the base irradiation are given as histograms of the linear power vs. time for twelve axial zones in the rod.

FIG. 2a) shows the experimental linear power history of five sectors selected as examples, averaged as sequences of constant power steps. The final power ramp is seen as a vertical line since it develops in a shot time interval. In Figure 2b) the curves represent the simulation with DIONISIO 2.0 of the centre temperature of those individual sectors. The results of the predictions of the participant codes fall in a range of values which is superimposed for comparison. In Figure 2c) and d) the curves express respectively the simulation of the fission gas released by the whole rod and the internal pressure. The contributions of the twelve sectors are taken into account in the calculations. In these figures also the vertical segment represents the range of results obtained with the codes that participated in the experiment.

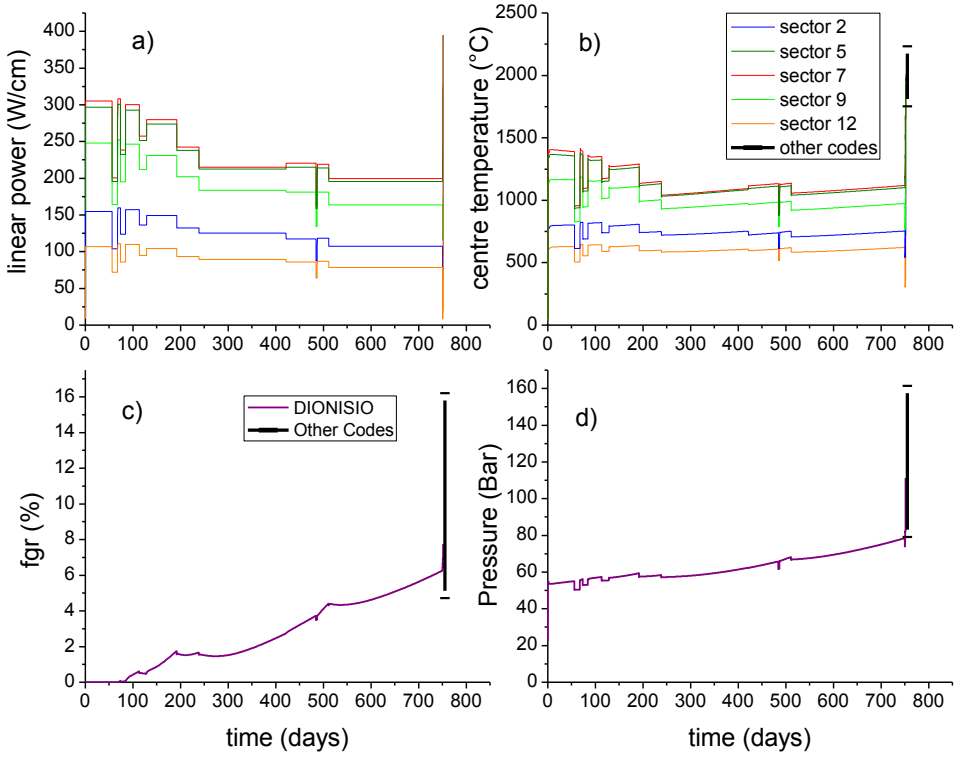

FIG. 2a) Experimental data of the linear power in five selected sectors of the BD8 rod. b) Centre temperature for those sectors. c) fgr and d) pressure in the whole rod. In b), c) and d) the curves represent the simulations with DIONISIO 2.0 and the points the maximum and minimum predictions of other codes.

A wide set of experiments compiled in the IAEA data bank [14, 15] were simulated to test the performance of the code in its present form. They are listed and briefly described in Table 1.

TABLE 1. EXPERMENTS USED TO VALIDATE THE VERSION 2.0 OF DIONISIO

Experiment name	*N° of rods*	*Rreactor type /Ffuel type*	*References*
'IAEA_Blind'	3	PHWR, CANDU / UO_2	[16]
Contact	3	PWR / UO_2	[17]
FUMEX I	10	PWR / UO_2	[18]
CNEA_ MOX	2	PHWR, CANDU / MOX	[19]
PRIMO	1	PWR / MOX	[20]
AECL-bundle	4	PHWR, CANDU / UO_2	[20]

Experiment name	*N° of rods*	*Rreactor type /Ffuel type*	*References*
EFE-Ro	2	PHWR / UO_2	[21]
Regate	1	PWR / UO_2	[22]
IFA507	2	BWR / UO_2	[23]
IFA535	4	BWR / UO_2	[24]
IFA597	1	BWR / UO_2	[25]
IFA534	2	PWR / UO_2	[26]
IFA 429	7	PWR / UO_2	[27]
IFA 432	5	BWR / UO_2	[28]
IFA 533.2	1	BWR / UO_2	[29]
IFA 562.1	12	BWR / UO_2	[30]
Osiris	2	PWR / UO_2	[31]
Kola3	9	WVVER / UO_2	[32]
Riso2	16	PWR / UO_2	[33]
Riso 3	15	PWR / UO_2	[34]
Tribulation	19	PWR / UO_2	[35]
Hbep	79	PWR, BWR / UO_2	[36]
Gain	4	PWR, UO_2-Gd_2O_3	[37]
InterRamp	20	BWR, UO_2	[38]
SuperRamp	44	PWR/BWR, UO_2	[39]
Demo Ramp I/II	13	BWR, UO_2	[40]
Over Ramp	39	PWR, UO_2	[41]
Trans Ramp	18	PWR/BWR, UO_2	[42]
Sofit	7	VVER, UO_2	[43]
Br3	5	PWR, UO_2	[44]
Irdmr	7	PHWR, UO_2	[45]
Uspwr16x16	9	PWR, UO_2	[46]
Spc-Re	20	PWR, UO_2	[47]

To test the quality of the predictions of concentration of different elements a large number of experiments were simulated and compared with the data. Fig. 2 shows the comparison between calculated and measured content of total Uranium and Plutonium corresponding to experiments listed in Table 1. In the plots dotted parallel lines are drawn at both sides of the line of perfect agreement to underline the good accord between calculations and measurements. In particular for Pu, 98% of the nearly 500 plotted points fall within the fringe ± 0.5 wt% at both sides of the bisector of the first quadrant. Equivalently, the mean value of the absolute difference between calculated and measured values represents 15.4% of the mean value of the measured data, expressing also the good quality of the approximation reached with the simulations.

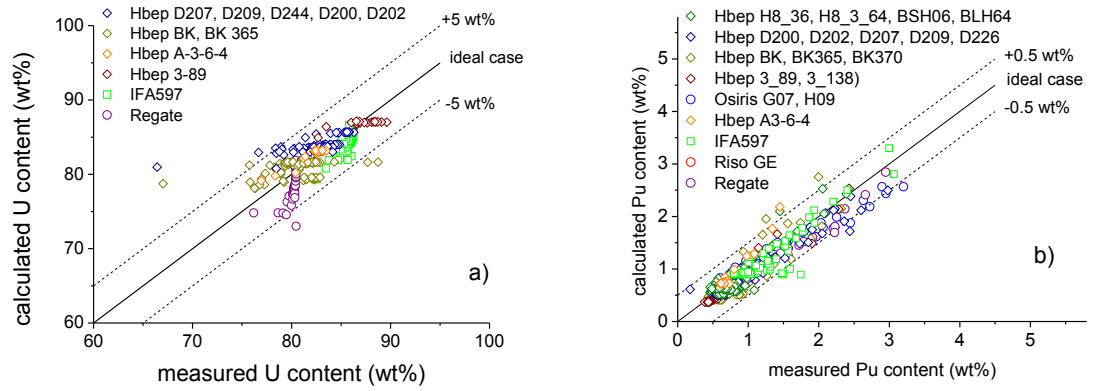

FIG. 2. Calculated vs. measured values of local concentration of a) U and b) Pu.

As in Figure 3, calculated and measured values of average burnup, centre temperature, FGR and internal pressure for experiments selected from Table 1 are compared in Fig.4.

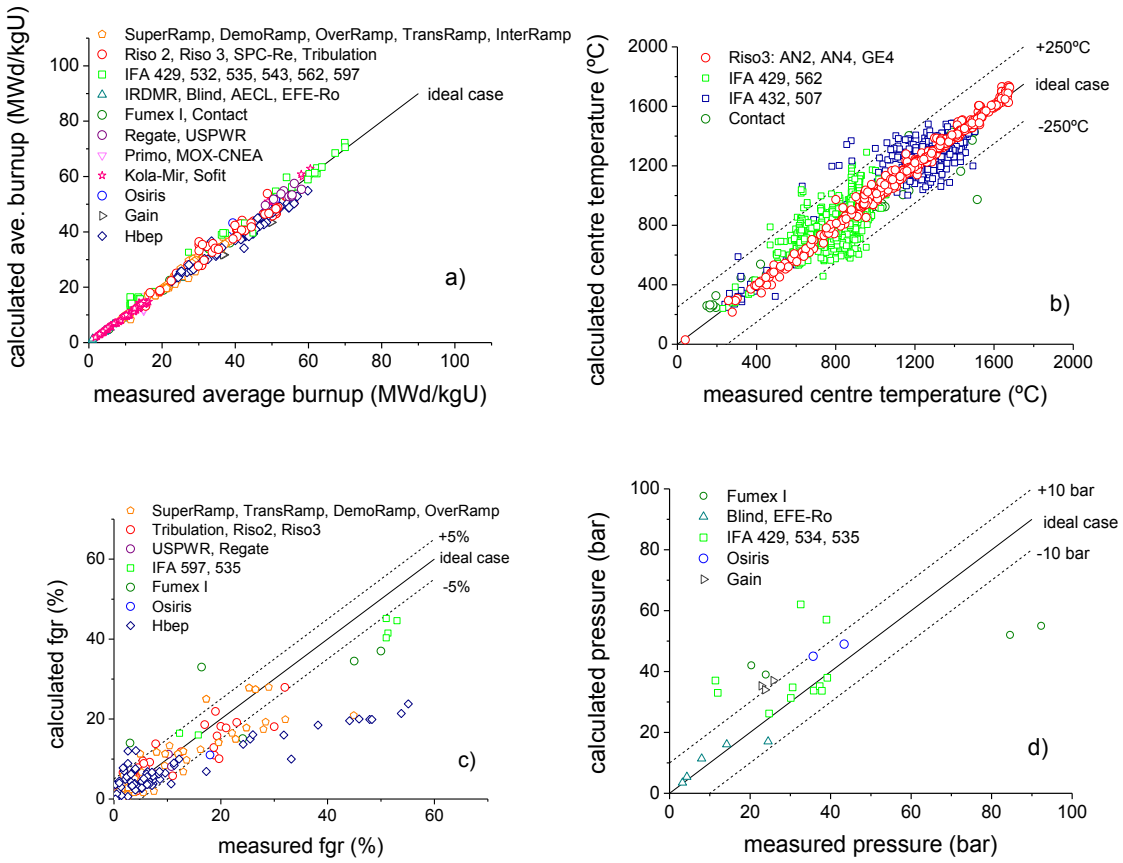

FIG. 3. Calculated vs. measured data of a) average burnup, b) centre temperature, c) FGR and d) internal pressure for experiments selected from Table 1.

Due to thermal expansion and mechanical restrictions, the pellet experiences a non-uniform deformation: the initially cylindrical pellet surface distorts, bending outwards, the top and bottom faces being displaced further than the central belt [5]. If the pellet strain is sufficiently large, it may come into contact with the cladding (PCMI), particularly in regions next to the pellet-pellet contact surfaces, giving place to a bamboo type differential deformation in the

cladding evidenced by the presence of equidistant circumferential ridges. The two-dimensional structure of DIONISIO along with the model of mechanical contact included in it allows an acceptable description of the bamboo effect and the radial cladding deformation. As an example a comparison is made in Figure 4a) between measurements and simulations corresponding to the ABS rod from the IRDMR experiment. The plot shows the evolution of the pellet strain at the middle pellet plane (minimum strain) and at the pellet-pellet interface (maximum strain). In Fig. 4b), the simulated pellet and internal cladding radii corresponding to the plane of maximum strain are plotted vs. burnup; the scale is given at the right side. The hoop stress is also plotted in the left axis.

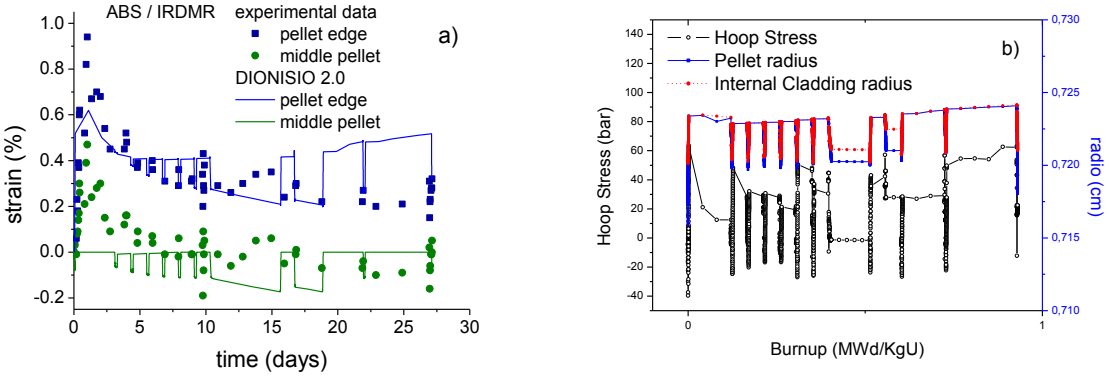

FIG. 4a) Comparison between measurements and the predictions of DIONISIO for the eevolution of strain in the ABS rod of the IRDMR experiment. b) Evolution of pellet, internal cladding radius and hoop stress for the same rod.

4. CONCLUSIONS

The present architecture of the code allows a more realistic simulation of the fuel rod behaviour since each axial section can be modeled starting from the local values of linear power and coolant temperature. Due to the non-uniformity of the conditions to which the different portions of fuel rod are subjected during operation, several phenomena can start at (or take place only in) the central part of the bar and begin much later (or never happen) at the rod ends. The release of fission gases and the pellet cladding mechanical contact are just two examples of phenomena of these characteristics. The previous version of DIONISIO assumed a uniform power in the whole rod length. The choice of this value as the average linear power can lead to underestimation of the amount of gas released or to overestimation of the time for initiation of release, and vice versa if the simulation is carried out assuming the whole rod at the maximum power. Evidently, a correct calculation of gas release, as for its volume or initiation time, plays a significant role with reference to the prediction of all the physical parameters of the rod (internal pressure, temperature distribution, etc.) A similar difficulty is probably present in those codes that perform the rod simulation in a one-dimensional approximation.

With the improvements recently introduced, involving subroutines for the physical and chemical properties of the fuel material in the high burnup range, the code DIONISIO in its version 2.0 evidenced a good performance in the numerous simulations of experimental situations typical of PWR, BWR and PHWR fuels. On this basis, DIONISIO 2.0 can be regarded as an adequate simulation tool for average burnup levels as high as 60 MWd/kgU.

REFERENCES

[1] DENIS, A., PIOTRKOWSKI, R., Simulation of isothermal fission gas release, J. Nucl. Mater. **229** (1996) 149–154.

[2] SOBA, A., DENIS, A., ROMERO, L., VILLARINO, E., SARDELLA, F., A high burnup model developed for the DIONISIO code, J. Nucl. Mater. **433** (2013).

[3] LEMES, M., Estudio analítico y numérico de los efectos de la irradiación hasta alto quemado en combustibles de reactores de potencia, Master Thesis, (2013) Instituto Sabato, University of San Martín, Argentina.

[4] SOBA, A., DENIS, A., LEMES, M., sent for publication.

[5] LASSMANN, K., WALKER, C., van de LAAR, J., LINDSTRÖM, F., Modelling the high burnup UO_2 structure in LWR fuel, J. Nucl. Mat., **226** (1995) 1-8.

[6] LASSMANN, K., SCHUBERT, A., van de LAAR, J., Recent developments of the TRANSURANUS code with emphasis on high burnup phenomena, International Conference on Nuclear Fuel for Today and Tomorrow (2003).

[7] PALMER, I., HESKETH, K., JACKSON, P., in: J. Gittus (Ed.), Water Reactor Fuel Element Performance Computer Modelling, Applied Science, Barking, UK, 1983, p. 321.

[8] VILLARINO**,** E., CONDOR calculation package PHYSOR 2002, Seoul, Korea, Republic of, October 7-10, 2002.

[9] GRANT, C., Manual del sistema HUEMUL, versión 4. Informe Interno CNEA, MCO-06-REC-1. *code* (in preparation).

[10] BLAIR, P., Modelling of fission gas behaviour in high burnup nuclear fuel, PhD Thesis, École Polytechnique Federale de Lausanne, Suiza (2008).

[11] KHVOSTOV, G., MIKITYUK, K., ZIMMERMANN, M., A model for fission gas release and gaseous swelling for the uranium dioxide fuel coupled with the FALCON code, Nuc. Eng.& Des. **241** (2011) 2983-3007.

[12] Van UFFELEN, P., PRIMO, PWR reference irradiation of MOX fuels, Data of a ramped MOX Ffel rod, SCK-CEN, Mol, Belgium, (2002).

[13] OTT, L., Mixed-oxide (MOX) fuel performance benchmark. Summary of the results for the PRIMO MOX rod BD8. NEA No. 6291 (2009).

[14] http://www.iaea.org.

[15] http://www.oecd-nea.org/science/fuel/ifpelst.html.

[16] SAH, D., VISWANATHAN, U., VISWANADHAM, C., UNNIKRISHNAN, K., RATH, B., Blind prediction exercise on modelling of PHWR fuel at extended burnup, J. Nucl. Mater. 383 (2008).

[17] IFPE/CONTACT Rev.1. Database for CONTACT experiments irradiated at CEA Grenoble. J A Turnbull, (1998).

[18] Fuel Modelling at Extended Burnup, IAEA–TECDOC–998, IAEA (1998).

[19] MARINO, A., PÉREZ, E., ADELFANG, P., Irradiation of argentine (U,Pu)O_2 MOX fuels. Postirradiation results and experimental analysis with the BACO code, J.Nucl. Mater. 229 (1996).

[20] ARISMESCU, V., NEA-1596 IFPE/AECL-BUNDLE, Chalk River, ONTARIO. (2000).

[21] PARASCHIV, M.C., Romanian irradiation tests, OECD/IAEA, IFPE Database, (2001).

[22] NEA-1696 IFPE/REGATE L10.3.

[23] NEA-1729 IFPE/IFA-507-TF3-TF5 (2004).

[24] TOSI, V., The effect of pressurisation on fission gas release in high burnup BWR-type fuel rods (IFA-535.5 - 6), HWR-198, NEA-1548/01 (1987).

[25] MALÉN, K., MICSKI, A., SCHRIRE, D., NILSSON, B., PIE of high burnup BWR

fuel rod IFA-597.3 (Rod8), Studsvik Nuclear AB SwedenHRP-356/U. (1997).
[26] NEA-1684 IFPE/IFA-534.14REV.1 (2005).
[27] NEA-1546 IFPE/IFA-429 (1997).
[28] NEA-1488 IFPE/IFA-432 (1996).
[29] NEA-1549 IFPE/IFA-533.2 (1997).
[30] NEA-1547 IFPE/IFA-562.1 (1997).
[31] IFPE/OSIRIS, NEA-1622/04.
[32] IFPE/KOLA-3-MIR-RAMP, NEA-1766/02.
[33] NEA-1502 IFPE/RISOE-II, IFPE/RISOEII, Fuel Performance Data from Transient Fission Gas Release (1995).
[34] IFPE/RISOEIII, NEA-1493/17.
[35] NEA-1536 IFPE/TRIBULATION R1
[36] NEA-1510 IFPE/HBEP-3 REV.1, High Burnup Effects Programme. Final Report, DOE/NE/ 34046-1 [HBEP-61(3P27)].
[37] NEA-1625 IFPE/GAIN.
[38] FINAL REPORT OF THE INTER-RAMP PROJECT Studsvik Staff (1979).
[39] FINAL REPORT OF THE SUPER-RAMP PROJECT, Seved Djurle Studsvik (1984).
[40] DJURLE, S., Final Report of the STUDSVIK DEMO-RAMP I Project, STUDSVIK-STDRI-18 (1983); STUDSVIK-STDRII-13; THE STUDSVIK DEMO-RAMP II Project. Final Report (1981).
[41] NEA-1556 IFPE/OVER-RAMP (1997); STUDSVIK-STOR-37, THE STUDSVIK OVER-RAMP PROJECT FINAL REPORT (1981).
[42] DJURLE, S., STUDSVIK-STTRI-10 Final Report of the TRANS-RAMP I Project (1985); NEA-1648 IFPE/TRANS-RAMP-I, II and IV (2003); STUDSVIK/SlTRIV-25 (1994).
[43] Losonen, P., Verification of TRANSURANUS code against temperature data from VVER type test tie1 rods from SOFIT experiments, IAEA/OECD Data Base Training Meeting, Halden, Norway (1996).
[44] EA-1560 IFPE/BR3-HBFRHCP (2003).
[45] NEA-1777 IFPE/CANDU-IRDMR (2007).
[46] LYON, W., US-PWR 16x16 LTA Extended Burnup Demonstration Program Summary File (2005).
[47] SOFER, G., van SWAM, L., SPC-re-ginna: Annular-Pellet Barrier-Clad Fuel Assemblies at the R.E.Ginna PWR: Hotcell Examinations EP 80-17. Final Report, Volume 1 (1997).

SIMULATION OF HIGH BURNUP FUEL FRAGMENTATION IN HIGH TEMPERATURE TRANSIENTS

Z. HÓZER, B. SOMFAI, K. KULACSY

Hungarian Academy of Sciences Centre for Energy Research
Budapest, Hungary
zoltan.hozer@energia.mta.hu

Abstract. Fragmentation and relocation of the high burnup fuel pellets was observed in Halden LOCA tests and in Studsvik hot cell experiments. A simple model has been developed for the analysis of the mechanical behaviour of the fuel pellet to explain the fragmentation mechanism. High pore pressure and porosity can cause such stresses in high burnup fuel pellet that can lead to fragmentation of UO_2.

1. INTRODUCTION

Significant fragmentation and relocation of high burnup (92 MWd/kgU) fuel pellets was observed in IFA-650.4 LOCA test in the Halden reactor. Cladding burst occurred at 790 °C and part of the fuel fragments were released from the ballooned section of the cladding into the coolant (Figure 1). Under similar test conditions the fresh fuel pellets remained intact in other tests in the same reactor. Later experiments with high burnup pellets also showed the fragmentation and relocation process. On the basis of these observations could be concluded that there are some burnup dependent phenomena or mechanisms that are the driving forces for fuel fragmentation.

FIG. 1. Fragmented high burnup fuel pellet in Halden LOCA test [1].

Recently another tests series was performed with irradiated fuel segments (72 MWd/kgU) in Studsvik hot cells. The simulated high temperature LOCA scenarios also indicated that fuel fragmentation can take place in high burnup fuel during accidents conditions [2]. In these tests also significant fuel dispersal was observed during the experiment.

In order to identify the causes for the observed pellet fragmentation and to develop numerical models for prediction of the potential consequences of this phenomenon on reactor accidents, an analytical study has been carried out in the MTA Centre for Energy Research, Hungary. In the present paper the steps of model development and some calculated results are summarised.

2. ANALYSES OF THE POTENTIAL CAUSES OF PELLET FRAGMENTATION

The high burnup fuel pellets are characterised by high content of fission product and formation of high burnup structure at the external surface of the pellets. The gaseous fission

product (e.g. Xe and Kr) cannot remain in the fuel matrix, they migrate to the grain surfaces and form gas bubbles (pores).

For high temperature transients the heat-up of the pellets leads to the increase of pressure inside these bubbles. The high pressure in pores creates high mechanical stresses in the pellet and it can initiate the formation of crack and facilitate crack propagation along the gains. In our study it was investigated if such an effect could lead to the fragmentation observed in the Halden and Studsvik experiments.

2.1. Fracture strength

The integrity of the fuel pellet is determined by the fracture strength of UO_2 (normal stress at the beginning of fracture). If the stress is higher than the fracture strength local crack formation and fragmentation of the pellet can be expected. Fracture strength data versus temperature is seen in Figure 2 [3]. The rise of the temperature causes a slight fracture strength increase. The fracture strength measurements, however, show a large scattering. The fitted line (Knudsen equation) in Figure 3 was used in our study to predict fracture strength.

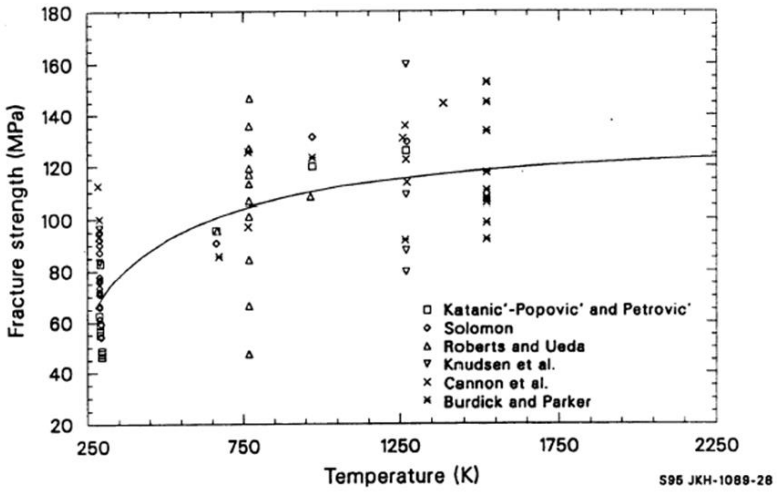

FIG. 2. Comparison of equation in the elastic regime with out-of-pile UO_2 fracture strength data normalised to 10 μm grain size and 95% theoretical density [3].

Figure 3 shows the calculated fracture strength versus porosity for different grain sizes. With increasing porosity fracture strength decreases exponentially. The initial fracture strength drops from ≈150 MPa to ≈100 MPa with 20% porosity. The dependence on grain size seems to be not very strong.

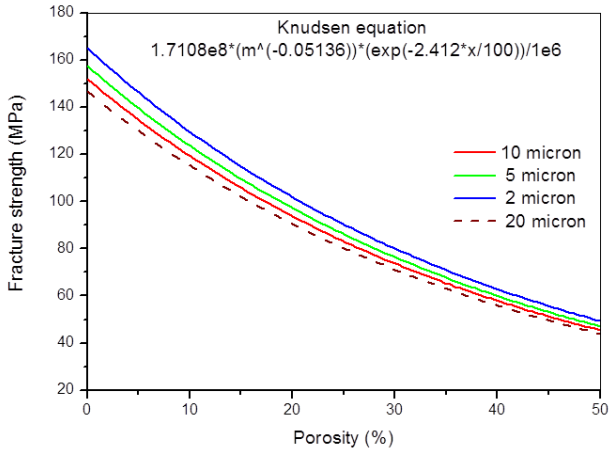

FIG. 3. Fracture strength versus different porosity fractions.

2.2. Pore pressure

Koo et al. [4] have calculated pore pressure in the rim as a function of pellet average burnup and pore radius as seen in Figure 4. With increasing burnup the pressure increases due to collection of more gases in the pores. According to their model calculations the gas pressure in the pores of high burnup fuel can be as high as several hundreds MPa, and the pressure is higher in small pores than in large pores.

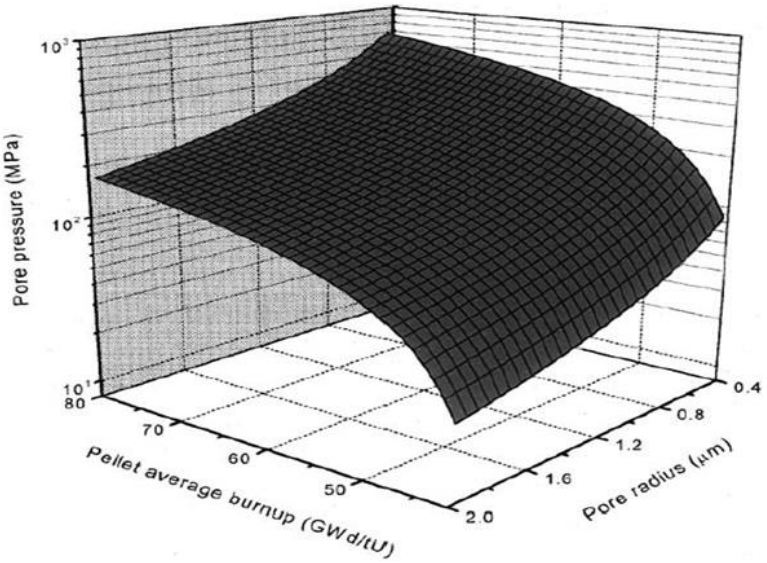

FIG. 4. Calculated pore pressure in the rim [4].

2.3. Stresses in the pellet

A simple model has been developed for the analysis of the mechanical behaviour of the fuel pellet. The pellet was divided into elementary cells and the forces were determined for cell boundaries. The calculated stresses were compared to fracture strength.

It was assumed that the pore size is uniform and the pore pressure is the same throughout the whole pellet. The location of pores is equidistant on peripheral line parallel to the pellet surface and their shape is spherical. Stress was calculated between two pores along the peripheral line as seen in Figure 5.

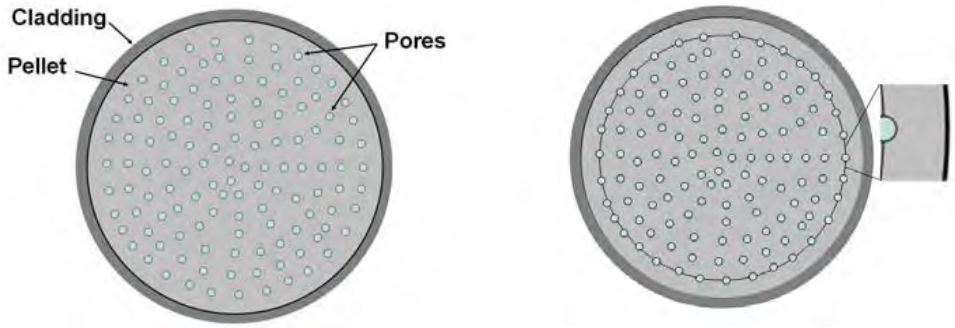

FIG. 5. Schematic figures of the pellet and the elementary cell.

In case of normal operation mechanical equilibrium exists between the internal pressure in the pores and the stresses in the cladding, the pellet therefore remains intact (Figure 6, left). During LOCA accident the ballooning process creates a gap between the pellet and the cladding and the mechanical equilibrium can be lost (Figure 6, right). The high internal pressure in pores can initiate fracture development along the grain boundaries and this process can lead to pellet fragmentation.

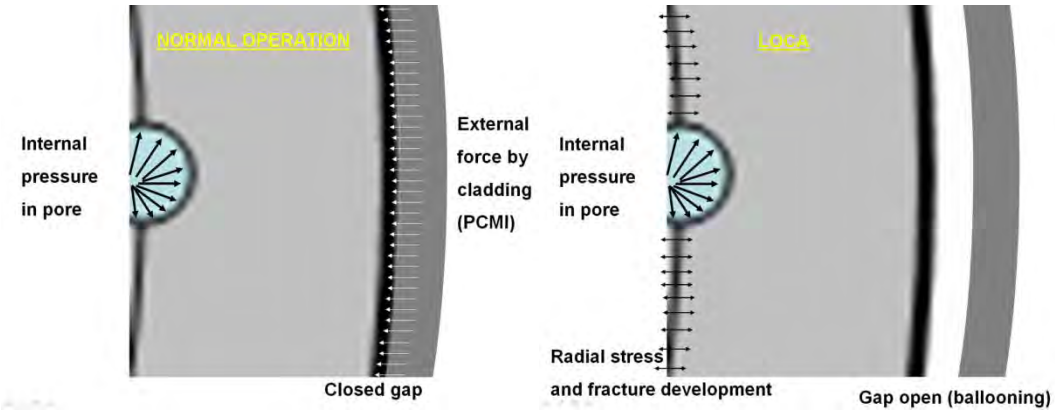

FIG. 6. Stresses in the pellet in case of normal operation (left) and LOCA (right).

Stresses were calculated along the external ring (Figure 5) between two pores. The bubble size was considered 1 μm. The distance between the bubbles was determined using the porosity and the geometrical parameters corresponding to uniform distribution of pores as shown in Figure 5. Calculations were carried out with different pressure values (between 100 and 300 MPa) as seen in Figure 7. These pressure values seem to be realistic data according to Figure 4. The created stresses are rather high: several hundreds MPa. The fracture strength (Figure 3) is in the same order or even less for high porosity cases. For this reason can be concluded that the stresses formed in the high burnup pellets during LOCA accidents can create stresses higher than the fracture strength and it can result in formation of crack in the uranium oxide pellet.

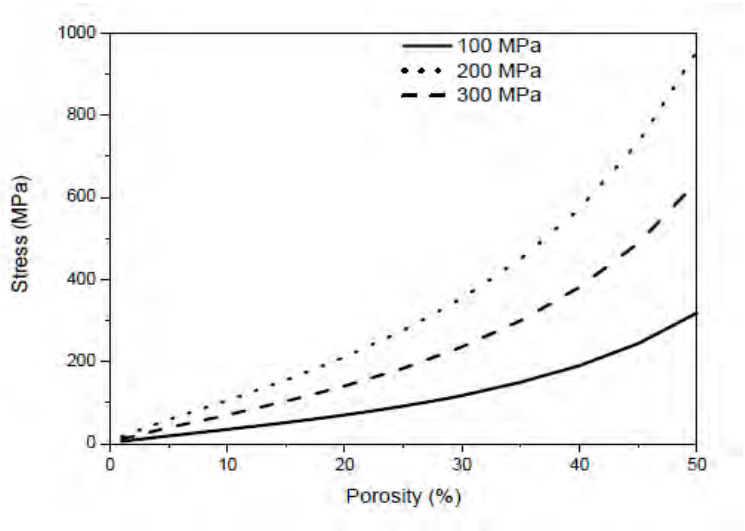

FIG. 7. Stress versus porosity for different pore pressures.

It was concluded on the basis of the above analysis with idealised pellet geometry, that high pore pressure and porosity can cause stress in high burnup fuel pellet that can lead to fragmentation of UO_2. This can explain the fuel fragmentation observed in the Halen and Studsvik experiments. It was also pointed out that more detailed calculations would be needed to determine a threshold value and the conditions of fuel fragmentation and simulate the behaviour of real pellet structure.

3. SIMULATION OF PELLET FRAGMENTATION DURING LOCA

The IFA-650.5 experiment was calculated in the framework of an OECD benchmark using different fuel behaviour codes [5]. The codes describe the thermal and mechanical behaviour, but do not simulate fuel fragmentation. For this reason, using the results of a code calculation and some specific data on pore size distribution a special calculation was carried out to describe the changes in the microstructure of the high burnup pellet during the in-pile LOCA test. In this chapter the calculations details are presented.

3.1. Objectives of the numerical simulation

During a LOCA accident the high burnup structure at the rim of the pellets with a high burnup may fragment into microscopic pieces and the fine debris may relocate into the ballooned section of the cladding, decreasing the coolability of the fuel pin. Moreover, the fragmentation releases some of the gas trapped in the pores of the HBS, increasing the pressure inside the pin. The main objectives of this study were the followings:

- determine when the fragmentation occurs under LOCA conditions,
- calculate the amount of fission gases getting into the free volume from the pores and
- refine the existing models: take the pore size distribution into account on mechanical basis

3.2. Steady state and transient conditions

The IFA-650.5 test was used for modelling. The segment burnup was 83.4 MWd/kgU. The target cladding temperature was 1100°C and the burst occurred at 750°C.

Normal operation and LOCA simulations of the segment made with the fuel behaviour code TRANSURANUS [6]. The TRANSURANUS results were generally in good agreement with

the measured data, especially for the quantities used in the model. During the LOCA the maximum surface temperature of the pellets was calculated to be between 1000 and 1200 °C. The final HBS was 1.8 mm thick and the burnup at the pellet rim was above 140 MWd/kgU.

3.3. Pore size distribution

The pore size distribution was an important parameter in this study. In order to get reliable data a ceramographic picture of cross sections of the test rod was analyzed. Using image analyses software, the pore sizes and their distribution at certain positions was determined.

Since it was intended to use the model at different axial elevations and radial positions, it was necessary to determine the local pore size distribution at different burnups where measured or calculated data are not available. The available data are shown in Figure 8. These data cover the average pellet burnup range from 56 to 102 MWd/kgU which match to local burnup range from 81 to 174 MWd/kgU. Within this range interpolation was used to determine the pore size distribution and out of the range extrapolation was applied with adequate foresight.

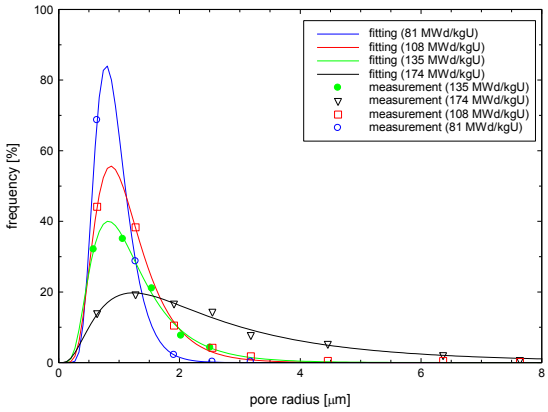

FIG. 8. Frequency versus pore radius at different burnups (measured data).

Log-normal fitting was done and some of the interpolated curves are seen in Figure 9. 2/3 of the pores are smaller than 2.2 micron. Pores above 5 micron diameter were not counted, because the mechanism of their formation may be different.

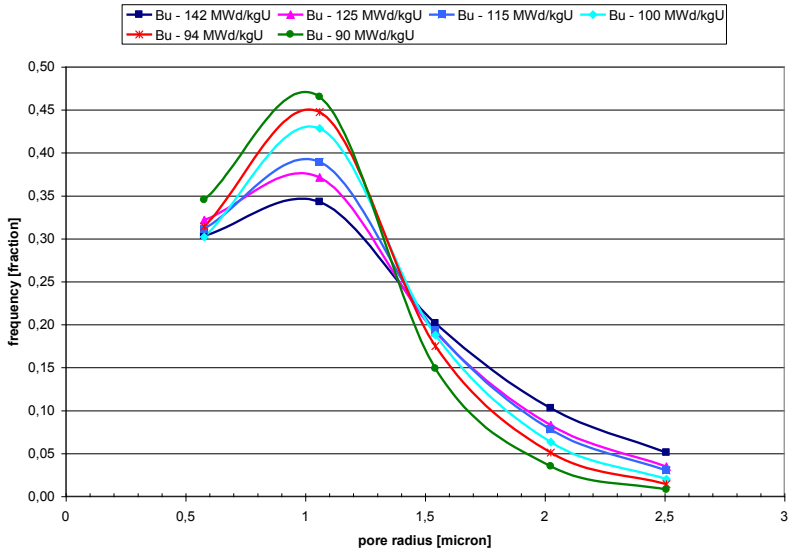

FIG. 9. Frequency versus pore radius at different burnups (fitted curves).

3.4. Pore pressure calculation

For the pore pressure calculation the assumptions were the followings: along the pellet radius the typical pore size is the same, the pore size distribution is changing and the amount of the pores are changing. The porosity of the pellet at different positions was taken from the TRANSURANUS calculation.

The amount of the fission gases in the different pores were needed for the calculation of the pore pressure. The TRANSURANUS calculations provided the amount of produced fission gases for a volume unit of UO_2 and these fission gases were distributed among the pores.

In Figure 10 the pressure of the different size pores can be seen after the base irradiation at room temperature. The pressure is the highest in the smallest pores, it is $\approx 1{,}8 \cdot 10^8$ Pa. The model was compared with the method of Koo pore pressure calculation [4]. The Koo model does not count with pore size distribution, only the average pore size is used, although it has a big influence on the pressure. The two methods show good agreement.

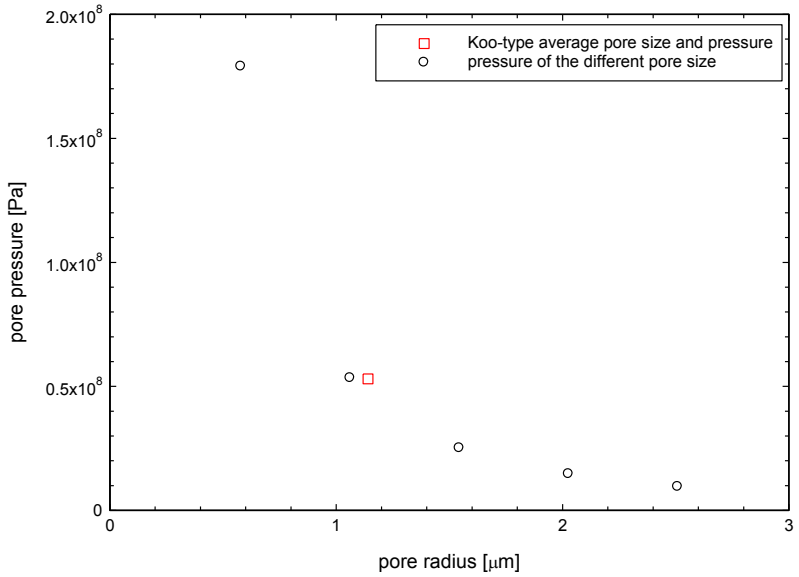

FIG. 10. Pore pressures as function of pore radius.

3.5. Simulation of test conditions in IFA-650.5 test

The temperature of the pellet surface and the rod pressure history under LOCA experiment can be seen in Figure 11. On the pressure curve a small increase can be found from 126 second until the burst. It could have been caused by the fragmentation so the fission gases get into the free volume which can cause pressure increase.

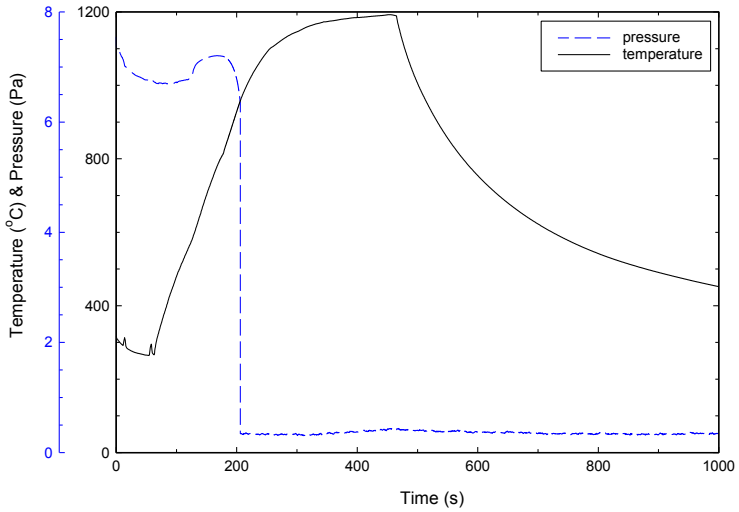

FIG. 11. Pressure and temperature histories in IFA-650.5 experiment.

According to our model only the small pores cause stress high enough to fragment the HBS. If the stress is higher in the UO_2 matrix between 2 pores than the valid fracture strength at given conditions the pellet will fracture most probably. The fracture strength is described by the Knudsen equation. It depends on the porosity so the fracture strength is different in every radial position.

The stress histories are shown with the continuous curves (Figure 12) and the dashed curves are the solutions of the Knudsen equation. The red curve shows the temperature history. It can be seen that first, in the outermost ring, about 110 seconds the stress curve crosses the fracture strength curve which belongs to it. It means the ring of the pellet fragmented at this time. The main fragmentation occurred in the interval of 140 to 160 seconds and 640 to 750 °C. It is worth noting that the time concurs with the increase of pressure in Figure 10 and the temperatures overlap with the literature data. Figure 12 shows that the last rig which was fragmented is number 41 out of 50. This rig corresponds to 0.899 relative radius. The developed HBS structure was thicker but the gas content of the pores, because of the lower burnup, are not enough to cause fragmentation. In other axial position, because of different local parameters (burnup, power, temperature) the fragmented region was, of course, not the same.

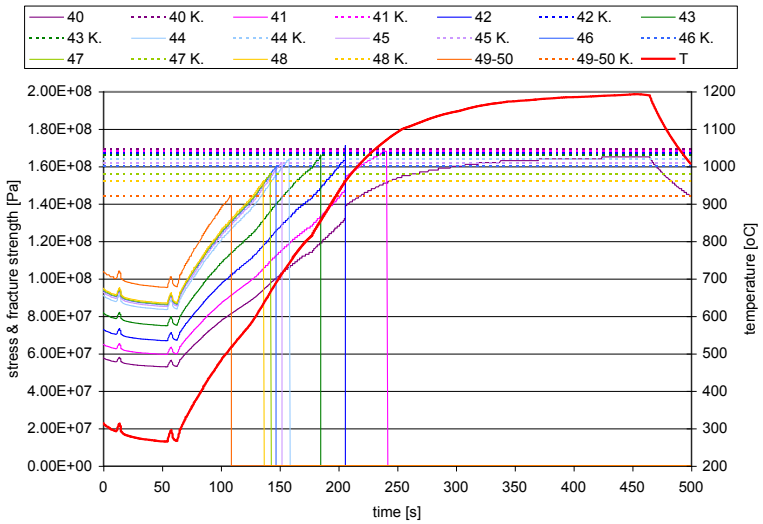

FIG. 12. Calculated stress in different regions of the pellet as function of time and temperature history of IFA-650.5 test.

These pores contain approximately 15-16% of the gas in the porosity which can escape to the pin free volume during fragmentation. According to the calculations the amount of gas from the small pores caused 4% pressure increase (produced as an integral of gas releases in each axial position) and the measured increase was app. 7%.

The model predicted that a nearly 0.5 mm thick outer HBS layer would fragment. This is in agreement with the post irradiation examinations.

4. CONCLUSIONS

The fuel fragmentation of high burnup pellets during LOCA accidents was analyzed in the present study.

It was pointed out that accumulated fission gases in the pores can produce very high pressure that is enough to initiate crack formation in the pellet.

The following parameters were determined for a selected experimental scenario:

- the burnup dependent pore size distribution in the HBS,
- the accumulated fission gas pressure in the different sized pores,
- the stresses in the material between the pores,
- threshold value of fracture strength where the pellet fragments,
- the fragmentation fraction of pellet volume and the mass/volume of fission gases released due to fragmentation.

The present model is suitable for predicting the fragmentation of the HBS of the fuel pellets with average burnups between 56 and 102 MWday/kgU and the ensuing extra fission gas release during LOCA. With temperature history similar to IFA-650.5 LOCA test, the estimated fragmentation limit is ≈90 MWd/kgU local burnup.

ACKNOWLEDGEMENTS

The authors are grateful to Mr Csaba Győri for performing TRANSURANUS calculations and to Mrs Anna Csordás Pintér for image analysis of ceramography pictures.

REFERENCES

[1] OECD NUCLEAR ENERGY AGENCY, Safety significance of the Halden IFA-650 LOCA test results, NEA/CSNI/R(2010)5, OECD, Paris (2010), https://www.oecd-nea.org/nsd/docs/2010/csni-r2010-5.pdf.

[2] RAYNAUD, P.A.C, Fuel fragmentation, relocation, and dispersal during the loss-of-coolant accident, NUREG-2121, US RNRC (2012), http://pbadupws.nrc.gov/docs/ML1209/ML12090A018.pdf.

[3] SIEFKEN, L.J, CORYELL, E.W., HARVEGO, E.A., HOHORST, J. K., ARNDT, S.A., SCDAP/RELAP5/MOD 3.3 code manual MATPRO - A library of materials properties for light-water-reactor accident analysis, NUREG/CR-6150, Vol. 4, Rev. 2 INEL-96/0422, US NRC (2001), http://pbadupws.nrc.gov/docs/ML0103/ML010330363.pdf

[4] KOO, Y.H., LEE, B.H., CHEON, J.S, SOHN, D.S., Pore pressure and swelling in the rim region of LWR high burnup UO_2 fuel, J. Nuc. Mat., **295** (2001) 213.

[5] OECD NUCLEAR ENERGY AGENCY, Benchmark calculations on Halden IFS-6506 LOCA test results, NEA/CSNI/R(2010), OECD, Paris (2010), https://www.oecd-nea.org/nsd/docs/2010/csni-r2010-6.pdf.

[6] LASSMANN, K., TRANSURANUS: a fuel rod analysis code ready for use, J. Nuc. Mat. **188** (1992) 295.

EXPERIMENTAL AND COMPUTATIONAL STUDIES OF VVER HIGH BURNUP FUEL BEHAVIOUR UNDER LOCA CONDITIONS (MIR-LOCA/60 TEST)

P.V. FEDOTOV[a], A.V. KUMACHEV[a], O.A. NECHAEVA[a], V.V. NOVIKOV[a], A.V. SALATOV[a], M.V. SYPCHENKO[a], A.V.ALEXEEV[b], A.V. GORYACHEV[b], I.V. KISSELEVA[b], V.N. SHULIMOV[b]

[a]JSC «VNIINM», Moscow, Russian Federation
+7(495)190-80-39,
avs@bochvar.ru

[b]JSC«SSC-RIAR», Dimitrovgrad, Russian Federation

Abstract.

The MIR-LOCA/60 experiment with VVER high burnup fuel was performed in the MIR research reactor (SSC-RIAR) in 2010. Experimental fuel assembly with 16-th fresh and three refabricated VVER-1000 type test fuel rods with burnup of 58.1 - 58.6 MWd/kgU was tested.The purpose of MIR-LOCA/60 experiment was the study of thermomechanical behaviour of VVER high burnup fuel at typical conditions for LOCA design accidents. The maximum indications of fuel thermal couple (TC) didn't exceed the level of ~860 °C, TC registration for fresh fuel rods cladding was about 820°C. The duration of cladding temperature holding at the level of more than 700 °C was about one minute.As a result of PIE of the tested FA deformations and corrosion of claddings and structure of fresh (unirradiated) and spent fuel pellets were defined.In experiment there was a rupture of four fresh fuel rods. Refabricated fuel rods were remained intact. Fracture and relocation of fuel pellets of refabricated fuel rods weren't observed.Post-test neutron, thermohydraulic and thermomechanical calculations were carried out. As a result the estimations of temperature regime for refabricated fuel rods were received. The assessment of the maximum temperature of refabricated fuel rod claddings is in the range of ~ 700 - 800 °C.

1. BRIEF DESCRIPTION OF EXPERIMENT

The MIR-LOCA/60 experiment with VVER high burnup fuel was performed in the MIR research reactor (SSC-RIAR) in 2010. This work was performed in cooperation of the organizations: JSC«SSC-RIAR», Research Centre Kurchatov Institute, JSC «OKB Gidropress», JSC«OKBM Afrikantov», JSC«VNIINM», JSC«TVEL» [1].

Experimental fuel assembly (EFA) containing 16 fresh test fuel rods and 3 refabricated fuel rods of VVER-1000 type with burnup of 58.1 - 58.6 MWd/kgU was tested.

The purpose of MIR-LOCA/60 experiment was the study of behaviour of VVER high burnup fuel at typical conditions for LOCA:

- Research of deformations and rupture conditions of claddings, and oxidations of claddings;
- Research of fuel pellets destruction conditions and fuel relocation in the ballooning area of cladding.

The active area and the reflector of the MIR reactor in cross section (Figure 1) has form of a hexagon inscribed in circle with diameter of 975 mm. Core height - 1000mm. Green colour in Figure 1 marks the position of the experimental assembly in the core.

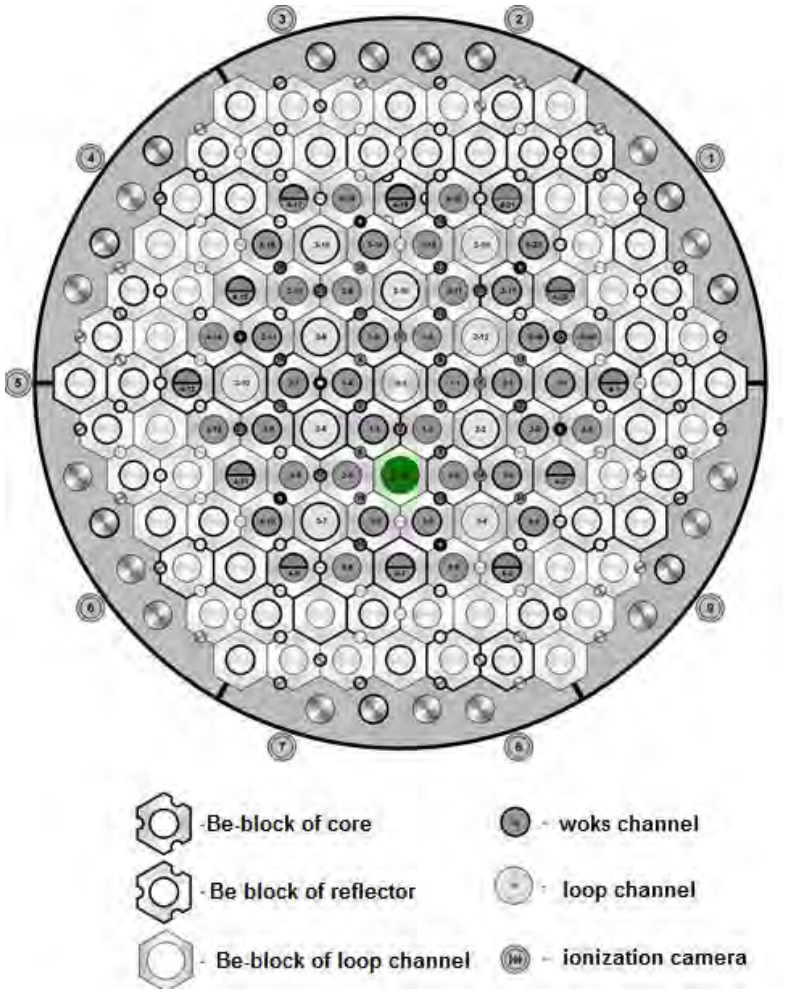

FIG. 1. EFA position in the reactor form.

Parameters of refabricated fuel rods before and after irradiation in Balakovo NPP during four cycles are presented in Table 1.

TABLE 1. PARAMETERS OF REFABRICATED FUEL RODS BEFORE AND AFTER IRRADIATION

Parameters of the original fuel rod before irradiation in VVER-1000		Parameters of the refabricated fuel rod RFR-2	
Cladding material	E110	Average fuel burn-up, MW*d/kgU	58.1
Diameter of fuel rod, mm	9.1	Fuel stack length, mm	977
Inner diameter of fuel rod, mm	7.72	Average cladding diameter, mm	9.03
Fuel material	UO_2	Filling gas	He
Pellet diameter, mm	7.57	Filling gas pressure, MPa	2.2
Diameter of central hole, mm	2.35	External oxide thikness, mkm	≤6
Pellet height, mm	9-12	Hidrogen concentration in cladding, ppm	≤80

Arrangement of fuel rods on the section of EFA and instrumentation of assembly are presented in Figure 2–3.

During test the experimental measuring system was efficient (see Figure 4–6), so the information for the computer modelling of thermal-mechanical behaviour of fuel rods was received.

The maximum indications of fuel thermocouple (TC) didn't exceed the value of ~860°C, for the TC of fresh fuel rods cladding was about ~820 °C, duration of holding of cladding at a temperature more than 700 °C was about 1 minute. (Figure 4–5).
The pressure sensors installed in one fresh fuel rod (# 18) and one refabricated fuel rod (# 16), showed that depressurization of these fuel rods in experiment didn't happen (Figure 6).

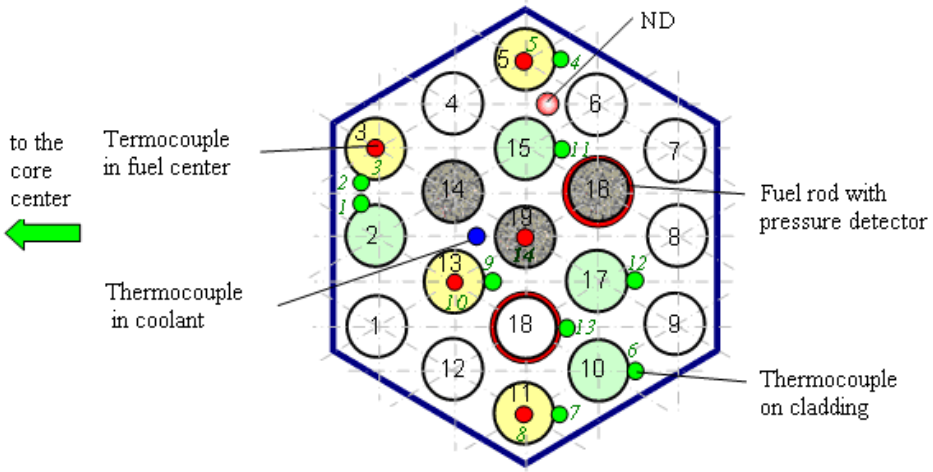

# 19	# 14	## 2,10,15,17	## 3,5,11,13	## 1,4,6, 7,8,9,12	# 18	# 16	between## 13,14,19
Refabricat. FR	Refabricat. FR	Fresh FR	Fresh FR	Fresh FR	Fresh FR	Refabricat. FR	
Fuel TC	Not instrument.	Cladding TC	Cladding TC (fuel TC)	Not instrument.	Pressure sensor and cladding TC	Pressure sensor	Coolant TC
T14		T1,T6,T11, T12	T2(T3),T4 (T5),T7(T8), T9 (T10)		T13		

FIG. 2. Arrangement of fuel rods in EFA section.

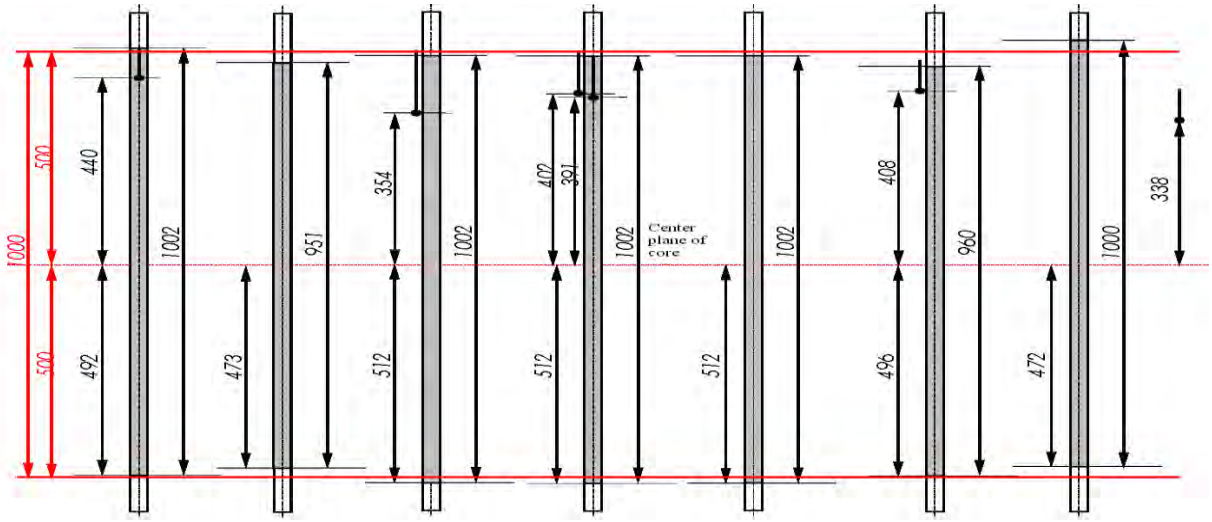

FIG. 3. Coordinates of thermocouples installed in EFA fuel rods.

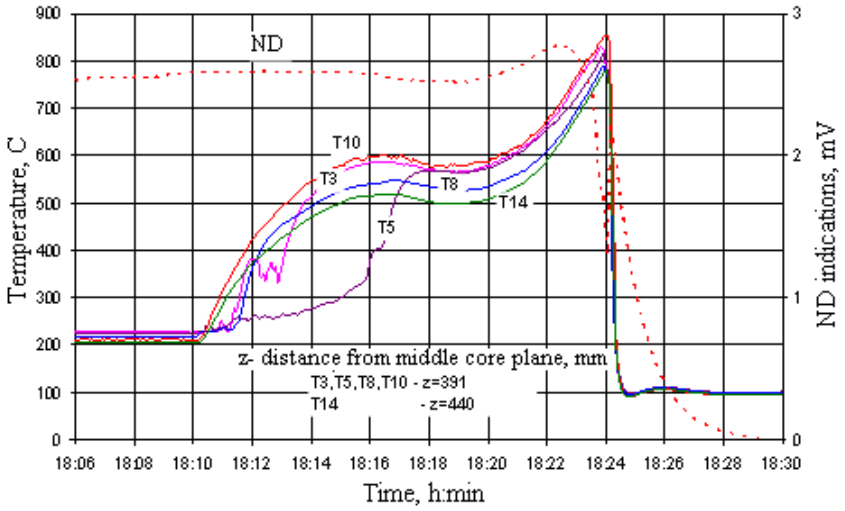

FIG. 4. Indications of neutron detectors and fuel thermocouples.

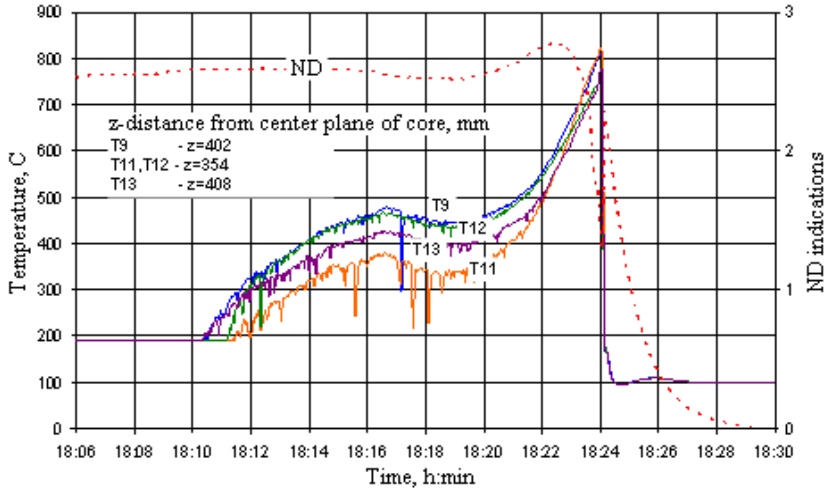

FIG. 5. Indications of neutron detectors and cladding thermocouples.

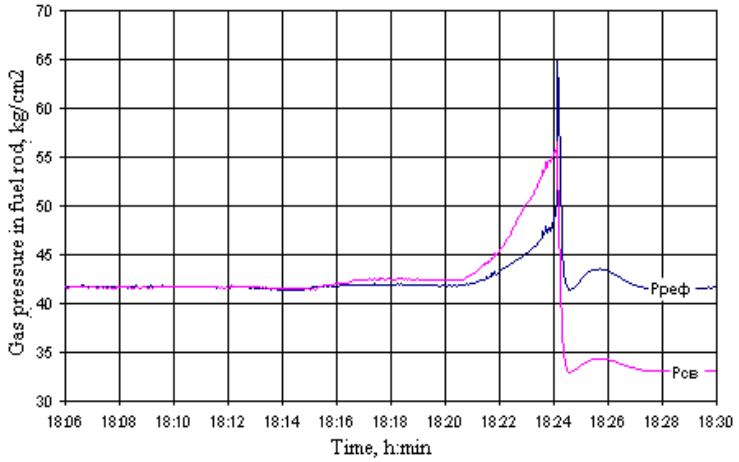

FIG. 6. Gas pressure in fresh (P_{fresh}) and refabricated (R_{ref}) fuel rods.

The axial temperature distribution of the fuel rod cladding in MIR/LOCA-60 experiment upon reaching the maximum (before the reactor scram) is presented on Fig. 7.

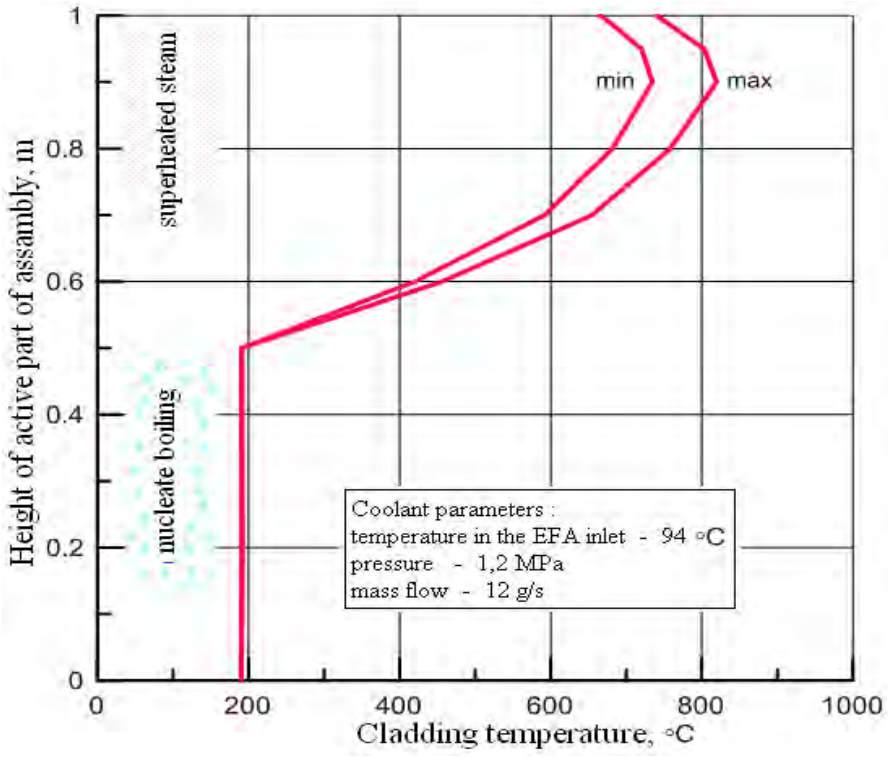

FIG. 7. The axial temperature distribution of the fuel rod cladding.

2. CONTENT OF PIE

Post-irradiation examinations of EFA after MIR-LOCA/60 experiment, executed by SSC-RIAR, included the following operations:

- Survey and photography of EFA appearance after tests;
- Bunch dismantling on separate fuel rods;
- Gamma scanning of fuel rods;
- Measurement of claddings outer diameter by a method of a contact profilometry;
- Definition of quantity and gas composition of in free volume of intact fuel rods.

The complex of post-test calculations of experiment by specialists of SSC-RIAR, Research Centre Kurchatov Institute, OKB Gidropress, OKBM Afrikantov, VNIINM with the use of various neutronic, thermohydraulic and thermomechanical codes [2-6] was executed (Table 2).

Reproduction of a temperature mode of refabricated fuel rods in experiment was the purpose of post-test calculations.

TABLE 2. CODES USED FOR POST TEST CALCULATIONS OF MIR-LOCA/60 EXPERIMENT

	Neutronic calculations	Thermohydraulic calculations	Thermomechanical calculations
SSC-RIAR	MCU-RR	CANAL(TECH-97)	-
OKB Gidropress	-	CANAL(TECH-97) CORSAR/HP	-
Research Centre Kurchatov Institute	SAPFIR-2006	RELAP5/MOD3.3	FRAPCON-3.2, FRAPTRAN-1.1
OKBM Afrikantov	-	RELAP5/MOD3.3	-
VNIINM	-	-	RAPTA-5.2

All participants of TH-calculations developed sets of boundary conditions in the form of spatial time dependent tables for heat transfer coefficients from claddings of EFA fuel rods and coolant temperatures during experiment. Using these input data the thermomechanical calculations are carried out with the RAPTA-5.2 code.

3. RESULTS OF PIE

In experiment there was a rupture of four fresh fuel rod's claddings (Figure 8, Table 3). Claddings of other fuel rods have the various levels of deformation, remaining intact.

TABLE 3. MAXIMAL HOOP STRAIN OF CLADDINGS AT RAPTURE AREA

FR number	2	3	4	13
Cross-section coordinate, mm	810	781	779	820
Hoop strain of cladding, %	25,4	28,4	43,1	37,2

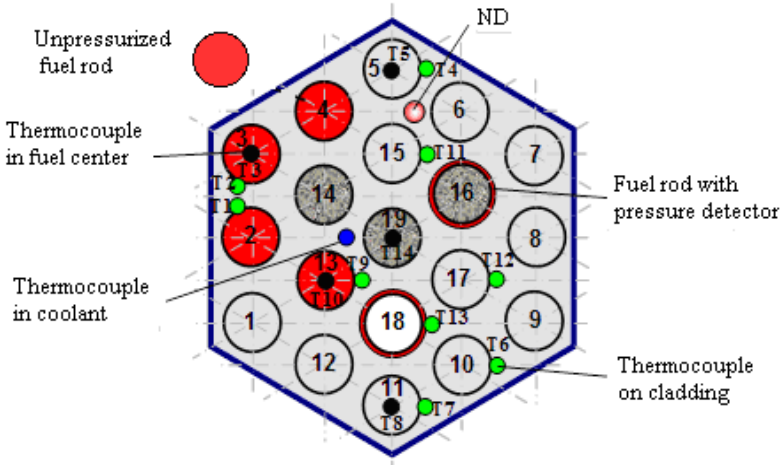

FIG. 8. Position of depressurized fuel rods. Refabricated fuel rods are located in cells: PT 02 – # 19, RT 03 – # 16, RT 04 – # 14.

In ballooning area of claddings of depressurized fuel rods there was a relocation of fuel fragments (Figure 9). Fuel pellets are fragmented on some large parts.

Measurements showed axisymmetric character of claddings deformation. Profile records of fuel rods (averaged by results of eight measurements) are provided on Figure 10.

The structure of claddings of studied unirradiated fuel rods is shown in Figure 11. Rupture of a cladding has plastic character with full local thinning. Thickness of the oxide film formed on an external surface of claddings was about 2-3 microns.

Claddings of refabricated fuel rods in the field of the maximum temperature are deformed by the internal gas pressure, but kept tightness. Deformation of a cladding led to formation of cracks in an oxide layer on their external surface in the top part of fuel rod (section of 773 mm, Figure 12). On sites of the formed cracks small oxidation of a surface of free metal is observed. Change of an oxide thickness on an external surface out of cracks doesn't exceed an error of measurements ± 2 microns. In the section with the coordinate of 100 mm hydrides are visible; in the section of 773 mm hydrides are absent.

It isn't revealed any differences micro- and macrostructures of fuel pellets of refabricated fuel rods in sections with the maximum temperature of tests and in the bottom sections, including fuel porosity in the rim-layer and in the fuel centre region, the grain size, fragmentation of pellets (Figure 13).

The gas composition in refabricated fuel rods which have kept tightness is measured by a method of gas mass spectrometry (Table 4).

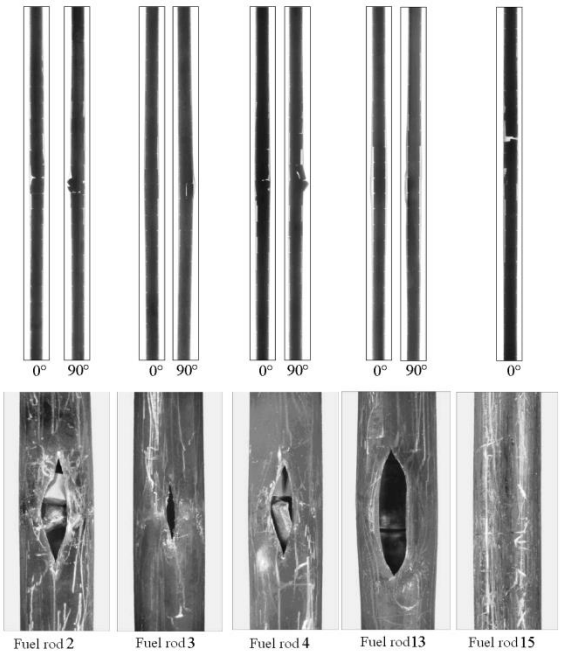

FIG. 9. Destruction of a fuel column and appearance of claddings in the field of ballooning.

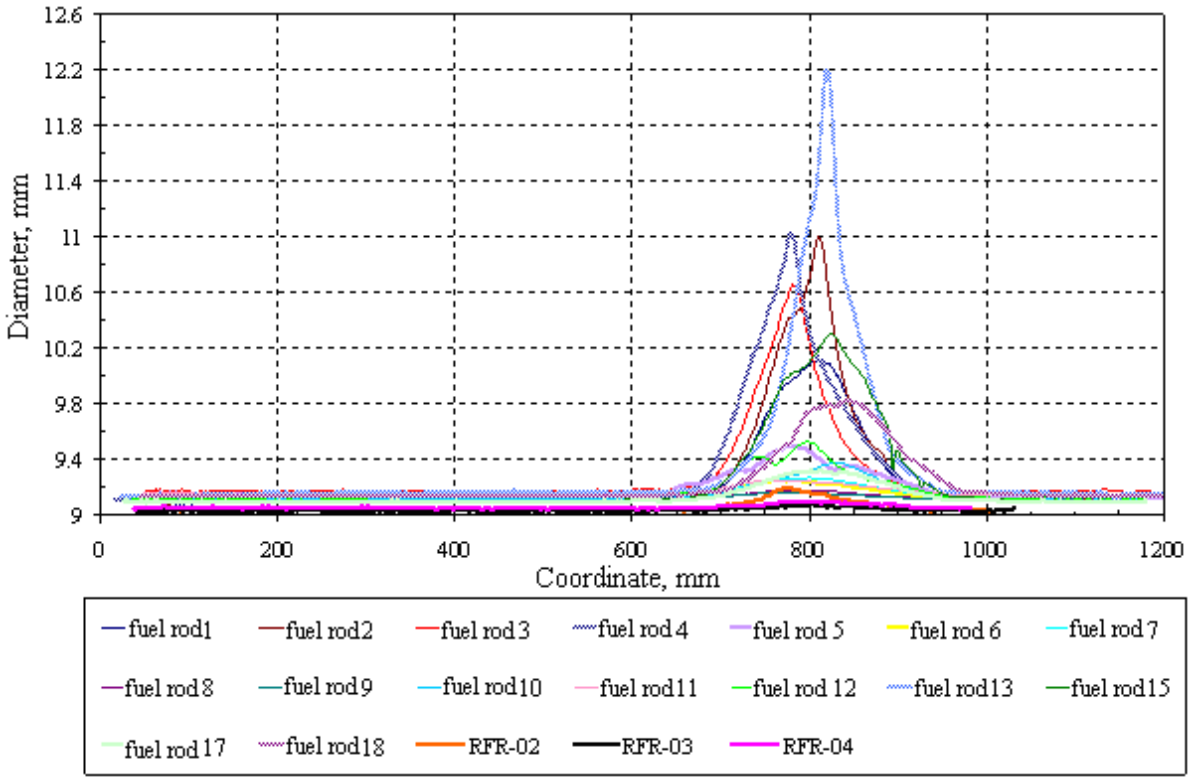

FIG. 10. Distribution of claddings diameter on height of active part of fuel rods.

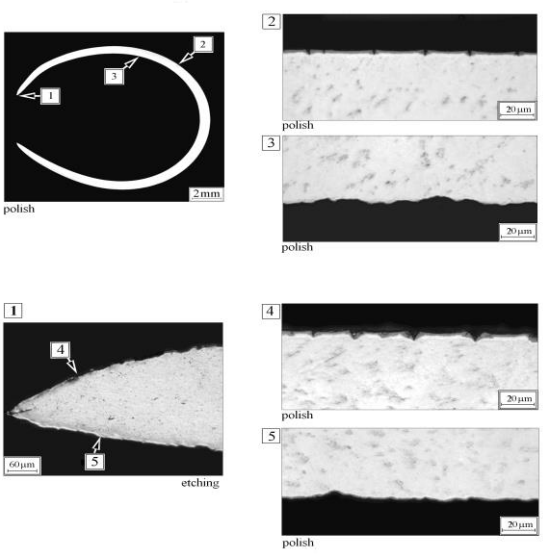

FIG. 11. Structure of a cladding of failed FR # 2.

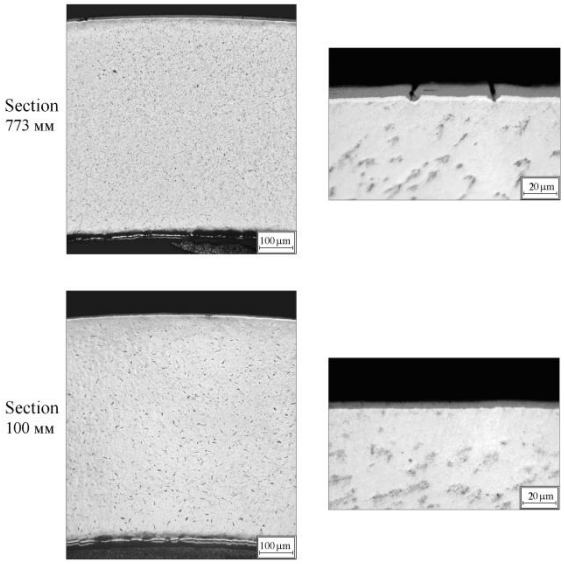

FIG. 12. Structure of a cladding of refabricated FR # 19 (PT-02).

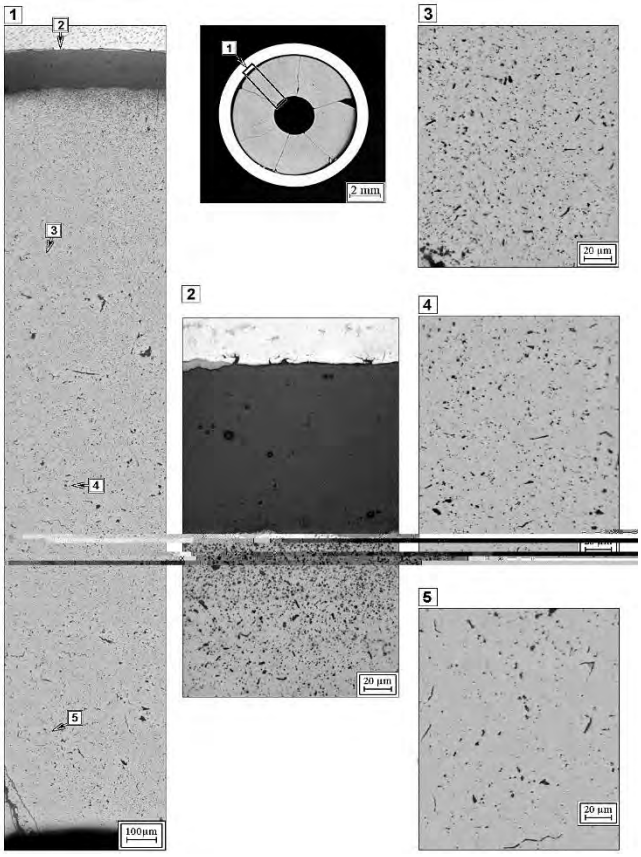

FIG. 13. Fuel structure of refabricated FR # 19 (PT-02) in cross-section 773 mm (polish).

TABLE 4. MEASUREMENT RESULTS OF GAS COMPOSITION IN REFABRICATED FUEL RODS

FR number	Free volume in FR, cm^3	Gas volume by normal conditions, cm^3	Gas pressure in FR, MPa	Gas mixture content, volume fraction, %						
				He	N_2	O_2	Ar	CO_2	Kr	Xe
RFR-04	11,6	243,0	2,10	94,12	1,39	0,21	0,009	-	0,293	4,05
RFR-02	12,1	254,4	2,11	96,75	0,85	0,17	0,007	-	0,168	2,049

4. RESULTS OF POST-TEST CALCULATIONS

The dependence of EFA power history, accepted as basic data for carrying out post-test calculations, was set on the basis of indications of the ionization camera (see Figure 14).

Axial distribution of power in fresh and refabricated fuel rods was specified on the basis of results of post-test gamma scanning. As an example the distribution of Zr-95 reflecting a profile of energy release in fuel during test is shown in Figure 15. Points in drawings marked out the values accepted for the subsequent calculations of relative energy release in fuel rods of EFA and on height of each fuel rod.

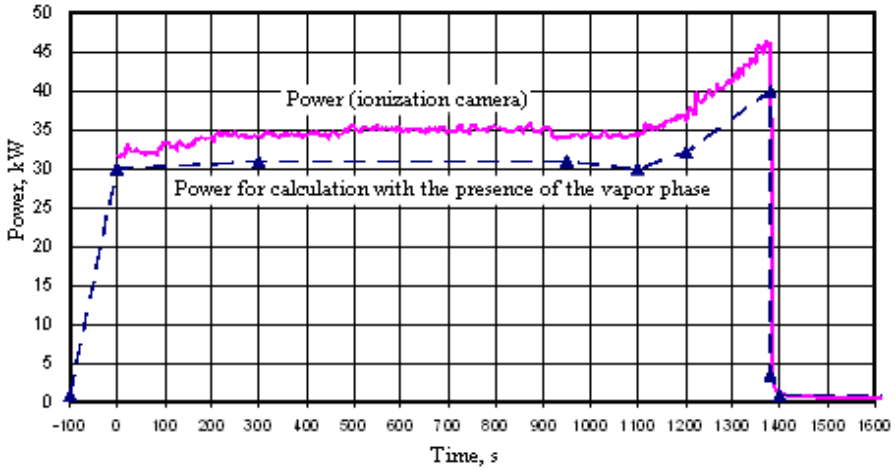

FIG. 14. Change of EFA power in the course of experiment.

A) FR # 3

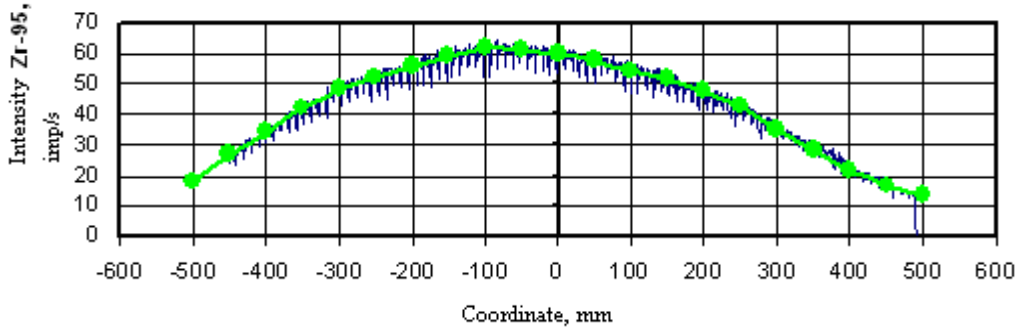

B)FR #19 (RFR-02)

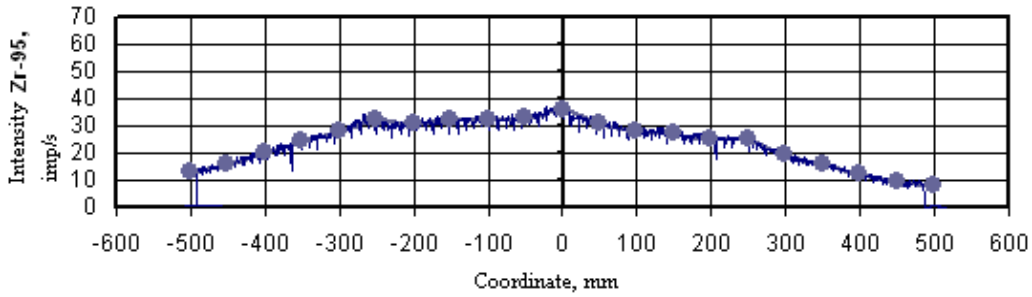

FIG. 15. Distribution of Zr-95 on height of fresh and refabricated fuel rods.

In Figure 16 the energy release distribution of EFA fuel rods on the basis of gamma scanning measurements, neutron calculations of SSC-RIAR and neutron calculations of Research Centre Kurchatov Institute are presented.

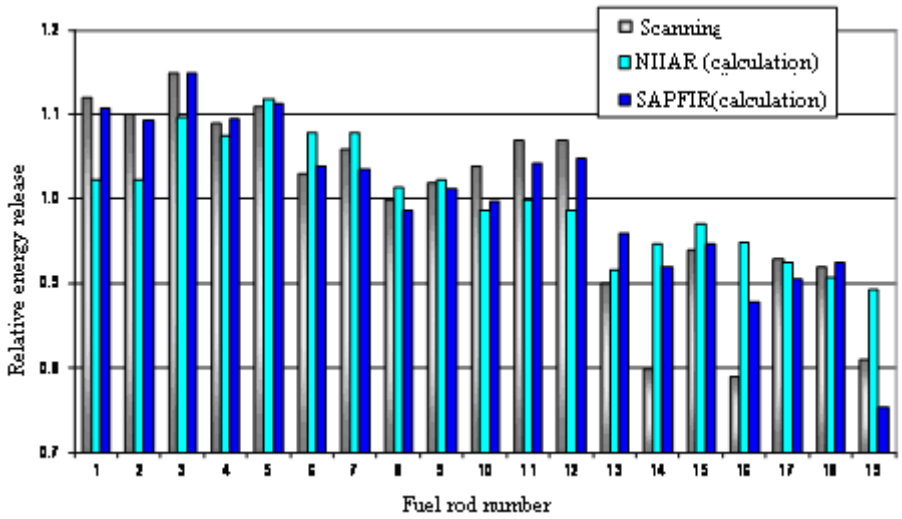

FIG. 16. Energy release distribution on EFA fuel rods on the basis of results of gamma scanning, neutron calculations of SSC-RIAR and neutron calculations of Research Centre Kurchatov Institute.

As a result of thermohydraulic calculations using various codes the sets of boundary conditions in the form of tabular dependences of heat transfer coefficients from EFA fuel rods claddings to coolant and coolant temperature during experiment were received. With use of these input data the thermomechanical calculations by RAPTA-5.2 code were carried out.

The maximum calculated values of cladding temperatures of the instrumented fuel rods are given in Table 5, received in TM-calculations by the RAPTA-5.2 code with the use of results of TH-calculations by various codes (axial coordinates and the time moments of computed and experimental maxima generally don't coincide). As a result of TH-calculations the considerable dispersion of the maximum temperatures of refabricated fuel rods is received:

– for FR # 14 (PT 04) – from 696 to 801 °C,

– for FR # 16 (PT 03) – from 694 to 813 °C,

– for FR # 19 (PT 02) – from 722 to 800 °C.

TABLE 5. MAXIMUM EXPERIMENTAL AND CALCULATED VALUES OF CLADDING TEMPERATURES OF INSTRUMENTED AND REFABRICATED FUEL RODS (° C)

FR #	Temperature, °C / Coordinate from bottom, m			
	Initial data of OKB Gidropress, CANAL	Initial data of OKB Gidropress, CORSAR	Initial data of Kurchatov Institute, RELAP	Initial data of OKBM Afrikantov, RELAP
2	841.8 / 0.85	838.3 / 0.85	832.6 / 0.75	777.4 / 0.9
3	836.7 / 0.85	824.3 / 0.85	844.3 / 0.65	780.3 / 0.9
5	843.9 / 0.85	838.2 / 0.85	829.6 / 0.75	780.2 / 0.9
10	790.1 / 0.85	804.2 / 0.85	804.5 / 0.75	777.9 / 0.9
11	764.2 / 0.85	780.2 / 0.85	814.8 / 0.75	780.3 / 0.9
13	796.8 / 0.85	808.5 / 0.85	794.8 / 0.75	755.3 / 0.9
15	810.0 / 0.85	823.0 / 0.85	804.4 / 0.75	757.8 / 0.9
17	801.8 / 0.85	815.1 / 0.85	783.8 / 0.75	757.7 / 0.9
18	792.5 / 0.85	807.9 / 0.85	803.6 / 0.75	754.3 / 0.9
14 (RFR 04)	792.4 / 0.85	801.2 / 0.85	782.9 / 0.75	696.5 / 0.9

FR #	Temperature, °C / Coordinate from bottom, m			
	Initial data of OKB Gidropress, CANAL	Initial data of OKB Gidropress, CORSAR	Initial data of Kurchatov Institute, RELAP	Initial data of OKBM Afrikantov, RELAP
16 (RFR 03)	794.9 / 0.85	813.6 / 0.85	760.7 / 0.75	694.0 /0.9
19 (RFR 02)	783.6 / 0.85	800.8 / 0.85	723.9 / 0.75	722.8 / 0.9

As an example in Figure 17 schedules of FR # 19 cladding temperatures in a hot spot are provided.

It is necessary to notice that the received distinctions of settlement temperatures at TC indications about 800 °C cause qualitatively various calculated estimates of deformation behaviour of a cladding – from almost absent deformation to the large deformation up to the cladding rupture.

The maximum values of the measured hoop strain of claddings of depressurized and refabricated fuel rods are given in Table 6 in comparison with the corresponding calculated values received in TM-calculations by the RAPTA-5.2 code with use of TH-calculation results by various codes. Essential divergences of computed and experimental deformations are caused by divergences of calculated and experimental temperature regime of claddings.

Oxidation of claddings in experiment was insignificant. Calculated estimates of oxide films on an external surface of claddings obtained by the RAPTA-5.2 code were up to 2 microns, calculated estimates of the oxide film of refabricated fuel rods were up to 0.8 microns. Thus, the total oxide thickness taking into account the initial oxide thickness is about 8 microns that corresponds to PIE results.

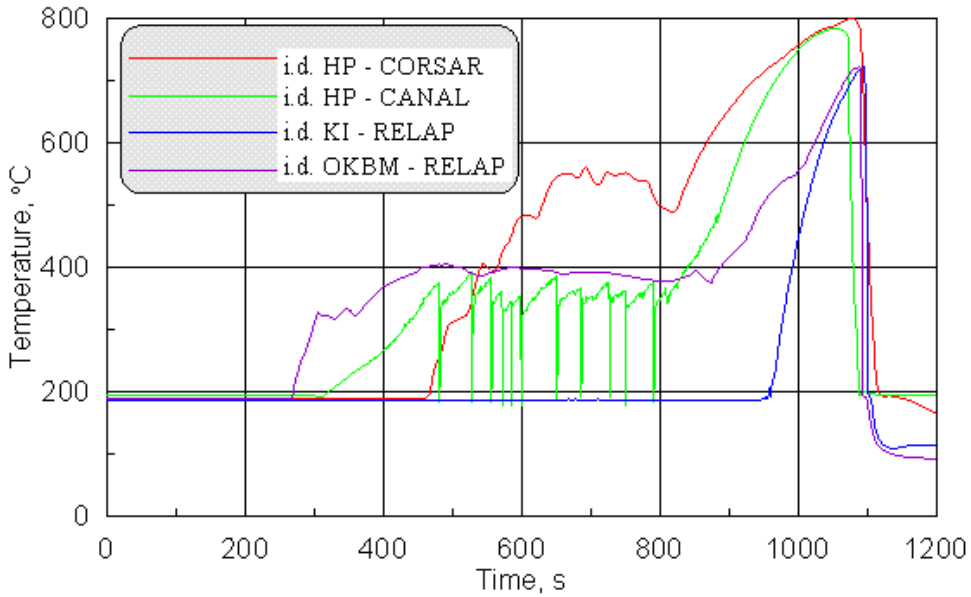

FIG. 17. Change of cladding temperature of FR # (PT 02) in a hot spot by results of RAPTA-5.2 code calculations with use of various boundary conditions.

TABLE 6. CALCULATION RESULTS OF EFA FUEL RODS CLADDINGS IN EXPERIMENT

FR #	Logarithmic hoop strain, unitless / rupture forecast on deformation criterion (R)				
	Experiment	Initial data (i.d.) from OKB Gidropress, CANAL	Initial data from OKB Gidropress, ORSAR	Initial data from Kurchatov Institute, RELAP	Initial data from OKBM Afrikantov, RELAP
2	0.226 (25.4 %)	0.3003 / R	0.3393 / R	0.1554 / R	0.0415
3	0.25 (28.4 %)	0.3348 / R	0.3319 / R	0.3059 / R	0.0565
4	0.358 (43.1 %)	0.0113	0.2075 / R	0.2137 / R	0.0391
13	0.316 (37.2 %)	0.1214 / R	0.1573 / R	0.0700 / R	0.0419
14	<0.005 (0.5 %)	0.0059	0.0630	0.0309	0.0051
16	<0.005 (0.5 %)	0.0783 / R	0.1037 / R	0.0197	0.0253
19	<0.02 (2 %)	0.0536	0.0677 / R	0.0075	0.0097

5. CONCLUSIONS

The MIR-LOCA/60 experiment with VVER high burnup fuel was perfomed in the MIR research reactor (SSC-RIAR) in 2010. Experimental fuel assembly with 16 fresh (unirradiated) test fuel rods and 3 refabricated fuel rods of VVER-1000 with burnup of 58.1 58.6 MWd/kgU was tested.

The purpose of MIR-LOCA/60 experiment was the study of behaviour of VVER highburnup fuel at typical conditions for LOCA.

The maximum indications of fuel TC did not exceed ~ 860 °C, TC of fresh fuel rods cladding ~ 820 °C, the duration of cladding temperature more than 700 °C was about 1 minute.

Post-test neutron, thermohydraulic and thermomechanical calculations were carried out. As a result the estimations of temperature mode of refabricated fuel rods were received. The assessment of the maximum temperature of refabricated fuel rod claddings is in the range of ~ 700 800 °C.

As a result of PIE of the tested FA cladding deformations and corrosion, the structure of fresh and spent fuel pellets were defined.

In this test there was a rupture of claddings of four fresh fuel rods with large hoop strain deformations. There was cracking of pellets into large fragments and shift of fragments in the ballooning area.

Refabricated fuel rods kept tightness. In the hot area maximum hoop strain of a cladding was not more than 2%, there was a separation cladding from fuel, change of fuel pellets state in hot area didn't happen.

Thus, in this test there was no condition for destruction of fuel pellets with burnup ~ 58 MWd/kgU.

In 2014, the following LOCA experiment with a single VVER fuel rod with burnup 72 MWd/kgU is planned in MIR reactor. The main goal of the experiment is investigation the fragmentation and relocation of fuel in a LOCA conditions, planned maximum cladding temperature in the experiment is 1000 °C, the modernization of the irradiation device will allow direct measurement of cladding temperature.

REFERENCES

[1] FEDOTOV, P.V., KUMACHEV, A.V., NECHAEVA, O.A., NOVIKOV, V.V., SALATOV, A.V., SYPCHENKO, M.V., ALEXEEV, A.V., GORYACHEV, A.V., KISSELEVA, I.V., SHULIMOV, V.N., BYKOV, M.A., MAHIN, V.M., ZAITSEV, S.I., ZAKUTAEV, M.O., LIOUTOV, K.V., PYLEV, S.S., TEBIN, V.V., TSHEPETILNIKOV, E.YU., GUSEV, A.S., PIMENOV, YU.V., Experimental and settlement studies of VVER fuel rods behaviour under LOCA conditions (MIR-LOCA/60 experiment), (Enlarged Halden Programme Group Meeting), Storefjell Resort Hotel, Gol, Norway, 10th – 15th March, 2 vols, (2013)

[2] ProgramTECH-97 (ТЕЧЬ-97). RF Regulatory Body, SEC NRS (Scientific and Engineering Centre of Nuclear and Radiation Safety), Certificate of Computer Code № 112 of 02.09.1999.

[3] Program CORSAR/HP (КОРСАР/ГП). RF Regulatory Body, SEC NRS (Scientific and Engineering Centre of Nuclear and Radiation Safety), Certificate of Computer Code № 263 of 23.09.2009.

[4] RELAP5/MOD3 Code Manual, User's Guide and Input Requirements, NUREG/CR-5535, INEL-95/0174, Vol.1.2 Rev.1, August 1995.

[5] FRAPTRAN: A Computer Code for the Transient Analysis of Oxide Fuel Rods NUREG/CR-6739, Vol. 1, PNNL-13576.

[6] Program RAPTA-5.2 (РАПТА-5.2). RF Regulatory Body, SEC NRS (Scientific and Engineering Centre of Nuclear and Radiation Safety), Certificate of Computer Code № 299 of 29.09.2011.

OPERATING EXPERIENCE AND LESSONS
(SESSION 2)

Chairperson

G. Ruggirello

Argentina

FUEL FAILURE ISSUES RELATED TO INCREASED BURNUP

O. YOUSAF, R.S. NAZIR, M. ASLAM, Q. SHAKIR
Nuclear Power Engineering
DNPER, N-Block, PAEC HQ
Islamabad, Pakistan
omeryousaf9211@hotmail.com

Abstract.

Nuclear energy is currently facing challenges regarding its competitiveness. In order to stay at current position, one of the methods is to reduce the fuel cycle costs. Increasing burnup is one of the technique that can be used to meet this goal, with enhanced safety features. However there is a number of fuel failure causes related to increased burnup, as follows. 1) Effect of increased burnup on fuel cladding corrosion and water chemistry parameters that accelerates the corrosion rate. 2) Effect of hydrogen pickup and stresses, as it effects mechanical properties of cladding. 3) Mechanical and chemical interactions between pellet and cladding. 4) Internal pressure of fuel rod. 5) LOCA impact of increased burnup. It is believed that failure tendency may increase with increased burnup due to the embrittlement of the cladding. However, at the same time one has to keep in mind that the reactivity of the fuel decreases with burnup. Higher failure rate at higher burnup is caused by mechanical and chemical degradation of cladding material. In this paper current and potential mechanisms related to fuel failure are discussed.

1. INTRODUCTION

One of the major present challenges to nuclear energy lies in its competitiveness. To stay competitive the industry needs to reduce maintenance and fuel cycle costs, while enhancing safety features. In spite of the relatively small contribution of fuel to the overall cost of generating electricity in an NPP, it is also an expensive item, and thus it is desirable to reduce the cost of the fuel used [1].

There are several approaches to reducing the rate of spent-fuel production, among which a high burnup strategy is a realistic and cost effective one. The current attention in the nuclear industry is focused on power uprates, which might encourage a modest burnup increase. However, the government is obviously more concerned about spent fuel. The waste disposal repository design has to incorporate the appropriate spent fuel characteristics as initial conditions [2].

The performance of the critical fuel components is the result of a complex interaction of a large number of variables that challenge the evaluation of the mechanisms in progress and the prediction of their behaviour at extended and more severe conditions. The technologies involved include just about every aspect of materials science imaginable: properties of materials, metallurgy, structural mechanics, coolant chemistry, physical chemistry, and their basic mechanisms just to mention a few examples. In addition, exposure to radiation changes all of the physical properties and processes: the properties of the structural materials and of the coolant change, transformations in structure and composition occur in all the materials (true alchemy!), and these processes occur in a non-homogeneous and nonequilibrium manner throughout the core.

Test reactors offer a good tool for evaluating a limited number of variables and mechanisms and have provided some valuable data, however, the operation and use of these reactors is expensive. The final performance evaluation is in the power reactor itself since it provides all the variables of importance; however, the lack of instrumentation, the inability to control testing time, as well as the difficulty of separating variables makes interpretation of ongoing processes difficult. The final evaluation of new materials and fuels for high burnups

progresses necessarily through the stages mentioned: ex-reactor testing, test reactor evaluation of samples, power reactor evaluation of samples or full fuel assemblies [1].
The degree of success achieved in fuel performance to date has been remarkable considering the lengthy evaluation process required and the tough conditions the fuel assembly is exposed to in service.

2. INCENTIVES FOR HIGH BURNUPS

The list below represents the incentives that existed in the early days of the nuclear industry for operating fuel to high burnups. Most of the incentives are still valid however, the value of and the emphasis on each one is slowly changing with time. The incentives are:

- Economics – lower fuel cycle costs.
- Capability for longer cycles – increased capacity factors, decreased radiation doses.
- Improved resource utilization – decreased amount of uranium, Separative Work Units (SWU) and fuel assemblies.
- Increased margin to storage capacity. However, the inability to send fuel for reprocessing or to a permanent storage site has caused a spent fuel assembly log-jam in the spent fuel pools and effectively eliminated this high burnup incentive.
- Eventual decreased offsite shipping and storage costs. However, the significantly increased time required for high burnup fuel to decrease its decay heat in a spent fuel pool before it can be loaded into an intermediate dry storage cask and the unknown schedule for shipping the fuel from the dry cask to a permanent storage site prevents a reliable estimate for the capacity and cost required for the intermediate wet and dry storage facilities.

In the opinion of this author, based on this and other factors discussed, extension of burnup to levels that require >5% enrichment are highly unlikely.

The reduction in margins to nuclear, thermal and safety analysis limits poses challenges to fuel management methods in order to maintain the desirable as well as the licensing margins. Modified fuel designs and fuel management methods have succeeded to meet the design and licensing limits with 4.95% as well as 5.95% enriched fuel. The major modifications have been the increased amount of burnable absorbers to hold down the increased reactivity and nuclear calculations for their accommodation. Detailed studies of designs >5%enrichment may reach nuclear or thermal limits [1].

2.1. Potential failure mechanisms at high burnups

It appears that increased burnup may result in the following failure modes during normal operation and anticipated operational occurrences:

- Corrosion;
- Hydrides;
- PCI/PCMI;
- Dimensional changes;
- ‘brittle’ fuel rods failure during LOCA resulting in ‘non-coolable fuel geometry’;
- Fuel dispersal during RIA.

The effect of increasing burnup on failure modes are discussed below.

2.1.1. Corrosion

The oxidation of zirconium alloys is one of the most studied processes in all of the nuclear industry.

$$Zr + 2\ H_2O \longrightarrow ZrO2 + 2\ H_2$$

Increased burnup will increase the degree of zirconium alloy material corrosion since higher burnup also means in general longer residence time in the reactor. However, the developments of new PWR alloys have significantly reduced corrosion rates compared to that of Zry-4 and thus increased the margins towards corrosion failures. The improved corrosion performance of new materials will however most likely be used to increase the corrosion duty (higher power, longer residence time and use of different water chemistries) of the fuel thus decreasing the margin to corrosion failures. It is the belief of the authors that corrosion will always limit the burnup.

To reach higher burnups, the enrichment of the fuel must increase and therefore, the fuel rod power over its lifetime will increase. This situation tends to increase the fuel clad temperature that for PWRs will increase the corrosion rate (since the corrosion rate is much less dependent on temperature in BWRs, similar effect will not be seen in BWRs).

Also, higher enrichment fuels in PWRs will require an increase in the LiOH coolant concentration. This since reactivity control in PWRs is to a large extent controlled by the boron concentration in the coolant, and increased fuel reactivity will require an increase in the boron coolant concentration that in turn will require an increase in the LiOH coolant concentration to maintain the optimum pH. The tendency for increased fuel rod power with increased burnup may result in increased tendency for subcooled boiling in the hottest channels and may together with the increased LiOH coolant content tend to deteriorate protectiveness of the zirconium oxide layer with accelerated corrosion as a result.

Both in PWRs and BWRs it appears that hydrides at the metal/oxide interface may accelerate corrosion rate, thus with increased burnup, corrosion produced hydrogen absorbed in the zirconium alloy material will increase. This hydrogen may eventually precipitate out as hydrides and as such may accelerate the corrosion rate. Again, the development of new corrosion resistance PWR alloys will also reduce hydrogen pickup (that is the product of corrosion rate and hydrogen pickup fraction) reducing the tendency for hydride driven corrosion acceleration late in life.

The enhancement in the corrosion rate in the presence of fast neutrons depends upon neutron intensity, temperature, dissolved oxygen in the water and oxide layer thickness. There are also some other important water chemistry changes results in a more aggressive corrosion environment that may limit fuel burnup.

2.1.2. Hydrides effect

Hydrogen diffuses into the zirconium alloy cladding forming zirconium hydrides. The hydrogen production process also mechanically weakens the rods cladding because the hydrides have lower hardness, ductility and density than zirconium or its alloys, and thus blisters and cracks form upon hydrogen accumulation. This process is also known as hydrogen embrittlement.
Hydrogen in excess of about 100 – 150 wtppm will precipitate out as zirconium hydrides that may embrittle the material to various extent dependent upon not only the hydride concentration but also how the hydrides are distributed and oriented in the material. Generally following can be said:

- Increased fraction of hydrides will reduce ductility and fracture toughness.
- Non-uniform distribution of hydrides reduces ductility and fracture toughness more than uniformly distributed hydrides.
- The fuel cladding will become more embrittled, by formation of hydrides that are oriented perpendicular to the major tensile stress direction.

The embrittlement effect of hydrides facilitates fuel failure as:

- Fuel outer channels and grids during seismic loading.
- Fuel rods during transport container drop.
- Fuel assembly hits the pool wall during outage handling operation.
- During a RIA event, Figure 1.
- Fuel rods during LOCA quenching or post-LOCA events, Figure 2.

Other effects of hydrogen are the following:

- Presence of hydrogen and hydrides will expand the material and therefore result in the dimensional changes.
- Hydrides at zirconium/metal interface increase the corrosion rate.

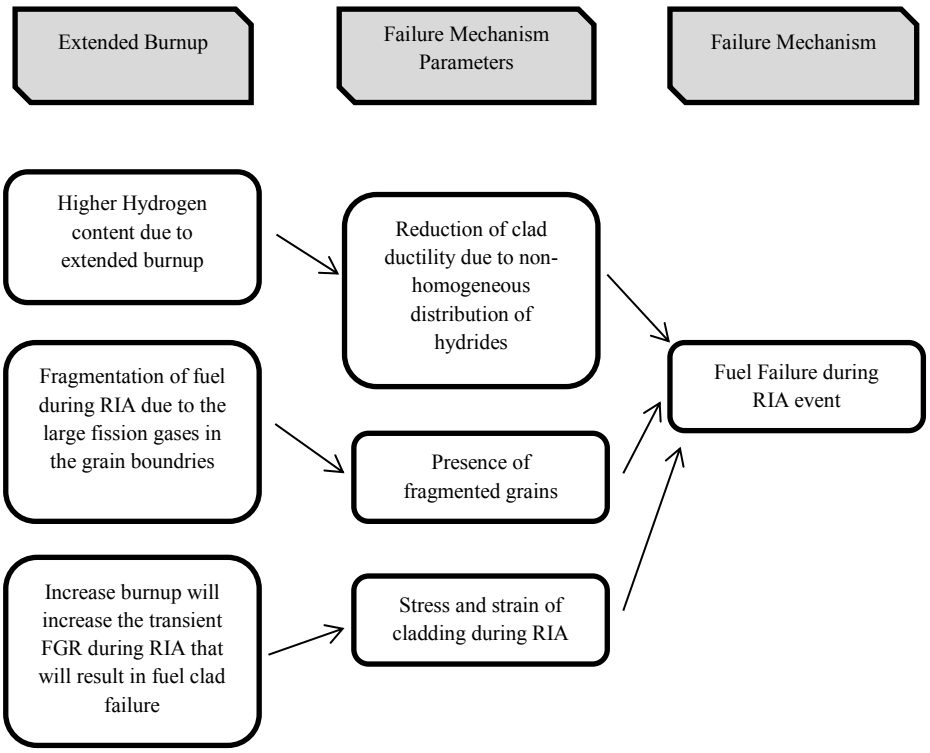

FIG. 1. Effect of increased burnup on RIA fuel.

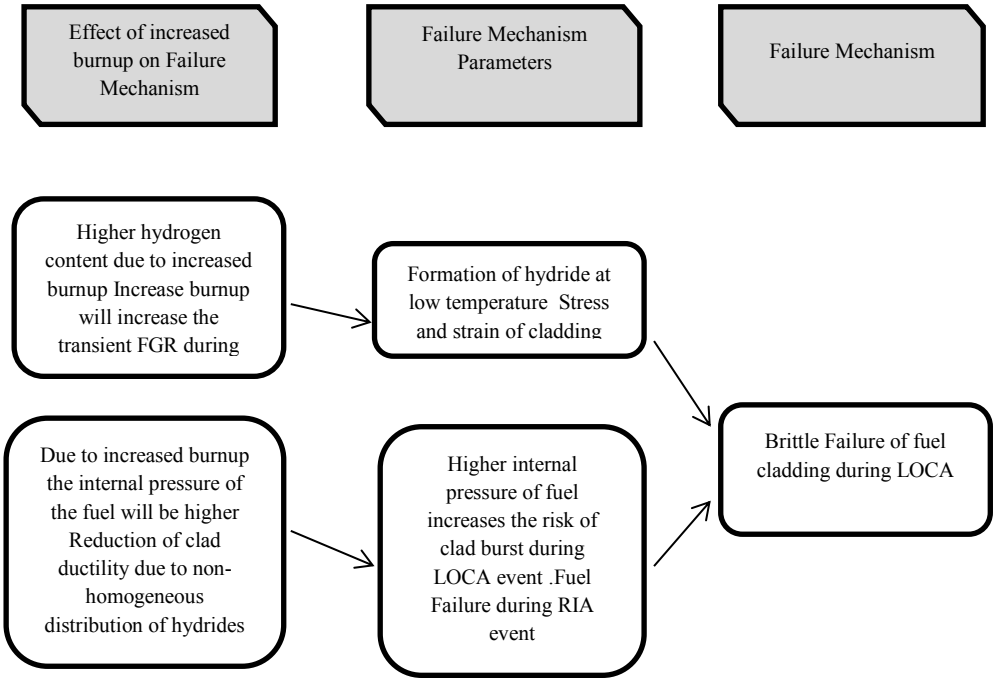

FIG. 2. LOCA impact of increased burnup.

2.1.3. Dimensional changes

Both hydrogen in solution and hydrides will expand the material and therefore contribute to dimensional changes (elongation, bowing) of components of fuel.

2.1.4. PCI/PCMI

Increase burnup will result in:

- More fission products produced;
- Increased Fission Gas Release, FGR;
- Increased Transient Fission Gas Release, TFGR;
- Increased swelling.

The increased fuel rod internal pressure with burnup facilitate excessive clad embrittlement during the LOCA clad oxidation phase. The increased rod internal pressure may also increase the tendency for fuel clad ballooning and fuel relocation during the LOCA event.

Figure 3 shows the potential impact of increasing burnup on PCI/PCMI failure tendency. It is believed that the failure tendency may increase with increased burnup due to the embrittlement of the cladding. However, at the same time one has to keep in mind that the reactivity of the fuel decreases with burnup and thereby there is a decrease in failure tendency with increased burnup. For example, if a control rod in a BWR is pulled adjacent to a fresh fuel assembly the power increase will be much higher compared to a similar situation but adjacent to an old assembly with low reactivity.

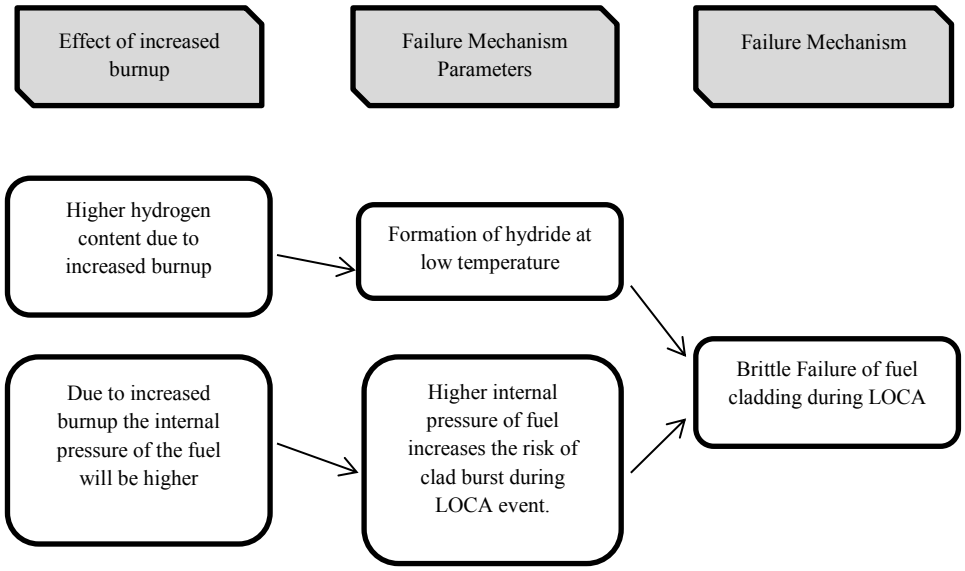

FIG. 3. Effect of increased burnup on the PCI/PCMI failure tendency.

3. SUMMARY

In this paper different potential for fuel failure are studied related to increased burnup. Following are the major causes:

- Corrosion of zirconium alloy cladding and the water chemistry parameters that accelerate corrosion rate.
- Dimensional changes of zirconium alloy components.
- Hydrogen (H) pickup and redistribution as it affects mechanical properties of the cladding.
- Pellet-cladding interactions (PCI) and pellet-cladding mechanical interactions (PCMI).

The only items above that have posed limits to extending burnups have been corrosion and dimensional changes in both BWRs and PWRs and PCI in BWRs. Improved materials and operating procedures have been able to exceed all of these limits and have not reached new limits within current operating strategies.

REFERENCES

[1] RUDLING., P., ADAMSON, R., BRIAN COX., FRIEDRICH, G., STRASSER, A., High burnup fuel issues, Vol. 40 No.1, (2008).
[2] KAZIMI, M. S., TODREAS, N. E., Nuclear Power Economic Performance: Challenges and Opportunities, *Ann. Rev. Energy Environ.*, 24, 139 ~1999.

HIGH BURNUP FUEL TECHNICAL AND ECONOMICAL LESSONS LEARNED AT SWISS NUCLEAR POWER PLANTS

F.E. JATUFF
Kernkraftwerk Gösgen-Däniken AG
CH-4658 Däniken
Switzerland
Email: fjatuff@kkg.ch

Abstract.

The nuclear power plants in Switzerland have followed since long the strategy to upgrade burnups, aiming fundamentally at front-end incentives to reduce the assembly production and intermediate storage costs. Some of them implemented a rather aggressive high burnup strategy, like the Gösgen nuclear power plan;its core design and fuel management needed to be adapted and the safety of high burnup fuel had to be consequently demonstrated through long-term experimental programs. In particular, new zirconium-based alloys were tested and fuel behaviour during normal and transient conditions required extensive analytical and experimental validation. The paper shows a summary of the basic results of these programs for Gösgen, leading to the current licensed burnup limits that represent record commercial values for this reactor type (70, 75 and 82 GWd/t_{HM} for maximum fuel-assembly average, maximum fuel rod average and maximum local burnups, respectively). Additionally to the technical and nuclear safety challenges that this effort required, the economic aspects of the introduction of high enrichment, high burnup core loadings on the front- and back-end frontsare briefly summarised.

1. INTRODUCTION

The three pressurized water reactors (PWR Beznau 1, Beznau 2 and Gösgen) and the two boiling water reactors (BWR Mühleberg and Leibstadt) in Switzerland have undergone significant enrichment and burnup upgrades since many years, to the point of having achieved world-record values in the past. At recent times, definitively discharged irradiated fuel assemblies for the five reactors show burnup values belonging to the highburnup interval 52.3 58.5 MWd/kg_{HM} (values for the year 2011), with the BWRs on the lower side (Mühleberg 52.3 and Leibstadt 52.4 MWd/kg_{HM}) and the PWRs on the upper side (Gösgen 57.0, Beznau 2 57.5 and Beznau 1 58.5 MWd/kg_{HM}). Especially the Swiss PWRs are moving to fully achieve equilibrium cores for optimal burnups, with Beznau running a 6-region and Gösgen a 5-region core strategy with enrichments of ca. 4.8% and 5.0%, respectively. The meaning of optimal burnup and the incentives and reasons lying behind this strategy are given in Section 2.

The Gösgen nuclear power plant (KKG), in particular, has a license to go to very high burnups of up to limiting 70 MWd/kg_{HM}fuel-assembly average, 75 MWd/kg_{HM} fuel rod average and 82 MWd/kg_{HM} local ('pellet-average') for UO_2 fuel, and correspondingly 65, 70 and 77 MWd/kg_{HM} for MOX fuel, for annual cycles and 5-year fuel assembly life. At the present time, without MOX and with a 5-region core / 5% enrichment loading almost in equilibrium, it is expected to achieve in the practice a batch-average discharge burnup of ca. 65 MWd/kg_{HM}. The work performed to support the extension of burnup limits specifically for KKG, basically addressing technical and nuclear safety aspects of front-end and fuel management, is given in Section 3.

Somewhat less considered were the back-end aspects associated to high enrichment, high burnup fuels. In particular, the criticality safety of storage pools, transport and transport/storage casks, as well as dose rate limits at surfaces of these casks due to the very high neutron source in high burnup fuel, represent very difficult challenges to solve nowadays, in the context of ageing plants subject to ever-increasing safety standards. The

reprocessing of highburnup fuel is also feasible but more complicated. Additionally, the transportability of the fuel assemblies following a long-term dry-storage is considered problematic for fuels above 45 MWd/kg_{HM}, because of possible long-term barrier degradation, e.g. associated to cladding creep. A summary of the current technical and nuclear safety aspects considered relevant today with respect to the back-end of high burnup fuel is given in Section 4.

The original strategy addressed fundamentally front-end incentives to reduce the assembly production costs, by reducing the number of fuel assemblies loaded in the core and by optimizing the plutonium production: less fuel assemblies to handle means in principle fewer items to be transported and stored. Having introduced thus a highburnup strategy already since several years, it is possible to assess concretely the associated front-end savings rather accurately. Intermediate storage and transport costs of highburnup fuels were more uncertain at the time. Today, the technology accompanied some of these trends and higher burnups belong to the current status quo. Costs, however, have changed significantly and some other financial impacts remain still open. We illustrate relevant financial aspects and we give the final conclusions in Section 5.

2. INCENTIVES FOR HIGHER BURNUPS

2.1. By extending cycle lengths or by reducing the batch size

In the last few years several studies on the optimal burnup of UO_2 fuel in PWRs have been performed and published in the open literature, using a variety of methods and assumptions, with the purpose of investigating the existence of an optimal fuel and waste management strategy [1-4]. Naturally some external cost assumptions play an important role in these studies, but so do the initial ^{235}U enrichment, the length of the time between refuelling (*cycle length*) and the number of cycles a certain batch remains in the core (*batch fraction*); these parameters influence the fuel utilization from the most physical viewpoint and have therefore an impact on costs.

From the mentioned studies, however, it is difficult to conclude universally about the best fuel and waste management strategy because the results depend strongly on local assumptions; e.g., in some cases the cycle length is fixed [4], in others the batch fraction is kept constant [2, 3]. Both approaches are justified in practice, because the constantly increasing burnup allows utilities to lengthen the cycle length from 1 year to $1^1/_2$ or even 2 years. This increases the availability of the plant and helps to increase the capacity factor. Some other utilities argue that their refuelling outages are so short by virtue of in-parallel maintenance, sometimes only two weeks, that longer than annual refuelling is not necessary. These utilities present therefore a higher number of fuel ages in the core, typically up to five or six, and they benefit from higher fuel utilization. As a result, the available studies did not span widely the range of variation of all these variables simultaneously, in part because this requires an enormous systematic core physics computational effort.

The outcome is a wide scenario bracketed by limiting cases represented by assuming, on the one hand, fixed cycle length, burnup increase through decreasing batch fraction, zero burnable poison penalty and full low leakage loading patterns (promoting very high burnups), mainly followed in part of Europe, and on the other hand, fixed batch fractions, burnup increase through extended cycle length, gadolinia poison residual absorption and non-optimized loading patterns (not promoting very high burnups), mainly followed in the United States.[1]Very interestingly, the need for plant maintenance during operation or, instead, highly

concentrated during outage, plays an enormous role governing the cycle and outage lengths and thus the incentive to go to higher burnups by reducing batch size or by extending cycles.

In any case it is necessary to target in advance the achievable discharge burnups when changing enrichment, batch size or cycle length. The typical basic relationship for LWRs between these parameters is illustrated in Fig. 1 for German Konvoi reactors, where the reciprocal reload fraction (RRF) is the inverse of batch fraction in the core, i.e. a reciprocal reload fraction of 3 means that the fuel remains in the core up to 3 cycle lengths (given normally in effective full power days, EFPD), each batch representing 1/3 of the core loading. The basic relationship for other light water reactor types looks similar in principle.

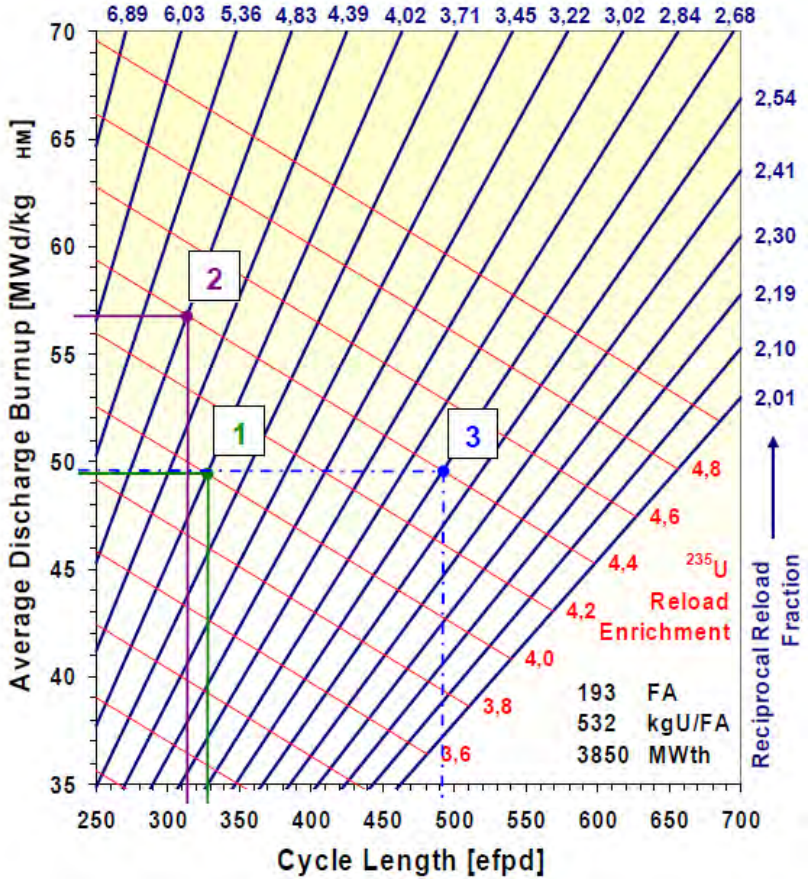

FIG. 1. Typical average discharge burnups obtained in function of batch size, cycle length and enrichment, for UO_2-fuelled Konvoi-reactors [5].

In Figure 1, three scenarios are given to illustrate these alternatives. The first one, for 4.0% enrichment and a 4-region core (RRF = 4.02), predicts an average discharge burnup for an equilibrium core of ca. 50 GWd/t_{HM}; the other two scenarios correspond to an increase to 4.4% enrichment, which may lead either to a discharge burnup increase by keeping the cycle length almost unmodified (RRF = 4.83, batch size of 40 fuel assemblies), or to a cycle length extension, essentially keeping the discharge burnup unmodified (RRF = 2.68, batch size of 72 fuel assemblies).

2.2. Optimal burnup and high burnup strategies in Swiss PWRs

There are a number of simplifications used to achieve the scheme in Figure 1, but at the basis of the burnup increase in Swiss reactors there is an incentive to optimize the plutonium buildup and its burnup and to keep the cycle lengths at an annual level. The optimization of the fissile material burning is represented normally by the *fuel utilization*, computed in FIFA, which gives the number of fissions produced per initial fissile atom. The optimization of the fuel utilization takes place because, for very low burnups, the production of a prominently fissile plutonium vector implies FIFA values larger than one. It is also intuitive that, for very high burnups, the plutonium and minor actinide vectors produced by neutron capture become less multiplicative, whereas neutron-absorbing fission products continue to build up with burnup, such that further enrichment increases will not necessarily increase the fuel utilization. This leads to an optimum burnup, which could be defined as the one maximizing the fuel utilization measured in FIFA. This is graphically shown in Figure 2, where Westinghouse / EPRI results are compared with our lattice depletion calculations using CASMO-4 [6] combined with simplified core depletion calculations which account for power distribution effects [7], allowing us to study the variation of the cycle length and the batch fraction flexibly and including limiting cases.

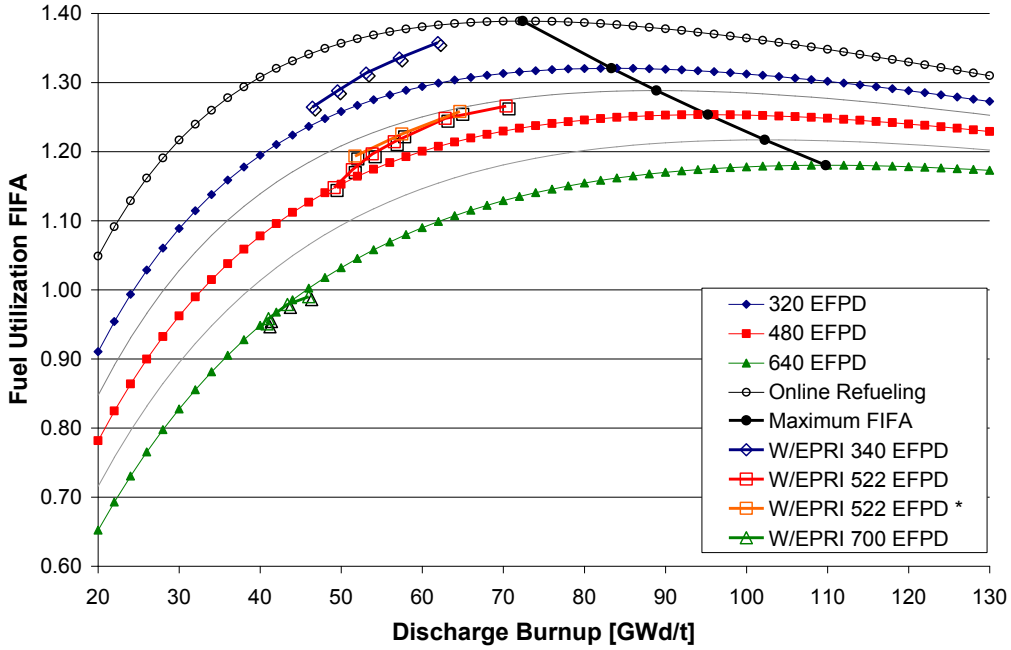

FIG. 2. Fuel utilization FIFA vs. discharge burnup studied with CASMO-4, parametrically for given cycle lengths (including extrapolation to zero cycle length or online refuelling), compared to other published results.[1] The maximum FIFA values from the CASMO-4 results are approximately linked with a line corresponding to enrichment values lying in the range 5-7%.

From the CASMO-4 calculations, saturation of the fuel utilization (FIFA maxima) is found for a given enrichment, depending on the cycle length, with a superior FIFA value at about 1.40 for the extrapolated case of online refuelling for ca. 5% enrichment. It can also be observed that in several publications the fuel utilization expected show similar trends; the lack of agreement is due to the simplicity of the lattice and core evaluations based on our CASMO-4 calculations on the one hand, as well as the several different assumptions and methodologies used by other organizations on the other hand. In particular, the attained FIFA in the PSI study [4] with annual refuelling was considerably higher than in the Westinghouse/EPRI, the MIT and the OECD evaluations with longer than annual refuelling.

It can be shown that in the range 5-7% enrichment an optimal burnup is achieved maximizing FIFA for cycle lengths going from on-line refuelling to almost two years. This is consistent with the minimization of uranium ore requirements[4] and with a 5- to 6-region core (fuel assemblies 5 to 6 cycles in the core) implemented at Gösgen and Beznau, which thereby oriented their fuel management to optimize the fuel utilization and minimize the need of uranium ore, thus contributing to the conservation of resources and improvement of the consequent environmental impact.

3. FRONT-END ASPECTS OF HIGH-BURNUP FUEL

Having ~5% enriched fuel almost 5-6 years in the core required extensive research through technical, scientific and nuclear safety high-burnup programmes. The most straight-forward characteristic of commercial[1] high burnup fuel rods is that they content a higher concentration of fissile material, typically ^{235}U in the case of uranium rods, and that they remain longer in the core to produce more energy; this requires checking the longer-life behaviour of pellets, cladding and fuel assembly structure. The pellet behaviour is to be monitored, on the one hand, because the mechanical and thermal properties of the pellets in the presence of higher concentration of fission products are to be assessed. This means in particular the retention of fission gas in the pellet matrix (or the need to increase the fuel rod plenum to keep more fission gas at a given maximum pressure), the grain structure and fragmentation of the pellets, and their physical dimensions (densification and swelling). The cladding is subject to longer irradiation and is susceptible to enhanced corrosion, oxidation and hydrogen uptake, with the potential to degrade its mechanical properties. Also the fuel rod plastic deformation in the form of diameter change and elongation or growth is relevant. For fuel assembly structure material, the channel bowing in BWRs and the elongation and bowing of guide tubes in PWRs is of importance.

For KKG, an ambitious, decade-long high burnup programme was developed together with the fuel vendor AREVA GmbH, including analytical activities but fundamentally addressing experimental research based on commercial and especially prepared test rods subjected to post-irradiation examinations at the KKG pool, at the Paul Scherrer Institute in Würenlingen and at the EC JRC Transuranium Institute in Karlsruhe, to develop a database for code validation. The basic results are described in the following Sections.

3.1. Pellet behaviour at very high burnups

Essentially the main concern is about the pellet swelling and structure behaviour of the fuel matrix due to enhanced fission-product concentration, particularly due to the fission gas produced and partly retained in the matrix itself, and partly released to the space between pellets and fuel cladding (plena and gap) [8]. The fission gas release is important to account for enough plenum space for high burnup fuel rods, in order to limit the maximum internal pressure, particularly by postulated transients or accidents. The pellet swelling is related to pellet-cladding interaction during the fuel life.

[1]Experimental high burnup programmes are fundamentally based on the irradiation of specially designed high burnup test rods allocated in 'normal' (low or mid-burnup) assemblies; these test rods are moved, following end-of-life of the original assembly, to other normal assemblies to continue the irradiation, and in some cases far beyond their target burnup (they are over-burnt, approaching practically an equilibrium by burning fissile plutonium isotopes built up from neutron capture in ^{238}U and daughters). This over-burning is especially useful to test cladding properties but is not directly representative of pellet behaviour, because plutonium burning in the rim structure can dominate the entire pellet burnup. This goes sometimes unnoticed and this is why we introduce the 'commercial' high burnup properties, i.e. those obtained in a commercial nuclear power plant, which may differ substantially from research high burnups.

The rim or high burnup structure at the pellet periphery differs significantly from the structure of the pellet centre, subject to much higher temperatures. This aspect is also of relevance, and extensive information from KKG fuel has been already published [9-11].

The relevant pellet behaviour for a wide burnup range going up to about 80 GWd/t_{HM} is depicted in Figure 3, for different pellet production methodologies, including enriched reprocessed uranium and doped fuel. On the pellet swelling side, the measurements on burnt fuel show a continuous pellet swelling above 60 GWd/t_{HM}, achieving pellet expansions compatible with as low as 90% of the theoretical pellet density, consistently with the prediction models.

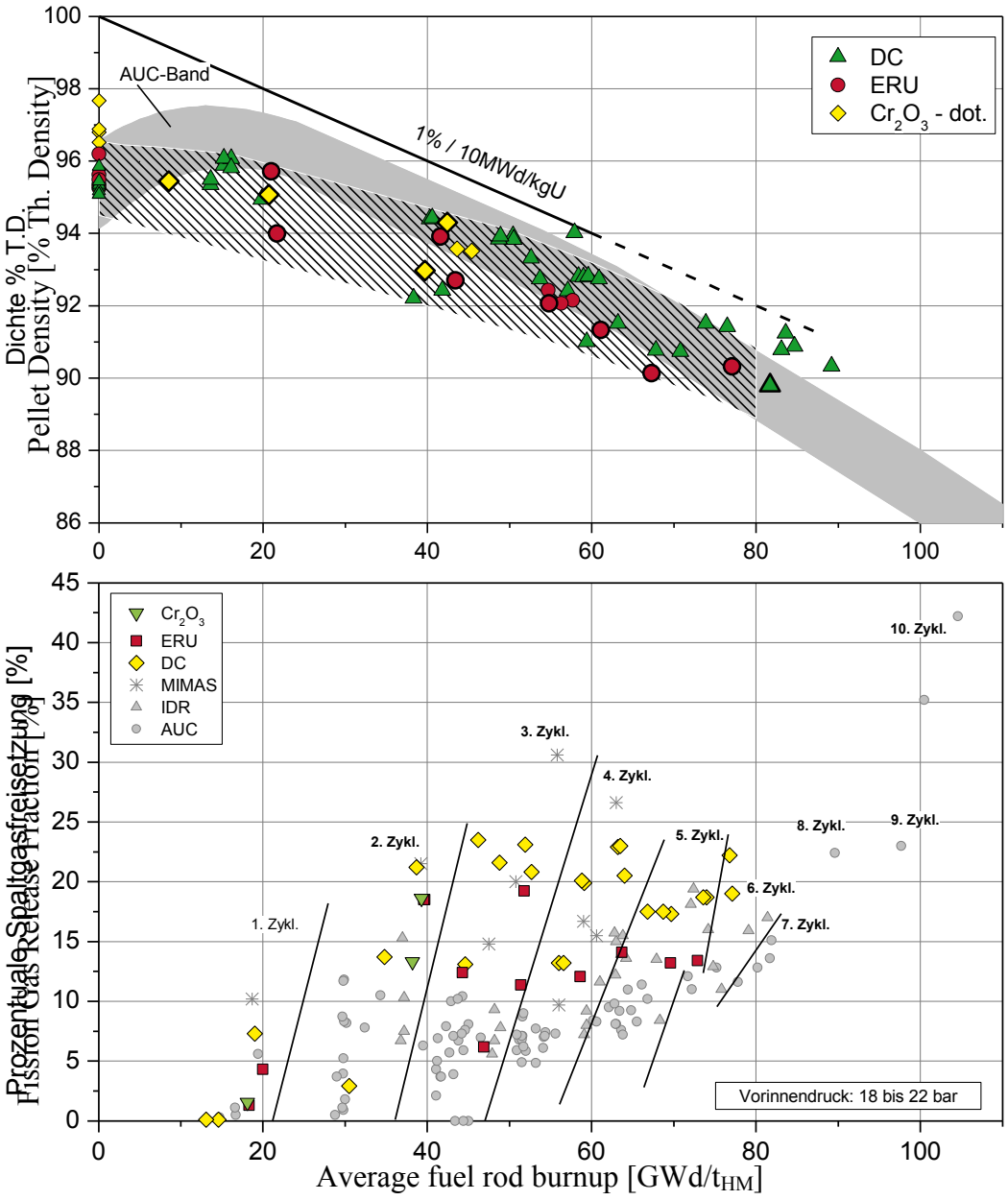

FIG. 3. Pellet behaviour at high burnup ranges: Pellet density as per cent fraction of the theoretical density (top), and fission gas release as per cent fraction of total fission gas produced (bottom).

Fission gas release in commercial fuel rods is bound by a level of ca. 25%. Especially over-burnt fuel rods (with one rod showing a maximum of 10-cycle annual irradiations and ca.

120 GWd/t_{HM} local burnup to test cladding properties) have also been investigated for pellet behaviour. These non-commercial, ultra-high burnup test rods showed fission gas release fractions somewhat below 45%.There is expectation on a significant reduction of the fission gas release in doped fuel, particularly >50 GWd/t_{HM}due to the higher intra-granular fission gas retention and lower amounts of gas bubbles interconnected on grain boundaries. Research is being performed at the present time; preliminary results on one- and two-cycle-burnt doped fuel rods do not show so far promising improvements for KKG normal operation, transient behaviour being still under study.

3.2. Cladding behaviour at very high burnups

The basic concern is associated to increased oxidation and hydrogen uptake as well as the metallic behaviour and cladding deformation at very high burnups, both highly related to the integrity of the cladding during reactor operation but with important consequences for the back-end. The most important oxidation results obtained are given in Figure 4.

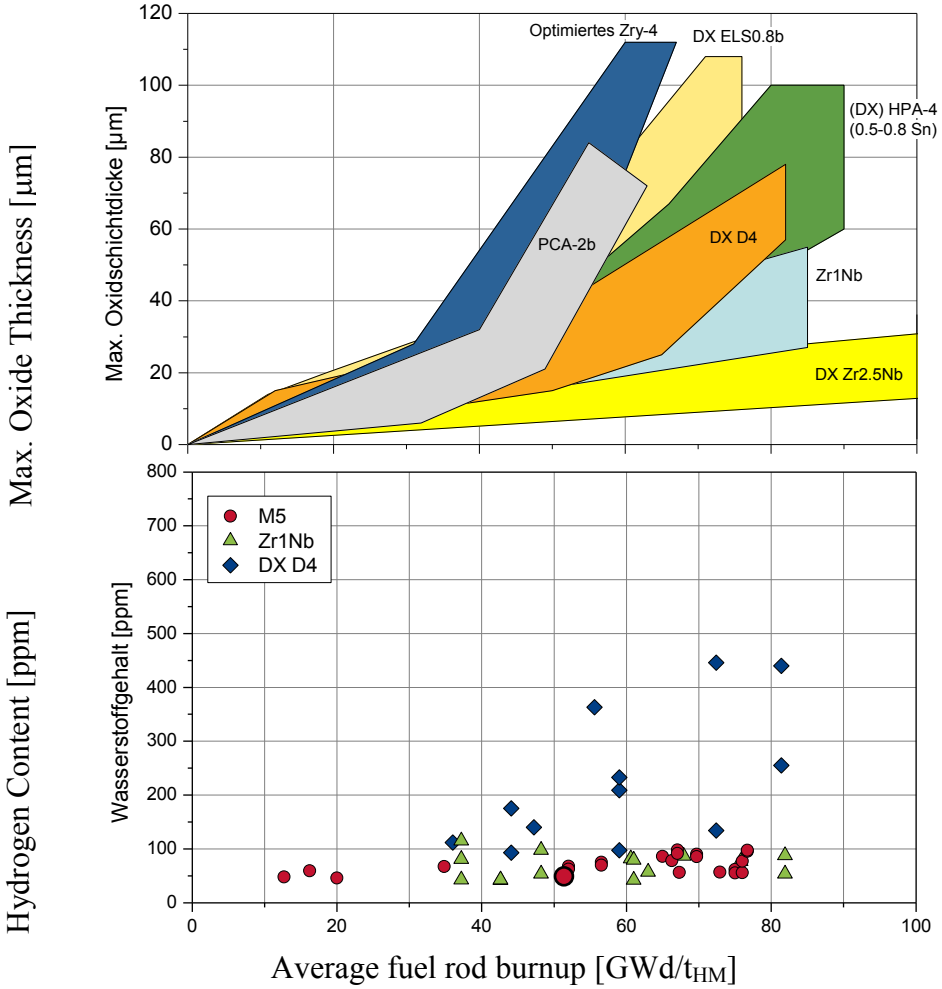

FIG. 4. Maximum oxide thickness (top) and hydrogen content (bottom) vs. burnup for selected zirconium-based alloys tested at KKG.

The analysis of oxidation and hydrogen uptake for different cladding alloys at high burnup conditions allowed the derivation of the corresponding hydrogen pick-up fractions used for code validation. Figure 5 depicts one of the databases used to validate pick-up fraction predictions in the fuel rod design code for KKG.

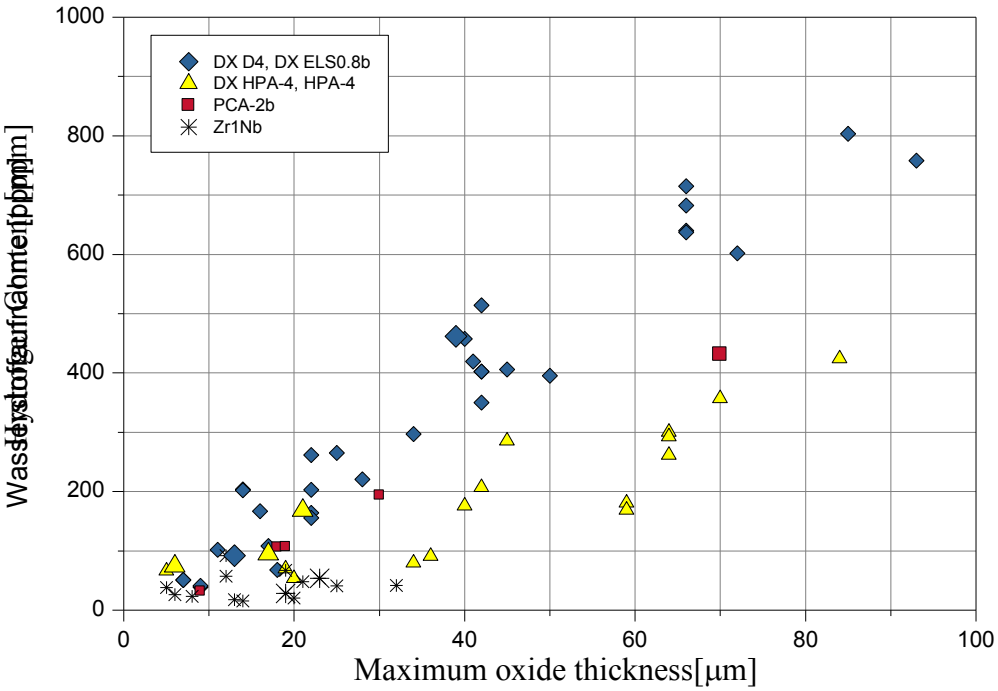

FIG. 5. Hydrogen content vs.maximum oxide thickness for selected zirconium-based alloys tested at KKG. The experimental information was used to develop hydrogen pick-up fraction relationships.

The geometry of the cladding is known to change with the neutron fluence, depending on the fabrication process and metallurgy employed, fundamentally by the plastic reduction of the cladding diameter and its corresponding axial growth. Figures 6-7 depict the geometry variation of the fuel rod for a variety of KKG pellet and cladding combinations at high burnups. The driven forces are associated to external and internal rod pressures, mechanical interaction with initially sintered but shortly thereafter swollen pellets, and grain structure variation of the cladding alloy matrix under neutron irradiation. The diameter variation measured confirms a relatively stable behaviour well above 60 GWd/t_{HM}, rod elongations remaining below~1%.

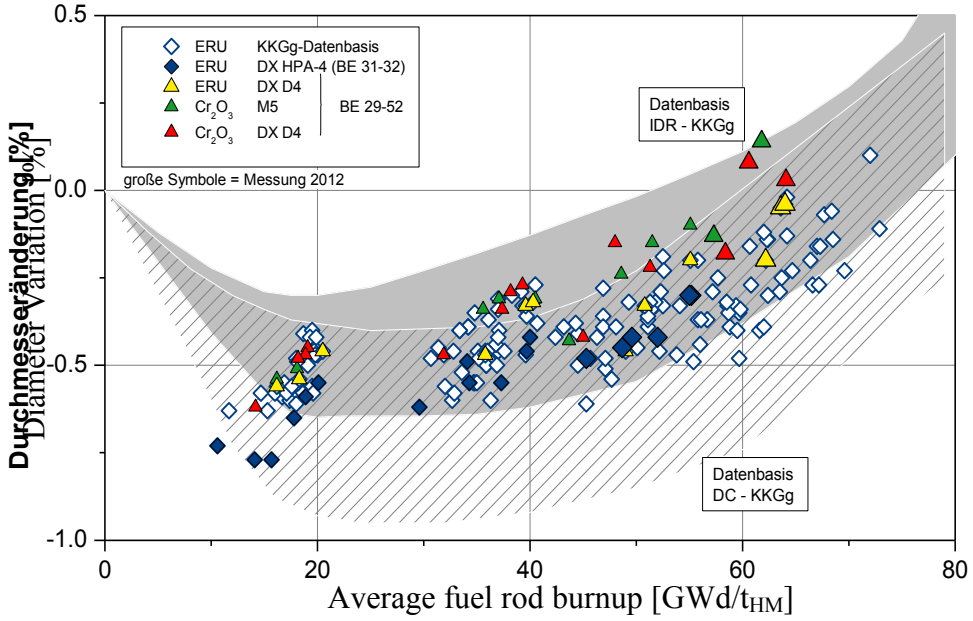

FIG. 6. Cladding diameter variation vs. burnup for selected zirconium-based alloys tested at KKG.

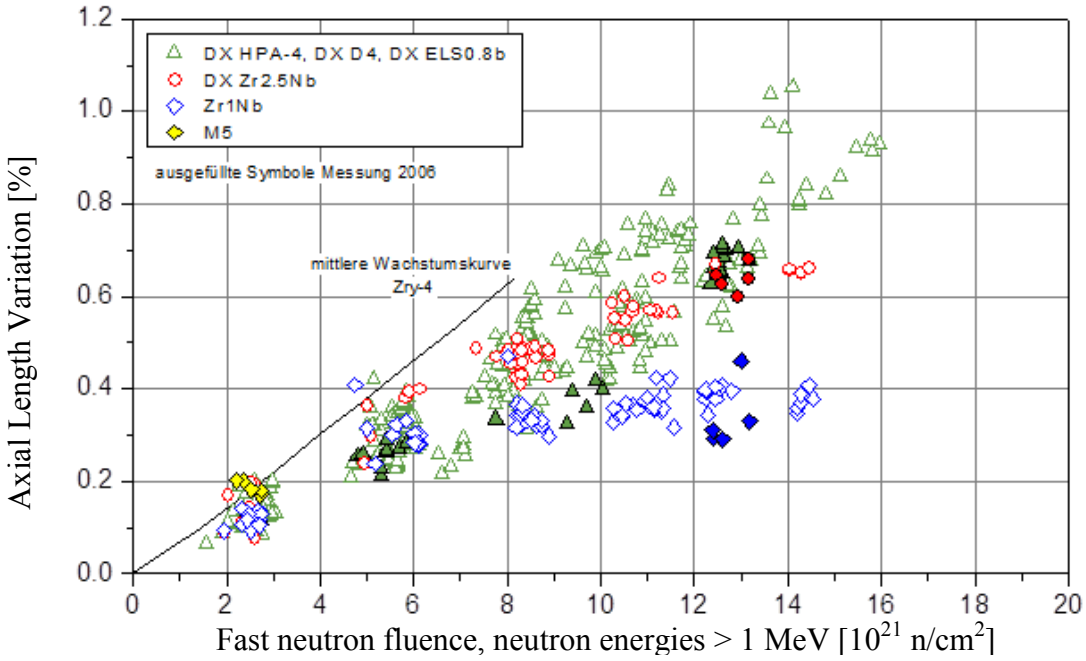

FIG. 7. Rod length variation vs. burnup for selected zirconium-based alloys tested at KKG.

3.3. Guide tube behaviour at very high burnups

Similarly, different structural guiding tube zirconium-based alloys were experimentally investigated following irradiation of their assemblies up to high burnups. The fuel assembly growth, which depends on the elongation of these guiding tubes subject to the spring holding forces on the top nozzle, showed a predictable behaviour also above 60 GWd/t_{HM} (values below or at 0.2% in Figure 8).

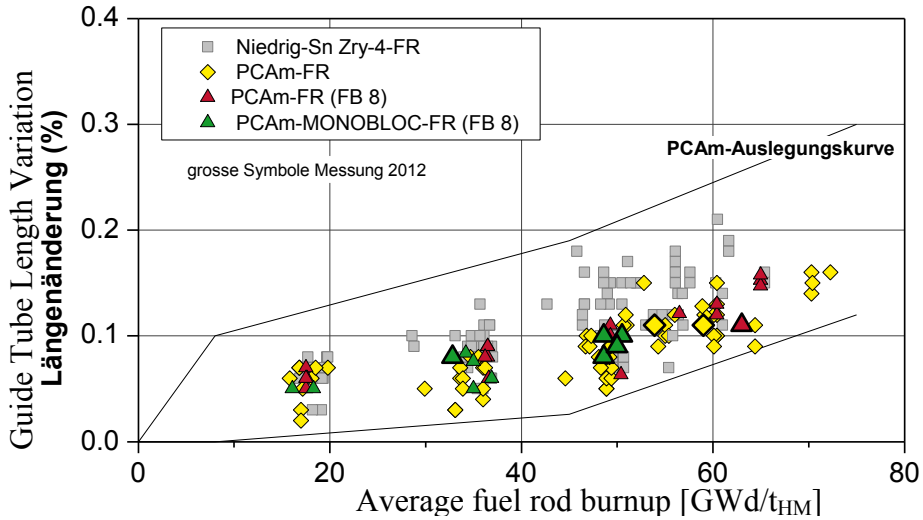

FIG. 8. Guide tube length variation vs. burnup for selected zirconium-based designs tested at KKG.

3.4. Other extensive research programmes for Swiss high burnup fuel

A vast Swiss physics database has been generated and is updated regularly. Many other fields relevant in the context of high burnup physics have also been deepened up to high burnup values, and interesting information is available in the open literature. These include, among others, safety studies associated to criticality and burnup credit [12], LOCA and transient behaviour [13-15], reactivity loss and neutron source increase with burnup [16], detailed

characterisation of density and isotopic compositions of high burnup fuel [17-20], etc. Due to space limitation, the interested reader is necessarily invited to turn to this material separately.

3.5. KKG fuel assembly modifications implemented for very high burnups

The high burnup programme developed demonstrated that the basic KKG fuel parameters behaved monotonically and in a smooth way, from the burnups considered high in the open literature (45 GWd/t_{HM} in theUnited States) to values beyond ca. 80 GWd/t_{HM}, thus supporting the licensing criteria mentioned above. The design of the fuel assemblies was upgraded in any case following the programme outcomes to improve further the rod and assembly robustness. The main modifications included:

- Use of cladding alloy DX-D4 instead of DY ELS0.8b to improve corrosion resistance;
- Reduction of the cladding liner thickness about 7%;
- Reduction of the holding spring force at the assembly top nozzles;
- Optimization of the plena volume above and below the pellet column in the rod;
- Increase of the pellet density to compensate the length reduction of the pellet column;
- Introduction of the Monobloc-Guide Tube design.

4. BACK-END ASPECTS OF HIGH BURNUP FUEL

Following the Fukushima accident and despite the robustness of the Swiss nuclear power plants demonstrated by the EU-Stress Tests in 2012, the Swiss Government took the decision to phase out nuclear power generation, though not immediately. The electricity demand would be supplied through expansion of hydropower, the development of new renewables, and in general more efficient usage. If this is insufficient the building of gas powered stations and an increase in electricity imports are postulated. The evaluation of the potential sites for the deep geological disposal facility and the process for gaining public acceptance in the form of regional conferences are taking place. All the potential sites are located in the north of the country, where the industry is concentrated as these are the best sites from a geological perspective.

The quality of the experimental database available for front-end aspects of high burnup fuel, as described in Section 3, is outstanding. The solid back-end concept of the Swiss nuclear fuel cycle requires, however, renewed efforts to address some open technical questions and safety aspects associated to the fact that it is very difficult to characterise spent fuel following a very long intermediate storage: experimental values would require for example opening a cask with representative high burnup fuel assemblies after say 40 years. For long-term wet and dry storage, and for the operations following them, namely transport and handling, packing and disposal, more experimental data are necessary to show that possible degradation mechanisms are not taking place(or at least to a very lesser extent).

Worldwide, existing final disposal concepts are being re-assessed thus leading to increasing dependence on interim storage. The need to re-license interim storage systems initially approved for 40 years will be a challenge. This challenge can be greater if it is needed to re-license transport systems. In particular, there are fundamental differences between the behaviour of fuel in wet and dry storage, and further differences between dry storage systems [21]. In the case of dry storage there does not appear to be enough data to support defining appropriate limits, with available but rather modest experimental values bound essentially to low burnups [22]. Furthermore any limit would also need to take into account the design basis for each of the technologies. It was suggested that the International Atomic Energy Agency

Technical Working Group on Nuclear Fuel Cycle Options and Spent Fuel Management should be working to define a common set of criteria, for instance based on mechanical properties, criticality safety, retrievability, etc. The obvious importance of considering back-end effects of front-end developments is again an important topic. The advantages of higher discharge burnups / MOX can be negated by the necessity to dispose of the fuel in a deep geological repository too early.

Some dry storage programmes are being developed at bilateral and multilateral levels, with results partly available [23, 24] and partly being mainly of a commercial and thus restricted nature. Some of the most important aspects to clarify possible degradation mechanisms during dry storage include:

- Creep at temperature above 250ºC and for cladding hoop stresses above 100 MPa, to satisfy a creep limit of <1%: Phenomena are under consideration and it has been observed that hydrogen in solid solution can considerably increase the creep rate, for example for recrystallized, annealed Zircaloy. Hydrides, on the contrary, significantly reduce these rates by blocking the dislocation motion.It is thus very difficult to predict creep behaviour without a clear separation between these two distributions, added to a clear understanding of the matrix texture at hand, when both hydrides and hydrogen in solid solution are present.
- The drying process of transport or transport/storage casks is being revisited again, since this process is performed differently in different countries. In the USA this is done under a gas flow in order to restrict the temperature variations. The vacuum process in Europe implies higher temperature steps, in sequence. This is particularly difficult in relation with the possible hydride dissolution and radial reorientation; accepted criteria include cladding temperatures <400ºC and hoop stresses <120 MPa to prevent this phenomenon. In order to study this effect, the Paul Scherrer Institute is conducting with the support of the Swiss nuclear industry a number of tests on LWR irradiated cladding, by quantifying the number of radial hydrides before and after temperature cycles representative of vacuum processes [25]. Typical results are given in Figure 9, suggesting that very significant hydride reorientation may take place for hoop stresses much lower than 120 MPa (even in the compression range). More work is still necessary before coming to definitive conclusions about temperature and hoop stresses for the radial reorientation phenomena; here we simply try to emphasize that much more will be necessary for the back-end of high burnup fuel, particularly to guarantee the integrity of high burnup fuel during transport and handling operations, following ageing in dry conditions under relatively high temperatures and pressures during several decades.

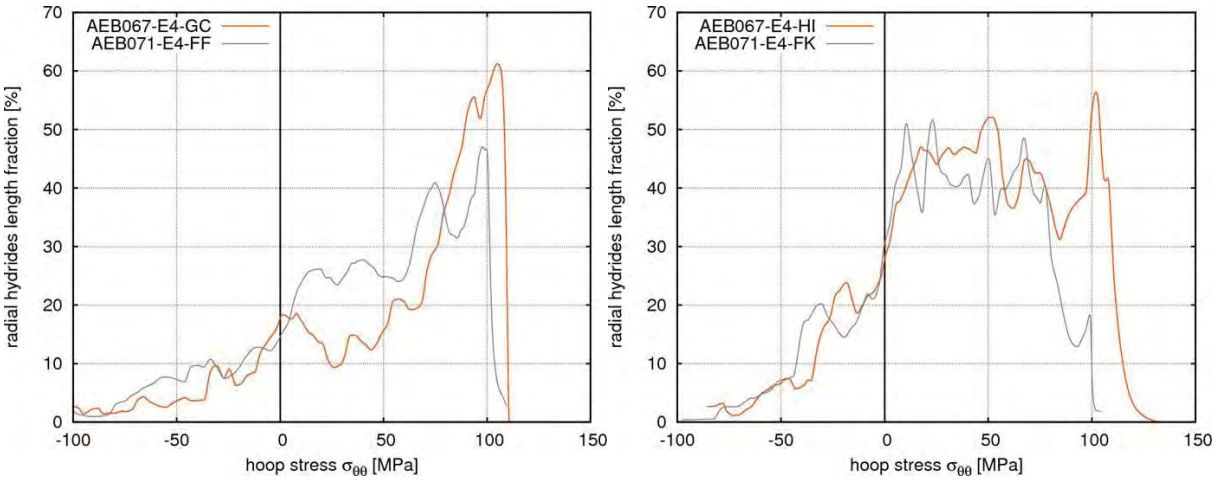

FIG. 9. Hydride reorientation following thermal cycles, in function of the hoop stress for two BWR spent fuel cladding samples.[25] Left: one cycle, reorientation threshold round 50 MPa, lower radial hydrides fraction at compressive hoop stress. Right: three cycles, reorientation for a lower threshold once hoop stress is positive.

Due to these uncertainties, the USNRC has recently stopped granting licenses for transport and storage casks and even for new nuclear power plants, till an issue on the waste confidence rule is solved. In this context, the US department of Energy launched recently a research project over five years, led by EPRI, to characterize spent fuel following dry storage, in a representative 1:1 scale, using an instrumented cask. Unfortunately some time will be necessary before representative results are available.

5. ECONOMIC ASPECTS AND CONCLUSIONS

Section 2 illustrated how concentrating initial fissile material in less fuel assemblies, together with some optimization of the fuel utilization through plutonium buildup, lead to a reduction of the batch size. The first conclusion is that the utility can spare fabrication costs, proportional to the number of assemblies per batch. The costs associated to the enrichment increase necessary for this purpose are somewhat more complex, because it depends on the enrichment tails and the amount of uranium feed on a physical side, and on the spot- or term-market values on the other side. In the case of KKG, it was possible in the last 30 years to reduce the fuel costs about 25%, at an average reduction rate of about 0.022 cents of Swiss franc per kWh and per year. With an annual production of round 8×10^9 kWh, this rate meant a reduction of about 1.7 million francs per year on the front-end.

Not accounted in this estimation are the costs associated to the back-end. Some investments were made to guarantee the transportability and storability of 5%-enriched fuel. The intermediate storage at KKG is at the moment under wet conditions. High neutron source intensities of high burnup fuel will impact on the costs of transport/storage casks, if KKG needed to opt for this solution. The final disposal in repository casks could also be more complicated, by requiring for instance less fuel assemblies in the cask to cope with increased decay heats. This is also still uncertain, because it depends on when exactly the assemblies are going to be transported and packed in the final casks. Consequently, these financial allocations remain still open, with a trend to become positive or negative depending on how soon the final repository will enter into operation in Switzerland.

The basic conclusion from our perspective is that high burnup fuel design, fabrication and operation in the plant is a mature activity supported initially by solid research programmes and, now, by considerable experience in several utilities. The associated costs are known and

rather stable. More work is necessary, however, on the back-end, at technical, safety and financial levels, without which important questions will remain open.

REFERENCES

[1] ORGANISATION FOR THE ECONOMIC AND COOPERATION DEVELOPMENT, Very High Burnups in LWRs, OECD-NEA No. 6224, ISBN 92-64-02303-8 (2005).

[2] XU, Z., KAZIMI, M.S., DRISCOLL, M.J., Impact of High Burnup on PWR Spent Fuel Characteristics, Nucl. Sci. Eng. **151**(2005)261-273.

[3] SECKER, J., JOHANSEN, B.J., STUCKER, D.L., OZER, O., IVANOV, K., YILMAZ, S., YOUNG, E.H., Optimum Discharge Burnup and Cycle Length for PWRs, Nucl. Technol. **151**(2005)109-119.

[4] BROGLI, R.,KRAKOWSKI, R., Degree of Sustainability of Various Nucler Fuel Cycles, PSI Report 02-14, Paul Scherrer Institute (2002).

[5] BERGER, H.-D., Frederic Joliot – Otto Hahn Summer School in Reactor Physics, Topic 2.1 (2006).

[6] EDENIUS, M., EKBERG, K., FORSSEN, B.H., KNOTT, D., CASMO-4: A fuel Assembly Burnup Program - User's Manual, Studsvik Report SOA-95/1, Studswik of America (1995).

[7] GRAVES, H.W., Jr., Nuclear Fuel Management, Chap. 12 – In-Core Fuel Management. John Wiley and Sons, ISBN 0-471-03136-4 (1979).

[8] KHVOSTOV, G., MIKITYUK, K., ZIMMERMANN, M.A., A Model for Fission Gas Release and Gaseous Swelling of the Uranium Dioxide Fuel Coupled with the FALCON Code, Nucl. Eng. Design **241** (2011) 2983-3007.

[9] HELLWIG, Ch., HORVATH, M.I., BLAIR, P.R., CHAWLA, R., GÜNTHER, D., Fission Gas Distribution and Behaviour in the High-Burnup Structure, Proc. of the 2007 International LWR Fuel Performance Meeting, San Francisco, California, Sept. 30th – Oct. 3rd 2007, Paper Nr. 1029 (2007) 291-300.

[10] ROMANO, A., HORVATH, M.I., RESTANI, R., Evolution of Porosity in the High-Burnup Fuel Structure, Jour. Nucl. Mat. **361** (2007) 62-68.

[11] GOLL, W., HELLWIG, Ch., HOFFMANN, P.B., SAUSER, W., SPINO, J., WALKER, C.T., UO_2 Fuel Behaviour at Rod Burnups up to 105 MWd/kg_{HM}, Kerntechnik **52**, (2007) 95-102.

[12] KOLBE, E., GRIMM, P., VASILIEV, A., FERROUKHI, H., Criticality Safety Evaluation of a Swiss Wet Storage Pool including Limited Burnup Credit and Uncertainty Analysis, Proceeding of the International Conference on Nuclear Criticality ICNC, 2011, Sept. 19-22, 2011, Edinburgh, Scotland (2011).

[13] AOUNALLAH, Y., Simulation of HALDEN IFA-650 Loss-of-Coolang Accidents Tests with TRACE, Kerntechnik**77** (2012) 316-323.

[14] KHVOSTOV, G., WIESENACK, W., ZIMMERMANN, M.A., LEDERGERBER, G., Some Insights into the Role of Axial Gas Flow in the Fuel Rod Behaviour during the LOCA based on HALDEN Tests and Calculations with the FALCON-PSI Code, Nucl. Eng. Design **241** (2011) 1500-1507.

[15] FLANAGAN, M., ASKELJUNG, P., Observations of Fuel Fragmentation, Mobility and Release in Integral, High-Burnup, Fuelled LOCA Tests, U.S. NRC Staff Report, (available in pbadupws.nrc.gov/docs/ML1225/ML12257A284.pdf), 12. October 2012.

[16] MURPHY, M.F., JATUFF, F., GRIMM, P., SEILER, R., BROGLI, R., MEIER, G., BERGER, H.-D., CHAWLA, R., Reactivity and Neutron Emission Measurements of Highly Burnt PWR Fuel Rods, Ann. Nucl. Energy **33** (2006) 760-765.

[17] CARUSO, S., MURPHY, M.F., JATUFF, F., CHAWLA, R., Determination of Within-Rod Caesium and Europium Isotopic Distributions in High-Burnup Fuel Rods through

Computarised Gamma-Ray Emission Tomography, Nucl. Eng. Design **239** (2009) 1220-1228.
[18] CARUSO, S., MURPHY, M.F., JATUFF, F., CHAWLA, R., Validation of ^{134}Cs, ^{137}Cs and ^{154}Eu Single Ratios as Burnup Monitors for Ultra-High Burnup UO_2 Fuel, Ann. Nucl. Energy **34** (2007) 28-35.
[19] GÜNTHER-LEOPOLD, I., KOBLER WALDIS, J., KIVEL, N., LINDER, H.P., WERNLI, B., LWR-PROTEUS Programme Phase II: Final Report, PSI TM-43-06-05, Paul Scherrer Institute (2007).
[20] CARUSO, S., MURPHY, M.F., JATUFF, F., CHAWLA, R., Non-Destructive Determination of Fresh and Spent Nuclear Fuel Density Distribution through Computarised Gamma-Ray Transmission Tomography, J. Nucl. Sci. Technol.**45** (2008) 828-835.
[21] Meeting Report, 11th Meeting of the Technical Working Group on Nuclear Fuel Cycle Options and Spent fuel Management (TWGNFCO), 5th-7th June 2013, IAEA, Vienna (2013).
[22] EINZIGER, R.E., TSAI, H., BILLONE, M.C., HILTON, B.A., Examination of Spent Pressurized Water Reactor Fuel Rods after 15 Years in Dry Storage, Nucl. Technol., **144** (2003) 186-200.
[23] BERTSCH, J., Mechanical Integrity Testing of Fuel Claddings, GRS Project and Workshop on Structural and Release Behaviour of LWR High-Burnup Fuel under Transport Accident Conditions, 4th-5th December 2008, Hannover, Germany.
[24] GOLL, W., SPILKER, H., TOSCANO, E.H., Short-time Creep and Rupture Tests on High-Burnup Fuel Rod Cladding, Jour. Nucl. Mat. **289** (2001), 247-253.
[25] VALENCE, S., Influence of Hydrides on the Mechanical Behaviour of Claddings, PSI-ENSI Meeting on Dry Spent Fuel Storage, 13th October 2011.

POST IRRADIATION VISUAL INSPECTION AND METROLOGY OF A NEW DESIGN ATUCHA I FUEL ELEMENTS

G. RUGGIRELLO, H CALABRONI, J. FABIAN, P TRIPODI

Gerencia Ciclo Combustible Nuclear.
Comisión Nacional Energía Atómica,
Buenos Aires, Argentina

Abstract.
Atucha I NPP started its operation on June1974 using natural uranium fuel and since 1995 the core has been converted to SEU (U 0.85% enrichment). Moreover, in the recent years CNEA Fuel Engineering has developed a program to increase the U mass that involves a new structural design of the fuel element (FE), in order to achieve a higher burn up and reduce the frequency of on-line refuelling.
According to these developments a number of activities were planned for the follow-up and periodic control of the FEs in service. In this presentation the poolside facilities to perform visual inspection and fuel rod metrology are described, in special the applied techniques for the measurement of the axial growth at burn ups higher than those for the original FE designs. Contribution of these results to this program is also presented.

1. INTRODUCTION

Atucha 1 is Argentina's first NPP and began its commercial operation in 1974. It is a PHWR designed by Siemens, with a gross electrical power of 360 MWe. The reactor core has 253 vertical coolant channels (CC) in which the FE are irradiated and separates the primary coolant from the moderator. Refuelling is made periodically during operation. Power regulation is made through three absorber rods made of stainless steel for coarse control, three rods made of Hf for fine control, and additional rods of both types for shut down. All rods are inserted at different angles, thus allowing online fuel shuffling by the refuelling machine. Up to date the plant has operated with a 77 % load factor.

Being originally a natural uranium prototype reactor, Atucha 1 has undergone constant improvements in order to get a better efficiency in the utilization of the FEs, as well as concerning safety in operation.

The first action taken was to increase the enrichment to 0.85 w% U235, this program was began during 1993 and concluded when the core was fully converted to SEU in 2000 [1]. At the same time, a second program to increase U mass was implemented through a modification in the design of pellet geometry and a reduction in the inner free volume of the rod [2]. The result of this program was an increase of 2.5 w% in U mass.

The last action in the U mass increase program is the replacement of the structural rod by an active one which adds up to 5.3 w% of U mass to the original design. This modification involved the redesign of the elastic pad which adjusts the FE to the CC; this pad was originally fixed to the structural tube and now it is fixed to the spacer grid. Then, this new FE design consists of a circumferential array of 37 rods with an active length of 530 cm, assembled by fifteen rigid spacers. The rod adjusts to each spacer through three rigid pads welded to the rod at specific axial positions.

The Table 1 [3] shows the main features of the new design FE in comparison with the original one and also the improvements in the average discharge burnup and the refuelling frequency. In addition the FEs are now working at a lower maximum linear power, getting a flatter axial power profile.

TABLE 1. CHARACTERISTICS AND OPERATIONAL PARAMETERS OF Fes OF NEW DESIGN

	Changes introduced in Fuel Elements	
	Original design	New design
Assembly geometry	Circular Array	
Fuel rods	36	37
Structural rod	1	none
Enrichment	natural	0,85%(SEU)
Uranium mass (Kg/FE)	152,5	160,5
Tie plate	1	
Rigid spacer Grids	15	
Active length (mm)	5300	
Cladding material	Zircaloy-4	
Outside diameter (mm)	11.90 mm	
Cladding wall thickness (mm)	0.55 mm	
UO_2 pellet density (g/cm^3)	10.60	
Elastic sliding pad for adjusting to the CC	In structural rod	In spacer
Average discharge burnup (MWd/KgU)	**5,8**	**11,3**
Refuelling frequency (FE/FPD)	**1,4**	**0,7**

Summarizing, the main modification were the replacement of the structural rod for active one (N° 37) and the modification of the design of the elastic sliding pad to fit the FE with the CC. Figure1 shows both designs of elastic pad. The elastic pad at spacer N° 15 has more strength to bear the incoming coolant flow.

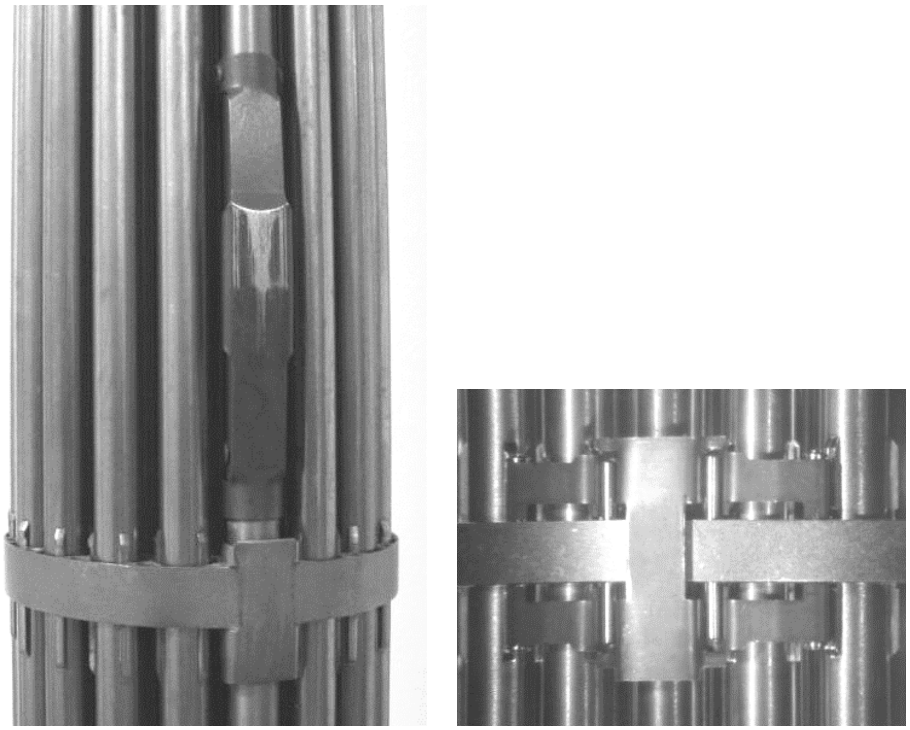

Original design; elastic pad fix to structural rod

New design with 37 active rod and elastic pad fix to the spacer grid.

FIG. 1. Original and new designs of elastic pad.

The steps on the implementation were firstly the corresponding off core test at experimental thermal hydraulic loop test and after an irradiation program was implemented in progressive's

stages. The first stage was the irradiation of 12 FEs (demonstration series) that had been started in 2004 and finished in 2011 and for the follow up of the behaviour a program for visual inspection and metrology control of the fuel rods was implemented at the spent fuel pool (SFP).

2. VISUAL INSPECTION AND METROLOGY OF THE FUEL ROD

For this purpose an upgraded version of an inverted periscope was implemented at the SFP (Figure 2) which added now the associated equipment for performing the metrology of the fuel rod and allows the acquisition of digital image.

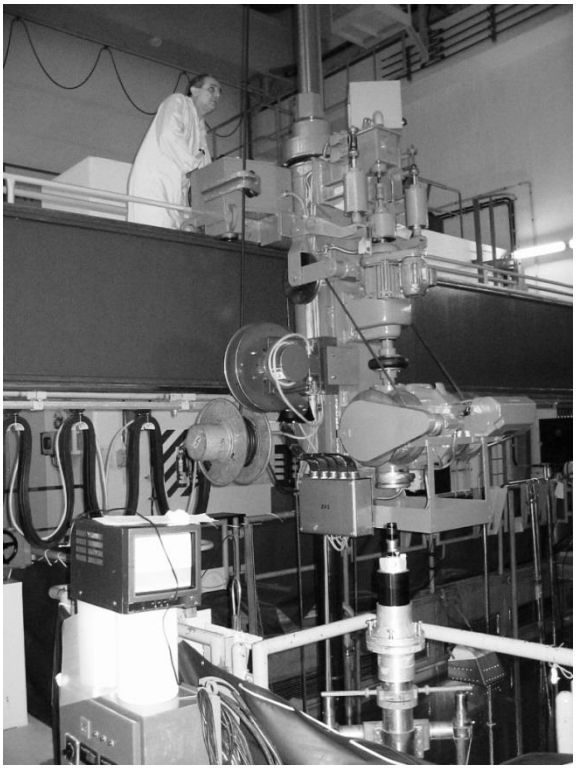

FIG. 2. Inverted periscope and associated equipment for visual inspection and fuel rod metrology at spent fuel pool.

2.1. By visual inspection can be analyzed

a) The general state of the elastic pad and spacer grid of new design, to detect possible interaction, wears or fretting marks in the contact area with the CC.
b) Relaxation of the elastic pad, the evaluation of the relaxation of the elastic pad fixed to the spacer is done by comparison of its gap -in reference to spacer- from an image taken during pre-irradiation inspection. Fig. 3 shows the lateral side view of the elastic pad. The reduction of gap respect to the spacer can be measured by image analysis taken during pre and post irradiation inspection. The geometric interference respect to the maximum permissible internal diameter of the CC is estimated with an error less than of 0.1mm. This inspection is important because the original material (SS A268) was replaced with Inconel 718 for compensate the relaxation generated by higher neutron dose [4].
c) To evaluate the twist and the bowing of the FE; the evaluation is done by axial and rotational displacement of the FE in front of the periscope and observed at the graduated scale in the monitor.

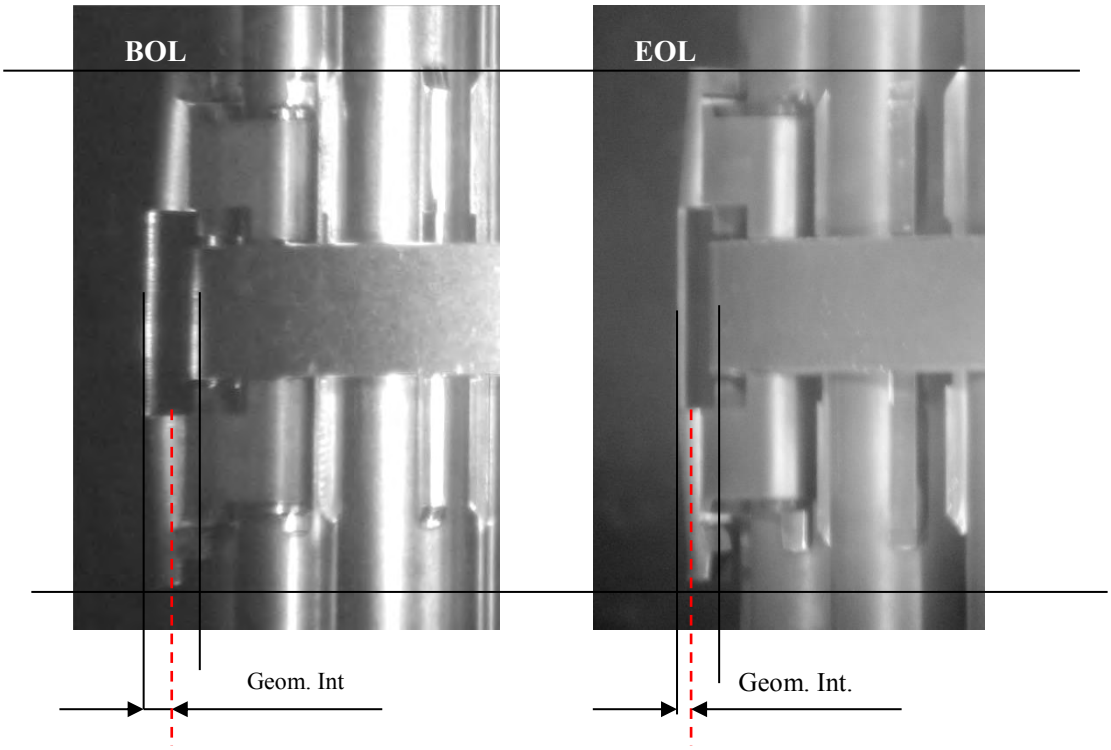

FIG. 3. Lateral side view of the elastic pad.

2.2. By metrology

Can be analyzed the axial growth of the fuel rod. The measurement of total and partial elongation along the rod gives information about irradiation growth according with the linear power axial profile, determine the possible hard Pellet-Cladding Interaction and assess the effects of U mass increase.

Partial elongation is obtained measuring the change in length (pre and post irradiation) in four sections of one outer rod. Each section is setting by the limits between the sharp edges of the rigid pads of the rod corresponding to spacers 1 to 4, 4 to 7, 7 to 10 and 10 to 15 and total length is considered between the spacers 1 to 15. Length measurements are performed observing the displacement of the mast of the crane bridge, when the FE is lifted in front of the periscope. A Laser Distance Meter (precision 0.1 mm) attached to the mast measures the displacement while the pad edge level is observed on the TV screen from the periscope view. Figure 4 shows the edge levels corresponding to the upper and lower spacers between which *Δ length* is measured.

Other measurement of interesting is the differential growth observed among the rod of different ring of the FE as consequence of higher fast neutron dose in the inners rods. This differential growth is measurement from the images analysis of the bottom end of the FE.

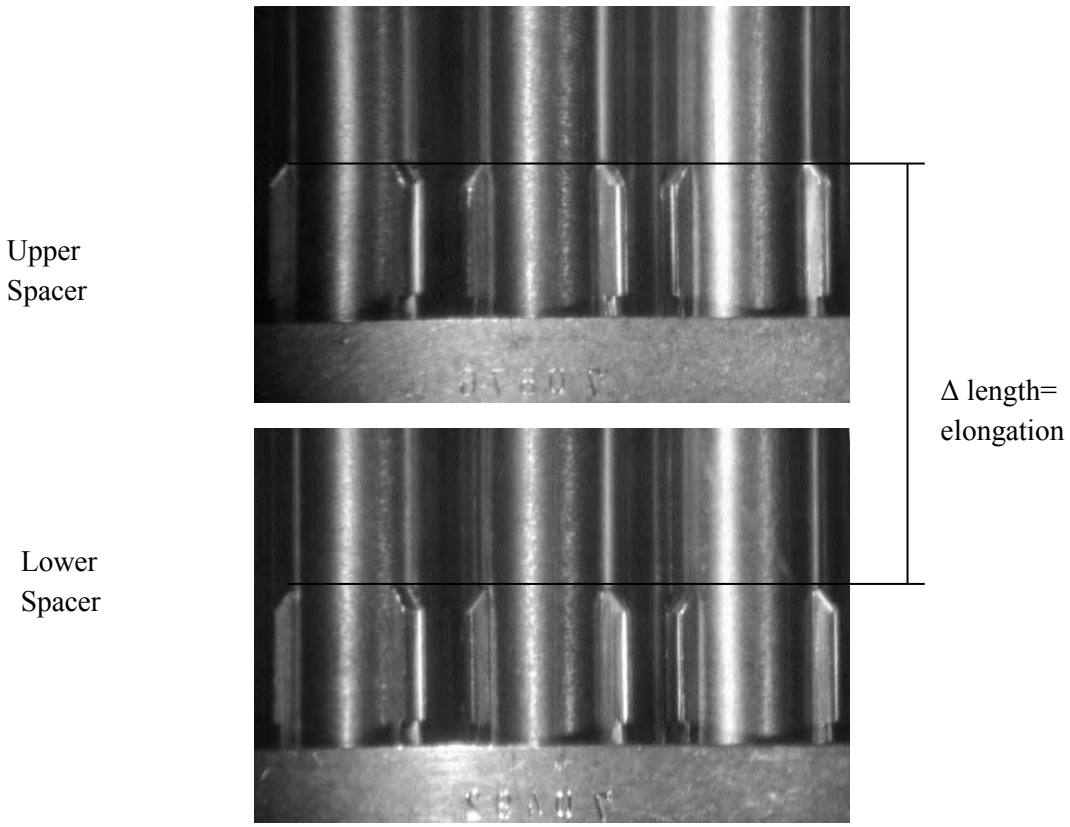

FIG. 4. Reference levels are taken at the rigid pads from an image of the periscope to measure the rod length (resolution ~ 0.5 mm).

3. INSPECTION RESULTS

By visual inspection no structural abnormalities, fretting wear or deformation were observe relative to the new fuel design.

3.1. Wear at elastic sliding pad

No significant wearing mark was observed in all spacers. Figure 5 shows interaction marks of elastic pad of spacer number 13 with CC.

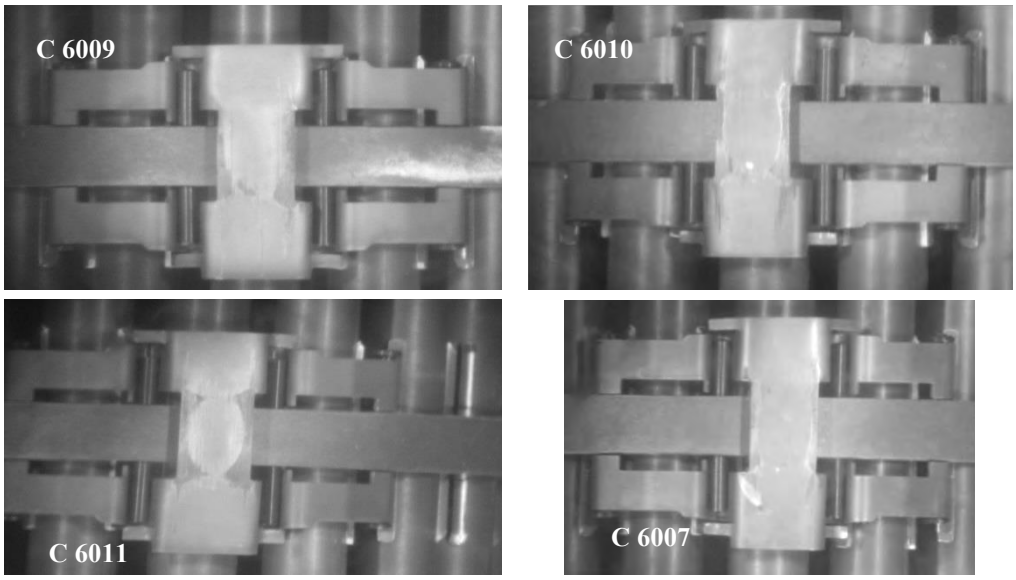

FIG. 5. Frontal view of spacer number 13 of four FE. No significant wearing marks were noticed.

3.2. Elastic pad relaxation

Figure 6 shows the remaining gaps at End of Life (EOL) for FA C6010 at spacers 1, 4, 7, 10 and 15. The measured geometric interference for these spacers is 0.7mm. These comparisons are not enough to fit deformations to axial profile pattern. Table 2 [5] shows details the initial values measured at factory (BOL) and the EOL condition in which the elastic relaxation and the remaining force is estimated as geometric interference. Elastic sliding shoes 1 to 14 has a good agreement in relaxation force under irradiation compared to the design estimated. Force in pad 15 is little less to the predicted value but still acceptable.

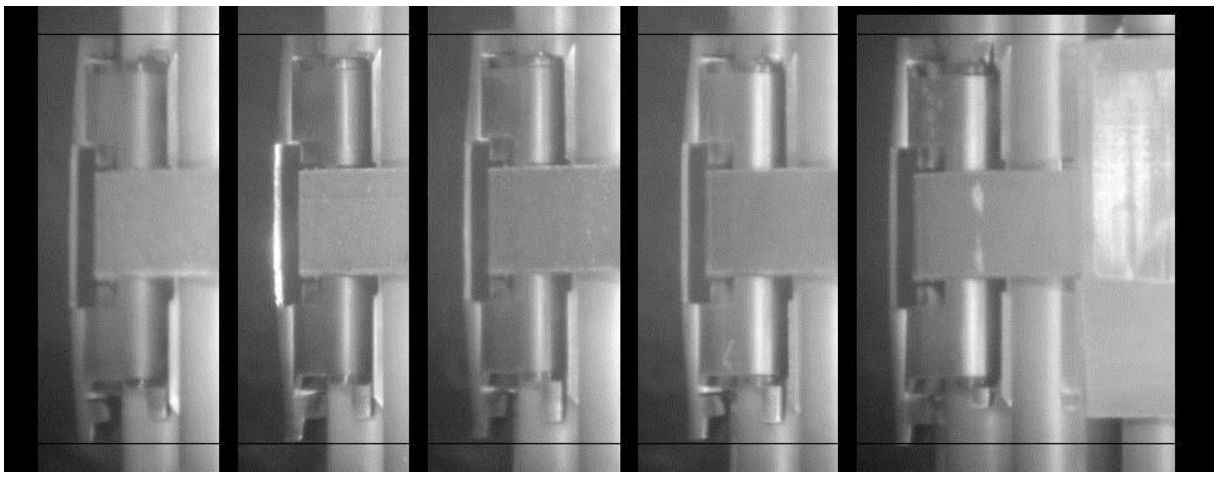

FIG. 6. Remaining gaps at EOL for FA C6010 at spacers 1, 4, 7, 10 and 15.

TABLE 2. MEASURED AND ESTIMATED CHARACTERISTICS OF SPACER GRIDS AT BOL AND EOL

Spacer grid	BOL		EOL			
	Geometric interference (mm)	Spring force (N) by design	Geometric interference (mm)	Relaxation (%)	Spring force (N)	
					resulting	prediction
1 a 14	1,5	30/35	0,7±0.2	40-53	12-16	13 a 20
15	1,5	70/75			28-45	45

3.3. Axial fuel rod growth

Figure 7 shows axial growth measured in each segment and a simulated conservative axial growth. There is no pattern of segmented axial growth that can be remarked, so it is not possible to assure the existence of a hard contact neither the pattern of axial neutron fluence.

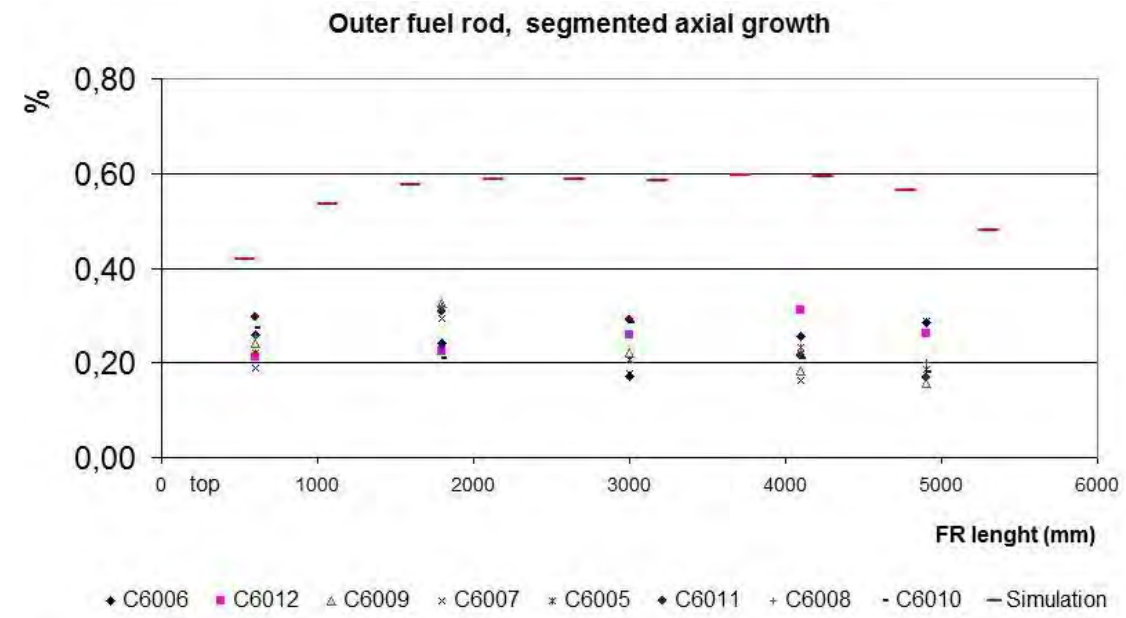

FIG. 7. Axial growth measured in each segment and a simulated conservative axial growth.

Figure 8 shows axial growth measured in centre and outer rods, and a simulated conservative case. The axial elongations measured are always less than the simulated conservative case.

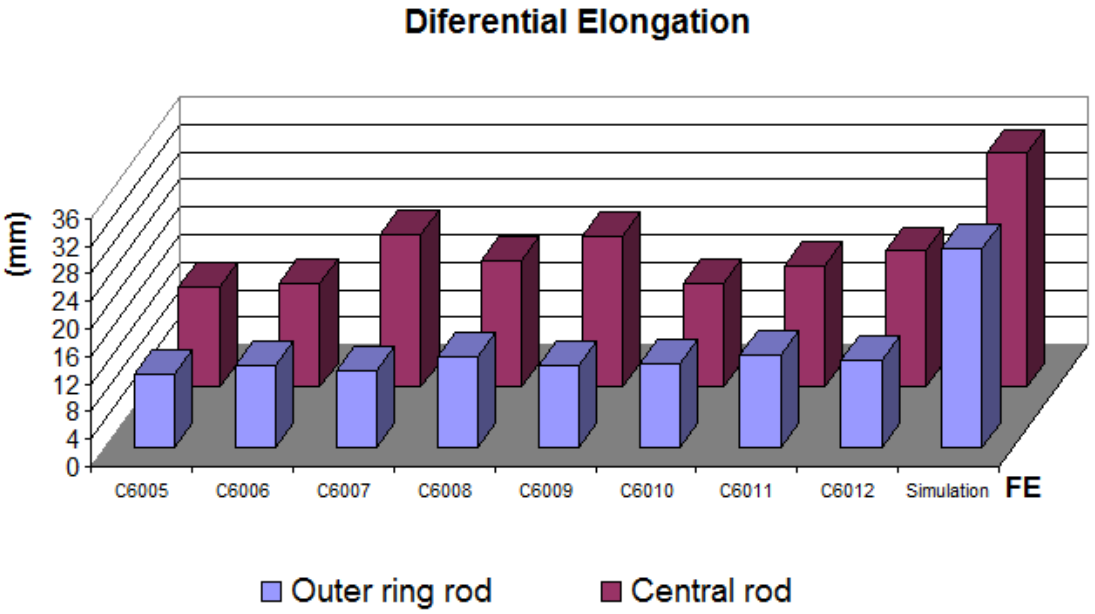

FIG. 8. Axial growth measured in centre and outer rods, and a simulated conservative case.

Figure 9 shows the tree different pattern in which the different elongation of each fuel rod ring can be clearly observed. Figure 10 summarizes differential elongation observed on FE of this inspection.

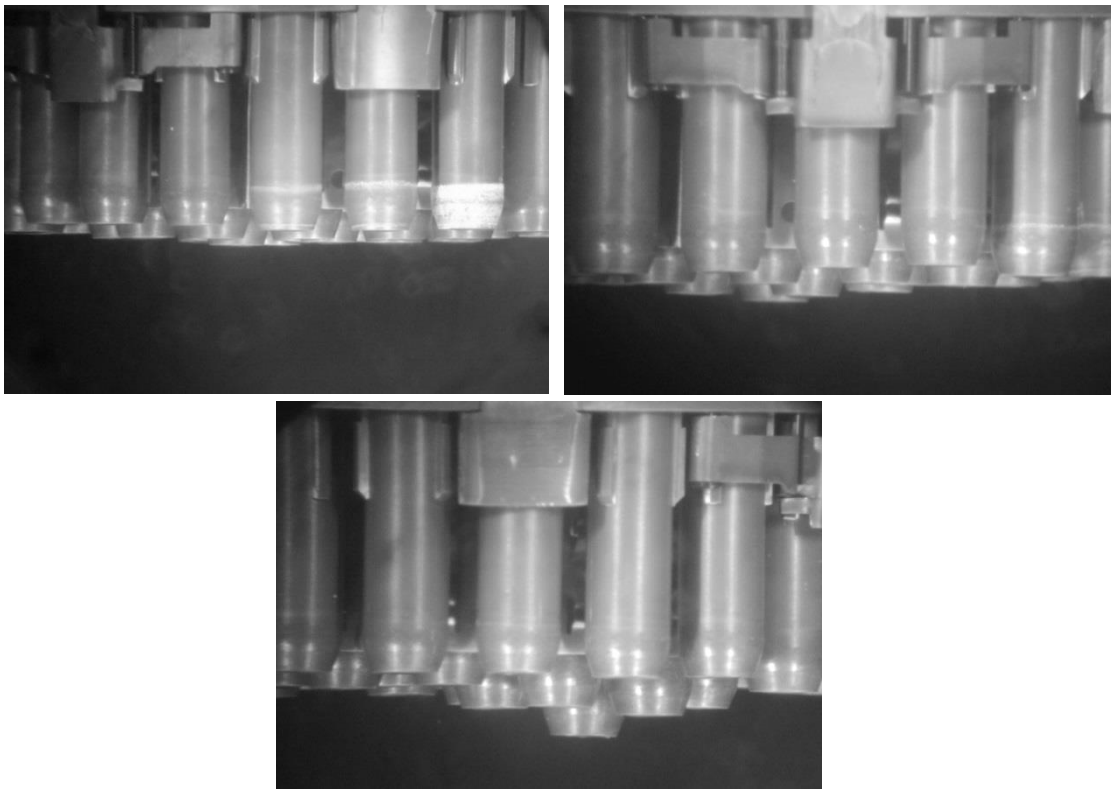

FIG. 9. Different patterns in which the different elongation of each fuel rod ring can be clearly observed (3, 5, 11 mm respectively).

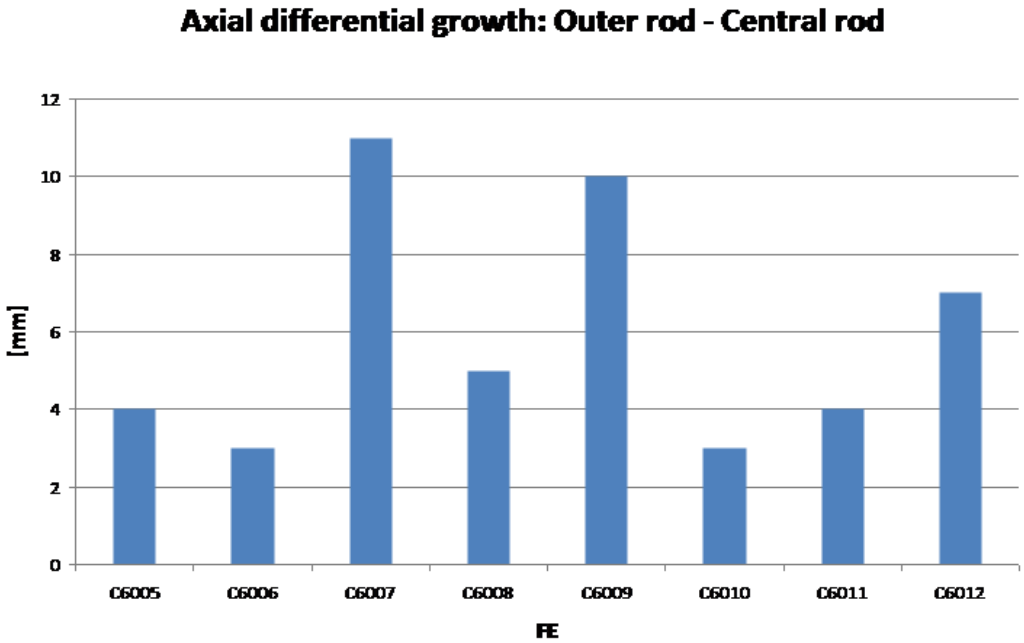

FIG. 10. Differential elongation observed in inspected fuel element.

4. CONTRIBUTION OF THESE RESULTS TO THE HIGH BU PROGRAM

Visual inspection and fuel metrology are key parameters of fuel performance surveillance. Structural failure, fretting wear or deformed elastic pad were not detected by inspection.

The measurements realized during post-irradiation inspection are significantly lower than the

predicted values by simulation of a conservative case. This assures that the design basis and criteria utilized on new design by the Fuel Engineering Department are conservative enough to prevent systematic failure of fuel elements.

Since these good post-irradiation results, the program advanced to the stage of full core load with this new fuel design. Nowadays the core is 80% loaded with 37 fuel rod assembly.

5. FINAL REMARKS

Underwater inspection and metrology techniques are being applied for the monitoring of fuel element's behaviour, as useful tools to assure the safety in operation of Atucha 1 NPP.

The visual inspection and metrology controls assured the progressive implementation of the U mass increase program. As a result of this, nowadays a fuel discharge burnup of about twice the original value has been achieved and the refuelling frequency has been reduced to one half of the previous one, which means a huge improvement in fuel economy.

REFERENCES

[1] ALVAREZ, L., CASARIO, J. A., VALESI, J., Fuel burn up extension to improve the competitiveness of argentine nuclear power plants. INTERNATIONAL ATOMIC ENERGY AGENCY, High burnup fuel experience and economics, (Proc. TM, Bulgaria 2006).

[2] ALVAREZ, L., CASTAÑIZA, S., Fuel engineering considerations for mixed cores experience at the argentine Atucha-1 PHWR. Fuel Design and Licensing of Mixed Cores for Water Cooled Reactors, Vienna (2011).

[3] BUSSOLINI, A.A., TRIPODI, P., ALVAREZ, L., Preliminary design studies to evaluate the utilization of SEU in Atucha-2 fuel rods. INTERNATIONAL ATOMIC ENERGY AGENCY, Proc. TM on Pressurized Heavy Water Reactor Fuel: Integrity, Performance and Advanced Concepts, Mumbai, India, April 2013, IAEA-TECDOC-1751 2014 Vienna 269-282.

[4] ALVAREZ, L., CASARIO, J., FINK, J., PÉREZ, R., HIGA, M., Extended burn up with SEU fuel in Atucha-1 NPP. Technical and economic limits to fuel burn up extension, Bariloche (1999).

[5] CASARIO, J.A., VALESI, J.A., NOTA IEC Nº 034/99.

FUEL DESIGNS AND FUEL CYCLES
(SESSION 3)

Chairperson

C. Cottrell

Canada

STATUS OF FUEL ENGINEERING ACTIVITIES ON EXTENDED BURNUP FUEL FOR THE ARGENTINE FLEET OF PHWRS

A.A. BUSSOLINI, J.A. VALESI, L.A. ALVAREZ

National Commission on Atomic Energy (CNEA) - Fuel Engineering Department
Del Libertador Av. 8250, Buenos Aires, Argentina (C1429BNO)
Tel: + (54 11) 6772 7430, Fax: + (54 11) 6772 7407
bussolini@cnea.gov.ar

Abstract.
At the present there are two nuclear power plants in operation in Argentina, one is Embalse (CNE), a CANDU-6 design, and the other is Atucha-1 (CNA-1), a Siemens/KWU PHWR design. Fuel assemblies for CNE and CNA-1 are entirely manufactured in Argentina and over the years their designs have been improved as a result of the operational experience, fabrication evolution and technical and economic needs. One of the main modifications was the utilization of Slightly Enriched Uranium (SEU) in CNA-1 to replace the natural uranium considered initially in the design of this power plant. The introduction of the SEU fuel was performed between the years 1995 and 2000. Since then only SEU fuels have been in use in CNA-1. The fuel engineering activities for the SEU fuel were performed by the Fuel Engineering Department of the National Commission on Atomic Energy (CNEA) and have included among other tasks the preparation of drawings, the adjustment of product specifications, extensive fuel rod thermomechanical design verifications and the fuel performance evaluation of the first series of the SEU fuel.
Due to the utilization of SEU and the fuel design improvements in CNA-1 the fuel burnup was increased twice the original value. In this paper is given a brief definition of what is meant by extended burnup in the case of PHWR power plant and a description of the SEU Program to upgrade CNA-1 natural uranium core to SEU. Also the objectives, advantages and limitations of this program and the design and in pile performance are commented.
Nowadays the construction of Atucha-2 (CNA-2), the 3rd Argentine Nuclear Power Plant, is almost completed, the fuel assemblies have been loaded in the reactor and the commissioning phase of the project is in an advanced stage. Atucha-2 is also a Pressurized Heavy Water Reactor designed by SIEMENS-KWU. The fuel is natural uranium.
Considering the excellent results of the utilization of SEU fuel in CNA-1, feasibility and safety studies of SEU fuel utilization and core transition in CNE were performed. Based on the results of CNA-1 and the similarities between the designs of CNA-1 and CNA-2 fuels some fuel engineering preliminary studies about SEU fuel utilization in CNA-2 are being performed by CNEA. In this paper are summarized some key points of those studies.

1. INTRODUCTION

Argentina has two nuclear power plants in operation, one is Embalse (CNE), a CANDU-6 design, and the other is Atucha-1 (CNA-1), a Siemens/KWU PHWR design. Currently, the construction of Atucha-2 (CNA-2), the 3rd nuclear power plant of Argentina, is almost completed, the fuel assemblies have been loaded in the reactor and the commissioning phase of the project is in an advanced stage. This third reactor was also designed by Siemens/KWU. The construction started in the 80's, halted in the 90´s and was re-launched in 2006.

Fuel assemblies for CNE and CNA-1 are entirely manufactured in Argentina and over the years their designs have been improved as result of operational experience, fabrication evolution and technical and economic needs. The first core for CNA-2 was fabricated by the same national manufacturer. This is the first time that Argentina is in charge of the engineering and manufacturing of the first core for a nuclear power plant.

1.1. Atucha-1

Atucha-1 is a 357 MWe (1179 MWt) nuclear power plant with pressure-vessel design and moderated and cooled with D_2O.

The reactor core is approximately cylindrical in shape and consists of 253 slightly enriched uranium fuel assemblies located in the same number of coolant channels. Table 1 summarizes some key characteristics of CNA-1.

TABLE 1. CNA-2 AND CNA-1 NUCLEAR POWER PLANTS DATA [4, 6, 8 AND 9]

General Operating Conditions	CNA-2	CAN-1 *	CNE	Unit
Thermal reactor power	2160	1179	2109	MWth
Net electric power	692	335	600	MWe
Average specific fuel rod power	232.8	232.0	246.0	W/cm
Fuel burn-up at equilibrium	7500	11400	7350	MWd/Mg
Number of fuel assemblies in the core	451	253	4560	-
Number of fuel channels	451	253	380	-
Refuelling	on power	on power	on power	-
Primary system pressure	115,0	112,8	112	bar
Coolant and moderator	D_2O	D_2O	D_2O	-

(*) After plant commissioning and power uprating

Each fuel assembly consists of 36 fuel rods and one structural tube (in the outer ring) arranged in three concentric rings and a central fuel rod. The assembly also includes a tie plate, fifteen Zr-4 rigid spacer grids, one Inconel sheet spacer grid and a coupling system to connect the fuel assembly with the reactor internals. Each fuel rod consists of a 5300 mm long stack of UO_2 pellets, isolating pellets, a gas plenum and a compression spring enclosed by a thin walled zircaloy-4 free standing canning tube with welded end plugs at both ends to make it gas tight. Fuel assembly details are shown in Figure 1 and Table 2 shows some key characteristics.

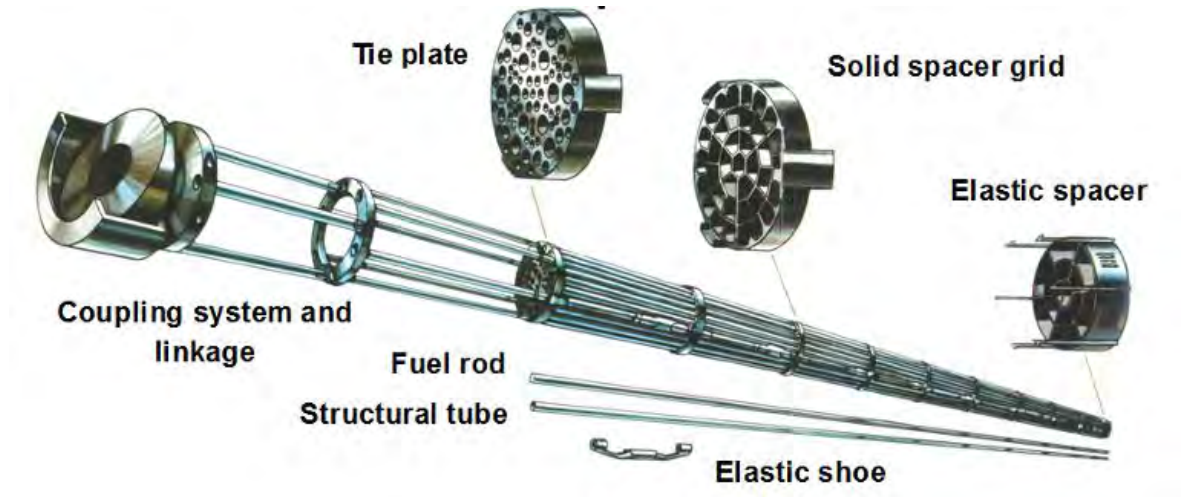

FIG. 1. CNA-1 fuel assembly design [10].

TABLE 2. CNA-2 FUEL ASSEMBLY DESIGN SUMMARY [4, 8]

	CNA-2	CNA-1 *	CNE
Fuel assembly			
Number of fuel rods per fuel assembly	37	36 (+1 structural rod)	37
Length	6027.8 mm	6028.5 mm	495.3 mm
Outside diameter (without elastic shoe)	107.8 mm	107.8 mm	102.77 mm
Type of spacer grids	Elastic (Raw material: sheet)	Rigid (Raw material: bar) + 1 elastic at the lower end	--
Number of spacer grids	13 (12 from Zry-4 and 1 at the lower end from Inconel 718)	16 (15 from Zry-4 and 1 at the lower end from Inconel 718)	--
Fuel rod			
Cladding material	Zircaloy-4	Zircaloy-4	Zircaloy-4
Cladding outside diameter	12.90 mm	11.9 mm	13.08 mm
Fuel column length	5300 mm	5300 mm	478.6 mm
Fuel rod length	5566.4 mm	5566.4 mm	492.5 mm
Fuel pellets			
Material	Uranium dioxide	Uranium dioxide	Uranium dioxide
Form	Cylindrical pellets with dishing on both end faces	Cylindrical pellets with dishing on both end faces	Cylindrical pellets with dishing on both end faces
Enrichment	Natural	SEU (0.85 w% U^{235})	Natural

(*) After plant commissioning and power uprating

The coolant channels are arranged vertically in a trigonal lattice within the moderator tank. The fuel assemblies are replaced on-line during reactor operation by a refuelling machine. The coolant channels are surrounded by the moderator (D_2O), which is contained in the moderator tank.

1.2. Atucha-2

CNA-2 was designed and built based on the design and experience of CNA-1 but scaled in size and power. CNA-2 will deliver approximately twice the power of CNA-1. This power increase is mainly due to the use of more FA in the core thus a greater amount of uranium. Some characteristics comparing both NPP are listed in Table 1.

The fuel assemblies for CNA-2 have the same geometrical arrange of CNA-1 but consist of 37 fuel rods without any specific structural tube. The fuel rods are kept in their positions using 12 zircaloy-4 sheet spacer grids and one Inconel spacer grid (lowest most). The main CNA-2 fuel details are shown in Figure 2 and listed in Table 2.

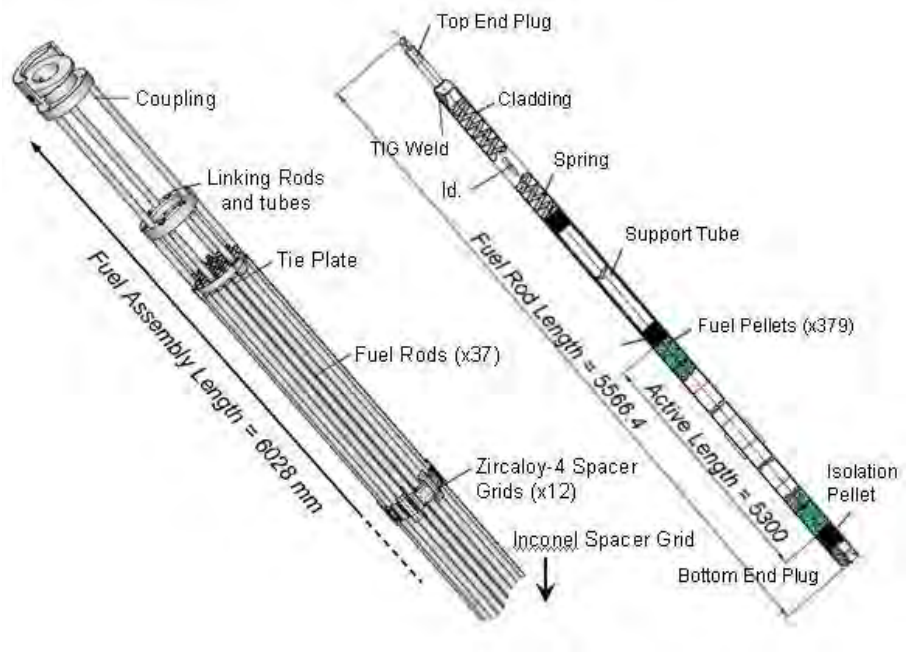

FIG. 2. CNA-2 fuel assembly design and fuel rod details [11].

The internal designs of CNA-2 and CNA-1 fuel rods are very similar including the cladding free standing concept. CNA-2 FAs are currently fuelled with natural uranium.

1.3. Embalse

Embalse is the second Argentine nuclear power plant which is operating since 1983. The reactor is a CANDU-6, designed and built by AECL of Canada. Table 1 summarizes some key characteristics of the reactor and fuel bundle details are listed in Table 2.

2. EXTENDED BURNUP IN PHWR

The burnup of LWR´s fuel has doubled during the last three decades and the average burnup is in the range of 50,000 MWd/tU while in PHWR remains in the range of 7,000 MWd/tU. It can be expected that these burnups will be increased further [1, 2].

The current trend in LWRs and to some extent in PHWRs is to increase fuel burnup to high or ultrahigh levels. The target burnup for LWR and PHWR fuel is 60,000 - 80,000 MWd/tU and 15,000 - 20,000 MWd/tU respectively.

Considering absolute values, the typical burnup for PHWRs is significantly lower in comparison with the burnup for PWRs. On the other hand, the burnup increase between the original and the proposed new burnup limits expressed in percentage is higher in PHWRs (114% - 185%) than in PWRs (20% - 60%).

3. SEU PROGRAM IN ATUCHA 1

To reduce the impact of the cost of the fuel on the cost of the energy generated at Atucha-1 a program was initiated in August 1993 to introduce gradually slightly enriched uranium (SEU; 0.85 w% U^{235}) fuel. The introduction of SEU fuels started in 1995 and by 2000 the whole core was converted to this new type of fuel. The program was divided in three phases with an

upper limit of number of SEU FA in the core [3] in each phase. Since then only SEU fuel is in use.

3.1. Main objectives and advantages of SEU utilization

The main benefits from the use of SEU in comparison with natural uranium (NU) are the following [4]:

- Extension of fuel discharge burnup.
- Fuel cycle costs decrease.
- Uranium resources savings.
- Spent fuel volume decreases.

Other beneficial consequences of using SEU fuel in CNA-1 are [4]:

- Extension of fuel residence time.
- Reduction of FA consumption.
- Reduction of frequency of refuelling and fuel shuffling (on power). Less utilization of the fuelling machine.
- Reduction of fresh fuel stock and fuel transports.
- Impact on spent fuel storage pool capacity.

3.2. Design criteria and limitations

The fuel rod was designed so that design criteria are satisfied during normal operation in order to prevent excessive fuel temperatures, excessive internal rod gas pressure and excessive cladding stresses and strains. The detailed fuel rod design establishes and considers such parameters as pellet size and density, clad/pellet gap, gas plenum size, cladding dimension, helium pre-pressure, radial relocation of pellet fragment, density changes, fission gas release, cladding creep and other physical effects.

These design criteria are related with some SEU life limiting aspects. The main design guidelines for SEU FA were [4]:

- Maintain the fuel ability to operate reliably to the proposed extended burnups levels.
- The reduction of the operational flexibility at the power plant must be as low as possible.
- Maintain the safety margins as close as possible to the margins for natural fuel operation.

The main fuel operating parameters affected by the utilization of SEU fuel instead of NU are:

- Discharge Burnup.
- Residence time.
- Local burnup at the time of fuel reshuffling (power ramps).
- Maximum burnup at high power.

Other parameters such as power levels, water chemistry and sheath and coolant temperatures are not significantly affected.

The most relevant aspects in Atucha-1 FA performance analyzed were those affected by the higher burnup and the increase in the residence time. The most significant were:

- Fission gas release and how it affects the internal gas pressure.
- Fuel cladding creeps down and sheath strain.

- Relative length changes between the fuel stack and the cladding.
- Relative length changes between different fuel rods at different positions in the same FA.
- Fuel cladding axial growing.
- Fuel assembly structural integrity, including the effectiveness of the interactions between fuel rods and spacer grids and between elastic sliding shoes and coolant channel (to hold fuel rods and fuel assemblies in their positions through the whole irradiation).
- Power ramp behaviour.
- Waterside corrosion and deuterium uptake.

In the particular case of power ramps, they are produced during the irradiation as a result of fuel reshufflings, fresh fuel loading, reactor start-ups and reactor power changes and their associated control rod movements. Power ramps may lead to the occurrence of fuel failures associated to PCI-SCC. The PCI prevention criteria were reviewed by CNEA and a new set of recommendations was defined to consider the SEU operation at higher burnup. The new criteria are based on the combination of linear power before and after the ramp and burnup at the time of the ramp. Considerations about maximum allowable power increase rates were also included. The operator of the power station translated these criteria into operational instructions which refer to data obtained from the fuel management calculations. As a result of the new criteria the time to reach full power in a plant start-up increased from 28 to 35 hours.

3.3. Fuel design verifications

Several analysis were performed to fulfill regulations requirements and to update the safety analysis report. Fuel rod calculations were performed to evaluate the fuel performance in the new operating conditions. Conservative design parameters were used as input data and conservative power histories were also selected according to the parameter to be verified. The main objective of these calculations was to demonstrate that the fuel performance safety margins are not affected by the utilization of SEU.

Several power histories representative of different new irradiation routes were analyzed.
The main performance parameters included in the fuel rod calculations were:

- Maximum fuel temperature.
- Internal fuel rod pressure.
- Long term sheath strain.
- Short term strains.
- Waterside corrosion and deuterium pick-up.
- Fuel rod axial growing.
- Relative elongations of the pellets stack and the cladding.
- Relative elongations between fuel rods at different positions of the FA.

3.4. Fuel design modifications

Several changes have been introduced in the design of the fuel rod and the FA to optimize them to the new SEU operating conditions:

- The plenum length was increased to provide more volume for gas release.
- Bearing pads with longer contact surfaces were adopted to assure reliable interaction between spacers and fuel rods during the whole life of the fuel.

- The ductility of the cladding material was increased to reduce the fuel rod susceptibility to PCI failure on power ramps.
- Inconel-718 was selected to replace the original elastic sliding shoes material (SS A286) to compensate the higher stress relaxation produced by the increase of the neutron fluence.

3.5. Program phases

The introduction of SEU fuel started in 1995 and finished in 2000. The program was divided in different phases with an increasing upper limit of SEU FA in the core. Licensing documentation and authorizations from the Nuclear Regulatory Authority (ARN) were required for each Phase and a Safety Report was prepared for each stage of the program.

Phase 1 consisted in the introduction of SEU FA not exceeding 12 at any time in the core.

Phase 2 was initially defined as the transition period from 12 to 60, but was later extended to 99 SEU FA in the core.

Phase 3, from 100 to full SEU core.

Phase 1

Fresh SEU FAs were introduced in six predetermined channels as shown in Figure 3.

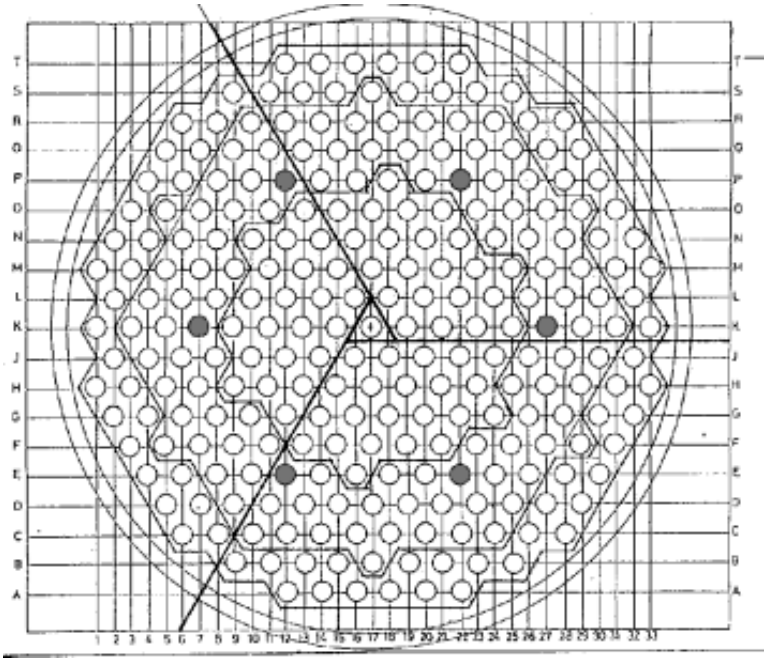

FIG. 3. CNA-1 core section. Location of the six predetermined channels for SEU FA introduced during phase 1.

The main objectives were:

- Verify the performance of the SEU fuel in the core with discharge burnups close to the values expected for the equilibrium full SEU core. In particular, to verify the behaviour in power ramps produced during refuelling operations, reactor power increases, and startups from low power.
- Reach discharge burnups of 10,000 MWd/tU.

- Verify predictions of neutronic calculations like reactivity gain, channel power increase and detector flux increase when introducing SEU fresh FA.
- Test operating procedures developed for SEU fuel.

Phases 2 and 3

- The average discharge burnup of the SEU fuel was increased to 11,000 MWd/tU. The main objectives were:
- Verify the performance of the SEU fuel in the different zones of the reactor at burnups at which they were going to be moved from one channel to another in the SEU core.
- Verify the performance of the SEU fuel at discharge burnups similar to the foreseen for the full SEU core.
- Verify the global behaviour of the core with an increasing fraction of SEU fuel.
- Prepare the location of SEU FA in the core for the transition to a full SEU core.

3.6. Design and in-pile performance

As predicted, the operation of the plant showed no unexpected impacts due to the use of SEU fuels. An evaluation of SEU fuel performance data shows that power ramps, discharge burnups and dwelling times satisfy previous estimations without any negative impact on the fuel performance. In particular, the new criteria to prevent PCI failures in power ramps for higher burnup SEU fuel in refuelling operations, plant startups or power cycling has been effective [3]. The results of post-irradiation pool-side visual examinations and fuel rod length measurements were satisfactory and in agreement with previous estimations and models [5]. In Figure 4 are showed the results of fuel rod length measurements at different burnups.

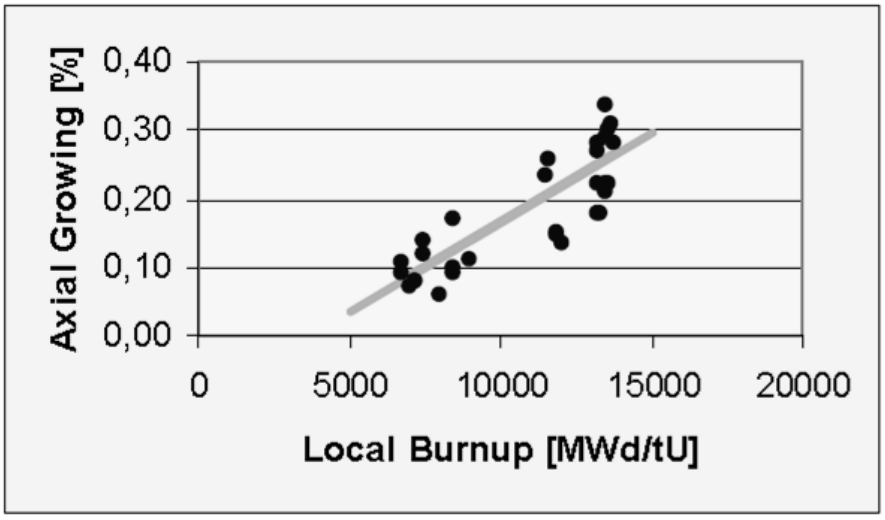

FIG. 4. CNA-1 SEU fuel rod axial growing (%) measurements at different local burnups.

Relevant data to point out is [5]:

- The increase of the average discharge burnup, from 5,900 with natural uranium to 11,300 MWd/tU.
- The maximum local burnup, close to 15,000 MWd/tU.
- The reduction of the refuelling frequency, from 1.31 to 0.7 FA/fpd.
- The dwelling time, from 300 to 500 fpd, almost doubling the corresponding value for natural uranium.

- The reduction of spent fuel volume, about 42 %.

In Table 3 are compared some key parameters. The fuel costs dropped gradually during the program approximately 30 % to 40 % [3, 6]. As a result the SEU program has been an important contribution to the reduction of Atucha-I operating costs and to the competitiveness of nuclear power generation against other sources of generation in a deregulated electrical market in Argentina [3].

TABLE 3. CNA-1 FA PERFORMANCE [4, 6]

Enrichment	**Natural U**	**SEU (0.85 w% U^{235})**
Average discharge burnup [MWd/kgU]	5.9	11.3
Refuelling frequency [FA/efpd]	1.31	0.7
Quantity of FA/year [F_L • 85 %]	396	208
Consumption of uranium [tU/year]	61	44

During the three phases of the transition program and also during the operation with full SEU cores no failures associated with the introduction of the SEU with 0.85 % U-235 or with the new operating conditions were reported. Table 4 shows the evolution of the quantity of failures and the average fuel discharge burnup during the last three years of operation.

TABLE 4. CNA-1 QUANTITY OF FAILURES AND AVERAGE FUEL DISCHARGE BURNUP EVOLUTION [9]

Year	**2010**	**2011**	**2012**
Number of Fuels Discharged	248	213	219
Number of Fuel Assemblies with leaking Fuel Rods	4	0	0
Average Fuel Discharge Burnup [MWd/tU]	10563	10649	10696

4. OTHER PROJECTS TO INCREASE FUEL BURNUP

4.1. CNE SEU fuel program [8]

Based on the advantages listed in the section 3.1 and the excellent results obtained with the implementation of the SEU program since 1995 in CNA-1, the Argentinean nuclear power plant operator (NA-SA) together with AECL and CNEA have been analyzing under the framework of a cooperative program the feasibility of using Slightly Enriched Uranium (with 0.9 w% ^{235}U) fuel in CNE. Using SEU fuel would produce a significant increase in the fuel discharge burnup, from the currently achieved burnup with natural uranium (NU) to about 14 MWd/kgU. This would result in similar benefits as those listed in the previous section with the CNA-1 SEU fuel program.

Among the activities related with the assessment of the CNE fuel performance up to SEU typical burnups, CNEA has performed preliminary calculations to evaluate the behaviour of the fuel in nominal design conditions using envelope power histories. The main parameters analyzed were fuel center temperature, internal gas pressure and cladding strains. Fuel calculations were performed using the same calculation tools like for the original design. These preliminary results are encouraging and allow predicting a very limited impact of the higher burnup on the fuel performance for the current design conditions.

In case of SEU implementation in CNE with the same enrichment as in CNA-1 (0.85 w% U^{235}) the savings (only in fuel) were estimated [6] around 19 %. The relative fuel cost

reduction is lower in comparison with CNA-1 because CNE fuel is cheaper than CNA-1 and CNA-2 fuels and has less impact on the total energy cost.

4.2. CNA-2 SEU fuel studies

Based on the NPP and FA similarities between CNA-1 and CNA-2, the excellent results obtained with the SEU program in CNA-1 and the extensive experience acquired in this process, a preliminary feasibility of a similar SEU program at CNA-2 has been under evaluation by the CNEA Fuel Engineering Department.

In this preliminary feasibility study [7] fuel design criteria were reviewed, CNA-2 and CNA-1 fuel designs were compared and some fuel rod thermomechanical behaviour calculations were performed with conservative input data. The most relevant parameters analyzed for this study were:

- Fuel burnup;
- Center line fuel temperature;
- Fuel rod internal pressure;
- Fuel and cladding relative deformations.

The results obtained in this preliminary study together with the excellent results obtained with the SEU program in CNA-1, allow anticipating that no systematic failures in Atucha-2 fuel rods due to the implementation of SEU are expected. No major design modifications arise to be necessary but some minor modifications in the fuel rod have to be evaluated to optimize them for SEU requirements.

Further studies like the evaluation of the higher relaxation produced by the increase in neutron fluence in the elastic spacer grids and particularly in their cantilever springs also were proposed.

The realization of this project in CNA-2 would have an important impact in the plant costs of the generated energy, similar to the one in CNA-1 due to the similarity between both types of fuels [6].

5. FINAL REMARKS

Competitiveness of the electricity generated in PHWR NPP requires a constant effort to minimize the cost of the fuel and to improve the utilization of natural resources. These are the main driving forces for the study and implementation of fuel upgrade programs for the Argentinean fleet of PHWRs.

The main goals of these programs are to increase the fuel discharge burnup and to increase uranium content in order to extend the dwelling time. In this paper were detailed the SEU programs for extending the fuel discharge burnup and their advantages.

The particular case of CNA-1 where a successfully SEU fuel program with a gradual transition from a natural uranium core to a SEU core (0.85 % ^{235}U) has been completed and has been successfully applied for more than 10 years with cores loaded completely with SEU fuels is encouraging in order to continue with similar programs in the two other Argentinean NNP and for PHWRs in general.

REFERENCES

[1] INTERNATIONAL ATOMIC ENERGY AGENCY, Impact of extended burnup on the nuclear fuel cycle, Proceedings of an Advisory Group Meeting, IAEA, Vienna, 2-5 Dec. 1991, IAEA-TECDOC-699 (1993).

[2] INTERNATIONAL ATOMIC ENERGY AGENCY, Experiences and Trends of Manufacturing Technology of Advanced Nuclear Fuels, IAEA-TECDOC-1686, Vienna (2012).

[3] FINK, J.M., HIGA, M., PÉREZ, R., PIÑEYRO, J., SIDELNIK, J., CASARIO, J.A., ALVAREZ, L., Overview of the SEU project for extended burnup at the Atucha-I NPP. Four years of operating experience, INTERNATIONAL ATOMIC ENERGY AGENCY, TM on Technical and economic limits to fuel burnup extension, Bariloche (15-19 Nov. 1999), IAEA-TECDOC-1299 Vienna (2002) 170-180.

[4] CASARIO, J.A., ALVAREZ, L.A., Developments in slightly enriched uranium for power reactor fuel in Argentina. Impact of extended burnup on the nuclear fuel cycle, Vienna (1991).

[5] ALVAREZ, L., CASARIO, J., FINK, J., PÉREZ, R., HIGA, M., Extended burnup with SEU fuel in Atucha-1 NPP, Proceedings of an Advisory Group Meeting,Vienna, 2-5 Dec. 1991, IAEA-TECDOC-699 Vienna (1993) 15-22.

[6] NOTARI, C., REY, F. C., Uranio levemente enriquecido en Atucha I: Un desarrollo tecnológico relevante de la CNEA y el sector nucleoeléctrico. CNEA (2001).

[7] BUSSOLINI, A., TRIPODI, P., ALVAREZ, L., Preliminary Design Studies To Evaluate the Utilization of SEU in Atucha-2 Fuel Rods, Pressurized Heavy Water Reactor Fuel: Integrity, Performance and Advanced Concepts, IAEA-TECDOC-CD-1751 (2014) 269-282.

[8] ALVAREZ, L., CASARIO, J.A., MORENO, C., Status Report about Candu Type Fuel Activities in Argentina, Eighth International Conference on CANDU Fuel, Honey Harbour (2003).

[9] ALVAREZ, L., BUSSOLINI, A., TRIPODI, P., Revisiting the experience with advanced fuels in the argentine heavy water reactors, Pressurized Heavy Water Reactor Fuel: Integrity, Performance and Advanced Concepts, IAEA-TECDOC-CD-1751 (2014) 215-224.

[10] LEMOS, L. S., VALESI, J. A., Zircaloy-4 spacer grids for CNA-2 Fuel Element, PHWR Fuel Design, Fabrication and Performance, IAEA TM, Buenos Aires (2009) http://www.iaea.org./OurWork/ST/NE/NESeries/Working Materials/PHWR-fuel-WM-pdf.

[11] CASTAÑIZA, S., ALVAREZ, L, Simulation of CNA-2 Fuel Rod Behaviour under Normal Operation, PHWR Fuel Design, Fabrication and Performance, IAEA TM, Buenos Aires (2009) www.iaea.org./OurWork/ST/NE/NESeries/WorkingMaterials/PHWR-fuel-WM-pdf.

CORE MANAGEMENT IMPROVEMENTS AT ANGRA UNIT 1 USING AN ADVANCED 16X16 WESTINGHOUSE TYPE PWR FUEL ASSEMBLY

L.F. PANETO
Indústrias Nucleares do Brasil S.A. – INB
Rodovia Presidente Dutra, Km 330 –
Engenheiro Passos.
Resende – R.J. Brasil
Fax: +552433218678
Email: lélia@inb.gov.br

Abstract.
Industrias Nucleares do Brasil (INB) and Westinghouse Electric Company (WEC) are jointly designing an advanced 16x16 Westinghouse type Pressurized Water Reactor (PWR) fuel assembly. This advanced 16x16 (called 16x16 Next Generation Fuel or 16NGF), which will be implemented in Angra Unit 1 (in Brazil) is an integral part of the utilities fuel management strategy. The major reason for initiating this joint development program is to update the current 16STD. The current 16STD-fuel assembly contains an non-optimized fuel rod diameter for the fuel rod pitch, parasitic neutron absorption in assembly components (i.e. Inconel Mid grids), no Intermediate Flow Mixer (IFM) grids, and other dated mechanical features.
The advanced 16NGF fuel assembly is being designed for peak rod average burnups of up to 75 GWd/MTU and will use an optimized fuel rod diameter, low parasitic neutron components (i.e. ZIRLO™ Mid grids), ZIRLO™. The 16NGF, the Fuel Rod Diameter Optimization study analyzed a reduction in fuel rod diameter, keeping the same rod pitch for geometrical compatibility reasons. The optimized fuel rod diameter must satisfy the reactor safety requirements. The trend of the nuclear industry is to extend the cycle length and increase enrichment by using advanced fuel designs. It must be emphasized that this design change gives rise to economical advantages, for example, reduced costs for uranium utilization and enrichment with a net gain in reactivity.
The design objective of 16NGF regarding the FROD is to select the diameter that gives the highest reactivity. As a consequence the rod diameter selected would meet the lowest fuel assembly cost. In conclusion, due to the customer's requirement for longer cycles and the upper limit that exists in the enrichment to be used in Angra 1, as well as Westinghouse previous experience, it was proposed as optimized FROD the 0.360 inches.

1. INTRODUCTION

Industrias Nucleares do Brasil (INB), KEPCO Nuclear Fuel Company, Ltd. (KNFC), and Westinghouse Electric Company (Westinghouse) are jointly designing an advanced 16x16 Westinghouse type Pressurized Water Reactor (PWR) fuel assembly. This advanced 16x16 Westinghouse type PWR fuel assemblies, which will be implemented in Angra Unit 1 (in Brazil), is an integral part of the utilities fuel management strategy. The project incorporates Westinghouse improvements in the fuel design for better fuel performance under economic and safety standpoint. The use of more advanced materials and the changes allowing more thermal margin will allow higher burnups and longer cycles of operation. In this paper we will describe the front-end nuclear fuel management activities utilized by the joint development team and describe how these activities played an integral part in defining the direction of the fuel assembly design.

2. OBJECTIVES

The major reason for initiating this joint development program is to update the current 16x16-fuel assembly, which is also called 16x16 Standard or 16STD. The current 16STD-fuel assembly contains a non-optimized fuel rod diameter for the fuel rod pitch, parasitic neutron absorption in assembly components (i.e. Inconel Mid grids), no Intermediate Flow Mixer (IFM) grids, and other dated mechanical features. The advanced 16x16 fuel assembly (called

16x16 Next Generation Fuel or 16NGF [1]) is being designed for peak rod average burnups of up to 75 GWd/MTU and will find the diameter of fuel rod that allows to achieve a better technical performance (neutronic) resulting in economic gains in the fuel cycle, low parasitic neutron components (i.e. ZIRLO™ Mid grids), ZIRLO™ Intermediate Flow Mixer (IFM) grids to improve Departure from Nucleate Boiling (DNB) margin, and many other mechanical features that improve design margins.

3. OPTIMIZED FUEL ROD DIAMETER

The 16STD design for Angra-1, Kori 2 and Krsko is not an optimized design with respect to neutronic and burnup considerations. This results in a conservative Hydrogen/Uranium (H/U) ratio that gives rise to a harder neutron spectrum that reduces its reactivity. For 16NGF, the Fuel Rod Diameter Optimization study analyzed a reduction in fuel rod diameter, keeping the same rod pitch for geometrical compatibility reasons. By increasing the H/U ratio it is possible to obtain a net gain in reactivity due to higher moderation, i.e., a stronger neutron thermalization. The optimized fuel rod diameter must satisfy the reactor safety requirements. The trend of the nuclear industry is to extend the cycle length and increase enrichment by using advanced fuel designs. It must be emphasized that this design change gives rise to economical advantages, for example, reduced costs for uranium utilization and enrichment with a net gain in reactivity.

The reference Fuel Rod Outside Diameter (FROD) for the 16STD-fuel assembly by Westinghouse is 0.374 inches. To determine the optimized FROD for the 16NGF, it was proposed to make a systematic perturbation on the values of the FROD. The lower most reload cost for the same cycle length was the goal for the FROD, which complies with the economic optimization requirements. The following fuel rod diameters were selected for evaluation: 0.335, 0.345, 0.350, 0.356, 0.360, 0.364 inches and the current product FROD, 0.374 inches as the reference case.

The study was performed using the following assumptions to determine the geometric and design parameters used in the models:

- Fixed Equilibrium Loading Pattern based on current plant fuel management;
- Fixed energy output (Effective Full Power Days or EFPD);
- Fixed number of feed assemblies;
- Pellet diameter determined by a constant pellet/gap volume;
- Fixed axial blanket length and enrichment;
- Fixed core operating conditions;
- Fixed burnable absorber content.

Two parallel studies were conducted: one for Kori-2 with 48 Feed Assemblies (FA) and 430 EFPD (16 month fuel management scheme), and another for Angra-1 with 40 Feed Assemblies and 340 EFPD (annual cycle fuel management scheme).

Self-generating core models with equilibrium cycles for 340 and 430 EFPD and reload batches of 40 and 48 FA, respectively, were calculated in order to obtain the reload cost of each case. For each of the cases the following items that determine the relative reload fuel cost were recorded:

- Fuel Rod OD (FROD);

- Mid zone enrichment U^{235} w/o (adjusted to constant EOC 10ppm);
- Total core U-loading (KgU).

Using a fixed cost economic model the total reload fuel cost will be driven by Total U-loading (decreases with decreasing pellet OD), and U^{235} enrichment costs (increases with decreasing pellet resulting from the increased mid-zone enrichment to maintain fixed energy output). Other associated costs with the fuel assembly manufacture were fixed.

In order to check that the integrity of the Loading Pattern (LP) is maintained for the perturbation the following core parameters were checked for each case:

- Reactor Coolant System (RCS) boron, Hot Zero Power (HZP) All Rods Out (ARO) Beginning Of Cycle (BOC) (ppm);
- RCS boron, Hot Full Power (HFP) ARO BOC Equilibrium Xenon (ppm);
- Maximum fuel rod F-delta-H;
- Moderator Temperature Coefficient (MTC), HZP BOC ARO (pcm/degF).

Based on these it was determined that re-optimization of the LP for each case would only minimally impact the rod optimization conclusions. The biggest impact being the most positive MTC for the 48 FA case, which would require additional burnable absorbers for the 0.335 inches FROD case.

The results of the economic results of the fuel rod diameter optimization study are presented in Table 1.

TABLE 1. RESULTS OF RELOADS COST FOR EACH FUEL ROD OUTSIDE DIAMETER

Fuel Rod Diameter	**Relative Reload Cost**	
	48 FA – 430.7 EFPD	**40 FA– 340 EFPD**
0.374 inches	1.000 (reference)	1.000 (reference)
0.364 inches	0.969	0.969
0.360 inches	0.961	0.959
0.356 inches	0.955	0.953
0.350 inches	0.950	0.947
0.345 inches	0.951	0.947
0.335 inches	0.958	0.956

Figures 1 and 2 summarize the economic approach for 430 and 340 EFPD and reloads batch of 48 and 40 FA, respectively.

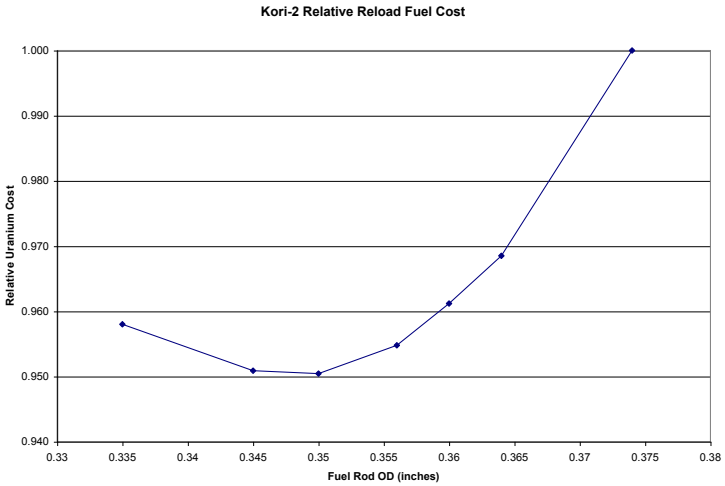

FIG. 1. Relative reload uranium cost for 430 EFPD and reload batch of 48 FAs.

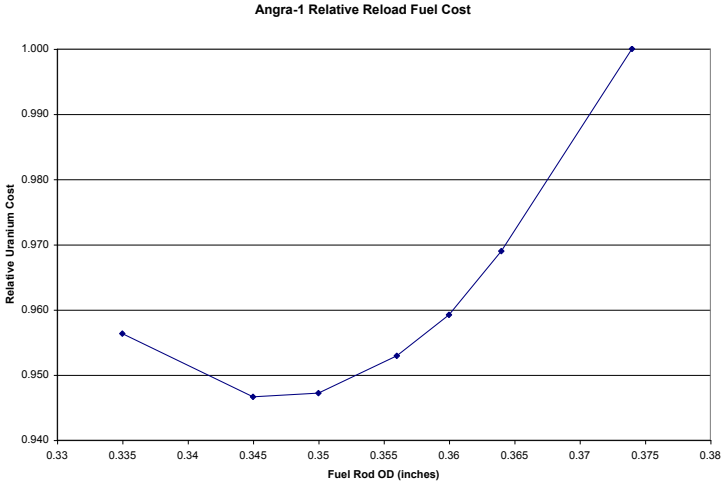

FIG. 2. Relative reload uranium cost for 340 EFPD and reload batch of 40 FAs.

Two analyses were initially carried out in order to select the optimum FROD. In the first one, as mentioned above, the cost optimizations as well as the nuclear reactivity were considered. In that scenario the 0.350 inches FROD seems to be the optimized one.

In addition, the analysis also considered the fuel cycle management point of view. In this analysis, FROD less than 0.360 inches was shown to be undesirable for a cycle length longer than 18 month due the U^{235} w/o enrichment approaches the upper bound licensing limit.

Figure 3 summarizes the fuel cycle management approach for Numbers of Feed Assemblies versus EFPD for reloads batches of 40, 44, 48, and 52 FAs. All the cases considered 5.0 w/o U^{235} enrichment.

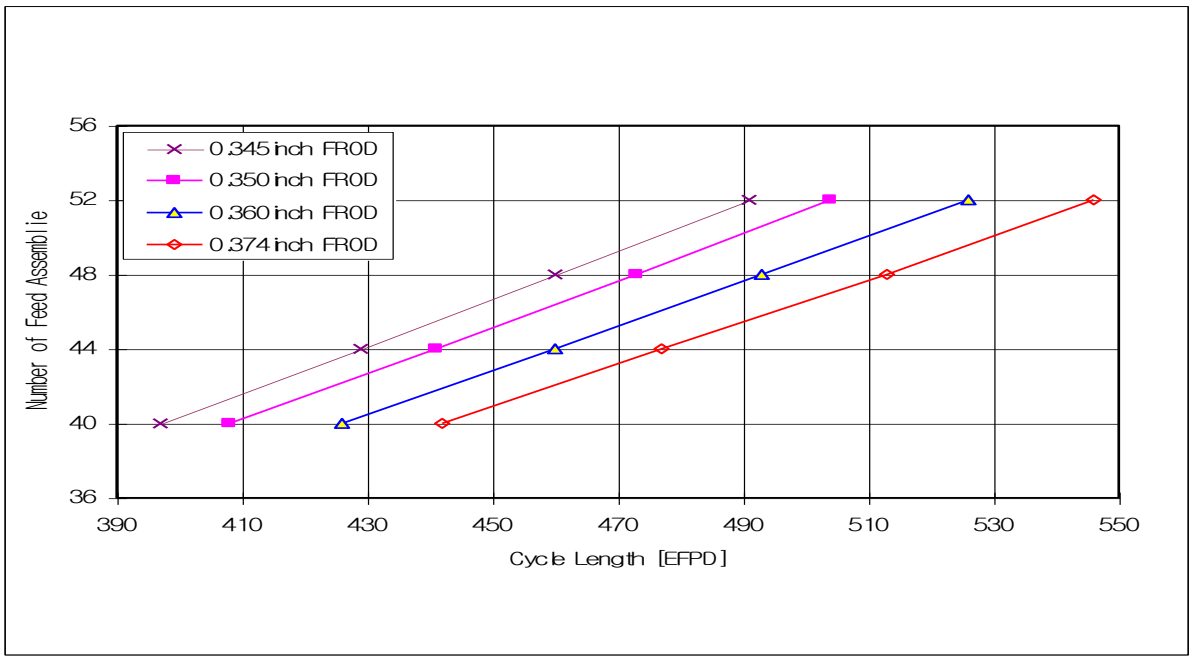

FIG. 3. Fuel cycle management approach for numbers of feed assemblies versus EFPD for reloads batches of 40, 44, 48, and 52 FAs.

3.1. Fuel rod optimization - Results and Conclusions

The design objective of 16NGF regarding the FROD is to select the diameter that gives the highest reactivity. As a consequence the rod diameter selected would meet the lowest fuel assembly cost.

In conclusion, due to the customer's requirement for longer cycles and the upper limit that exists in the enrichment to be used in Kori 2, Angra 1 and Krsko, as well as Westinghouse previous experience, it was proposed as optimized FROD the 0.360 inches.

Based on the past 10 years experience with FROD 0.360 inches used in 17x17 Westinghouse optimized PWR type designs, the 16NGF FROD should not be lower than 0.360 inches.

Furthermore, with this extensive experience of Westinghouse in the use of this FROD in similar reactors, it will be possible to take advantage of similar results from the safety analysis carried out by Westinghouse for this fuel rod diameter in other reactors. Therefore, since 0.360 very close to the optimized diameter, this one was selected as the optimized one for use in Kori 2, Angra 1, and Krsko. Additional consideration would be the increased DNB penalty for a rod thinner than 0.374 inches as described in section 5.

4. HIGH BURNUP CAPABILITY

A higher discharge burnup means better uranium utilization, reducing the uranium requirements and the amount of fuel assemblies disposed during the utility life. The peak rod burnup up to 75 GWd/MTU and region burnup up to 55 GWd/MTU are the targets for 16NGF project. In this new design, many features are implemented to reach this goal.

An important feature is the use of ZIRLO^{TM} cladding tubes for the fuel. This alloy has much higher corrosion resistance than Zircaloy 4 that is currently being used, besides that is less

sensitive to the hydrogen embrittlement. All the mechanical components are designed taking in account the higher fluence that will be achieved. In addition, the fuel rods have to accommodate more gaseous fission products that are released to the plenum.

5. IMPROVED THERMAL MARGIN

In support of obtaining the maximum thermal margin with the 16NGF fuel assembly design, the following information shows the reasons for choosing the 16NGF Mid and IFM grid vane patterns, the 16NGF Mid and IFM grid vane shapes, and the number of IFM's to be added.

Consideration was given for the Mid / IFM grid vane patterns to minimize both fuel assembly and fuel rod vibration. Also consideration was given for the Mid / IFM grid vane features for improved flow blockage area and resultant improved DNB margin.

One of the goals of the 16NGF program is to increase DNB performance by 20% over 16STD (10% in power). Adding IFM's improves DNB performance by approximately 20% due to the increase in turbulence and mixing. Conversely, reducing the rod diameter penalizes DNB performance since there is less heat transfer surface area available for the same power. For example, a reduction from 0.374 to 0.360 inches decreases DNB performance by about 7.8%. Therefore, the net DNB benefit in this example would be 20-7.8 = 12.2%. To meet the program objective of 20% DNB margin benefit, DNB effects of mid-grid design changes (improved vane design) need to be considered to increase DNB performance. Therefore, the effect of the grid design on DNB margin should also be taken into account. This effect is called 'grid benefit'.

The design of the 16NGF mid-grid is employing the latest Westinghouse DNB-improvement technology and lessons learned from the previous Robust Fuel Assembly (RFA) development efforts. Based on experience the RFA grid benefit ranged from 8 to 10%. In the case of the 16NGF design, this 8-10% grid benefit should offset the 7.8% rod diameter penalty for reducing the fuel rod diameter.

Therefore, the preliminary best estimate of the DNB performance improvement for 16NGF is approximately 20-22%. These estimates are based on Westinghouse experience with 17x17 DNB data, as there is currently no 16x16 DNB data available. Taking this uncertainty into account, it can be concluded that a DNB margin gain of at least 20% is likely achievable through:

a. The addition of IFM's.
b. Appropriate mid-grid design modifications based on Westinghouse experience.

6. LOW PARASITIC NEUTRON ABSORPTION USING ZIRLOTM MID GRIDS

The 16NGF design uses ZIRLO^{TM} instead of Inconel in the grids in the active length of the fuel (Mid Grids and IFM Grids). This is to take advantage of the lower neutron absorption in the ZIRLO^{TM} material, leading to a reduction in the fuel cycle cost.

Two core models were evaluated to quantify the benefit of using ZIRLO^{TM}. One used Mid Grids made of ZIRLO^{TM} and the other Inconel. Both cases considered full core with 16NGF at equilibrium cycle and cycle length fixed in 444 EFPD. The result showed an economy of 1.6% using ZIRLO^{TM} (see Table 2).

TABLE 2. FUEL CYCLE COST FOR CORE MODELS USING INCONEL AND ZIRLO™ MID GRIDS

Core Models (Case)	*Mid Grid Material*	**Mid-zone FA U_{235} Enrichment (w/o)**	*Relative Fuel Cycle Cost*
1	Inconel	4.664	1.000
2	ZIRLO™	4.600	0.984

Table 3 gives a brief description about grids in the 16NGF and 16STD.

TABLE 3. 16NGF AND 16STD GRIDS TYPES

Grid Type	**16NGF**		**16STD**	
	Quantity	**Material**	**Quantity**	**Material**
Top Grid	1	Inconel	1	Inconel
Mid Grid	6	ZIRLO™	6	Inconel
IFM Grid	3	ZIRLO™	-	-
Bottom Grid	1	Inconel	1	Inconel
Protective Grid	1	Inconel	-	-

7. BURNABLE ABSORBER FLEXIBILITY

Burnable absorbers are neutron-absorbing materials used to compensate the excess of reactivity in the beginning of cycle and to control power peaking. To comply with the technical specification limit for MTC, the use of BA allows the reduction in soluble boron concentration needed to provide enough reactivity hold down during cycle length.

Two BA types, (described below) gadolinia, and IFBA were given the primary focus in 16NGF program. A third BA type of Wet Annular Burnable Absorber (WABA) was also considered. The WABA consists of absorber rods placed in the fuel assembly guide thimble tubes and is therefore, limited to the number of guide thimble tubes in the assembly (20 in the case of the 16X16 lattice). These different BA types were implemented and verified in the bounding core models generated for 16NGF designing purpose. The core design models are based on the equilibrium cycle considering the design goals of 16NGF such as rod peaking factor limit, peak rod burnup, and least negative MTC limit. The results showed that they are satisfied above the design goals. The increase in thermal margin and the use of these burnable absorbers allow more flexibility to get a more optimized loading pattern that uses low leakage strategy. Core models with IFBA and gadolinium rods showed that it is possible to implement strategies for 12 or 18 months cycle length and with normal or 6.3% uprate in power. In case of WABA, discrete burnable absorber, the results showed difficulty for long cycle above 16 months to control the of the boron concentration at BOL. More optimized loading patterns would be required. The WABA design is not currently being considered but was used primarily in the fuel rod diameter optimization study since this BA type is not associated with the fuel.

The specifications of BAs such as poison enrichment, axial length and radial configurations in an assembly used the typical values that were applied in current fuel design and based on previous experience in other reactors. However, to maximize the merit of 16NGF, a burnable absorber optimization study determining the optimum BA specifications will be performed before 16NGF region implementation.

IFBA fuel rod contains lower poison than WABA and Gad fuel rods; thus more IFBA rods are required to accomplish the same reactivity holddown as a given number of WABA or Gad rods. As a result, the fuel manufacturing facilities without IFBA capability will have more cost impacting with this BA type.

The primary BA for consideration by INB and KNFC is Gadolinium with IFBA being utilized by the Westinghouse design for Krsko. The next two sections give more detail about these BA types.

7.1. Gadolinium rod

Gadolinium Burnable Absorber (Gad) consist of fuel rods with mixed Gd_2O_3 and UO_2 that are placed in some fuel rod positions in the fuel assembly. Different quantities and pattern configurations are possible for the Gadolinium rods, providing flexibility on loading pattern optimization. The Gadolinium rods have a partial stack length (120 in) in the center of the rod with UO_2+Gd_2O_3 pellets. The top and bottom of the rod have standard UO_2 pellets or axial blankets.

The U^{235} enrichment in Gadolinium region has to be lower than non-Gadolinium rods due the degradation in thermal conductivity. The bounding core models, with 5.0 w/o enrichment in U^{235}, were generated based in this assumption, resulting in 3.5 w/o U^{235} enrichment in the Gadolinium region. The 6 w/o enrichment in Gadolinium was assumed.

7.2. IFBA

The Westinghouse Integral Fuel Burnable Absorber (IFBA) design consists of a thin ZrB_2 on the outer surface of the fuel pellet. The fuel rods containing IFBA pellets are assembled with UO_2 fuel rods in diversified patterns. The 16NGF adopts the same IFBA patterns as 16STD, these patterns are standardized and provide options from 20 to 148 IFBA rods in a fuel assembly.

The IFBA pellets are placed in the central axial stack region of the fuel rod optimized for axial shape and FQ control, the bottom and top axial regions in the rod are filled with UO_2 pellet or axial blanket pellets. IFBA pellets have the same U^{235}enrichment as non-IFBA rods. The loading of the absorber material B^{10} is determined based on reactivity holddown considerations. The use of Annular Axial Blanket is required in IFBA rods to comply with the rod internal pressure limits. Krsko plant has been successfully using IFBA in several reloads with 16STD.

8. AXIAL BLANKET

The axial blanket (low enrichment pellets at the top and bottom of the fuel stack) is a new feature for the 16NGF. The Kori unit 2 and Angra unit 1 currently do not use Axial Blanket as a design characteristic. Krsko plant has been using this feature for their 16STD fuel.

The main purpose of the axial blanket optimization study is to determine which axial blanket enrichment and length would provide the better fuel cycle cost-benefit.

Since Angra 1 as well as Kori 2 intend to use gadolinia as burnable absorber of choice, the study has focused on this BA. Also, it considered only solid fuel axial blanket pellets.

In order to evaluate only the axial blanket influence the cycle length and loading pattern for each cycle to be analyzed was fixed. The batch size was set as 48 FA in the reload. For each axial blanket length and enrichment the mid-zone FA enrichment that meets the above fixed

requirements was calculated. The average discharge burnup for this study is 45,955 MWd/MTU and the highest assembly and peak rod burnup were found very similar for all of the cases, approximately 55,600 MWd/MTU and 61,150 MWd/MTU respectively.

For each of the cases studied the following parameters were recorded to evaluate the cost-benefit:

- Axial blanket pellet enrichment (U^{235} w/o);
- Mid-zone enrichment (U^{235} w/o);
- Maximum peaking factor FQ;
- Axial blanket length (top and bottom).

In order to evaluate the economic impact on the fuel cycle cost, the reload costs for each case was simulated. The fuel cycle cost-benefit is relative to the base model and the fabrication costs were not considered. The market price values used in this study are the same as in section 3.

8.1. Axial blanket cost-benefit

The results indicate 1.8 w/o enrichment and 8 inches length (on each extremity of the rod) as the best option from the fuel cycle cost-benefit standpoint relative to no blanket (reference) as shown in the Figure 4. The fuel cycle cost-benefit determined to be on the order of 1.8%.

The difference in the reload cost in the range between 1.5 and 2.6 w/o enrichment and also for the 6 and 8 inches length is not significant. From the Local Peaking Factor (F_Q) limit standpoint (decreases with higher blanket enrichment) and also for longer cycle length requirements (increases with shorter length and higher blanket enrichment), the higher axial blanket enrichment (2.6 w/o) is recommended with the 6-inch blanket case.

The decision for the best axial blanket strategy will be determined following the reload transition safety analysis for 16NGF region implementation.

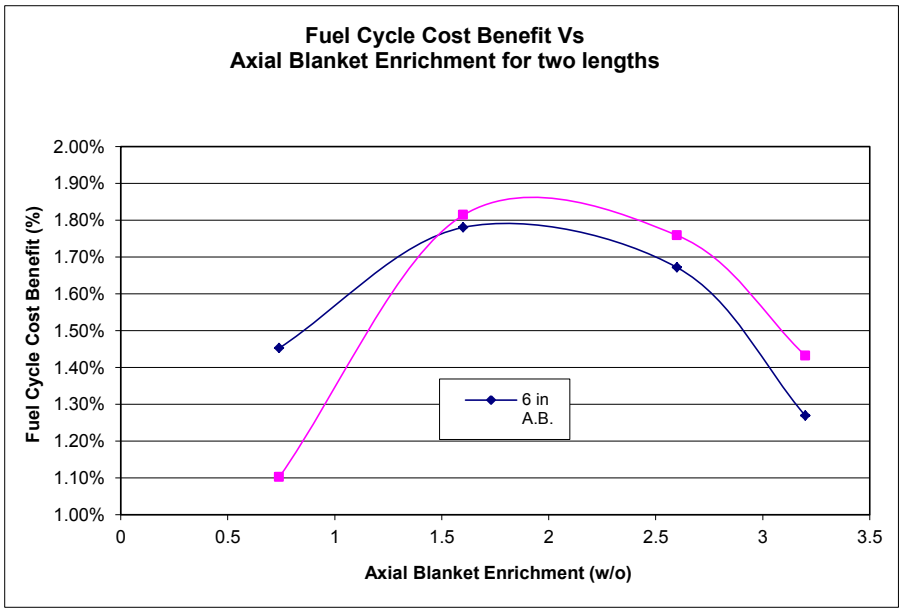

FIG. 4. Fuel cycle cost-benefit vs. axial blanket enrichment for two lengths.

9. SUMMARY AND CONCLUSIONS

During the recent years Westinghouse has improved the fuel design aiming at incorporating the recent design improvements that will assure a better fuel performance under economic and safety standpoint. Industrias Nucleares do Brasil (INB), KEPCO Nuclear Fuel Company, Ltd. (KNFC), and Westinghouse Electric Company (Westinghouse) are jointly designing an advanced 16x16 Westinghouse type PWR fuel assembly. This advanced 16x16 Westinghouse type PWR fuel assembly, which will be implemented in Angra Unit 1 (in Brazil), Kori Unit 2 (Korea, Republic of), and Krsko Unit 1 (Slovenia), is an integral part of the utilities fuel management strategy. The front-end nuclear fuel management activities utilized by the joint development team have been presented to describe how these activities played an integral part in defining the direction of the fuel assembly design.

The 16NGF fuel team proposed to analyze all the design features already implemented and tested in different Westinghouse fuel designs and to implement those most adequate for complying with the customer design requirements. That is not an easy task taking into account that really there are three customers to be satisfied at same time. The major improvements that give direct impact in the fuel costs can be summarized as:

- Fuel rod diameter optimization – really this is a major task already reported in this paper. It contributes within 4 to 5% savings in the overall reload cost. Also, some side benefits can be achieved in the back end costs due to the use of less Uranium for the same cycle length. Savings in the natural uranium consumption has not been analyzed despite of being expected.
- The savings due to the use of ZIRLO^{TM} mid grids when compared with the Inconel mid grids of the 16STD was estimated in 1.6% in the fuel cycle costs. That evaluation took also into account the impact in the enrichment and Uranium reload costs.
- The use of an optimized axial blanket could add to this economic saving evaluation an extra 1.8% in the reload cost when compared with the 16STD without this feature.
- The increase in F-delta-H due to the increase in the overpower margin, expected to be more than 10%, will provide enough flexibility for carrying out more aggressive Loading Pattern which certainly will give rise to a better efficiency in the use of Uranium.

Besides the above, the design improvements aim a flawless fuel, with better performance than the current design and capable to reach burnup up to 75 GWD/MTU.

The figures above on the savings evaluation were carried out based on the current (year 2012) market prices applicable into the United States. Of course some differences would be expected when the same evaluation can be made in each one of the countries that participate in the project.

REFERENCE

[1] 16NGF Final Design Closeout Package, 16NGF-03D-143 Rev.1, Pennsylvania (2004) 375 pp.

LIST OF PARTICIPANTS

Faria, Eduardo
Indústrias Nucleares do Brasil S.A. – INB
Rodovia Presidente Dutra, Km 330 – Engenheiro Passos.
Resende – R.J. Brasil
Fax: +552433218678
Email: faria@inb.gov.br

Sadde, Luciano
Indústrias Nucleares do Brasil S.A. – INB
Rodovia Presidente Dutra, Km 330 – Engenheiro Passos.
Resende – R.J. Brasil
Fax: +552433218678
Email: sadde@inb.gov.br

R&D AND FABRICATION
(SESSION 4)

Chairperson

R. B. Bhatt

FABRICATION OF (UO_2- 0.4% PuO_2) MOX FUEL FOR PHWRS

R.B.BHATT, A.K. MISHRA, ANIRUDDHA KUMAR, AMIT KULSHRESTHA, P.G.BEHERE MD AFZAL, ARUN KUMAR

Advanced fuel fabrication facility,
Bhabha Atomic Research Centre,
Tarapur complex,
India
Email: rbbhatt@barctara.gov.in

Abstract.

Indian Pressurised Heavy Water Reactors (PHWR) have been operated over the years using natural UO_2 bundles. Recently high burn up fuels have drawn the attention. As part of the High burn up fuel experimental irradiation, AFFF (Advanced fuel fabrication facility) has taken up the fabrication of MOX fuel for PHWRs. The MOX fuel pellets containing 0.4 wt % of PuO_2 have been used for this purpose. The PHWR MOX bundles consist of two inner rings of MOX fuel pins and an outer ring of 12 Nat UO_2 fuel pins. This paper describes fabrication and quality and process control of MOX for PHWR along with the design changes made in fuel element. TIG welding has been chosen instead of resistance for end plug joint. Advantages associated with the changes have also been described. Fuel economics have also been presented regarding the burn- up and residence time.

1. INTRODUCTION

Presently, Pressurized Heavy Water Reactors (PHWRs) form the most important part of Indian nuclear power programme. These reactors make use of natural uranium dioxide as fuel. In order to conserve the natural uranium resources, a number of advanced fuel cycle options have been studied. These are (1) use of depleted uranium, (2) use of recycled uranium from light water reactors (LWRs), (3) use of natural uranium – plutonium mixed oxide (MOX) and (4) use of thorium – plutonium MOX [1]. As a part of the work on development of high burnup fuels for PHWRs, MOX fuel bundles have been fabricated in the BARC facilities at Tarapur. This will permit about 40% higher burn up as compared to the burn up achievable in conventional natural uranium dioxide (UO_2) fuel bundles resulting in conservation of natural uranium [2]. Advantages associated with this MOX fuel in PHWR are fuel cost reduction, increase in burn up compared to natural uranium and reduction of the refuelling frequency [4].

The MOX fuel pellets containing 0.4 wt % of PuO_2 have been used for this purpose. The PHWR MOX bundles consist of two inner rings (seven) of MOX fuel pins and an outer ring (twelve) of natural uranium dioxide fuel pins. Technology for Gas Tungsten arc welding (GTAW) of end plugs for PHWR MOX fuel pins has also been developed. The end plugs were specially designed to meet the requirement of GTAW and inspection by X-ray radiograph. The fabrication of uranium dioxide – plutonium dioxide MOX fuel is carried out in gloveboxes because of high radio toxicity of plutonium.

This paper deals with the fabrication procedure of MOX fuel and its quality control. Design changes in process have also been described. Fuel performance is also mentioned.

2. FABRICATION OF MOX FUEL

Process flow sheet for the fabrication of MOX fuel along with quality control steps is shown in Figure 1. Configuration of MOX fuel bundle with MOX and natural uranium dioxide fuel

pins is shown in Figure 2. Figure 3 shows the photograph of a 19 element PHWR MOX bundle.

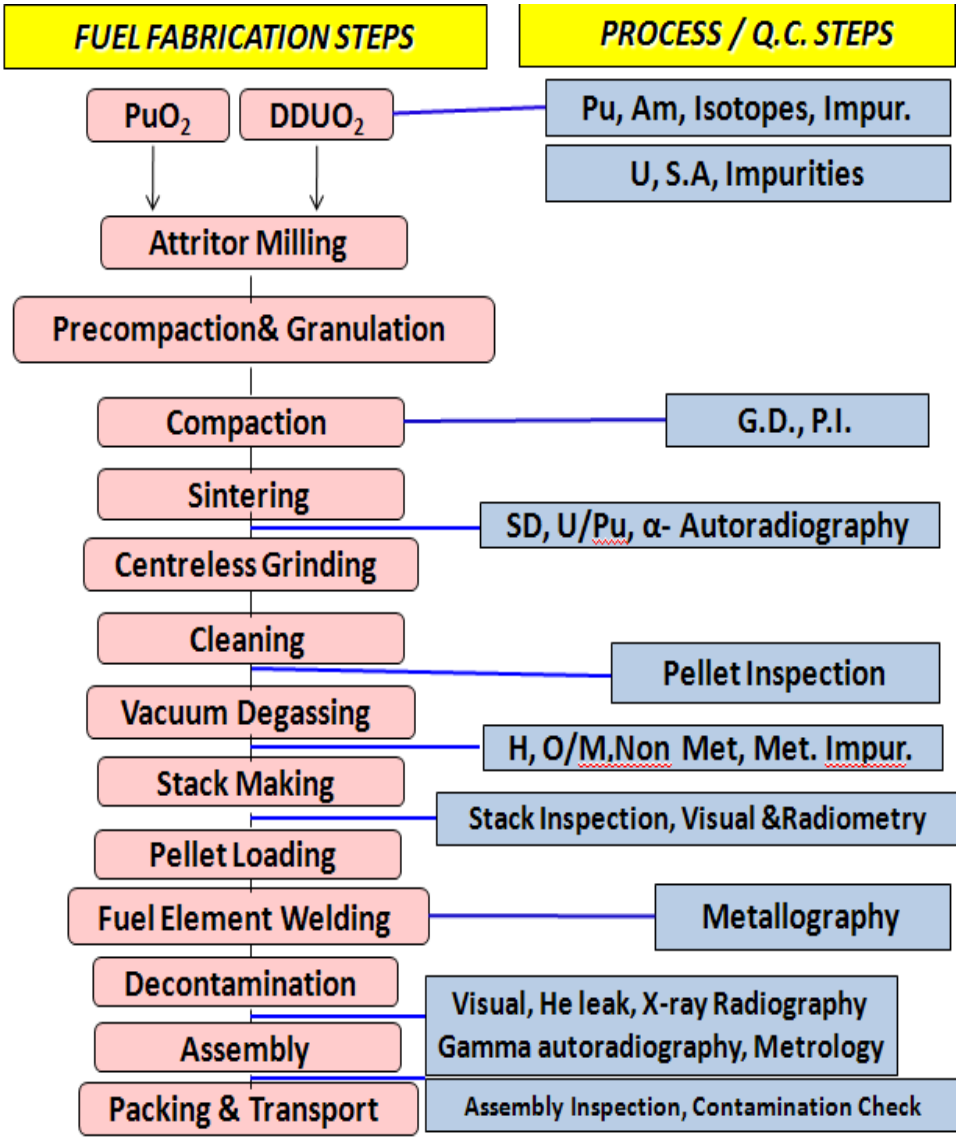

FIG. 1. PHWR MOX process flow sheet.

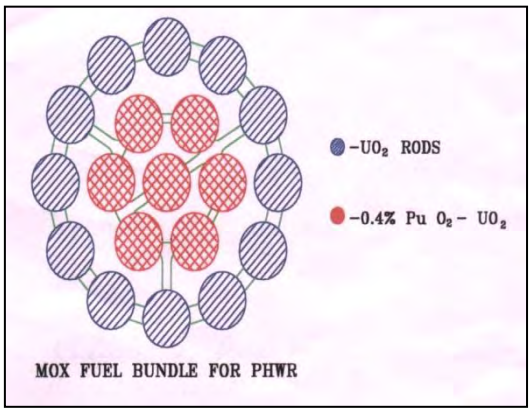

FIG. 2. PHWR fuel element configuration bundle.

FIG. 3. PHWR 19 element fuel bundle.

MOX fuel pellets are produced by conventional powder metallurgy technique. Process starts with the calcination of plutonium dioxide powder for 4 hours. Natural uranium and plutonium are weighed in proportions to make a batch. Mixing & milling is carried out to mix the powders homogeneously and to reduce the particle size. The fabrication specification for the maximum plutonium rich particle size is in the range of 200-400 microns. The analysis shows that the agglomerates can cause spikes in fuel temperatures of about 300-500°C depending upon the size and concentration of plutonium in the agglomerate [3].

Both the powders along with Poly Ethylene Glycol (binder) and Oleic acid (lubricant) are mixed and milled in an attritor. 100 grams of powder sample after mixing and milling is analyzed in Neutron Well Coincidence Counting (NWCC) to confirm the plutonium dioxide percentage. Isotopic composition is required to for determining the plutonium dioxide percentage through NWCC. MOX powder is pre compacted to obtain granules of desired size to improve flowability.

Pre compaction is carried out to get uniform density of the pellet. Pre compacting the MOX powders using Hydraulic/ Mechanical press at 70-110 MPa load. Pre-compacted pellets feed to oscillatory granulator. The crushed compacts pass through a sieve and the out put of granulator is granules with narrow size range from 400-1300 μm.
A double acting hydraulic press is used for the final compaction to achieve desired density. Final compaction is done in double action mode with 250-300 MPa load there by achieving green density 5.6 to 6 g/cm^3. Sufficient green strength is required for handling the pellets to sintering furnace.

Molybdenum charge carriers filled with green fuel pellets are loaded in a resistance heating batch type sintering furnace. Molybdenum is used as a heating element under reducing atmosphere. (W + 25-26%Re) & (W + 3-5%Re) thermocouple is used for the measurement of temperature in reducing atmosphere. Sintering of fuel pellets is carried out at a temperature of 1575 ± 50^{o}C for 4-6hrs in reducing atmosphere [N_2 + 7%H_2]. The oxygen by metal ratio (O/M) should be 1.99 to 2.02. Specification for density of the sintered pellet is 10.55 ± 0.20 g/cm^3.

Density is measured on sample basis. Ceramography is also carried out to find the grain size and structure of the pellet. Specification for grain size is 5 to 50 microns. Micro homogeneity is checked by alpha autoradiography. Uranium and plutonium analysis is carried out on sintered pellets by chemical analysis. Oversize pellets are ground to acceptable size by a centre less grinding machine. The ground pellets are cleaned using an ultrasonic cleaner and are dried at 100 ^{o}C. The pellets are inspected for physical integrity by visual inspection and

the inspected pellets are loaded in one end welded clad tube. Table 1 gives important specifications of the fuel pellets.

Rejected MOX pellets were recycled for making fresh fuel pellets. The Clean Rejected Oxide (CRO) was calcined at 650 to 700°C for 2 hours. Powder made by microwave denitration of CRO was also used for making the pellets.

TABLE 1. SPESIFICATIONS OF PELLETS

Density (g/cm^3)	10.55 ± 0.20
Diameter (mm)	14.29 ± 0.03
Grain size (μm)	5 to 50
Max. allowable size of Pu agglomerate (μm)	< 200
PuO_2 (%)	0.4 ± 0.1
Equivalent Boron Content (EBC) (ppm)	< 1.5
O/M	1.99 to 2.02

3. ENCAPSULATON

Zircaloy–4 clad tube is used in Indian PHWRs. The end plug welding of natural uranium fuel pins for PHWR is carried out using resistance welding technique. For end plug welding of MOX pins GTAW technique is chosen as adapting and operating a resistance welding machine inside the glovebox train is difficult. Further resistance welding produces an outside upset on the weld which is to be machined. GTAW technique doesn't give rise to any upset on the weld. One end of the clad tube is welded outside glovebox (inactive condition) using argon atmosphere. The degassed one end welded clad tubes and end plugs are introduced inside the glovebox for loading of degassed MOX pellets. The MOX pellets are stacked as per specified length and loaded into the one end welded clad tubes. The top end plug welding is carried out in a specially designed GTAW chamber under helium atmosphere. GTAW parameters were optimized and machine and operator qualification was carried out as per the specification. Set up welds and process welds were evaluated at the start and end of the shift respectively. Figure 4 shows the photograph of end plug welding chamber. PHWR MOX fuel pin is shown in Figure 5.

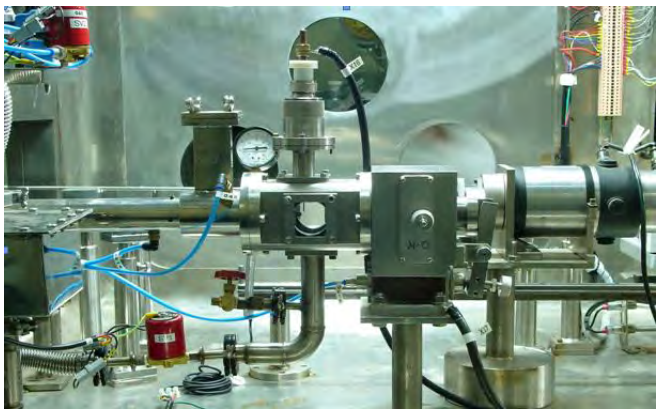

FIG. 4. TIG welding chamber.

FIG. 5. PHWR fuel pin joint with end plug.

End plug design was changed to suit for GTAW technique and the schematic diagram is shown in Figure 6. The changes in the end plug led to a decrease of < 1 % in the stack length compared to the natural uranium dioxide stack. Decontamination of the welding elements is carried out before taking the pins out of glovebox. The fuel pins are then subjected to various quality checks such as helium leak testing, X-ray radiography, gamma auto radiography, metrological inspection, visual examination and passive gamma scanning.

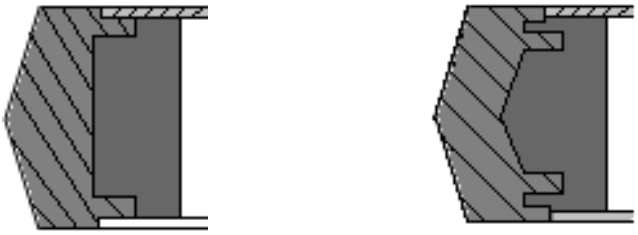

FIG. 6. Joint design for GTAW and Resistance welding.

4. BUNDLE ASSEMBLY

Zircaloy-4 end plates are welded at both ends using resistance welding as shown in Figure 7. Elements are loaded in a jig to maintain inter elemental gap. The central element (one position) and the intermediate ring (six positions) of a 19 element bundle is taken by MOX fuel pins. The 12 natural uranium dioxide pins form the outer ring of a PHWR MOX fuel bundle. Argon is used as a shielding gas during welding.

FIG. 7. Resistance welding of endplate for PHWR bundle.

5. ECONOMICS OF MOX BUNDLE IRRADIATION

Fifty MOX bundles were irradiated in PHWR. Details of the loading pattern are reported elsewhere [5]. Few bundles have seen a peak Burn-up of nearly 20000 MWD/TeU. Highest burnup achieved by a bundle was 20332 MWD/TeU. Residence time for these bundles was nearly three years for central channels. Residence period increased for these MOX bundles. The zircaloy corrosion, hydriding and irradiation embrittlement behaviour for the bundle for the increased residence period was found satisfactory. Forty six bundles for 16 months and

four bundles in one channel for a longer period were irradiated. Average Burn-Up was greater than 10500 MWD/TeU compared 6700 MWD/TeU [6] with natural UO_2 bundle. The Delayed Neutron (DN failed fuel monitoring system) counts of these channels were steady, indicating good fuel performance of these bundles. The iodine activity in the coolant was maintained about 1 micro Ci/l. All discharged bundles were sniffed in spent fuel bay and found non defective.

6. CONCLUSIONS

Experience of fabrication and quality control of MOX fuel for experimental irradiation is presented. Technology for MOX fuel fabrication has developed. Design modifications in pellet fabrication, encapsulation and quality control checks are mentioned. Technique for GTAW for end plug welding inside glovebox has been developed. Economics related to MOX fuel irradiation compared to natural UO_2 bundles is presented. The successful irradiation based on prior design validated the fabrication and quality control procedures developed at AFFF.

REFERENCES

1. KAMATH, H.S., ANATHARAMAN, K., PURUSHOTHAM, D.S.C., MOX Fuel For Indian Nuclear Power Programme, Proc. of the IAEA Symposium held in Vienna, 17-21 May 1999, organized in co-operation with the OECD NEA on MOX Fuel Cycle Technologies for Medium and Long Term Deployment, IAEA, IAEA-CSP-3/P, Vienna (2000) 190-199.
2. PANAKKAL, J.P., AFZAL, M., BHATT, R.B., PRAKASH, A, MISHRA, A.K., KUMAR, S., KAMATH, H.S., Fabrication of U-Pu Mixed Oxide Fuel For Pressurized Heavy Water Reactors, Nuclear Technology, Vol. 179, Aug 2012.
3. P.D KRISHNANI BALTEJ SINGH, UMASANKARI KANNAN, R SRIVENKATESAN, Studies of Advanced Fuel Cycles In Indian PHWRs and AHWR, International Conference on Advances in Nuclear Science and Engineering in Conjunction with LKSTN (2007) 239-244.
4. BHARDWAJ, S.A., KUMAR .A.N., PRASAD P.N., RAVI M., Fuel Performance Design And Development In Indian Reactors, The International Conference on CANDU fuel, 2003.
5. PRASAD, P.N., et al., Design, Development and Operating Experience of Thorium and MOX Bundles in PHWRs, Proc.9th Int. Conf. CANDU Fuel, Ontario, Canada, Sep 18-25, 2005.
6. PARIKH, M.V., et al, Status Report on MOX-7 Bundles Loaded in KAPS-1 Core, May 2005, NPCIL Internal Report.

LOW TEMPERATURE SINTERING OF UO_2 AT REDUCING ATMOSPHERE AND ITS APPLICATION[2]

Y. W. RHEE, I. M. MOON, D. J. KIM, J. S. OH, J. H. KIM, K. S. KIM, J. H. YANG, Y. H. KOO

LWR Fuel Technology Division,
Korea Atomic Energy Research Institute,
Deajeon, Korea, Republic of
Email: youngwoo@kaeri.re.kr

Abstract. We tried to lower the sintering temperature of UO_2 under a commercially used H_2 atmosphere by using sintering additives and/or adapting the sintering schedules, such as two-step sintering. The densification of UO_2 is significantly enhanced by adding a small amount of MnO – of less than 0.2 wt%. MnO-doped UO_2 can be densified up to about 95 % of the theoretical density through sintering at 1250 °C in H_2 atmosphere. The sintering additive, MnO, also enhanced the densification of Boron-bearing UO_2 pellet. Two-step sintering enables us to obtain nano-structured bulk UO_2 pellet with about 300 nm-sized grains, which can be used as an analogue of a high burnup structure (HBS) or RIM structure. HBS-analogue bulk UO_2 pellets may be used to conduct many out-of-pile tests, which can provide valuable data for understanding and modelling the behaviour of HBS or RIM.

1. INTRODUCTION

Extending the fuel discharged burnup could result in reducing the fuel cycle costs and the total mass of spent fuels [1]. There must be a lot of requirements for increasing the LWR fuel burn-up. In this report, we are going to deal with two essential points. One is related with the increase of fuel loading. More fissile materials can be loaded by increasing U^{235} enrichment and/or by mixing UO_2 and high U-density materials such as UN and U_3Si_2. The other is related with providing a bulk UO_2 pellet with nano-sized grain for understanding the properties of high burn-up structure (HBS). This nano-grain-sized UO_2 pellet might be used as HBS-analogue for out of pile experiments.

These approaches to increase fuel loading are seriously being considered in developing an accident tolerant fuel (ATF) as well [2]. The candidates for ATF claddings such as coated zircaloy cladding or layered SiC cladding have disadvantages of using high neutron absorption cross-section materials for coating or the increased cladding wall thickness for SiC cladding. Thus, this shortage of fuel loading should be compensated by increasing the U^{235} enrichment or by adding high U-density materials.

In an aspect of fabricating or transporting nuclear fuels, the criticality should be considered in order to increase the U^{235} enrichment or to add high U-density materials to UO_2. Erbia-bearing super high burn-up (Er-SHB) fuel is presented as a solution of the criticality problem by Japanese researchers.[3] They reported that Er-SHB fuel could prohibit the criticality during fabrication and transportation by adding small amount of erbia to the raw UO_2 powder. Erbia could be replaced to any suitable neutron-absorbing materials such as boron compounds.

Recently, KAERI started to develop a boron-bearing UO_2 pellet in which boron-compound is homogeneously dispersed [4]. A previous study[5] reported that boron-dispersed UO_2 fuel pellet is very difficult to be fabricated with a sufficient level of boron retention and high

[2]This work was supported by the National Research Foundation of Korea (NRF) grant funded by the Korea government (MSIP) (2013000720).

sintered density (greater than 90 % of theoretical density (TD)) because of the volatilization of boron oxide. In order to solve this problem, it is necessary to reconsider the low temperature sintering of UO_2 in a reducing atmosphere.

Conventionally, uranium dioxide nuclear fuel pellets have been fabricated using sintering UO_2 compacts at high temperatures of above 1700 °C in H_2 atmosphere in almost all LWR fuel vendors. High temperature sintering is the most energy intensive and expensive process among unit processes of the nuclear fuel fabrication. Thus far, a number of attempts have been made on lowering the sintering temperature of UO_2 to reduce the fuel fabrication cost. However, these efforts were based on an improved sinterability in hyperstoichiometric UO_{2+x}, which was obtained by mixing U_3O_8 with UO_2 and sintering at inert or slightly oxidative atmosphere, such as Ar, N_2, and CO_2. It is known that a large degree of swelling may result from the entrapped large-molecule-size gases such as CO_2, Ar and N_2 in sintered UO_2 pellets during irradiation in a nuclear reactor.

A low temperature reductive sintering technique has a great significance not only for reducing the fabrication cost, but also for densifying a UO_2-based nuclear fuel with non-sinterable compound such as a boron compound or volatile minor actinide. B-compound dispersed UO_2 pellets may help solve the criticality problem, which is one of the main obstacles to increase fuel loading.

First, this paper deals with preliminary results on the densification behaviour of UO_2 and B-compound dispersed UO_2 during low temperature sintering in H_2 atmosphere. Secondly, a preliminary result on the fabrication of HBS-analogue UO_2 pellet is reported.

2. EXPERIMENTAL PROCEDURE

2.1. Low temperature sintering with sintering additive

Samples were prepared with the ADU-Route UO_2 powder, MnO powder and BN powder. Among various boron compound, BN was selected because of its thermal stability in high temperature. UO_2 powder was mixed with MnO and/or BN powder in a tumbling mixer for 2 h. A powder mixture was granulated with a 30 mesh sieve. The granules were mixed with a 0.3 wt% of zinc stearate in a tumbling mixer for 30 min. The compaction was conducted in a single acting press under about 3 ton/cm^2. The UO_2, UO_2-MnO, UO_2-BN and UO_2-BN-MnO powder compacts were sintered at the temperature range of 1100 to 1400 °C for 1 to 4 h in H_2 atmosphere. The sintered density was measured by a water immersion method. Microstructures were observed using an optical microscope after polishing the cross-section of the sintered pellet up to a 1 μm diamond polish.

2.2. Low temperature sintering with two-step sintering

ADU route UO_2 powder was used for a sample preparation. UO_2 powder was compacted in a single acting press with the die-wall lubrication of zinc stearate. Two-step sintering was conducted at various temperatures for 20 h in H_2 atmosphere. The temperature range of the first step was from 1250 °C to 1500 °C and that of the second step was from 1200 °C to 1400 °C. The sintered density was measured by a water immersion method. Microstructures were observed using a scanning electron microscopy.

3. RESULTS AND DISCUSSION

3.1. Low temperature sintering with sintering additive

Figure 1 shows typical densification curves of UO_2 during sintering in reducing atmosphere and oxidizing atmosphere.[6] It should be noted that the low temperature sintering of UO_2 is possible in oxidizing atmosphere, as shown in Figure 1. In oxidizing atmosphere, such as CO_2, Ar and N_2 gas atmosphere, the densification occurred even at very low temperature because of the enhanced uranium diffusivity induced by excess oxygen defects in

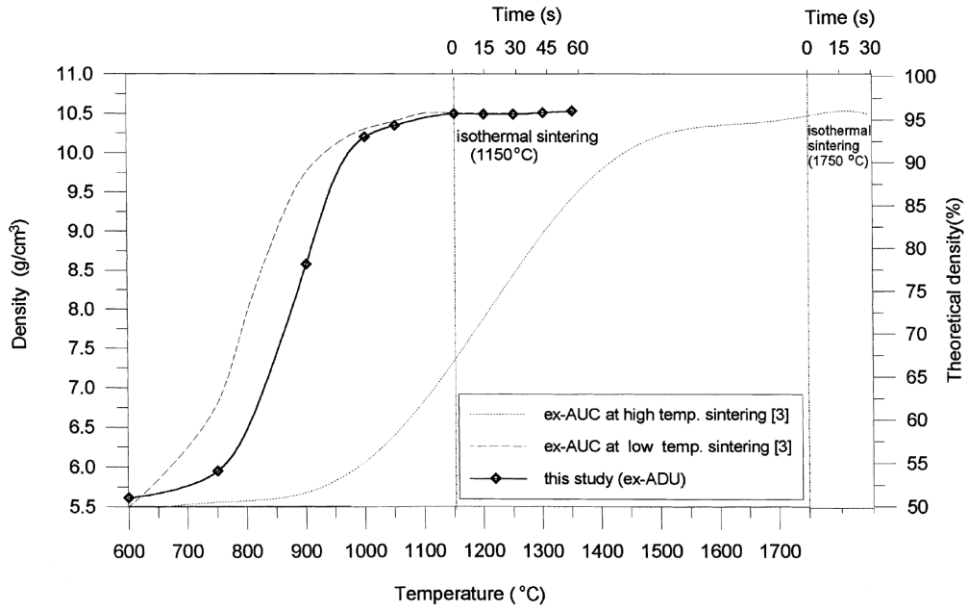

FIG. 1. Typical densification curves of UO_2 during high temperature sintering in reducing atmosphere and low temperature sintering in oxidizing atmosphere [6].

hyperstoichiometric UO_{2+x}. It is known that a large degree of swelling may result from the entrapped large-molecule-size gases in sintered UO_2 pellets during irradiation in a nuclear reactor.

Thus far, almost all LWR fuel vendors fabricate UO_2 fuel pellets through a high temperature sintering process in H_2 atmosphere. In reducing atmosphere, however, the densification occurred very slowly, and the high temperature of over 1600 °C is necessary to densify up to 95 %TD.

Recently, we found that the addition of MnO can accelerate the densification rate of UO_2-Gd_2O_3 compacts during the intermediate sintering stage in H_2 atmosphere.[7] As shown in Fig. 2, the densification of a MnO-added compact occurred faster than those of compacts with other sintering additives.

This enhanced densification kinetics of MnO-added UO_2-based system could be applied to lower the sintering temperature of UO_2 in H_2 atmosphere. Figure 3 shows the measured densities of MnO-added UO_2 pellets sintered at the temperature range of 1100 °C to 1400 °C for 1 h. With increasing the addition of MnO, the sintered densities of UO_2 pellets increased. MnO-added UO_2 pellet can be densified up to about 95 %TD after sintering at 1250 °C for 1 h in H_2 atmosphere.

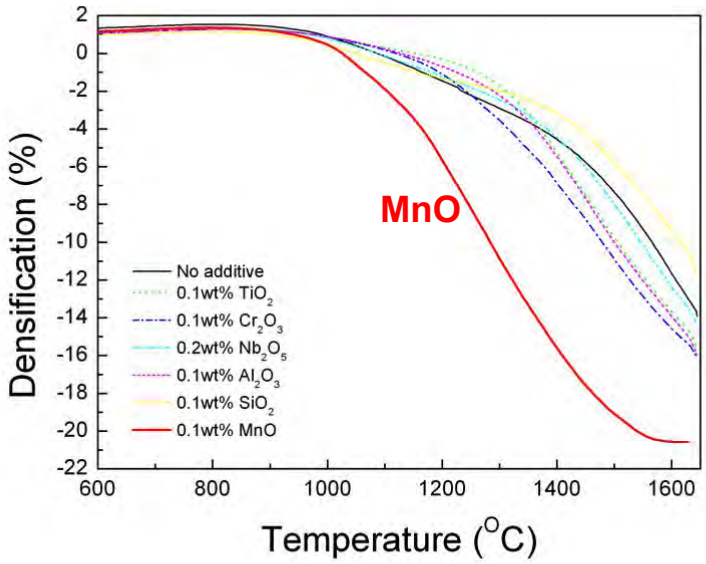

FIG. 2. Densification curves of UO_2-Gd_2O_3 compacts with various sintering additives [7].

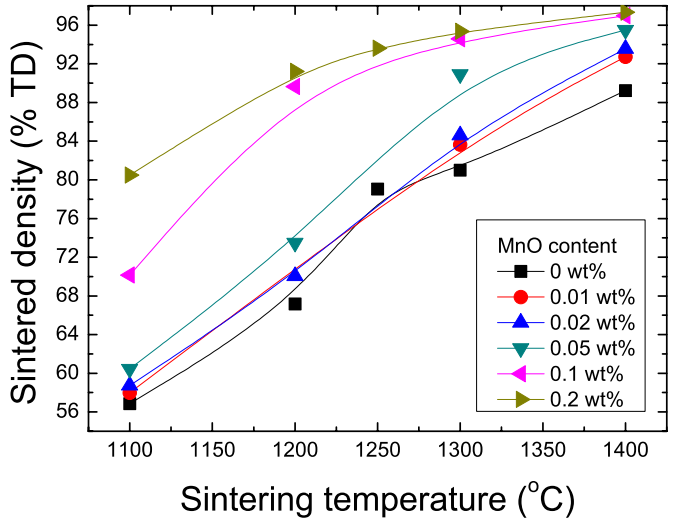

FIG. 3. Measured densities of MnO-added UO_2 pellets sintered at the temperature range of 1100 °C to 1400 °C for 1 h.

A low temperature sintering technique of UO_2 in H_2 atmosphere can be applied to sinter a UO_2 pellet with volatile materials such as boron compound and AmO_2 as well as to reduce the fabrication cost of UO_2 pellet. The sintering of boron-compound dispersed UO_2 was studied in 1960s.[5] They reported that it was difficult to densify a boron-dispersed UO_2 fuel pellet with a sufficient level of boron retention and high sintered density because of the evaporation of boron at high temperature as shown in Fig. 4.

Figure 5 shows the microstructure of B_4C-added UO_2 pellet sintered at 1250 °C. There are large pores in between B_4C and UO_2 matrix and it causes a poor sintered density. These large

pores are attributed to the evaporation of boron and/or the larger size of B_4C powder than that of UO_2 powder.

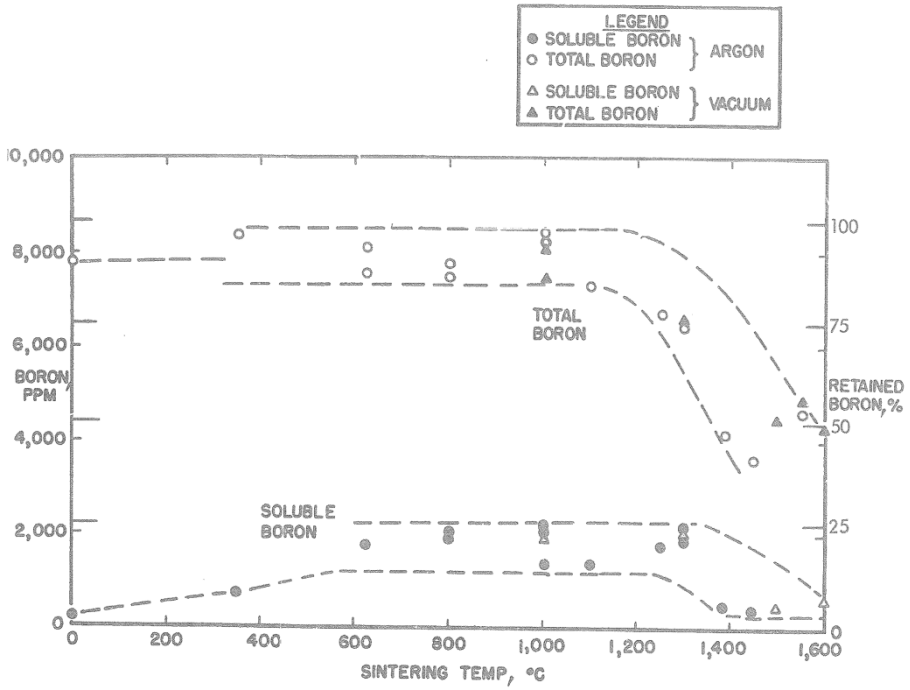

FIG. 4. Boron content in sintered pellet according to the sintering temperature [5].

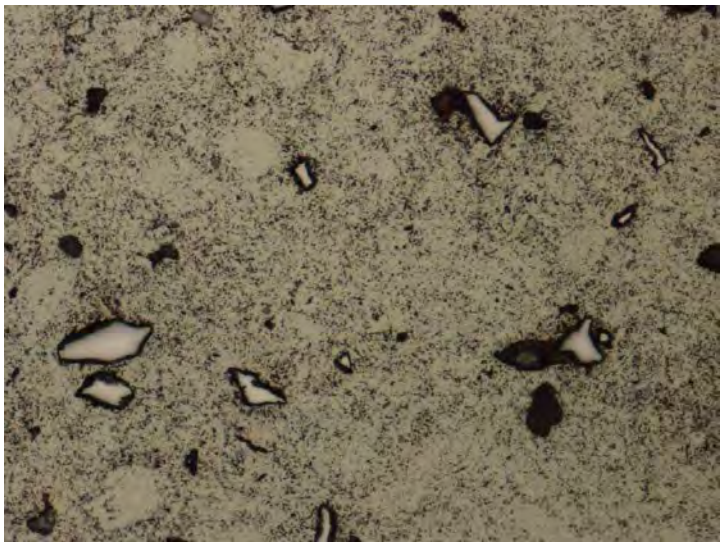

FIG. 5. Microstructure of B_4C-added UO_2 pellet sintered at 1250°C (x200).

Nano-sized BN powder was chosen after the thermochemical calculation and the screening test. BN appears to have better thermal stability than other boron compound. Figure 6 shows the sintered density of boron compound-added UO_2 pellet after sintering at 1100 °C in H_2 atmosphere. The sintered density of the UO_2 – 0.1 wt% BN pellet gradually increased with a sintering time up to about 87 %TD after sintering for 4 h. However, the UO_2 - 0.1 wt% BN –

0.2 wt% MnO pellet has a sintered density of about 94 %TD even after sintering for 1 h, and the sintered density increased up to around 96 %TD after sintering for 4 h.

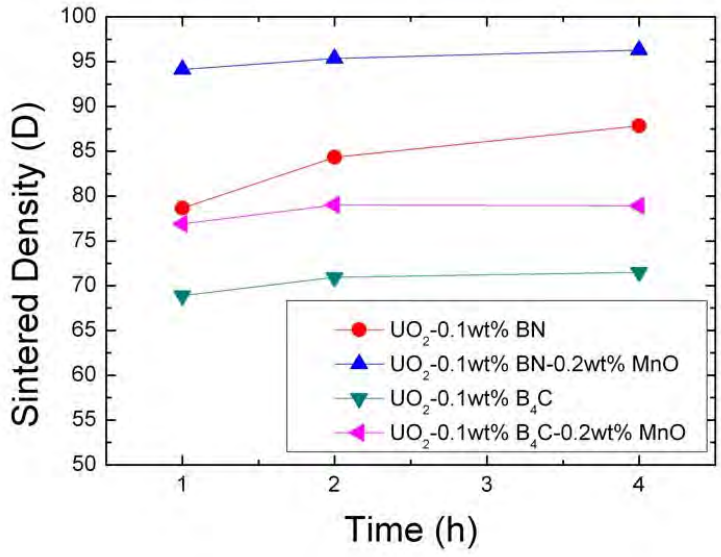

FIG. 6. Sintered density of boron compound-added UO_2 pellet after sintering at 1100 °C in H_2 atmosphere.

Residual boron content of the sintered BN-added UO_2 pellet was measured using PGAA (Prompt Gamma Activation Analysis) at HANARO. Measured residual boron contents of sintered pellets were represented in Figure 7 according to the initial boron contents. It appears that around 80 % of initial boron remains in the sintered pellet.

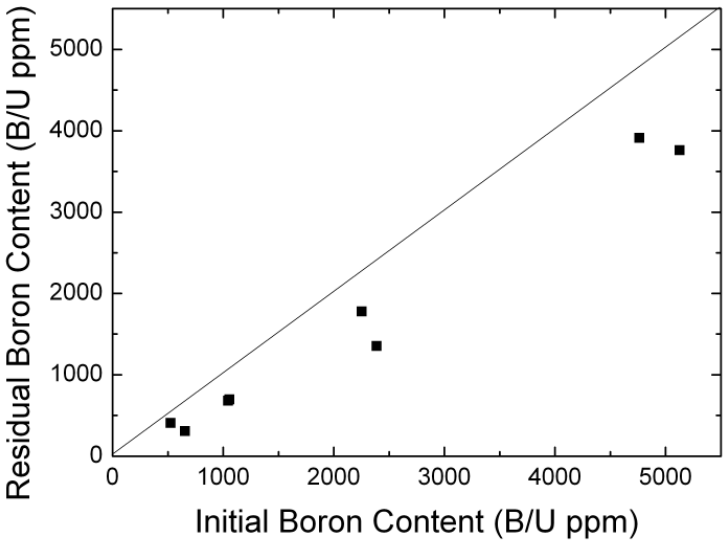

FIG. 7. Sintered density of boron compound-added UO_2 pellet after sintering at 1100 °C in H_2 atmosphere.

3.2. Low temperature sintering with two-step sintering

The microstructure of high burn-up structure is generally characterized by very small grain of about 300 nm in diameter, intergranular pores of 1-2 μm size and high porosity of 6-26 %. Recently, HBS-analogue bulk nano-crystalline oxide fuel was proposed for a new concept of an innovative materials option for increasing fission gas retention, plasticity, and radiation-tolerance [8]. Even though a number of considerations must be taken to prove the postulation and its in-pile properties, HBS-analogue bulk pellets can be used as good samples for various out-of-pile tests to understand the properties of HBS. Spino et al. [8] reported that HBS-analogue bulk nano-crystalline pellet was fabricated by using nano-sized YSZ (yttria stabilized zirconia) powder and PMMA bead as a pore former. They also reported that nano-sized UO_2 powder of 9-36 nm in diameter could be produced by a organic precursor decomposition method [9].

However, nano-sized powder usually has more difficulties to be dealt with in powder metallurgical processing than commercial powders. Thus, we tried to find a way to fabricate HBS-analogue nano-crystalline UO_2 pellet with commercial ADU-UO_2 powder of about 0.1 μm size.

It is well known that the densification and the grain growth simultaneously occur during sintering of ceramics. Figure 8 shows a typical trajectory of grain size and sintered density during sintering of UO_2. Generally, grain growth is significantly accelerated at a final stage of sintering (over 93 %TD). This is the reason why it is not easy to obtain nano-crystalline sintered pellet even if we started with nano-sized powder.

However, Chen et al. [10] suggested that two-step sintering enables us to densify nano-crystalline bulk pellet without final stage grain growth. At certain condition, densification can occur with almost no grain growth and it is called ‘microstructure freezing’.

Red circles in Figure 8 represent the results of two-step sintering of UO_2 pellet. Two-step sintering successfully prohibited grain growth of UO_2 during final stage of sintering. The UO_2 pellet can be densified up to 94 %TD with the grain size of about 300 nm. The microstructures of two-step sintered UO_2 pellets were compared with those of irradiated PWR HBS and previous study [8] in Figure 9. In this stage, it seems that HBS could be simulated by two-step sintered UO_2 in an aspect of grain size. Further efforts to simulate pore and porosity will be continued.

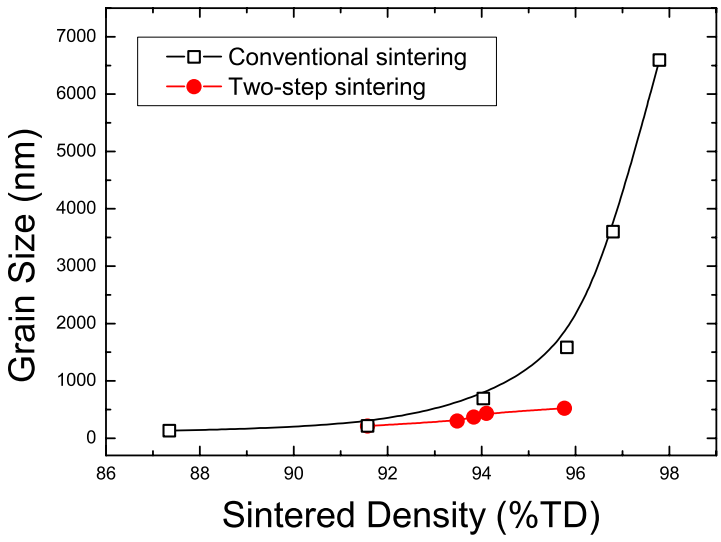

FIG. 8. Trajectories of grain size and sintered density during conventional sintering and two-step sintering of ADU-UO_2.

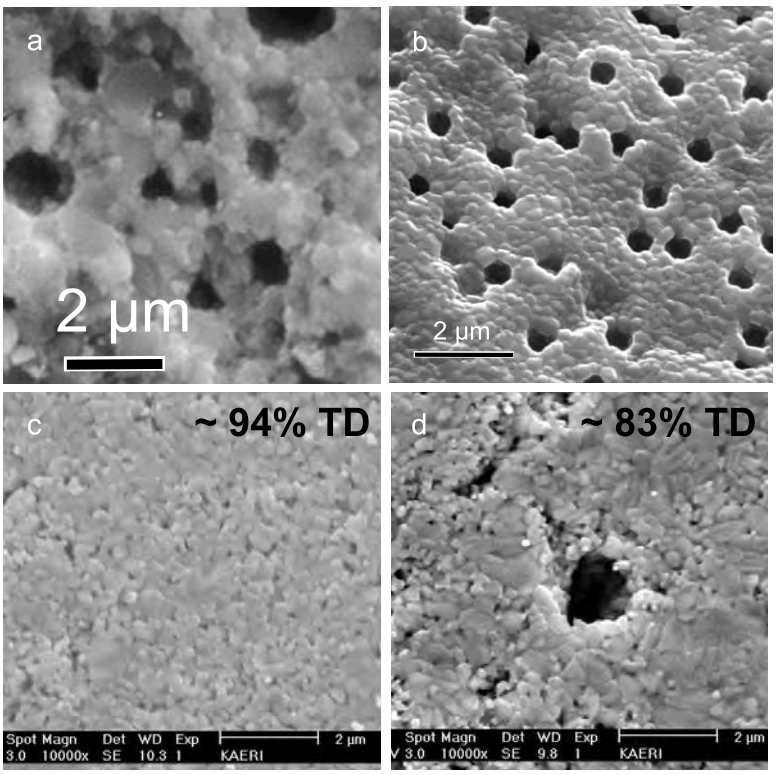

FIG. 9. Microstructures of (a) Typical HBS in irradiated PWR[8], (b) HBS-analogue YSZ pellet [8], (c) Two-step sintered ADU-UO_2 and (d) Two-step sintered ADU-UO_2 with pore former.

4. CONCLUSIONS

Low temperature sintering behaviour of UO_2 is investigated under commercial H_2 atmosphere. MnO-doped UO_2 can be densified up to about 95 %TD at 1250 °C, which is about 500 °C lower than conventional sintering temperature, 1700 °C.

A low temperature sintering technique might be applicable to sinter UO_2-based nuclear fuel with volatile materials, such as Boron compound and minor actinides (AmO_2 ...). By using low temperature sintering technique, BN-added UO_2 pellet can be sintered up to ~ 95%TD at 1100 °C in H_2 atmosphere with the slight evaporation of boron.

Two-step sintering method enables us to densify UO_2 pellet up to ~ 94%TD with very small grain size of about 300–400 nm. Porosity and pore size can be controlled with smaller uniform sized pore former through the further study. High Burn-up Structure might be simulated in an aspect of microstructure such as grain size and porosity by using two-step sintering and adding uniform sized polymer pore former. HBS-analogue UO_2 Pellet might give us good out-of-pile test samples for understanding the fuel properties of RIM (HBS) region.

REFERENCES

[1] Very high burn-ups in light water reactors, OECD/NEA No. 6224, 2006.
[2] Second Meeting on Increased Accident Tolerance of Fuels for LWRs, NEA Headquater, 2013.
[3] YAMASAKI, M., The Study on Erbia Credit Super-High-Burnup Fuel with Isotopically Modified Erbia, in: ANS 2010 Winter meeting, Las Vegas, NV, 2010.

[4] RHEE, Y.W., KIM, D.J., NAM, I.H., KIM, J.H., OH, J.S., YANG, J.H., KIM, K.S., Fabrication of Boron-containing Burnable Absorber Fuel Pellet, in: the Korean Nuclear Society Spring Meeting, Jeju, Korea, Republic of (2012).
[5] ANDREWS, M.G., TAYLOR, W.C., ZUROMSKY, G., Burnable Poison Additions to UO_2, CEND-3107-351, Combustion Eng. INC., Windsor, Connecticut (1969).
[6] AYAZ, B., BILGE, A.N., The possible usage of ex-ADU uranium dioxide fuel pellets with low-temperature sintering, J. Nucl. Mater., **280** (2000) 45-50.
[7] RHEE, Y.W., KIM, K.S., SONG, K.W., Densification Kinetics of MnO-doped UO_2-10 wt%Gd_2O_3 Compact, Thermochimica Acta, **455** (2007) 80-85.
[8] SPINO, J., SANTA CRUZ, H., JOVANI-ABRIL, R., BIRTCHER, R., FERRERO, C., Bulk-nanocrystalline oxide nuclear fuels - An innovative material option for increasing fission gas retention, plasticity and radiation-tolerance, J. Nucl. Mater., **422** (2012) 27-44.
[9] ZVORISTE-WALTERS, C.E., HEATHMAN, S., JOVANI-ABRIL, R., SPINO, J.L., JANSSEN, A., CACIUFFO, R., Crystal size effect on the compressibility of nano-crystalline uranium dioxide, J. Nucl. Mater., **435** (2013) 123-127.
[10] CHEN, I.-W., WANG, X.-H., Sintering dense nanocrystalline ceramics without final-stage grain growth, Nature, **404** (2000) 168-171.

WORK PLAN TO ACHIEVE THE TECHNOLOGY FOR THE INTRODUCTION OF OXYGEN MICRO-ADDITION AND BETA-NIOBIUM SECOND PHASE PARTICLES WITH OPTIMUM SIZE AND DISTRIBUTION IN THE ZIRCONIUM MATRIX OF ZR-1%NB ALLOY

P. A. FERREIRÓS, P.R. ALONSO, G.H. RUBIOLO

Gerencia de Materiales (GAEN-CAC), Comisión Nacional de Energía Atómica (CNEA), Av. Gral. Paz 1499, B1650KNA, San Martín, Buenos Aires, Argentina

Abstract.

If CNEA wants to handle the fuel elements technology for reactors of Generation III (high burn-up and cooling water at higher temperature and pH) must access to the technology of zirconium alloys low in Nb and free of tin. This paper present a roadmap to achieve, as semi-finished product, strips of Zr-1Nb-O alloy of about 27 mm wide and 1 mm thick which must reach the standards for the yield stress and creep resistance of the commercially available French M5™ alloy or Russian E110 alloy.

1. INTRODUCTION

In the paragraph dedicated to the FUTURE within the 2010-2019 CNEA strategic plans [1] is quoted: "In the area of nuclear fuels, we will continue with the development of fuel elements for CNA-II. Furthermore, we are developing new materials and processes for the production of high burn-up fuel elements for reactors of Generation III and IV".

As background of this strategy, CNEA has carried out the ULE (SEU) Project [2] where the original design of CNA-I fuel was changed, natural uranium was replaced by slightly enriched uranium (SEU) (0.85 % of the isotope U^{235}). The extraction burnup was increased from 6500 to 11500 MWd/tU producing a 40% decrease in fuel consumption and a reduction of about 30% in cost. The cladding material was Zircaloy-4 (Zry-4).

If CNEA wants to handle the fuel elements technology for reactors of Generation III (high burnup and cooling water at higher temperature and pH) must access to the technology of zirconium alloys low in Nb and free of tin. Examples of this are French M5 alloy (Zr – Nb-1wt% – 0.135wt% O) or Russian E110 alloy (Zr – 1wt% Nb – 0. 04 to 0.06 wt% O). These alloys currently used in PWR reactors of the United States of America, Europe and Russia have shown a significant decrease in the thickness of the oxide layer and the 'pick-up' of hydrogen compared to Zry-4 for burnt over 20,000 MWd/tU while they hold a creep resistance similar to Zry-4 [3].

The stable microstructure is the result of a low temperature process that produces beta-niobium second phase particles with optimum size and distribution in the zirconium matrix. The absence of tin as an alloying element results in very low corrosion and hydrogen pick-up rates at high burnup and reactor duty conditions [4]. The oxygen concentration is in the range of 0.02-0.05 %at. However, oxygen concentrations up to 0.1 %at are permissible, which provides a way of enhancing the alloy strength.

The main requirements for oxygen-containing alloying are as follows. They shall be free of any foreign matter, and they shall have a high enough melting point (close to that of zirconium), low vapor tension, and low dissociation pressures. The thermodynamic stability of alloying elements shall be significantly lower relative to ZrO_2 so that the entire amount of

oxygen could go into the melt while the alloy is still in a liquid state [5]. Moreover, oxide precipitation during ingot crystallization shall be precluded.

There are two potential mechanisms by which β-Nb may form during heat treatment [6]. The first is by classical nucleation and growth of new β-Nb directly from supersaturated α phase. This occurs when the alloy is rapidly quenched from the single phase β field to form α-martensite, supersaturated in niobium. The second occurs in alloys which are cooled at slow or intermediate rates from the single phase β field. In this case, retained β-Zr is present after cooling along grain boundaries. This phase is metastable, and on heat treatment the free energy of the system can be reduced by transformation to α and β-Nb. However, this process is complex and can involve intermediate steps. Furthermore, the kinetics of the transformation can be extremely slow, taking over 1000 h at 500ºC. The oxygen content affects both mechanisms of precipitation.

In this paper we present a work plan to achieve, as semi-finished product, strips of Zr-1Nb-O alloy of about 27 mm wide and 1 mm thick. Moreover, this product must present second phase particles with β-Niobium optimal size and distribution in the zirconium matrix reaching the standards for the yield stress and creep resistance commercially available.

2. SPECIFIC GOALS

1) Get an ingot (77 cm^3) of the alloy Zr-1wt% Nb-0.12wt% O by melting with consumable electrode arc in a two fusions process.

2) Deploying thermomechanical processes on the cast ingot to obtain strips with a microstructure of particles of β-niobium second phase with optimal size and distribution in the zirconium matrix.

3) Characterization of mechanical properties of the strips. Perform tensile and creep tests according to the ASTM standards [7].

3. ROADMAP

Specific goal 1

The method for manufacturing ingots will follow the procedures described in the U.S. patent 7.704.334 B2 [8] and the European patent EP 1 621 642 A1 [9]. The manufacturing process will be carried out by vacuum arc remelting (VAR). Crushed zirconium sponge will be used as the zirconium-containing material, niobium chips obtained turning a niobium bar of purity 99.99% will be used as the niobium-containing material, finally niobium pentoxide (Nb2O5) is the material used to compensate the composition of niobium and oxygen required. Niobium pentoxide with the melting temperature of 1780 °C, which is lower than the melting temperature of zirconium (1862 °C) is in its liquid state in the process of zirconium melting which ensures a uniform distribution of niobium and oxygen in an ingot.

The alloy will have the following composition by weight:

niobium - 0.81-1.2; oxygen - 0.090-0.180 and zirconium - rest

Impurities iron - 150-600 ppm; silicon - 25-120 ppm and sulfur - 0-35 ppm

Crushed zirconium sponge, niobium chips and niobium pentoxide powder with the required ratio in the alloy will be mixed; the particulate mixture will be pressed to form cylindrical briquettes of 20 mm diameter and 20 mm high. Various briquettes will be welded together with TIG welding to form the electrode for the first melting. The cylindrical ingot from first melting will be cut in quarter and these pieces will be used to assemble, with same welding technique, the electrode for the second melting. The ingot after second melting will be approximately 40 mm diameter and 50 mm high.

Specific goal 2

The ingot after second melting will be machined to get two bars 13x27 mm. Each of these bars will have the following thermomechanical treatments [10]:

a) β-quenched (maintained at 1020 ºC for 0.5 h and quenched into water at room temperature);
b) Hot-rolled (12%) at 580 ºC;
c) Annealed at 580 C for 3 h;
d) Cold rolled (45%) with three intermediate heat treatments at 570ºC for 2 h.

After these thermomechanical treatments we will obtain two strips of approximately 27 mm wide and 1 mm thick. These strips will be finally annealed at 580 ºC for 3 h so as to recrystallize the microstructure.

The oxygen composition of the alloy will be determined by vacuum fusion analysis.

For micro/nano-structural analyses, scanning and transmission electron microscopy (SEM and TEM) specimens will be made from the cold rolled and annealed samples. Both microscopes are equipped with an energy dispersive X-ray spectroscopy (EDS) detector. Also optical microscopy will be used to evaluate grain morphology and size. SEM microscopy will be used to identify and measure composition of second phases with median size while, TEM microscopy will do the same with the nanosized precipitates.

Specific goal 3

Tensile and creep specimens with a gage length of 25 mm and the width of 5 mm will be machined with the stress axis parallel to the rolling direction.

The tensile testing will be performed with a Shimadzu testing machine at room temperature and 300ºC.

The creep tests will be performed in air with a loading beam capable of maintaining a constant stress, within 1% of the initial stress, up total strains of the order of 10%. The elongation of the specimen will be measured by using LVDTs (Linear Variable Differential Transformers) which nucleus are attached to fused silica rods connected to the upper and Iower grips. The creep tests will be performed at 450, 480 and 500 ºC with the applied stress between 80 and 150 MPa.

Strain rate jump tests will be also performed at room temperature and 300 ºC to obtain the activation volume which can provide information about of the dynamic strain ageing caused by dissolved oxygen. The tensile samples will be initially strained at the strain rate of 10^{-4} s^{-1} up to a strain of 2.5% and then the strain rate will be changed to 10^{-2} s^{-1}.

4. CONCLUSIONS

CNEA has enough experience developing Zry-4 alloy, facilities and installations which are crucial for alloy developing are operational then just only need a political decision to start developing zirconium alloys low in Nb and free of tin.

REFERENCES

[1] Plan estratégico CNEA 2010-2019 (2010).

[2] HIGA, M., VILLAR, J., PEREZ, R., PIÑEYRO, J., SERRA, O., BLANCO, A., Power transients simulations in Atucha 1 nuclear power plant for mixed natural and slightly enriched uranium core, Proc. IAEA TM on Implications of Power Uprates on Safety Margins of Nuclear Power Plants-in cooperation with the OECD/NEA held in Vienna, 13-15 October 2003, IAEA-TECDOC-1418, IAEA, Vienna (2004) 19-25.

[3] MARDON, J.P., GARNER, G.L., HOFFMANN, P.B., M5®, a Breakthrough in Zr Alloy, Proc. LWR Fuel Performance Meeting / Top Fuel (2010) pp 577-586.

[4] TOFFOLON-MASCLET, C., GUILBERT, T., BRACHET, J.C., Study of secondary intermetallic phase precipitation/dissolution in Zr alloys by high temperature–high sensitivity calorimetry, J. Nucl. Mat. 372 (2008) 367–378.

[5] MARCOTTE, V.C., LARSEN, W.L., WILLIAMS, D.E., Phase relationships of the oxygen-containing 20 and 25 per cent zirconium-niobium alloys, J. Less-Common Metals 7 (1964) 373-382.

[6] ROBSON, J.D., Modelling precipitation in zirconium niobium alloys, J. Nucl. Mat. **377** (2008) 415–422.

[7] ASTM 8 EM. Standard test methods for tension testing of metallic materials. Annual book of standards, section 3: metals test methods and analytical procedures, vol. 03.01. ASTM, Philadelphia (2002).

[8] ZAVODCHICOV, S.Y., ARZHAKOVA, V.M., BOCHAROV, V., ZUEV, L.B., KOTREKHOV, V.A., ROZHDESTVENSKIY, V.V., TARASEVICH, S., PHILIPPOV, V.B., SHIKOV, A.K., Zirconium-Niobium-Oxygen containing alloy and method for producing said alloy, US Patent 7.704.334 B2 (2010).

[9] ZAVODCHICOV, S.Y., ARZHAKOVA, V.M., BOCHAROV, V., ZUEV, L.B., KOTREKHOV, V.A., ROZHDESTVENSKIY, V.V., TARASEVICH, S., PHILIPPOV, V.B., SHIKOV, A.K., Zirconium-Niobium-Oxygen containing alloy and method for producing said alloy, European Patent 1 621 642 A1 (2006).

[10] LEE, J.M., HONG, S.I., Design and mechanical characterization of a Zr–Nb–O–P alloy, Materials and Design **32** (2011) 4270-4277.

LICENSING AND REGULATORY ASPECTS
(SESSION 5)

Chairperson

J. Rovny

Slovakia

CHALLENGES FOR THE REGULATORY BODY DURING TRANSITION TO USE FUEL WITH HIGHER BURNUP

S.A. POPOVA

Chief Inspector
Division of Research and Analysis of Safety
Directorate of Safety Analyses, Assessment and Research
Nuclear Regulatory Agency
Bulgaria
S.Popova@bnra.bg

Abstract.

In the presentation will be disseminated the information about experience of the Bulgarian Nuclear Regulatory agency collected during licensing activities taken in relation of transition to the fuel with high burnup. Will be put in attention such problems as a compatibility of nuclear fuel during transitional cycles, neutron- physical characteristics of the core loaded with new fuel and necessity of further analysis, safety analyses for the particular unit (reactivity accidents, accidents with a large loss of coolant, etc.), characteristics of the fuel and unit's specification, as well as input data for accidents.

1. NUCLEAR PROFILE OF BULGARIA

Kozloduy NPP is located at 200 km north-west from Sofia and at 5 km east from Kozloduy, on the Danube River, Fig. 1. The plant construction activities started in 1969.

FIG. 1. Location of Kozloduy NPP in Bulgaria.

At present there are six units at Kozloduy NPP site of 3760 MW total capacity. Four units are VVER-440, model V-230 and other two units are VVER-1000, model V-320 (Fig. 2).

FIG. 2. Kozloduy NPP, Bulgaria.

The first two units - VVER-440, model V-230 of 880 MW capacities were shut down for decommissioning on December 31, 2002 in compliance with the Council of Ministers' Decision of December 19, 2002. The Units 1 and 2 are licensed until 2015 by the Nuclear Regulatory Agency as facilities for radioactive waste management, which are subjects to decommissioning.

Other two units - VVER-440, model V-230 of 880 MW capacities were shut down for decommissioning on December 31, 2006 in compliance with the Council of Ministers' Decision of December 21, 2006 for implementation of obligation under the Treaty of Accession of the Republic of Bulgaria to the European Union. The Units 3 and 4 are licensed until 2018 by the Nuclear Regulatory Agency as facilities for radioactive waste management, which are subjects to decommissioning.

Two units - VVER-1000, model V-320 of 2000 MW total capacity are in operation at present. The Unit 5 is licensed by the NRA for operation until 2017. The Unit 6 is licensed by the NRA for operation until 2019, Table 1. Spent Fuel Storage Facility is licensed by the NRA for operation until 2014. Scope – manipulation and storage of the spent nuclear fuel from the NPP Kozloduy reactors, in accordance with the conditions of the license. Dry Spent Fuel Storage Facility (DSFSF) has a permit for commissioning since 25.11.2011 year. Container system with using of CONSTOR 440/84 type of containers with natural convection air-cooling. Container's capacity – 84 fuel assemblies.

TABLE 1. KOZLODUY NPP, MAIN DATA

Unit	Reactor type	Start of operation	Fuel cycle at the moment/ the end of operation	End of the Licensee	Units shut down
Unit 1	VVER-440/V 230	Oct.1974	23	2015	2002
Unit 2	VVER-440/V 230	Nov.1975	24	2015	2002
Unit 3	VVER -440/V 230*	Dec.1980	23	2018	2006
Unit 4	VVER -440/V 230*	Jun.1982	22	2018	2006
Unit 5	VVER-1000/V-320	Sep.1988	20	2017	
Unit 6	VVER-1000/V-320	Dec.1993	19	2019	

***** Units 3 and 4 are an upgraded version of the V-230, with ECCS design equal to V-213

On 8 April 2005 the Government made a decision for construction of a new nuclear power generating capacity in Bulgaria. The decision specifies that the nuclear power plant shall have a maximum total capacity of 2000 MW electrical power generated by pressurised water reactors. On 29 March 2012 the Council of Ministers adopted a decision, which revoked all previous decisions related to the construction of 'Belene' NPP (Fig. 3). The adoption of this decision means that further (subsequent) actions related to the project 'Belene' are suspended.

FIG. 3. Belene NPP, Bulgaria.

2. REGULATORY FRAMEWORK

2.1. Act on the Safe Use of Nuclear Energy (ASUNE) [1]. This Act covers the activities associated with Plant Modification under Article 15, Paragraph 4, point 5 and Article 38

Article 15: (4) A permit shall be issued for:

Activities leading to modification of:

(a) structures, systems and components important to the safety of the nuclear facility;

(b) nuclear facility operating limits and conditions on which basis the operating licence has been issued;

(c) internal rules for carrying out the activity, including instructions, programmes, technical specifications, and other documents that are attached to the nuclear facility operating licence.

Article 38(1) Permits shall be issued to a licensee for:

Activities leading to modification of:

(a) structures, systems and components important to safety;

(b) limits and conditions for operation, that provide the basis for issuing of the operating licence;

(c) internal rules for conduct of licensee activities, including instructions, programmes, technical specifications and other documents attached to the licence.

(2) Permits covered under Item 1 of Paragraph (1) shall be issued if the requested modifications comply with nuclear safety and radiation protection requirements, standards and rules established by the regulation referred to in Article 26 (2).

Article 26:(2) Nuclear safety and radiation protection requirements, standards and rules for use of nuclear energy and sources of ionizing radiation, radioactive waste management and spent fuel management, including siting, design, construction, commissioning, operation and decommissioning of nuclear facilities and facilities with sources of ionizing radiation, shall be established by regulations adopted by the Council of Ministers on a motion by the NRA Chairman.

2.2. Regulations concerning for commissioning of new fuel – high burnup (HBU) fuel including

2.2.1. Regulation for the Procedure for Issuing Licenses and Permits for Safe Use of Nuclear Energy [2]

This Regulation establishes the procedure for issuing the permits under Article 15, Paragraph 4, point 5 of the Act on the Safe Use of Nuclear Energy (ASUNE).

Licenses and permits are issued, amended, renewed, suspended and revoked by the Nuclear Regulation Agency (NRA) Chairman according to the principles and under the conditions specified by the ASUNE.
The applicant shall comply with the conditions for issuing a license or permit or for to amendment and renewal of a license or permit when:

(i) All necessary documentation is submitted;
(ii) The NRA Chairman's instructions for providing additional documents are complied with;
(iii) All the conditions specified in preceding licenses, permits and other documents issued under the ASUNE and connected with issuing the respective license or permit are fulfilled;
(iv) The review and assessment of the applicant's submissions confirm the compliance with the requirements of the ASUNE and with all the regulations for the application of the ASUNE;
(v) All necessary licenses, permits and other administrative acts specified by the ASUNE as prerequisites for issuing the respective license or permit have been issued to the applicant by the competent administrative authorities.

Article 57(2) The following shall be attached to the application for issuing of a permit for modifications submitted by the licensee:

(i) Justification for the proposed modification and reasons for undertaking the modification;
(ii) Justification for the proposed time limit for performing the modification;
(iii) Assessment of the proposed modification impact on the limits and conditions for safe operation;
(iv) List of the standards applied to the activity;
(v) The amended parts or sections of the safety assessment report;
(vi) Analysis and assessment of the unfavourable external or operational conditions, including those connected with increase in the volume and activity of generated

Radioactive Waste (RAW), increase in the radioactive pollution, as well as with additional occupational radiation exposure;

(vii) Description of the modifications in the maintenance activities.

Article 57(3) In the case of issuing a permit for structures, systems and components modification, the following shall be attached:

(i) Technical design for the modification;
(ii) Schemes and drawings reflecting the state before and after modification;
(iii) Technical specification of the necessary equipment and components to be used for the modification;
(iv) Certificate for the modified structures, systems and components or description of the modes of production and assembling of the equipment and components;
(v) Description of the factory tests foreseen, the assembly and functional tests for confirming acceptance criteria, including the methods for verification and validation of computer codes related to operation;
(vi) Description of the operational state of the nuclear facility or of the respective part of it at which the modification is to be performed;
(vii) Quality assurance program applied to this activity and a plan for quality control.

2.2.2. Regulation on Ensuring the Safety of Nuclear Power Plants [3]

The regulation defines the basic criteria and rules of nuclear safety and radiation protection (safety) of nuclear power plants (NPP), as well as the administrative provisions and the technical requirements for ensuring safety during the stages of site selection, design, construction, commissioning and operation.Section II of this Regulation defines the scope of required safety assessment to issuing the permits for activities leading to modifications, including commissioning of the new fuel with high burnup (HBU).

Article 18 (1) Plant safety shall be analyzed using deterministic and probabilistic methods to verify and confirm the established design basis and the effectiveness of defence in depth arrangements. (2) Computer codes, analytical methods and plant models to be used in the safety analysis shall be verified and validated. Uncertainty of the results shall be quantified.

Article 20. Analyses results under Art. 19, paragraph 2 (analysis of the postulated initiating events) shall demonstrate:

1. Maintaining fuel cladding integrity - in states of categories 1 and 2;
2. Maximum fuel cladding temperature shall not exceed 1200 degrees centigrade, the local oxidation of the cladding shall not exceed 17% of the initial thickness, and the reacted amount of zirconium shall not exceed 1% of its mass in the reactor core, in cases of loss of coolant accidents of categories 3 and 4.

2.3. IAEA safety standards

2.4. International codes and standards

3. CHALLENGES FOR BULGARIAN REGULATORY BODY DURING TRANSITION TO USE FUEL WITH HIGHER BURNUP

Kozloduy NPP submitted a request for authorization to implement a technical solution 2903/11.12.2003 on 18 December, 2003. It was a phased transition from the fuel assembly TVS-M to TVSA design for unit 6.

Two years later Kozloduy NPP submitted a request for authorization to implement a technical solution 3064/20.09.2004 on 22 March, 2005. It was a phased transition from the fuel assembly TVS-M to TVSA design for unit 5.

Maximum-allowable burnup assemblies according to descriptive cataloguing for is 49 MWd/kgU for TVS-M and 55 MWd/kgU for TVSA respectively.

A set of documentation has been presented during the process of licensing in BNRA to justify the safety of the new fuel.

The model documents of safety analysis of a new type of fuel in operation of Units 5 (6) of Kozloduy NPP in different fuel cycles and extended power uprates is require for licensing process. (It can be seen in Appendix 1).

Some important recommendations have been established during the review and assessment of the documents which licensee had to pay more attention in preparation of the Terms of Reference (TOR) and choosing the design of the fuel in future.

All related analyses which are a part of new fuel licensing process are described below.

3.1. Analysis of the compatibility of fuel in transient cycles:

- Compatibility of geometry;
- Compatibility of neutron-physics characteristics (difference in water-uranium terms is compensated using proper enrichment of U^{235} and profiling);
- Thermomechanical compatibility (similar construction materials);
- Thermohydraulic compatibility.

3.2. Preparing a statement to prove the compatibility of the new fuel with existing systems and components of the reactor, equipment for the transportation, storage and handling of fresh fuel, and to confirm the design basis of the reactor and the efficiency of defence in depth.

3.3. Performing of neutron physics calculation for the respective unit using as input data the same fuel assemblies design which will be used during the transient fuel cycles and steady state cycle.

3.4. Transient core loading and fixed shall be formed in the way, which is expected to operate the block. For example, the core reloads of 42 fresh fuel assemblies in each cycle, 42 new assemblies for longer power effect of reactivity and 48 assemblies in the next cycle, etc.

3.5. Providing a preliminary reactor core analysis and checking if it needs for additional analyses.

3.6. For example, it is possible the coefficients of coolant-moderator temperature when reaching Hot zero power (HZP) to become a positive value or in range of uncertainly of the calculation when using a scheme of charging 48 fresh fuel assemblies at the beginning of each cycle.

3.7. According to Bulgarian legislation the reactivity coefficients of coolant-moderator temperature should be negative in all critical conditions.

Positive value of this coefficient when reaching HZP results in the imposition of additional measures - such as a fully sunk Control and Protection System Absorber rod (CPS AR) group 10 - working group. In this case it is necessary to submit to the BNRA further analyses of reactivity accidents of commissioning conditions with more than one partially sunk CPS AR group. It is necessary to implement a change in commissioning physical experiments (measure the effectiveness of working group) and also in the in-service documentation in case of reaching the HZP using additional CPS AR group/ groups with a fully sunk working group and banned its motion. It is necessary to assess the extent of analysis and operational documents requiring change.

For example, it is necessary to present these analyses and justifications:

- Analyses of reactivity accidents (RIA);
- Analysis of the cooling conditions of the reactor core (double-ended guillotine break (DEGB), instantaneous jamming of one reactor coolant pump, etc.);Analysis of nuclear safety of spent fuel/fresh fuel (SF/FF) management – storage, transport at the site and SF/FF handling of fuel with higher burnup. Analysis of criticality in transport containers in the fresh fuel storage (FFS), while refuelling in the core, emergency removal of fuel from the reactor core in spent fuel pool (SFP);Analysis of nuclear safety of the new type fuel storage at SFS - dry and wet;
- Assessment of the proposed change impact on the safety operations limits and conditions for safe operation of the unit. Assessment of the compliance with design limits for transients and accidents;
- Analysis demonstrating compatibility of the assemblies with existing CPS AR and the in-core instrumentation system (ICIS);
- Proof of compatibility of the assemblies with the existing Primary Coolant Chemistry regimes of VVER-1000 for different regimes of operation;
- Neutron fluence at the reactor pressure vessel analyses;
- Radiological consequences analyses and etc.

3.9. Safety analyses should be made taking into account the specific features of the unit and unit modifications, such as diameter of piping and steam lines, characteristics of the pumps, interlock systems for normal and emergency operation, signals to activate the safety systems and others.

3.10. It is necessary to consider whether previously used codes, calculated with sufficient accuracy the neutron-physics characteristics of the reactor core in transient and equilibrium cycles, using a new higher burnup fuel (respectively with a larger amount of fissile material), or it is necessary to adjust the constants libraries.

3.11. It is also necessary to check the selection of the input data for the analyses.

3.12. Data from the descriptive cataloguing of new fuel are operational limits for every assembly. This data became operation limits for safe operation of the particular unit when in safety analyses is demonstrated that the operation of the core loaded with this fuel does not violate criteria for safe operation of the reactor.

Moving to a new fuel operation requires update of the SAR of each unit. All further analyses were performed with updated input data, the selection of which are used conservative approach.

For example, as a result of reactor core analysis is received a value 53 Mwday/kgU at steady state loading of new fuel for a particular unit, on the other hand according to descriptive cataloguing limit burnup must not exceed 55 Mwday/kgU.

In this case, the data obtained from reactor core analysis at steady state reload for this unit shall be used as input data for safety analysis. In our example, this is data on 53 Mwday/kgU - maximum, reached an estimated value of burnup.

During the licensing process the lower value of burnup is taken as an operating limit (according to our example, this is 53 Mwday/kgU, which is lower than that presented in descriptive cataloguing) for this unit.

If the data obtained from reactor core analysis are at higher burnup than that presented in descriptive cataloguing of new fuel, then as a limit burnup for this unit is taken from the descriptive cataloguing, as a restriction from the fuel supplier.

4. CONCLUSIONS

The use of a new fuel with higher burn up required authorization and related safety documentation should be submitted for review and approval by the regulatory body in accordance with national regulations.

Management of the modification should be the responsibility of the operating organization.

It is necessary to prepare a thorough preliminary analysis already in selection process for obtaining permission to use a new type of fuel with higher burn up. The aim is to achieve greater efficiency, reduce the time and resources invested in the preparation of documentation in the licensing process.

Appendix 1

I. Justification documentation. Safety analysis of unit 5 (6) of Kozloduy NPP

1. Reactor core analysis for transient and steady state cycles of unit 5 (6) of Kozloduy NPP.
2. Justification of the efficiency of the fuel rods during steady state conditions, transients of normal operation, anticipated operational occurrences and design basis accident LOCA and RIA for unit 5 (6) of Kozloduy NPP.
3. Thermal hydraulic analyses for steady state in normal operation, anticipated operational occurrences, accidents, including severe accidents unit 5 (6) of Kozloduy NPP.
4. Analysis of nuclear safety during transportation with new fuel - analysis of criticality in transport containers in the fresh fuel storage (FFS), reloading the core, emergency removal of fuel from the core into spent fuel pool (SFP) in completely filled with new fuel SFP.
5. Analysis of nuclear safety during the storage in spent fuel storage (SFS) (under water) and in dry spent fuel storage (DSFS).
6. Analysis of the decay heat - in the core, with completely filled with new fuel SFP, after accidental removal of fuel from the core to the SFP in containers during transport and in SFS.
7. Analysis of fission products from the fuel and non-tight fuel elements in the coolant and coolant activity in normal operation.
8. Source term analysis during anticipated operational occurrences and accidents.

9. Analysis of the radiological consequences.
10. Analysis of the neutron fluence at the reactor pressure vessel, lifetime estimation.
11. Analysis of the neutron fluence at the reactor internals, lifetime estimation.
12. Compatibility analysis of the proposed nuclear and previously operated nuclear fuel in NPP (in transient refuelling).
13. Proofing of compatibility of existing fuel with water chemistry of the VVER-1000 reactors in different modes of operation.
14. Compatibility analysis of new assemblies with existing CPS AR and the ICIS
15. Compatibility analysis of new fuel with existing systems and equipment for the transportation, storage and handling of fresh fuel.
16. 16 Validation and verification reports for codes used for reactor processes analysis during normal operation, anticipated operational occurrences and accidents.
17. Feasibility study of the proposed new fuel to justify maximum economic efficiency of the fuel cycle.
18. Assess the impact of the proposed change on the limits and conditions of safe operation of the respective unit 5 (6). Analysis and assessment of compliance with design limits in transients and accidents.

II. Justifying documentation for licensing made by the licensee

1. Amended parts and sections of the respective SAR unit 5 (6), taking into account the new type of fuel, including evidence (statements, analyses, reports) to justify the safe and reliable operation of the units using new type of fuel.
2. New documents, instructions and procedures relating to the operation of the new type of fuel:
    - Programs for starting physical tests at HZP;
    - Programs for testing at power.
3. Draft amendments (new) Revision of Annex 2 of the License for operation of Units 5/6, which reported the new fuel, such as:
    - Technical specification for safe operation of Units 5/6 with VVER-1000 reactors;
    - Reactor operation instructions ;
    - Instruction on elimination of normal operation and accidents in reactor installation;
    - Program for quality assurance of safe operation of Units 5 and 6 of NPP Kozloduy;
    - Administrative instruction. Preparation of reports with neutron physical properties of reactor VVER-1000.
4. Updated information in Annex 4 of the license for operation of Units 5/6 - Data for nuclear fuel and radioactive waste related to the operation of Units 5/6".

REFERENCES

[1] Act on the safe use of nuclear energy, 1.07.2012.

[2] Regulation on the Procedure for Issuing Licences and Permits for Safe Use of Nuclear Energy, Promulgated in the State Gazette No. 41/18.05.2004, Amended SG No. 78/30.09.2005; 93/24.11.2009; 76/05.10.2012.

[3] Regulation on ensuring the safety of nuclear power plants, Published SG, No. 66 of 30 July 2004, amended SG No. 46 of 12 June 2007, and amended SG No. 53 of 10 June 2008.

LICENSING AND OPERATIONAL EXPERIENCE WITH HIGH BURNUP FUEL IN SLOVAK NPPS

J. ROVNY

Slovenske elektrarne, member of ENEL group
Bratislava
Slovak Republic
Email: juraj.rovny@enel.com

Abstract.

Slovenske elektrarne operate four units of VVER 440 V213 type. Nuclear fuel cycle is being continuously modified in order to satisfy current operational requirements as well as to optimize nuclear fuel cycle costs. These trends caused that fuel type has been modified practically every couple of years during the last decade, based on the fuel portfolio offered by the producer - TVEL. The latest fuel type, first time loaded into the reactor core in 2011, is designed to reach relatively high burnup values up to 72,5 MWd/kgU for fuel rod or up to 65 MWd/kgU for fuel assembly in six year fuel cycle. These values are substantially higher than previously reached values and are therefore subject to detail safety assessment during the licensing phase. In order to obtain license for the nominal design burnup values, Slovenske elektrarne had to launch a new initiative in order to summarise an adequate safety case. At the moment the licences are still limited for four years of operation only and utility is working on relevant documentation to be submitted to NRA for approval. The paper describes main technical issues and overall strategy selected in order to fulfill its licensing intent.

1. INTRODUCTION

Slovenske elektrarne (SE) is a major electricity producer in Slovak republic. Since 2006 Enel owns a 66% share in SE. Its net installed capacity amounts to 5,401 MW, of which 1,816 MW from nuclear energy and the rest from coal fired thermoelectric and hydroelectric power. Almost 90% of the produced electricity by Slovenske elektrarne is CO_2 free. Enel operates a net installed capacity of over 97,000 MW in 40 countries, serving more than 61 million customers.

SE operates 4 VVER-440 reactors in two sites: Bohunice and Mochovce. All of them are V-213 type with net installed electrical capacity of 470 - 500 MW each. Furthermore, a 2,775 billion Euro investment has been allocated to complete the Mochovce 3 and 4 (also VVER-440) nuclear power station being the largest overseas investment in the country.

All of the operating units significantly improved its performance over the last couple of years resulting in Unit Capability Factor beyond 93%. By doing so SE units belong nowadays to the best operated PWRs world-wide.

2. FUEL CYCLES APPLIED IN SLOVAK NPPS

Different fuel types and corresponding core designs have been applied over the history. Figure 1 shows schemes of profile and enrichment of particular fuel types loaded to reactor cores:

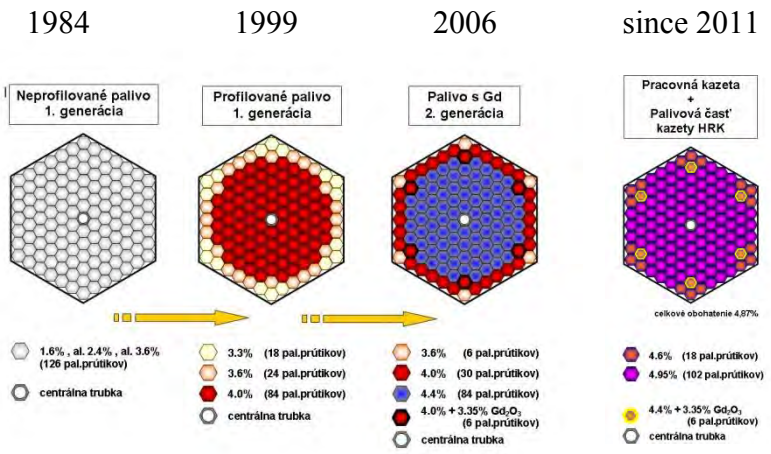

FIG. 1. Fuel types used in Slovak NPPs.

The only vendor and manufacturer of the fuel for NPPs in Slovakia has always been Russian company TVEL. This included also supply of enriched uranium product. Positive experience with very reliable fuels, support during licensing and practically no or only minor operational problems caused that an alternative fuel supplier has not been considered so far.

The currently used fuel type is fuel assembly (FA) consisting of rods with maximum enrichment 4.98%, 6 rods include Gadolinium as a burnable absorber and the total average FA enrichment is 4.87%. Selection of this type of fuel has been made in 2007 taking into account operational needs (as for example power uprate projects) and overall economy of fuel cycles.

3. HIGH BURNUP LICENSING

Generally, the question of highest possible burnup has not been addressed in a complex manner over the history in Slovakia. Therefore, there is no official regulatory limit. Urad jadroveho dozoru (UJD) – Nuclear regulatory authority of the Slovak republic always has been reviewing design of fuel cycles as a part of new fuel type licensing. With continuous improvement of fuel cycle economy the maximum discharge burnup of previous fuel types and cycles has gradually increased from values as 40 MWd/kgU (highest rod average) to 55 MWd/kgU and 62 MWd/kgU respectively. These values were in line with what could be denoted as general standard over the world and were, therefore, not subject to any particular assessment.

Nevertheless the situation has changed in 2009 when the latest fuel type licensing has been launched since the proposed fuel cycle design would result in burnup up to 72 MWd/kgU (highest rod average). This has attracted a particular attention of the regulator especially in the context of recent experimental results from the Halden reactor project (HRP). HRP IFA-650 LOCA tests series directed attention to possible fuel fragmentation and relocation effects as a result of high burnup fuel. Additional arguments and evidence of maintaining adequate safety of operation in high burnup conditions have been asked by UJD in order to finish licensing of new fuel type from the core design and fuel cycles strategy point of view.

It turned out to be that neither the fuel vendor nor the Technical Support Organization (TSO) contracted by SE during fuel licensing process are able to provide in a short term such evidence. Therefore, SE decided to address this issue by its own resources. This situation made visible another fact that both the utility as well as the local TSO to certain extend lost

part of its knowledge and competence in fuel engineering and such project would definitely contribute to reestablishment of it.

The following four areas were identified as required directions of further activities:

- Cooperation with fuel vendor
- Deep analysis of fuel safety criteria
- International experience mapping
- Experimental evidences

3.1. Cooperation with fuel vendor

TVEL has been asked to provide satisfactory justification of safe operation with high burnup fuel cycles based preferably on experiments. TVEL succeeded to submit results of operational experience with identical fuel type as SE use in its reactors up to burnup of 75 MWd/kgU. It has been based on experience with operation on both VVER-1000 as well as VVER-440 reactors in Russia and Ukraine. Higher burnup did not cause any operational problems or potential issues. Similarly post irradiation examination showed acceptable material degradation within set criteria up to the 75 MWd/kgU. In the area of postulated accidents, however, the evidence has not been provided for required value of fuel burnup. Despite the fact that performed experiments are showing excellent results these do not cover burnup beyond 65 MWd/kgU for LOCA conditions and 60 MWd/kgU for RIA conditions. Standpoint of the fuel vendor is that residual post-accident condition of the fuel allows for entitled assumptions to extrapolate these data also to higher burnup values.

3.2. Fuel safety criteria analysis

In the context of available experimental results one of the possible ways to grant a license for high burnup is to perform a correct technical interpretation of the high burnup phenomenon. Therefore, SE decided to deeply analyse this issue through the optics of fuel safety criteria, its justification and substantiation. Operational and engineering groups involved in fuel cycle tackled all relevant documentation, searching for evolution of fuel SCs in relation to fuel type modifications. Special attention is paid to relation between individual SC and burnup. This part of the job has not been finished yet but already now resulted into development of comprehensive, condensed and well-structured database of these facts and data. This will allow in the future better prepare for and manage any modifications from licensing point of view.

3.3. International experience

In order to avoid reinventing a wheel one of the very first initiatives launched in this project was mapping the way the other regulators and utilities addressed the high burnup phenomenon. Overview of existing regulatory limits has been summarised. In particular attentions were countries that use the same fuel vendor in the same reactor type, i.e. Czech Republic, Hungary and Finland.

Apart from that SE experts joined some of the international working groups (e.g. OECD NEA Working Group on Fuel Safety). It turned out that burnup limit is handled very differently in each individual country and no general approach can be identified as a common practice.

3.4. Experimental evidences

The last out of the four main components of high burnup license project initiative is the activity related to experiments devoted to this phenomenon. In order to gain an independent view on fuel behaviour under accidental conditions in addition to the experiments performed by fuel vendor it has been decided to actively join the Halden reactor project initiative. Slovak

republic has been represented in HRP by a TSO. In 2012 SE experts personally joined some of the steering committees and working groups. Main goals are to be an active partner, influence the type, scope and timing of experiments and to get information from first hand. Beside a running research project on LOCA conditions a new joint project is currently being prepared – Burnup accumulation of pre irradiated VVER fuel in period 2014 – 2016. A foreign TSO has been contracted to analyse and prepare interpretation of the previous Halden Reactor Project integral LOCA tests IFA-650 series in the context of the licensing process.

4. SUMMARY

Historically flawless processes of new fuel types licensing lead to high confidence in fuel vendor and local TSO that resulted in decision to select fuel type and fuel cycle with relatively high burnup without thorough consideration of all possible complications. Currently SE holds a license for fuel type as such, however with limited burnup. Additional evidence is needed in order the national regulator issues license for the original design burnup of 72 MWd/kgU.

For reasons described above SE decided to address this issue mainly by own resources (at least from the managerial point of view) and established a working group to perform this project. It is expected that during the year 2014 the question of burnup limit should be resolved.

Apart from this short-term goal it is desired to continue increasing in-house competences in core design and fuel performance areas and, therefore, it has been decided to insource core design competence and acquire and maintain solid knowledge in the area of fuel safety criteria assessment. From a long term perspective SE intend to regularly perform comprehensive economical evaluation of fuel cycle including the back end and monitor its performance.

ABBREVIATIONS

ADU	ammonium diuranate
AR	absorber rod
ARO	all rods out
ATF	accident tolerant fuel
BOL	beginning of cycle
BU	burnup
BWR	boiling water reactor
CANDU	Canadian type pressurised heavy water reactor (Canadian Deuterium Uranium)
CC	coolant channel
CPS	control and protection system
CRP	co-ordinated research programme
DEGB	double-ended guillotine break
DNB	departure from nucleate boiling
EFA	experimental fuel assembly
EFPDs	effective full power days
EOL	end of life
EOS	equiation of state
EPMA	electron probe microanalysis
FA	fuel assembly
fcc	face centred cubic
FCT	fuel centre temperature
FD	finite difference
FE	finite element
FGR	fission gas release
FPC	fuel performance code
FROD	fuel rod outer diameter
GTAW	gas tungsten arc welding
HBEP	high burnup effects programme
HBS	high burnup structure
HFP	hot full power
HRP	Halden Reactor Project
H/U	hydrogen/uranium
HWR	heavy water reactors
HZP	hot zero power
ICIS	in-core instrumentation system
IFBA	integral fuel burnable absorber

IFM	intermediate flow mixer
IFPE	International Fuel Performance Experiments database
IWGFPT	International Working Group on Fuel Performance and Technology
LOCA	loss of coolant accident
LP	loading pattern
LWR	light water reactor
MOX	mixed oxide fuel
MTC	moderator temperature coefficient
NEU	natural uranium equivalent
NSC	nuclear science committee of the OECD/NEA
NPP	nuclear power plant
NUE	natural uranium equivalent
NWCC	neutron well coincidence counting
PCI	pellet cladding interaction
PCMI	pellet cladding mechanical interaction
PCS	primary coolant system
PHWR	pressurised heavy water reactor
PIE	post-irradiation examination
PWR	pressurised water reactor
RCM	research coordination meetings
RCS	reactor coolant system
RFA	robust fuel assembly
RIA	reactivity insertion accidents
RRF	reciprocal reload factor
RU or RepU	reprocessed uranium
SCC	stress-corrosion cracking
SEM	scanning electron microscopy
SEU	slightly enriched uranium (slightly above natural concentration of ^{235}U)
SFP	spent fuel pool
SIMS	secondary ion mass-spectrometry
SWU	separative work unit
TD	theoretical density
TEM	transmission electron microscopy
TM	thermo-mechanical
TH	thermo-hydraulic
TSO	technical safety organisation
VVER	Russian designed pressurised light water reactor

XRF	X-ray fluorescence
WABA	wet annular burnable absorber

LIST OF CONTRIBUTORS

Alonso, P.R.	Comisión Nacional de Energía Atómica – CNEA, Av. General Paz 1499, San Martín, Buenos Aires, Argentina Tel: +54-11-4839-6710 Email: pralonso@cnea.gov.ar
Alvarez, L.A.	Comisión Nacional de Energía Atómica – GCCN-CAC-CNEA Av. General Paz 1499, San Martín, Buenos Aires, Argentina Tel: +54-11- 6772 7437; +54-11- 6772-7407; Email: lalvarez@cnea.gov.ar
Bhatt, R.B.	Bhabha Atomic Research Centre; AFFF, BARC Complex, Tarapur, P.O. Ghivali; Dist. Thane – INDIA 401502 Email: rbbhatt@barctara.gov.in
Boero, N.L.	TM Chairperson, President of the National Commission on Atomic Energy, Av. Del Libertador 8250 (1429) Buenos Aires, Argentina Tel: +54 11 4704 1000 Email: comunicacion@cnea.gov.ar
Bonelli, A.N.	Nucleoeléctrica Argentina S.A. Unidad de Gestión CNA-IV CN. PO Box No. 37, Ruta 9 – Km. 100 Lima, Buenos Aires, Argentina (B2806AEL) Tel: +54-11-3487-482007 Ext. 5882; +54-11-3487-482000 Ext. 5390 Email: abonelli@na-sa.gov.ar
Bussolini, A.A.	Comisión Nacional de Energía Atómica – CNEA Av. Libertador 8250 C.A.B.A. (1429) Argentina Tel:+54-11-6772-7430; +54-11-6772-7407 Email: bussolini@cnea.gov.ar
Boselli, A.	Comisión Nacional de Energía Atómica – CNEA Av. Del Libertador 8250 (C1429BNP); Buenos Aires, Argentina Tel: +54-11-4704-1181; +54-11-4704-1170 Email: boselli@cnea.gov.ar
Calabroni, H.N.	Comisión Nacional de Energía Atómica – CNEA Av. Libertador 8250 C.A.B.A. (1429) Argentina Tel:+54-11-6772-7435; +54-11-4125-8102 Email: hcalabroni@cae.cnea.gov.ar
Chocron, M.	Comisión Nacional de Energía Atómica – CNEA Av. Del Libertador 8250 (1429) Buenos Aires, Argentina Tel: +54-11-6772-7183; +54-11-6772-7153 Email: chocron@cnea.gov.ar
Ciarrocchi, A.V.	Comisión Nacional de Energía Atómica – CNEA Av. Libertador 8250 C.A.B.A. (C1498BNP), Buenos Aires, Argentina Tel: +54-11-6772-7430 Email: ciarrocchi@cnea.gov.ar
Correa, C.A.	Comisión Nacional de Energía Atómica – CNEA Auditoría Interna; Av. Del Libertador 8250 (1429) Ciudad Autónoma de Buenos Aires, Argentina Tel: +54-011-4704-1499 Email: correac@cnea.gov.ar
Cottrell, C.	Candu Energy Inc. 2285 Speakman Drive; Mississauga, Ontario, Canada L5K 1B1; Tel: +1 905-823-9060 Ext. 36264

	Email: catherine.cottrell@candu.com
D'Amico, N.	Nucleoeléctrica Argentina S.A. Unidad de Gestión CNA-IV CN. PO Box No. 37, Ruta 9 – Km. 100 Lima, Buenos Aires, Argentina (B2806AEL) Tel: +54-11-3487-482007 Email: ndamico@na-sa.com.ar
De Las Heras, M.E.	Comisión Nacional de Energía Atómica – CNEA Av. General Paz 1499, San Martín, Buenos Aires, Argentina Tel:+54-11-155369-2612 Email: belen@inti.gov.ar
Denis, A.	Comisión Nacional de Energía Atómica – CNEA; Laboratorio de Nanotecnología Nuclear, Centro Atómico Constituyentes, Av. General Paz 1499 (B1650KNA) Tel: +54 11 6772 7000 Email: adenis@cnea.gov.ar
Ferreirós, P.A.	Comisión Nacional de Energía Atómica – CNEA Av. General Paz 1499, San Martín, Buenos Aires, Argentina Tel:+54-11-6772-7247 Email: ferreiros@cnea.gov.ar
Hozer, Z.	Hungarian Academy of Sciences Centre for Energy Research; MTA Centre for Energy Research; P.O. Box 49; H-1121 Budapest Hungary Tel: 0036-1-2754083 Email: Zoltan.hozer@energia.mta.hu
Inozemtsev, V.	International Atomic Energy Agency, Vienna International Centre, PO Box 100 A-1400 **Vienna**, Austria Tel: (+431) 2600-22760 Email: V. Inozemtsev@iaea.org
Jatuff, F.E.	Kernkraftwerk Gösgen-Däniken AG; Kraftwerkstrasse; CH-4658 Däniken; Switzerland Tel: +41 62 288 21 06 Email: fjatuff@kkg.ch
Luca, V.	Comisión Nacional de Energía Atómica – CNEA Programa Nacional de Gestión de Residuos Radiactivos, Gerencia Quimica, Centro Atómico Constituyentes, Av. General Paz 1499 1650 San Martín; Bs. A. Argentina Tel:+54-11-6772-7018 Email: vluca@cnea.gov.ar
Marino, A.C.	Comisión Nacional de Energía Atómica – CNEA Centro Atómico Bariloche 8400 Argentina Tel:+54-294-4445256; +54-294-4445199 Email: marino@cab.cnea.gov.ar
Martinez, R.L.	INVAP S.E.; Av. Cmte. Luis Piedrabuena 4950 (ex RN 237) R8403CPV S.C. de Bariloche, Argentina Tel:+54-924-154696-889 Email: rmartine@invap.com.ar
Medina, J.P.	Comisión Nacional de Energía Atómica – CNEA Av. Libertador 8250 C.A.B.A. (C1498BNP) Argentina Tel: +54-11-6772-7999 Email: medina@cnea.gov.ar
Miceli, M.D.	Comisión Nacional de Energía Atómica – CNEA Av. Libertador 8250 C.A.B.A. Argentina

	Tel: +54-11-6772-7824; +54-11-6772-7345 Email: miceli@cnea.gov.ar
Mochi, I.	INVAP S.E.; Esmeralda 356 First floor Capital Federal, Buenos Aires, Argentina. Tel: +54-011-4394-3344 (6109); +54-011-4394-3543 Email: imochi@invap.com.ar
Motillo, L.I.	Comisión Nacional de Energía Atómica – CNEA Programa Nacional de Gestión de Residuos Radiactivos y Combustibles Gastados Av. Del Libertador 8250 (C1429BNP); CABA; Centro Atómico Ezeiza Presbítero Juan González y Aragón N°15, Ezeiza, Argentina Tel: +54-11-4125-8686; +54-11-4125-8535 Email: mottillo@cae.cnea.gov.ar
Paneto, L.F.	Industrias Nucleares do Brasil S.A. – INB ; Rodovia ; residente Dutra, KM330 – Engenheiro Passos – Resende ; RJ CEP 27555-000 Brazil Tel : 005524 3321 8650 Email: lelia@inb.gov.br
Pasqualini, E.E.	Comisión Nacional de Energía Atómica – CNEA; Laboratorio de Nanotecnología Nuclear, Centro Atómico Constituyentes, Av. General Paz 1499 (B1650KNA); Argentina Tel: +54-11-6772-7134 Email: pascua@cnea.gov.ar
Paz, M.L.	Comisión Nacional de Energía Atómica – CNEA Av. Libertador 8250 C.A.B.A. (C1498BNP) Argentina Tel: +54-11-6772-7430 Email: mpaz@cnea.gov.ar
Pedrozo, H.O.	Comisión Nacional de Energía Atómica – CNEA Av. Libertador 8250 C.A.B.A. (C1498BNP) Argentina Tel: +54-11-6772-7432 Email: pedrozo@cnea.gov.ar
Popova, S.A.	Bulgarian Nuclear Regulatory Agency; 69 Shipchenski prokhod Blvd; 1574 Sofia, Bulgaria Tel:003592-9406842 Email: s.popova@bnsa.bas.bg
Rhee, Y.W.	Korea Atomic Energy Research Institute; 989-111 Daedeok-daero, Yuseong-gu, Daejeon, Korea, Republic of Tel: +82-42-868-2815 Email: youngwoo@kaeri.re.kr
Rodrigues, L.M.	Comisión Nacional de Energía Atómica – CNEA Av. Del Libertador 8250 (1429) Buenos Aires, Argentina Tel: +54-11-6772-7183; +54-11-6772-7153 Email: chocron@cnea.gov.ar
Rovny, J.	Slovenske elektrarne – ENEL group; Mlynske nivy 47, 821 09 Bratislava 2, Slovak Republic Tel:00421-910673322 Email: Juraj.rovny@enel.com
Rubiolo, G.H.	Comisión Nacional de Energía Atómica – CNEA Av. General Paz 1499, San Martín, Buenos Aires, Argentina. Tel:+54-11-6772-7240 Email: rubiolo@cnea.gov.ar
Ruggirello, G.R.	Comisión Nacional de Energía Atómica – CNEA

	Av. Libertador 8250 C.A.B.A. (1429) Argentina Tel: +54-11-6772-7435; Email: ruggirel@cnea.gov.ar
Soba, A.	Comisión Nacional de Energía Atómica – CNEA; Laboratorio de Nanotecnología Nuclear, Centro Atómico Constituyentes, Av. General Paz 1499 (B1650KNA), Argentina Tel: +54 11 6772 7000 Email: soba@cnea.gov.ar
Sypchenko, M.V.	JSC A.A. Bochvar High-technology Research Institute of Inorganic Materials, Moscow, Russian Federation Tel: +7-495-190-80-39 Email: sypchenko@bochvar.ru
Syrewicz, M.C. MS	Nucleoeléctrica Argentina S.A. Unidad de Gestión CNA-IV CN. PO Box No. 37, Ruta 9 – Km. 100 Lima, Buenos Aires, Argentina (B2806AEL) Tel: +54-11-3487-482007 Ext. 5882; +54-11-3487-482000 Ext. 5390 Email: csyrewicz@na-sa.com.ar
Tripodi, P.C.	Comisión Nacional de Energía Atómica – CNEA Av. General Paz 1499, CP 1650; San Martín; Buenos Aires, Argentina Tel: +54-11-6772-7428 Email: tripodi@cnea.gov.ar
Valesi, J.A.	Comisión Nacional de Energía Atómica – CNEA Av. Libertador 8250 C.A.B.A. (C1498BNP), Argentina Tel: +54-11-6772-7430 Email: valesi@cnea.gov.ar
Van Der Heijdt, L.	Ministry of Infrastructure and Environment; P.O. Box 16191; 2500 BD; The Hague, The Netherlands Email: Bertie.vander.heijdt@ilent.nl
Wiss, T.	European Commission, DG JRC, Institute for Transuranium Elements, P.O. Box 2340; D-76125 Karlsruhe, Germany Tel: +49 7247 951 447 Email: thierry.wiss@ec.europa.eu
Yousaf, O.	Pakistan Atomic Energy Commission; PAEC HQ, P.O. Box 1114, Islamabad, Pakistan Tel: 051-9225255 Email: Omeryousaf9211@hotmail.com

IAEA
International Atomic Energy Agency

No. 24

ORDERING LOCALLY

In the following countries, IAEA priced publications may be purchased from the sources listed below or from major local booksellers.

Orders for unpriced publications should be made directly to the IAEA. The contact details are given at the end of this list.

BELGIUM
Jean de Lannoy
Avenue du Roi 202, 1190 Brussels, BELGIUM
Telephone: +32 2 5384 308 • Fax: +32 2 5380 841
Email: jean.de.lannoy@euronet.be • Web site: http://www.jean-de-lannoy.be

CANADA
Renouf Publishing Co. Ltd.
22-1010 Polytek Street, Ottawa, ON K1J 9J1, CANADA
Telephone: +1 613 745 2665 • Fax: +1 643 745 7660
Email: order@renoufbooks.com • Web site: http://www.renoufbooks.com

Bernan Associates
4501 Forbes Blvd., Suite 200, Lanham, MD 20706-4391, USA
Telephone: +1 800 865 3457 • Fax: +1 800 865 3450
Email: orders@bernan.com • Web site: http://www.bernan.com

CZECH REPUBLIC
Suweco CZ, s.r.o.
SESTUPNÁ 153/11, 162 00 Prague 6, CZECH REPUBLIC
Telephone: +420 242 459 205 • Fax: +420 284 821 646
Email: nakup@suweco.cz • Web site: http://www.suweco.cz

FRANCE
Form-Edit
5 rue Janssen, PO Box 25, 75921 Paris CEDEX, FRANCE
Telephone: +33 1 42 01 49 49 • Fax: +33 1 42 01 90 90
Email: fabien.boucard@formedit.fr • Web site: http://www.formedit.fr

Lavoisier SAS
14 rue de Provigny, 94236 Cachan CEDEX, FRANCE
Telephone: +33 1 47 40 67 00 • Fax: +33 1 47 40 67 02
Email: livres@lavoisier.fr • Web site: http://www.lavoisier.fr

L'Appel du livre
99 rue de Charonne, 75011 Paris, FRANCE
Telephone: +33 1 43 07 43 43 • Fax: +33 1 43 07 50 80
Email: livres@appeldulivre.fr • Web site: http://www.appeldulivre.fr

GERMANY
Goethe Buchhandlung Teubig GmbH
Schweitzer Fachinformationen
Willstätterstrasse 15, 40549 Düsseldorf, GERMANY
Telephone: +49 (0) 211 49 874 015 • Fax: +49 (0) 211 49 874 28
Email: kundenbetreuung.goethe@schweitzer-online.de • Web site: http://www.goethebuch.de

HUNGARY
Librotrade Ltd., Book Import
Pesti ut 237. 1173 Budapest, HUNGARY
Telephone: +36 1 254-0-269 • Fax: +36 1 254-0-274
Email: books@librotrade.hu • Web site: http://www.librotrade.hu

INDIA
Allied Publishers
1st Floor, Dubash House, 15, J.N. Heredi Marg, Ballard Estate, Mumbai 400001, INDIA
Telephone: +91 22 4212 6930/31/69 • Fax: +91 22 2261 7928
Email: alliedpl@vsnl.com • Web site: http://www.alliedpublishers.com

Bookwell
3/79 Nirankari, Delhi 110009, INDIA
Telephone: +91 11 2760 1283/4536
Email: bkwell@nde.vsnl.net.in • Web site: http://www.bookwellindia.com

ITALY
Libreria Scientifica "AEIOU"
Via Vincenzo Maria Coronelli 6, 20146 Milan, ITALY
Telephone: +39 02 48 95 45 52 • Fax: +39 02 48 95 45 48
Email: info@libreriaaeiou.eu • Web site: http://www.libreriaaeiou.eu

JAPAN
Maruzen-Yushodo Co., Ltd.
10-10, Yotsuyasakamachi, Shinjuku-ku, Tokyo 160-0002, JAPAN
Telephone: +81 3 4335 9312 • Fax: +81 3 4335 9364
Email: bookimport@maruzen.co.jp • Web site: http://maruzen.co.jp

RUSSIAN FEDERATION
Scientific and Engineering Centre for Nuclear and Radiation Safety
107140, Moscow, Malaya Krasnoselskaya st. 2/8, bld. 5, RUSSIAN FEDERATION
Telephone: +7 499 264 00 03 • Fax: +7 499 264 28 59
Email: secnrs@secnrs.ru • Web site: http://www.secnrs.ru

UNITED STATES OF AMERICA
Bernan Associates
4501 Forbes Blvd., Suite 200, Lanham, MD 20706-4391, USA
Telephone: +1 800 865 3457 • Fax: +1 800 865 3450
Email: orders@bernan.com • Web site: http://www.bernan.com

Renouf Publishing Co. Ltd.
812 Proctor Avenue, Ogdensburg, NY 13669-2205, USA
Telephone: +1 888 551 7470 • Fax: +1 888 551 7471
Email: orders@renoufbooks.com • Web site: http://www.renoufbooks.com

Orders for both priced and unpriced publications may be addressed directly to:

IAEA Publishing Section, Marketing and Sales Unit
International Atomic Energy Agency
Vienna International Centre, PO Box 100, 1400 Vienna, Austria
Telephone: +43 1 2600 22529 or 22530 • Fax: +43 1 2600 29302
Email: sales.publications@iaea.org • Web site: http://www.iaea.org/books

16-21461